Influence of Sidechain Structure and Interactions on the Physical Properties of Perfluorinated Ionomers

Christina Marie Orsino

Dissertation submitted to the faculty of the Virginia Polytechnic Institute and State University in partial fulfillment of the requirements for the degree of

Doctor of Philosophy
In
Chemistry

Robert B. Moore, Chair
Guoliang Liu
Louis A. Madsen
Michael W. Ellis

September 21, 2020
Blacksburg, Virginia

Keywords: perfluorosulfonate ionomers, Nafion®, PFSA, proton exchange membrane, semicrystalline ionomer, morphology, glass transition temperature, structure-property relationship

Influence of Sidechain Structure and Interactions on the Physical Properties of Perfluorinated Ionomers

Christina Marie Orsino

ABSTRACT

The focus of this dissertation was to investigate the influence of sidechain structure and sidechain content on the morphology and physical properties of perfluorosulfonic acid ionomer (PFSA) membranes. One of the primary objectives was to characterize the thermomechanical relaxations for short sidechain PFSAs developed by 3M and Solvay, as well as a new multi-acid sidechain perfluoroimide acid ionomer (PFIA) from 3M. Partial neutralization experiments played a key role in systematically manipulating the strength of the electrostatic interactions between proton exchange groups on each sidechain, leading to the elucidation of the molecular-level motions associated with multiple thermal relaxations observed by dynamic mechanical analysis (DMA). Particularly, 3M PFSA and Solvay Aquivion lack an observable β-relaxation in the sulfonic acid-form that is observed in the long sidechain PFSA, Nafion. By varying the strength of the physically-crosslinked network through exchanging the proton on the sulfonic acid groups for large counterions, we were able to conclude that the shorter sidechain length and increase in ion content in the 3M PFSA and Solvay Aquivion serves to restrict the mobility of the polymer backbone such that the onset of segmental motions of the main chains is not observed at temperatures below the α-relaxation temperature, where destabilization of the physically crosslinked network occurs. As a complementary technique to DMA for probing the relaxations in PFSAs, we introduced a new pretreatment method for differential scanning calorimetry (DSC) measurements that uncover a thermal transition in H^+-form 3M PFSA, Aquivion, and Nafion membranes. This thermal transition was determined to be of the same molecular origin as the dynamic mechanical α-relaxation temperature in H^+-form PFSAs, and the β-relaxation temperature

in tetrabutylammonium (TBA^+)-form PFSAs. The thermomechanical relaxations in multi-acid sidechain 3M PFIA were also investigated. Interestingly, the additional acidic site on PFIA led to unexpected differences in thermal and mechanical properties, including the appearance of a distinct glass transition temperature otherwise not seen in PFSA ionomers. We utilized small-angle X-ray scattering (SAXS) studies to probe the differences in aggregate structure between the PFIA and PFSA membranes in order to uncover the morphological origin of the anomalous thermomechanical behavior in PFIA membranes. Larger aggregate structures for PFIA, compared to PFSA, incorporate intervening fluorocarbon chains within the aggregate, resulting in increased spacing between ions that reduce the collective electrostatic interactions between ions such that the onset of chain mobility occurs at lower temperatures than the α-relaxation for PFSA. The SAXS profiles of PFSAs showed two scattering features resulting from scattering between crystalline domains and ionic domains distributed throughout the polymer matrix. In order to fit the "ionomer peak" to models used for the PFIA and PFSA aggregate structure determination, we presented a method of varying the electron density of the ionic domains by using different alkali metal counterions as a tool to make the intercrystalline feature indistinguishable. This allows for isolation of the ionomer peak for better fits to scattering models without any interference from the intercrystalline peak. Lastly, an investigation of annealing PFSAs of different sidechain structures in the tetramethylammonium (TMA^+) counterion form above their α-relaxation showed a profound crystalline-like ordering of the TMA^+ counterions within the ionic domains. This ordering is maintained after reacidification and leads to improved proton conductivity, which indicates that this method can be used as a simple processing method for obtaining improved morphologies in proton exchange membranes for fuel cell applications.

Influence of Sidechain Structure and Interactions on the Physical Properties of Perfluorinated Ionomers

Christina Marie Orsino

GENERAL AUDIENCE ABSTRACT

Hydrogen fuel cells offer an environmentally friendly, high efficiency method for powering vehicles, buildings, and portable electronic devices. At the center of a hydrogen fuel cell is a polymer membrane that contains ionic functionalities, which conduct hydrogen ions (protons) from the anode to the cathode while preventing conduction of electrons. The electrons travel through an external circuit to produce electricity, while the protons travel through the polymer membrane and meet with oxygen on the other side to produce water, the only byproduct of a hydrogen fuel cell. The efficiency of this process relies on the ability of the polymer membrane to conduct protons, and the lifetime of a fuel cell depends on the mechanical stability of this membrane. Perfluorosulfonic acid ionomers are good candidates for use as polymer membranes in hydrogen fuel cells due to their Teflon backbone that provides mechanical stability and their sulfonic acid functionalities that form channels for proton conduction. In this work, we probe the structure-property relationships of different perfluorosulfonic acid ionomers for use as fuel cell membranes. We focus on thermal analysis techniques to develop a fundamental understanding of the effect of chemical structure and sulfonic acid content on the temperature-induced mobility of the polymer chains in these ionomers. This mobility at elevated temperatures can be utilized to rearrange the morphological structure of perfluorosulfonic acid ionomer membranes in order to enhance proton conductivity and mechanical integrity.

This dissertation is dedicated to my mom.

You have been my constant support, biggest inspiration, and best friend through it all.

Acknowledgments

I would like to begin by thanking my PhD advisor, Dr. Robert Moore. I am incredibly grateful to have stumbled into your group, inspired by your enthusiasm during your symposium presentation to the incoming class of chemistry graduate students in 2015. You have guided me through the last five years with incredible ease and always recognized when I needed some extra support. I am proud to have spent my time at Virginia Tech working in a field in which you are well-known and highly respected. I truly feel that I have learned from the best. I have always, and will continue to, spread the word about what an incredible research advisor and mentor you are.

I would also like to thank my committee members: Dr. Guoliang (Greg) Liu, Dr. Louis A. Madsen, Dr. Michael W. Ellis, Dr. Johan Foster (former committee member), and Dr. Judy Riffle (former committee member) for their guidance and discussions. Thank you to the Chemistry Department Graduate Student Coordinator, Joli Huynh, and Graduate Program Director, Dr. John Morris, for answering all of my frantic emails and guiding me along in the PhD program successfully. I'm proud to have been a part of such a successful chemistry graduate program that runs so efficiently thanks to all of your efforts. Thank you to the Chemistry Department NMR staff, specifically Mr. Ken Knott for your time, assistance, and contributions to (our attempt at) running solid-state NMR experiments for this dissertation.

My graduate school career and this dissertation would not have been possible without my collaborations with the incredibly talented scientists at 3M. I'd like to acknowledge Dr. Mike Yandrasits and Matthew Lindell of the 3M Corporate Research Lab for your invaluable feedback and patience during my first couple of years as a graduate student working on the PFIA project. I learned and grew so much from our monthly discussions. I would also like to thank Dr. Denis Duchesne, Dr. Lisa Chen, and Dr. Gregg Dahlke of the 3M Advanced Materials Division. You

three have made monthly “industry updates” entertaining but meaningful. I cannot thank you enough for inviting me into your group for a summer internship, during which time I completed work for this dissertation and gained invaluable industry experience.

I must acknowledge the lifelong friendships I formed during my time here at Virginia Tech. First and foremost, thank you to my desk-mate of four years, Dr. Samantha Talley for being a person that I could talk to about all things SAXS- and cat-related. Your guidance and friendship meant so much to me during your time in our group, and you have continued to be a wonderful support system for me even after the completion of your PhD. My first few years in graduate school would not have been the same without Dr. Lindsey Anderson, Dr. Kristen Felice, and Dr. Lin Ju, who were wonderful colleagues and friends to me. Special thanks to Lindsey Anderson who introduced me to so many new friends, convinced me to join an intramural softball team, and invited me to move in with her into the “fun house” where we spent many weekends cooking out with our friends. I am so thankful for our friendship.

I would also like to thank former and current members of the Moore Group including Dr. Gregory Fahs, Melissa Novy, Glenn Spiering, Garrett Godshall, Zahra Mansouri, Michelle Pomatto, and Emily Plunkett who were a pleasure to work alongside and made graduate school fun. I cannot say enough good words about all of my fellow Moore Group members. You are all incredible scientists and I look forward to following along with your successes in the future. Thanks to Samantha Scannelli, Kearsley Dillon, and Ryan Carrazzone for your friendship and all of the fun times that we had throughout my last few years in grad school. To Chad Powell, who has been my biggest support system, the synthetic chemist to my physical chemist, and my best friend: thank you for everything. I can achieve anything with you by my side.

I express my deepest appreciation to my family, specifically my mom (Mary Connelly), dad (Robert Orsino), brother (Anthony Orsino), Grandpa Orsino, and Grandma Connelly. Thank you to my mom, who I have always looked up to as a smart, successful, and driven woman. She has been my biggest support and the first person that I call for advice, especially during my time in grad school. I would like to thank my dad for teaching me to never give up and always beaming with pride at my accomplishments. Both of my parents played such a huge role in my life and I owe so much of my success to them. Thank you to my brother and my grandparents for being my biggest cheerleaders and always expressing interest in my work. Lastly, I have to thank my group of close friends from home and from college who have been so supportive of my graduate school endeavors (and who came to visit me in Blacksburg several times over the last five years). I have no doubt that I would not be here without the support of my friends and family who have been cheering me on along the way.

Attributions

Professor Robert B. Moore – Research Advisor

Professor of Chemistry at Virginia Tech

Dr. Denis Duchesne – Research Scientist in the Advanced Materials Division at 3M

Collaborator on Chapters 3, 5, and Appendix A.

Dr. Gregg Dahlke – Research Scientist in the Advanced Materials Division at 3M

Collaborator on Chapters 3, 5, and Appendix A.

Dr. Lisa Chen – Research Scientist in the Advanced Materials Division at 3M

Collaborator on Chapters 3, 5, and Appendix A.

Dr. Michael Yandrasits – Research Scientist in the Corporate Research Lab at 3M

Collaborator on Chapters 4 and 7.

Dr. Steven Hamrock – Research Scientist in the Corporate Research Lab at 3M

Collaborator on Chapters 4 and 7.

Matthew Lindell – Chemist in the Corporate Research Lab at 3M

Collaborator on Chapters 4 and 7.

Melissa Novy – Moore Group member

Contributed to Chapter 4 by fitting the SAXS data to the modified hard cylinder model.

Glenn Spiering – Moore Group member

Contributed to Chapter 6 by assisting with the understanding of the SAXS data and scattering invariant calculations.

Dr. Gregory Fahs – Former Moore Group member

Wrote Mathematica code for the 1-D Correlation Function and Kinning Thomas Models used in Chapters 4 and 6.

Robert Smith – Former Moore Group undergraduate student

Contributed to Chapter 4 by performing partial neutralization of 3M PFIA and 3M PFSA membranes with Na^+ counterions.

Dr. Mingqiang Zhang – Former Moore Group Member

Contributed to Chapter 6 by laying the groundwork for the contrast variation phenomena observed in PFSA membranes.

Dr. Hang Ruang – Research Scientist at Nanosonic, Inc.

Collaborator on Appendix B.

Dr. Yuhong (Echo) Kang – Research Scientist at Nanosonic, Inc.

Collaborator on Appendix B.

Table of Contents

List of Figures

List of Tables

List of Abbreviations

AFM	Atomic Force Microscopy
APS	Advanced Photon Source
ATR	Attenuated Total Reflectance
CLTE	Coefficient of Linear Thermal Expansion
CSV	Cathodic Stripping Voltammetry
DES	Dielectric Spectroscopy
DLS	Dynamic Light Scattering
DMA	Dynamic Mechanical Analysis
DMFC	Direct Methanol Fuel Cell
DMSO	Dimethyl Sulfoxide
DPSV	Differential Pulse Stripping Voltammetry
DOE	Department of Energy
DPD	Dissipative Particle Dynamics
DSC	Differential Scanning Calorimetry
DVS	Dynamic Vapor Sorption
ECF	Electrochemical Fluorination
EW	Equivalent Weight
FTIR	Fourier Transform Infrared Spectroscopy
FWHM	Full Width at Half Maximum
GCE	Glassy Carbon Electrode
HOR	Hydrogen Oxidation Reaction
IEC	Ion Exchange Capacity
LSC	Long Sidechain
LSM	Local Segmental Motion
MD	Molecular Dynamics
MEA	Membrane Electrode Assembly
MHC	Modified Hard Cylinder
MTTMA	Modulated Temperature Thermomechanical Analysis
MW	Molecular Weight
NMR	Nuclear Magnetic Resonance

NN	1-Nitroso-2-Naphthol
OCV	Open Circuit Voltage
ORR	Oxygen Reduction Reaction
PEG	Proton Exchange Groups
PEM	Proton Exchange Membrane
PEMFC	Proton Exchange Membrane Fuel Cell
PFIA	Perfluoroimide Acid
PFICE	Perlfluoro Ionene Chain Extended Ionomer
PFSA	Perfluorosulfonic Acid
PFSF	Perfluorosulfonyl Fluoride
PS	Polystyrene
PTFE	Polytetrafluoroethylene
Q	Invariant
QENS	Quasi Elastic Neutron Scattering
RH	Relative Humidity
SANS	Small-Angle Neutron Scattering
SAXS	Small-Angle X-Ray Scattering
SLD	Scattering Length Density
SSC	Short Sidechain
TBA^+	Tetrabutylammonium counterion
TEA^+	Tetraethylammonium counterion
TEM	Transmission Electron Microscopy
TFE	Tetrafluoroethylene
TFSI	Bis(trifluoromethanesulfonyl)imide
TGA	Thermogravimetric Analysis
TMA	Thermomechanical Analysis
TMA^+	Tetramethylammonium counterion
USAXS	Ultra-Small-Angle X-Ray Scattering
VT	Variable Temperature
WAXD	Wide-Angle X-Ray Diffraction
WAXS	Wide-Angle X-Ray Scattering

Chapter 1.
Perfluorinated Ionomers: Development, Morphology, and Processing

1.1 Introduction

Perfluorosulfonic acid ionomers (PFSAs) are a group of semicrystalline random copolymers consisting of a polytetrafluoroethylene (PTFE) backbone and perfluoroether sidechains of various lengths containing sulfonic acid end groups.[1] These ionomers are most well-known for their chemical stability and physical properties due to their phase-separated morphology that results from the interactions between the backbone and side chains of the polymer. Dissimilarity between the polar sulfonic acid-containing sidechains and nonpolar backbone lead to phase separation on the nanometer scale, which is further enhanced with the introduction of water. This complex, phase-separated morphology in PFSAs gives rise to remarkable proton conductivity and chemical properties.[2] Specifically, PFSAs act as permselective membranes that allow for the transport of positively charged ions while rejecting the passage of anions. These desired properties, however, are the result of delicate balance between the polar sidechains that drive proton conductivity and the PTFE backbone that provides mechanical stability.

The first PFSA was developed by DuPont in the 1960s under the tradename Nafion®.[1] Nafion was originally developed as a separator membrane for the chlor-alkali cell industry due to its high permselectivity (e.g., ability to discriminate between cations and anions) but was adapted as a proton exchange membrane in hydrogen fuel cells for energy generation.[3] Now a product of Chemours, it has now become the most extensively studied material for use in fuel cell applications, and is widely recognized as the benchmark membrane in the fuel cell field.[1] A second PFSA with a shorter sidechain structure was developed by Dow Chemical in the 1980s,[4,5] but has

since been adopted by Solvay Specialty Polymers under the tradename Hyflon Ion®, more recently renamed as Aquivion®.[6] Since its development, many studies have focused on the difference in properties between the benchmark Nafion membrane, and the new short sidechain (SSC) PFSA membranes. Most recently, 3M Company developed their version of the PFSA structure, called 3M PFSA, that has an intermediate sidechain length between Nafion and SSC.[7] The structures for these three common PFSAs are shown in **Figure 1-1**, where the only difference between them is the structure/length of the functional sidechain.

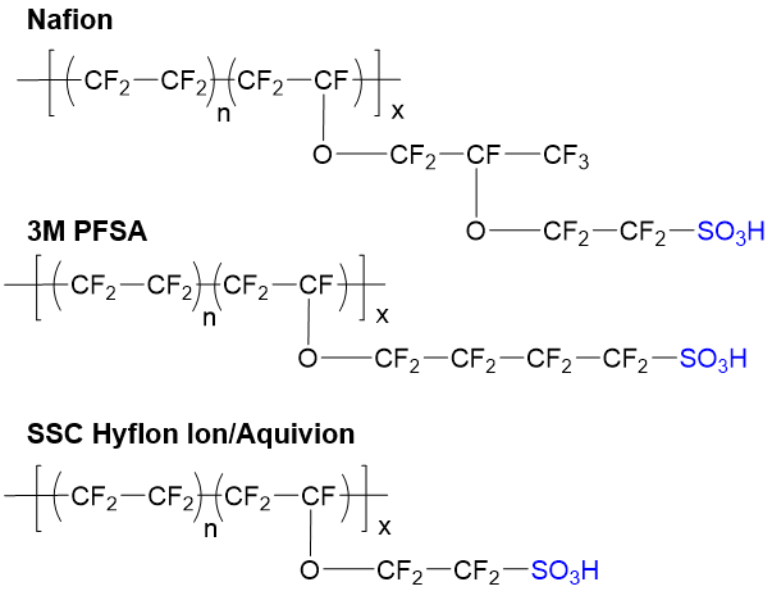

Figure 1-1. Chemical structures of the three commonly used PFSAs including Nafion, 3M PFSA, and short sidechain (SSC) Aquivion (formerly called Hyflon Ion).

1.1.1 Equivalent Weight and Ion Exchange Capacity

PFSAs are most commonly identified by their side chain length and their equivalent weight.[8] Equivalent weight (EW) is defined as the grams of polymer per equivalent of proton exchange groups (PEG) and is inversely related to the ion exchange capacity (IEC). The equivalent

weight is also related to the number of repeat units in the main chain and the molecular weight of the side chains. The relationship between different EW perfluorinated ionomers can be understood by the following equation:

$$EW = \frac{g\ polymer}{equivalent\ PEG} = \frac{1000}{IEC} = 100n + MW_{side\ chain} \quad (1)$$

Where *n* is the number of TFE units in the backbone and PEG is the number of proton exchange groups. Due to these relationships, the side chain length and number of TFE units between sidechains control the EW and chemical structure of the ionomer.

1.1.2 Applications

PFSAs have been most widely utilized as permselective barriers in chlor-alkali cells[9-13] and fuel cells,[14-19] but have also found use in applications including batteries,[20,21] actuators,[22-24] solar cell electrolytes,[25] solid acid catalysis,[26] and electrochemistry.[27-30] Their excellent chemical stability and ion transport properties make them ideal for use as a permselective membrane separator in chlor-alkali cells.[11] Chlor-alkali cells are used in the electrolysis of sodium chloride solutions to produce sodium hydroxide and chlorine. In this application, PFSAs are used as the separator between half cells containing water and aqueous sodium chloride.[8] Chloride ions from the sodium chloride brine in the first chamber are oxidized at the anode to generate chlorine gas. At the cathode in the second chamber, water is reduced to hydrogen gas and hydroxide ions. The PFSA membrane separating the two chambers allows the transfer of sodium ions between chambers while preventing any anionic species, such as hydroxide or chloride, from passing through. The sodium ions formed in the first chamber react with the hydroxide ions formed in the second chamber to produce the final product, sodium hydroxide.

While PFSAs were originally developed for use in chlor-alkali cells, an abundance of research has been aimed at use as a proton exchange membrane (PEM) in fuel cell applications. Proton exchange membrane fuel cells (PEMFCs) work by introducing hydrogen gas on one side of a PEM and oxygen gas on the other (**Figure 1-2**). Within catalyzed layers of a membrane electrode assembly (MEA), hydrogen molecules are split into protons and electrons on the anode side and the PFSA membrane facilitates the transport of protons through to the cathode. Oxygen reacts with the protons on the cathode side to create water, the only byproduct of these fuel cells. Electrons generated through this reaction travel through electrically-conductive electrodes and current collectors to the outside of the circuit where they do work.[14]

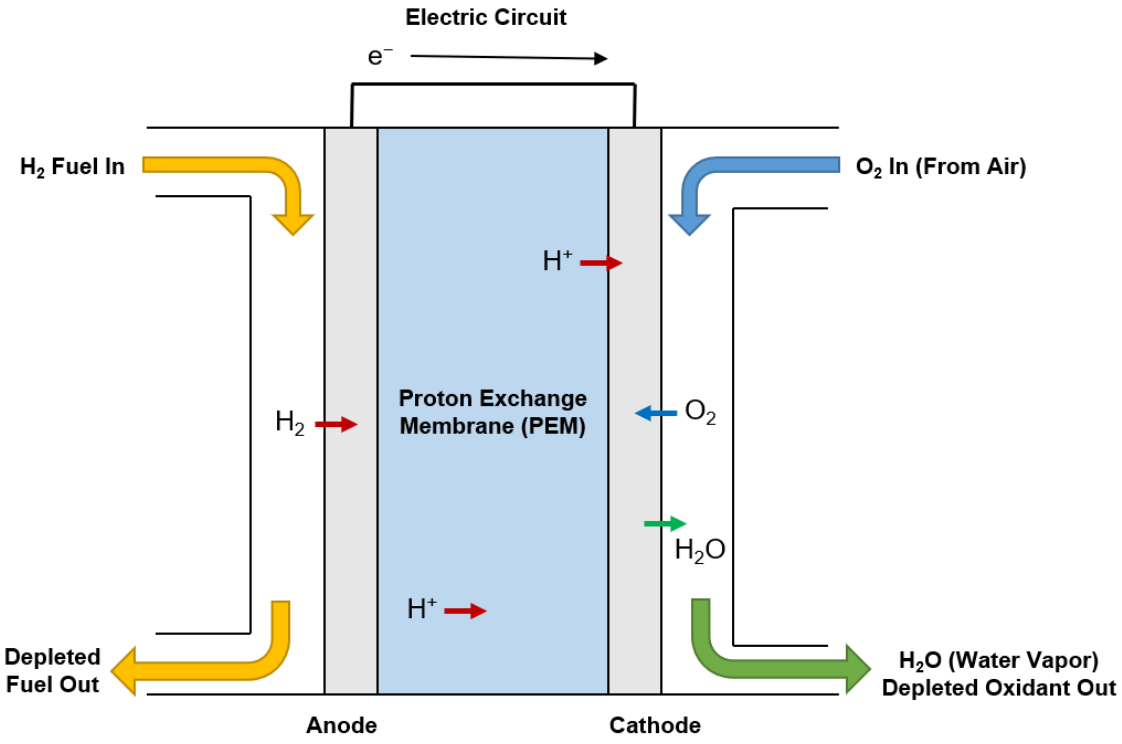

Figure 1-2. Schematic of a proton exchange membrane fuel cell.

The demanding operations of a fuel cell system require a membrane that has good proton conductivity as well as the capability to withstand stresses encountered within the fuel cell. PEMs must have high proton conductivity to maximize cell efficiency and be electrically insulated to prevent shortages.[16] These membranes also function as a gas barrier requiring that they have good mechanical properties and low permeability to oxygen and hydrogen gases. PEMs must be robust enough to withstand high temperatures, levels of humidity that cause swelling of the membrane and can lead to pinhole tears, acidic environments, and have good chemical stability toward peroxides produced during operation.[19] In addition to these hydrogen-oxygen fuel cells, PEMs are also utilized in direct methanol fuel cells (DMFCs) using a methanol/water mixture at the anode instead of hydrogen gas.

The automotive industry has spent between 6 to 10 billion dollars on research and development of fuel cell vehicles and have produced over 500 prototypes.[16] Currently, there are three fuel cell vehicles on the market: Honda Clarity, Toyota Mirai, and Hyundai Nexo. These vehicles are only available for purchase, however, at locations where the infrastructure is in place for hydrogen fueling stations (e.g., California and Japan). These vehicles offer a driving range of close to 400 miles before refueling is required with some of the new 2021 models boasting driving ranges slightly above 400 miles. In comparison, battery vehicles generally have a driving range of between 200 and 300 miles. Refueling also only takes about three to five minutes in a fuel cell vehicle compared to about eight hours to completely charge an average battery vehicle. The Department of Energy (DOE) has a specific Hydrogen and Fuel Cells Program with a mission to reduce greenhouse gas emissions, use of petroleum, and air pollution by advancing fuel cell technology and enabling the commercialization of fuel cells.[31] The DOE sets technical targets for MEAs, membranes, and catalysts used in fuel cell technologies that are updated every five years.

Some of the DOE targets for membranes in 2020 consist of area specific proton resistances of 0.02 Ωcm^2 at 80 °C and 0.03 Ωcm^2 at 30 °C, a maximum operating temperature of 120 °C, maximum hydrogen and oxygen crossover of 2 mA/cm^2, and chemical and mechanical durability over a minimum of 20,000 cycles, all while maintaining a cost of 20$/$m^2$.[32] While commercialization of fuel cells for the automotive industry is on the horizon, much research must be done to improve durability, performance, system design, and cost before the widespread use of these systems.[33]

1.2 Morphology of Perfluorinated Ionomers

The chemical and physical properties of PFSAs are governed by their phase-separated morphology. In general, ionomers are known to phase separate into hydrophilic and hydrophobic phases.[34] The hydrophilic domains are established from the aggregation of ions, while the hydrophobic domain is developed from the nonpolar backbone. Specifically, in perfluorinated ionomers the sidechains with pendant ionic groups form inter-connected aggregates that allow the transport of protons and water, while the PTFE backbone (and potential crystallization therefrom) forms hydrophobic domains that provide mechanical stability.[1]

1.2.1 General Morphology

The presence of a crystallizable backbone in ionomers allows for the development of crystalline regions that increase mechanical properties of the membrane. In PFSAs, the only way to increase the IEC is by adding additional functional sidechains to the copolymer, which decreases degree and rate of crystallization in ionomers due to the addition of noncrystallizable groups (defects) into a crystallizable backbone.[35,36] Higher EW PFSAs (lower IEC) contain longer segments of PTFE backbone between each ionic sidechain. This leads to longer crystallizable

segments and therefore higher degrees of crystallinity and rates of crystallinity in higher EW PFSAs as determined by SAXS[37] and DSC[38] studies. These runs of tetrafluoroethylene (TFE) are able to pack into crystalline domains having unit cell dimensions virtually identical to that of pure PTFE.[39] The overall degree of crystallinity for PFSAs is generally less than 10 wt % for 1100 EW Nafion®,[37] but can reach up to ca. 17 wt % in a 1000 EW 3M PFSA. Compared to pure PTFE (degree of crystallinity of ca. 55-75%),[40,41] PFSAs contain lower crystallinity due to the incorporation of sidechains and ionic groups that disrupt crystallizability of the PTFE backbone. This complicated, phase-separated morphology of crystalline and ionic domains in PFSAs remains the focus of many active investigations with the common goal of establishing a connection between molecular and morphological structure and resulting transport properties. Having a fundamental understanding of the link between structure, morphology, processing, and properties is necessary to guide the synthesis of next-generation ionomers.

1.2.2 History of Morphological Models for Ionomers

The foundation of morphological models of perfluorinated ionomers begins with early research in the 1970s and 80s on hydrocarbon ionomers including polyethylene- and polystyrene-based ionomers.[1,42] The concept of ion aggregation was established but the exact morphological analysis was widely debated in the literature. Most models of ionomers are based off of scattering profiles that only show very limited information allowing for guesswork and variation between the exact morphology of these membranes.[1] Much of the debate comes from the complex structure of these ionomers that can organize into ionic and crystalline domains with appreciable differences in dimensions. Many researchers attempt to match experimental scattering data with a model that can represent most of what is seen experimentally. Some of the proposed models can account for many experimental findings with perfluorinated ionomer membranes, such as permselectivity and

two-phase behavior, but most of the proposed models are lacking the ability to corroborate all of the properties of PFSAs.[8] In order to properly address the morphology of PFSAs, it is important to understand the previous models and their strengths and shortcomings.

1.2.2.1 Hydrocarbon-Based Ionomer Models

Morphological models of hydrocarbon-based random ionomers, usually in an alkali metal salt-form, were the first to be proposed and provided a basis for the PFSA morphological models to come.[43-45] Around the 1980s, significant work was being done to characterize the morphology of random ionomers in order to explain their unique physical properties. In specific, two-phase behavior was observed in ionomers above a certain ion content and there was a lack of a morphological explanation for this behavior.

The first qualitative model for hydrocarbon-based ionomers came from Bonotto and Bonner in 1968, based on an ethylene acrylic acid copolymer system.[44] In these semicrystalline ionomers, the authors observed shorter crystalline segments by FTIR, thermal analysis, and X-ray diffraction with greater degrees of ionization. The authors proposed that during crystallization, the polar groups are rejected from the crystallites, forming morphologically "blocky" domains containing ionic groups. Within these ionic domains, the electrostatic interactions act as physical crosslinks, analogous to chemical crosslinking, leading to increased mechanical stability over a larger temperature range with increasing ion content. Bonotto and Bonner also proposed the possibility that two ion pairs may exist within the same "amorphous pocket", likely to occur only at high ion contents and low degrees of crystallinity.

In the same year, Longworth and Vaughan published a model also based on an ethylene-acrylic acid copolymer.[45] The authors observed a peak in the X-ray diffraction data of the ionomers at a

scattering angle of 4° 2θ, corresponding to a characteristic distance of 20 Å, that persisted at temperatures well past the melting temperature of the ionomer. They attributed this peak to the ions, suggesting that the ions are separated into a separate phase with some periodicity between the ions. Additional electron microscopy data showed the presence of spherulites that exist in both the nonionic polyethylene and the ethylene-acrylic acid copolymer. Dynamic mechanical analysis showed that the ionomer had a glass transition temperature similar to branched low-density polyethylene, indicating that the polar ionic groups exist in the interlamellar phase of the ionomer. Based on these three experimental results, a three-phase model (shown in **Figure 1-3**), was proposed where the crystallites exclude the carboxylate groups, which then form clusters of ions about 100 Å in diameter arranged with some periodicity throughout the ionomer. In this model, both the clusters and crystallites are connected by amorphous polymer chains.

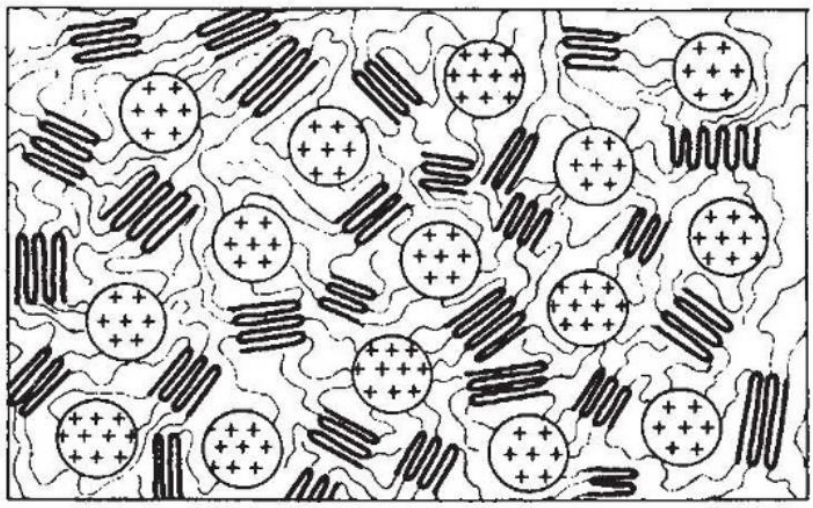

Figure 1-3. Three-phase model for ethylene-co-acrylic acid proposed by Longworth and Vaughan. The folded chains of polyethylene and carboxyl groups are attached by amorphous chains and distributed throughout the polymer matrix. Reprinted with permission from Springer Nature.[45]

In 1970, Eisenberg proposed the concept of "clustering" in ionomers where ions were said to exist as pairs or in higher-order multiplets that can withstand high temperatures.[46] The driving force of ion-pair aggregation is electrostatic interactions that exist over long ranges and are relatively strong in low dielectric constant matrix.[47] While multiplets were considered to be aggregates of ion pairs within close contact and containing no intervening hydrocarbon chains, these multiplets were proposed to cluster together to form larger domains that, due to steric reasons, must include some hydrocarbon material.[48] An experimentally observed second glass transition at high temperatures was attributed to the destabilization of these "clusters" when the elastic forces imposed on the aggregates from the covalently bonded polymer chains overcomes the electrostatic forces within the aggregate. Theoretical models proposed by Forsman,[49] Dreyfus,[50] Datye and Taylor,[51] focused on the competition between electrostatic and elastic forces based on the consideration that chain extension occurs near the aggregates. These models confirmed the findings of Eisenberg. However, Squires, Painter, and Howe later argued that there was no theoretical basis for the chain extension term in random ionomers and developed a new model based heavily on the electrostatic energy term.[48] Regardless, the concept of multiplets and clusters originally proposed by Eisenberg became the starting point for many of the morphological models to follow.

While the original concept of ionic aggregation was based on mechanical data that showed multiphase behavior in hydrocarbon ionomers, morphological models to follow aimed to explain the X-ray scattering data. The first two of such models focused on the "ionic" peak observed in X-ray scattering data of hydrocarbon ionomers. Marx, Caulfield, and Cooper proposed a model that described the ionomer peak as a measure of the average distance between ionic scattering sites and hydrocarbon matrix where small acid aggregates are distributed homogeneously throughout.[43] The

aggregates were said to exist in multiplets that increase from dimers up to septimers as acid content increases in the copolymer. Additionally, a peak at low scattering angles in X-ray scattering data were attributed to crystalline lamellae in the ethylene ionomers. Binsbergen and Kroon similarly attributed the ionomer peak to the electron density difference between ionic clusters and their surroundings, where increasing hydration reduces the electron density of the clusters and causes the ionomer peak to disappear.[52]

Further ionomer models aimed to explain the entire SAXS profile of hydrocarbon-based ionomers including a characteristic upturn at low scattering angles. MacKnight, Taggart, and Stein proposed the presence of ionic clusters of spherical geometry and on the order of 10 to 20 Å in size.[53] This model was termed the "core shell" model where the ionic clusters were suggested to be shielded by hydrocarbon chains and the ionic groups in the surrounding matrix are attracted to the cluster forming a "shell" around the hydrocarbon chains covalently attached to the cluster. Low angle scattering data was attributed to interferences between ionic groups around ionic clusters. An illustration of this core-shell model is displayed in **Figure 1-4b**. Roche and coworkers proposed a similar model to the core shell model but predicted that the ionic clusters are in a lamellar structure as opposed to a spherical geometry, surrounded by a "shell" of hydrocarbon chains.[54] In both of these models, the scattering peak is attributed to *intra*particle scattering as opposed to *inter*particle interference, resulting from the distance between the ionic cluster and the matrix ions (i.e., the width of the shell of hydrocarbon chains). Both of these models may account for the high temperature "cluster" glass transition due to the large size of the clusters proposed.

Yarusso and Cooper developed a modified hard sphere model that better fit the SAXS data at low scattering angles.[55,56] In this model, the ionomer peak was attributed to an interparticle interference between small ionic aggregates that are arranged in a liquidlike order with a "radius

of closest approach" consisting of hydrocarbon chains attached to the aggregate. An illustration of this model is shown in **Figure 1-4a**. Ionic aggregates on the order of 1 nm in diameter are surrounded by a "radius of closest approach" that represents preferred spacing between aggregates. While this model is an idealization based on perfectly spherical aggregates of uniform size, it is one of the most commonly utilized models for estimating size and spacing of aggregates in ionomers.[57] Ding and coworkers proposed a similar model to the Yarusso Cooper modified hard sphere model that focused primarily on the characteristic upturn in scattering at low angles.[58] In this study, the ionomer peak was attributed to scattering of hard spheres with liquidlike order, however, with a nonrandom distribution of lone ion pairs throughout the matrix that accounts for the characteristic upturn at low angles. In both of these models, mechanical properties were not considered.

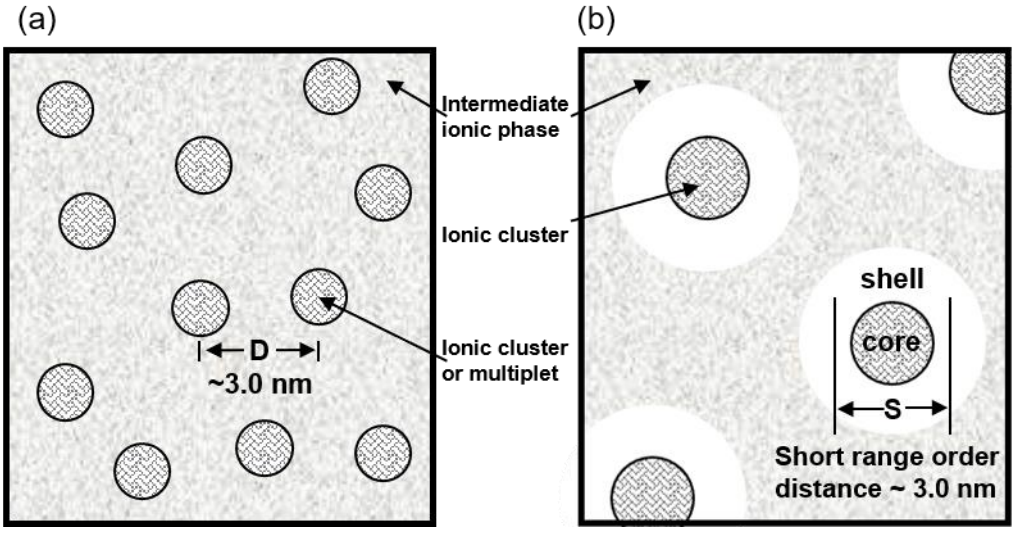

Figure 1-4. Interparticle vs. intraparticle scattering models. (a) the Yarusso Cooper modified hard sphere model depicting interparticle scattering and (b) the MacKnight core-shell model depicting intraparticle scattering. Adapted with permission from American Chemical Society.[1]

In 1990, a new multiplet-cluster model for the morphology of random ionomers was proposed by Eisenberg, Hird, and Moore (referred to as the EHM Model), that incorporated findings from

both dynamic mechanical and X-ray scattering studies.[42] SAXS studies of ionomers with variable-length sidechains showed that the ionomer peak position changes by varying sidechain length, indicating that the ionomer peak arises from interparticle scattering and the distance between scattering centers increases with increasing sidechain length.[59] Additionally, detailed dynamic mechanical studies on polystyrene ionomers indicated that clusters become dominant and perhaps contiguous above 6 mol % ion content.[60] In a series of polystyrene ionomers with varying ion content, the high temperature loss tangent peak associated with the cluster phase increases in both height and area with increasing ion content and even becomes the dominant relaxation at 6 mol % ion content. While the observed characteristic spacing from the ionomer peak of most ionomers have dimensions of less than 50 Å, it was predicted that in order to see a second glass transition temperature, the domains must have minimum dimensions of 50 to 100 Å. Thus, multiplet-cluster model, shown in **Figure 1-5**, was proposed to account for both SAXS and dynamic mechanical findings.

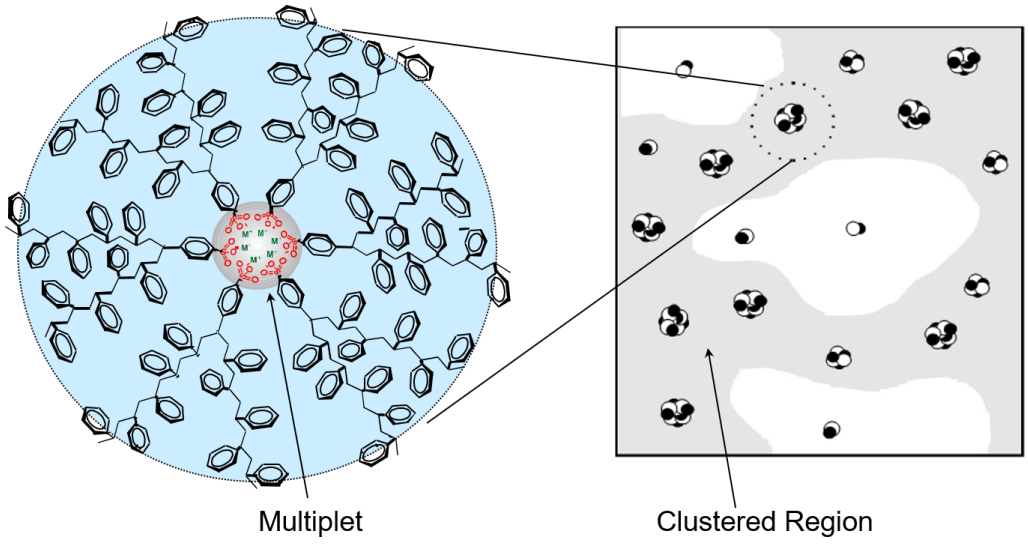

Figure 1-5. EHM multiplet-cluster model proposed by Eisenberg, Hird, and Moore.[42] The multiplet, which consists of only ionic material, anchors the polymer chains to which each ion pair is attached and creates a region of restricted mobility (highlighted in blue) surrounding the

multiplet. With increasing ion contents, the distance between multiplets decreases and overlap between the regions of restricted mobility form large, contiguous "clusters," which have their own glass transition.

In the EHM model, multiplets formed of only ionic material result from electrostatic interactions between ion pairs that are stronger than the elastic forces imposed by the covalently attached polymer chains.[42] Ion pairs within the multiplet anchor the attached chains to that multiplet site and effectively reduce the mobility of the chains within close proximity to the multiplet. This area of restricted polymer chains surrounding the multiplet is referred to as a "region of restricted mobility." In terms of dynamic mechanical data, the region of restricted mobility surrounding a multiplet would be too small to have its own glass transition, but may effectively act as a physical crosslink, increasing the T_g of the polymer. However, as ion content is increased and the distance between multiplets decreased, there is an overlap between regions of restricted mobility that form large, contiguous regions of restricted mobility referred to as a "cluster". The cluster has its own glass transition and exhibits behavior akin to a phase-separated region. This model accounts for the SAXS ionomer peak attributed to characteristic distances between multiplets, and the two-phase behavior observed in dynamic mechanical analysis. In contrast to previous models, this model does not assume a geometry of the clusters. This presence of a region of restricted mobility was further confirmed by Gao, Zhong, and Eisenberg[61] and Vanhoorne and coworkers[62] by probing polymer chain mobility of ionomers with solid state NMR.

A recent review on the morphology and structure-property relationships in random ionomers highlighted the technological importance of both the Yarusso Cooper and the EHM Model to the ionomer field.[57] These two models provided a basis for corroborating the X-ray and mechanical data for amorphous ionomer systems that allowed for more complicated semicrystalline ionomers, including PFSAs, to be better understood.

1.2.2.2 Perfluorinated Ionomer Models

One of the first notable and most long-standing morphological models for Nafion® comes from Gierke and coworkers in the early 1980s.[37,63,64] The standing hydrocarbon-based ionomer models of the time were the core-shell model,[53] a model of spherical clusters on a paracrystalline network,[43] and a lamellar model.[54] Gierke, Munn, and Wilson conducted a thorough SAXS study on Nafion in a range of equivalent weights, the unhydrolyzed precursor form, hydrolyzed acid form, and neutralized in the alkali metal sulfate form.[37] In the nonionic sulfonyl fluoride form, two scattering maxima were observed at ca. 0.5° 2θ and 18° 2θ, the second of which was superimposed on top of a broad amorphous halo. These scattering features were observed to increase in intensity with increasing EW and disappear at temperatures near the melting temperature of PTFE. Therefore, these two scattering features were attributed to crystallization of fluorocarbon chains.

In hydrolyzed acid-form Nafion, Gierke, Munn, and Wilson observed an additional scattering feature at 1.6 ° 2θ, corresponding to a Bragg distance of 3-5 nm, that was attributed to ionic clusters within the semicrystalline matrix.[37] It is important to mention here that the definition of clusters within the PFSA literature refers to nanophase separated ionic aggregates as opposed to the aforementioned clusters in the EHM Model, which refer to overlap between regions of restricted mobility.[1] This ionomer peak was shown to shift to lower angles and increase in intensity with increasing water content and decreasing EW (increasing ion content). Based on the early work by Eisenberg that proposed the aggregation of ions into multiplets,[46] and in combination with these experimental results, Gierke, Munn and Wilson proposed that the hydrated morphology of Nafion was best described as spherical clusters in an inverted micellar structure. To account for ion

transport properties, these clusters were suggested to be connected by narrow channels, approximately 1 nm in diameter. A schematic of what is now called the cluster-network model for Nafion is displayed in **Figure 1-6**.

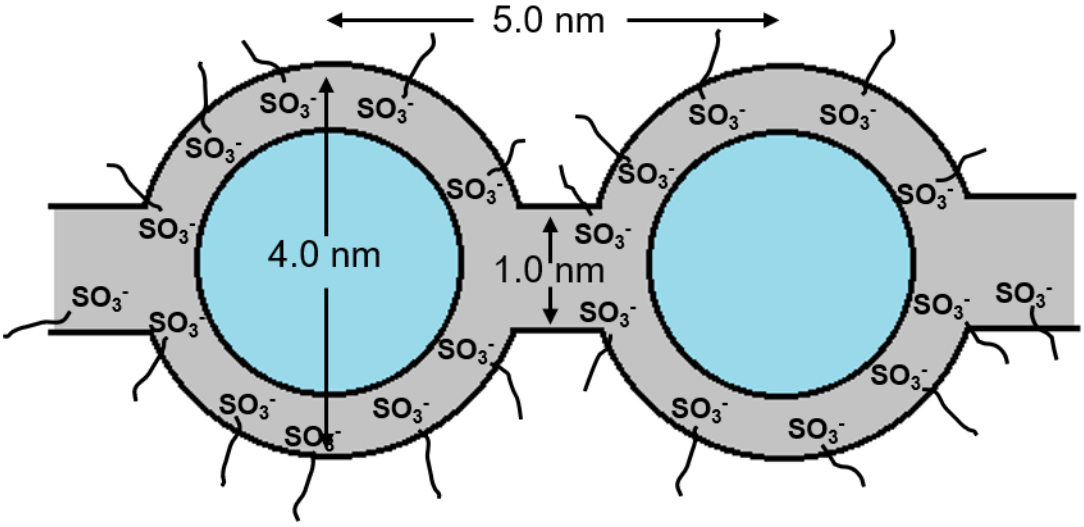

Figure 1-6. Cluster-network model for the morphology of Nafion®. Adapted with permission from Elsevier.[63]

In subsequent studies, Gierke and Hsu utilized the cluster-network model to calculate the cluster size, number of ion pairs per cluster, and number of water molecules per ion pair.[63,64] These values were all shown to increase with increasing water content.[63] The diameter of the cluster and ion pairs per cluster were observed to decrease with increasing EW. Additionally, exchanging the counterion for alkali metal counterions of different sizes showed a decrease in cluster size and number of water molecules per ion pair with increasing counterion size, while number of ion pairs per cluster increased. This was attributed to the binding affinity between larger counterions and the sulfonate groups, binding more tightly and reducing the hydrophilicity of the clusters.

In 1981, Yeager and Steck proposed a three-phase model for the morphology of Nafion based on counterion and water diffusion properties.[65] The authors of this model combined their diffusion

studies with two spectroscopic studies: one investigating luminesce quenching of large Ru(2,2'-bipyridine)$_3^{2+}$ counterions in Nafion conducted by Lee and Meisel,[66] and an infrared study of absorbed water in Na^+-form Nafion conducted by Falk.[67] An illustration of the three-phase model is shown in **Figure 1-7**. In this model, Region A is composed of fluorocarbon backbone and includes any of the crystallinity in the polymer. Region C consists of ionic clusters including ionic sulfonate sites, majority of the absorbed water, and some counterions. Region B is the interfacial region between Regions A and C that is considered to be of relatively large fractional void volume containing sidechain material, a small amount of water, some ionic sulfonates that were not incorporated into the cluster, and a fraction of counterions.

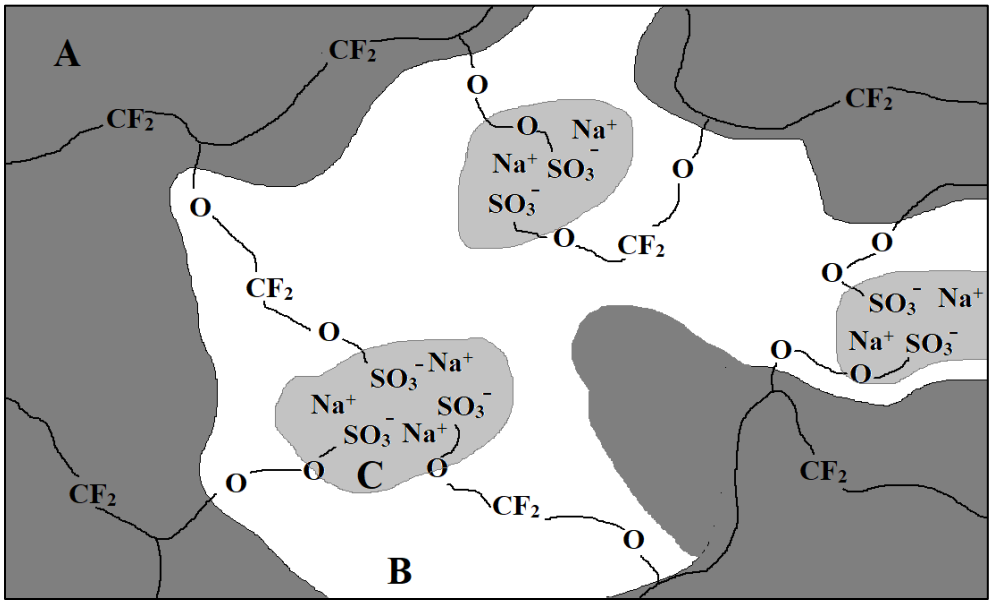

Figure 1-7. Three-phase model proposed by Yeager and Steck in 1981. Region A consists of fluorocarbon backbone and any crystallites. Region C is composed of sulfonate groups, some counterions and majority of absorbed water and Region B is the interfacial region between the two. Adapted with permission from The Electrochemical Society.[66]

Yeager and Steck utilized this proposed three-phase model to accurately depict the differences in diffusion coefficients between Na^+ and Cs^+ counterions by suggesting that the two counterions

are located within different phases in the model. For example, the authors suggest that relative proportions of counterions in Regions B and C depend on their size and charge density. Low charge density counterions such as Ru(2,2'-bipyridine)$_3^{2+}$ and Cs^+ are contained mostly in Region B, while large charge density and hydration energy ions such as Na^+ are found in the more aqueous phase of Region C. Both Regions B and C contribute to the overall transport diffusion properties of the membrane, but Region C is responsible for the peaks observed by SAXS and SANS and Region B provides a transport pathway among the clusters.

Around the same time, Roche and coworkers investigated the morphology of Nafion based on SAXS and SANS studies on membranes in the acid and neutralized forms in a range of water contents.[54,68,69] As-received Nafion was described as having three contrast regions consisting of the crystalline phase, ionic clusters, and inhomogeneous matrix phase. A low angle scattering peak at 0.5 ° 2θ, corresponding to a Bragg distance of 18 nm, that was also observed previously by Gierke and coworkers,[37] disappeared upon quenching to remove crystallinity. Therefore, this peak was attributed to interference between crystalline structures in the membrane. Upon quenching, the scattering feature of the hydrated ionic domains was probed by contrast matching SANS with mixtures of H_2O and D_2O swollen into membranes. Quenched membranes showed only an ionomer peak at 1.2 nm^{-1} and a low-angle scattering upturn. Scattering intensities were found to vary linearly with relative fractions of D_2O and H_2O, characteristic of two-phase behavior. The scattering maximum corresponding to the ionic clusters was observed over a wide range of water concentrations, indicating that a hard-sphere model is not sufficient to describe the scattering maximum because it is present even at very low water contents. Lastly, to account for the observed low-angle scattering upturn, the authors proposed a model of an inhomogeneous distribution of clusters within a fluorocarbon matrix. While this finding agreed with that of Gierke et al., Roche

et al. argued that the cluster-network model was unlikely, due to a lack of evidence of paracrystalline ordering.[68] Instead, it was proposed that the ionomer peak was due to *intra*particle scattering for which the maximum corresponded to characteristic distances in between structural elements within the aggregate. In subsequent SANS experiments, Roche, Pineri, and Duplessix observed that at high water contents, the polymer phase separates into essentially a two-phase system where the majority of water molecules are clustered in one phase and the majority of perfluorinated material are separated into another.[69] At low water contents, deviations from two-phase behavior were observed.

Fujimara and coworkers also conducted studies to assess the previously proposed morphological models.[39,70] The first study focused on the origin of the scattering maxima observed in Nafion ranging from 1100 to 1500 EW in H^+, Na^+, and Cs^+-forms.[70] In agreement with earlier studies, the low angle scattering maximum at 0.07 nm^{-1} was associated with crystallinity in the Nafion membranes. With increasing degree of crystallinity, the low-angle scattering maximum became more distinct, in agreement with observations by Gierke and coworkers,[37] and was thus attributed to the crystalline long period. The higher angle scattering maximum at 0.3 nm^{-1} was attributed to the existence of ionic domains and found to be dependent on the number of sidechains, the temperature, and level of hydration.

In a succeeding paper by Fujimura and coworkers, various standing models for the morphology of Nafion were evaluated to describe the origin of the ionomer peak.[39] In this study, theoretical simulations of the effect of water swelling and deformation on the scattering profiles of Nafion membranes were evaluated on the basis of two long-standing ionomer morphology models: the *inter*particle two-phase model and the *intra*particle core-shell model, both depicted previously in **Figure 1-4**. While computer simulations showed adequate fits of the scattering data

to both models, further investigations on microscopic vs. macroscopic swelling indicated that the core-shell model, proposed by MacKnight,[53] is the most probable morphology as opposed to the two-phase interparticle model, proposed by Yarusso and Cooper.[55] A later study by Miura and Yoshida also supported the core-shell model.[71]

In 1985, Dreyfus and Aldebert presented a local-order model based on scattering with neutrons and X-rays in which the local environment around an ionic aggregate has a tetrahedral symmetry at a distance D from the aggregate.[72,73] This model contained only two adjustable parameters and achieved reasonable fits over a broad scattering range. The authors concluded that the small-angle upturn and the ionomer peak were attributed to the existence and spatial distribution of ionic clusters. Utilizing this model, the number of exchange sites per cluster was calculated to range from 25 to 45 depending on degree of water swelling. While this model provided good fits for the SAXS data, the calculated number of charge sites per cluster was unrealistically large.[1]

In 1986, Kumar and Pineri utilized SAXS and SANS studies to elucidate cluster morphology.[74] The suggested model of noninteracting spheres was based on the lack of explanation for observed scattering and swelling data from the cluster-network model and unconfirmed assumptions made with applying Bragg's law to swelling in the core-shell model. Founded on this noninteracting hard sphere model, the number of exchange sites per cluster was found to decrease with increasing water content, as opposed to observations by Gierke, which was explained by macroscopic swelling increasing the elastic force on the polymer chains and forcing some ion pairs out of the cluster. This model also only showed a moderate decrease in ion pairs per cluster with increasing EW, again in contrast to the cluster-network model.

In the late 1990s and early 2000s, two similar lamellar-type models for the morphology of Nafion were proposed. Litt conducted a reevaluation of the morphology of Nafion, leading to the introduction of a lamellar model illustrated in **Figure 1-8a**.[75] This model was based on the assumption that long crystallizable regions in the ionomer will chain-fold to an average lamellar thickness and stack on top of one another, essentially forming a "micelle" with ionic groups lining the surface and interior consisting of amorphous chains. The amorphous region swells upon hydration, pushing the micelles apart and leading to a shift in the ionomer peak. Haubold and coworkers later presented a variation of this lamellar model, where the structure consisted of a "sandwich" geometry illustrated in **Figure 1-8b**.[76] The outer layers of the sandwich was essentially a shell containing sidechains and ionic groups, while the inner layer of the sandwich was a core containing the swelling solvent. To account for proton conductivity of these membranes, percolation pathways were proposed to form when the structural elements aligned such that the solvent-containing cores form a continuous pathway.

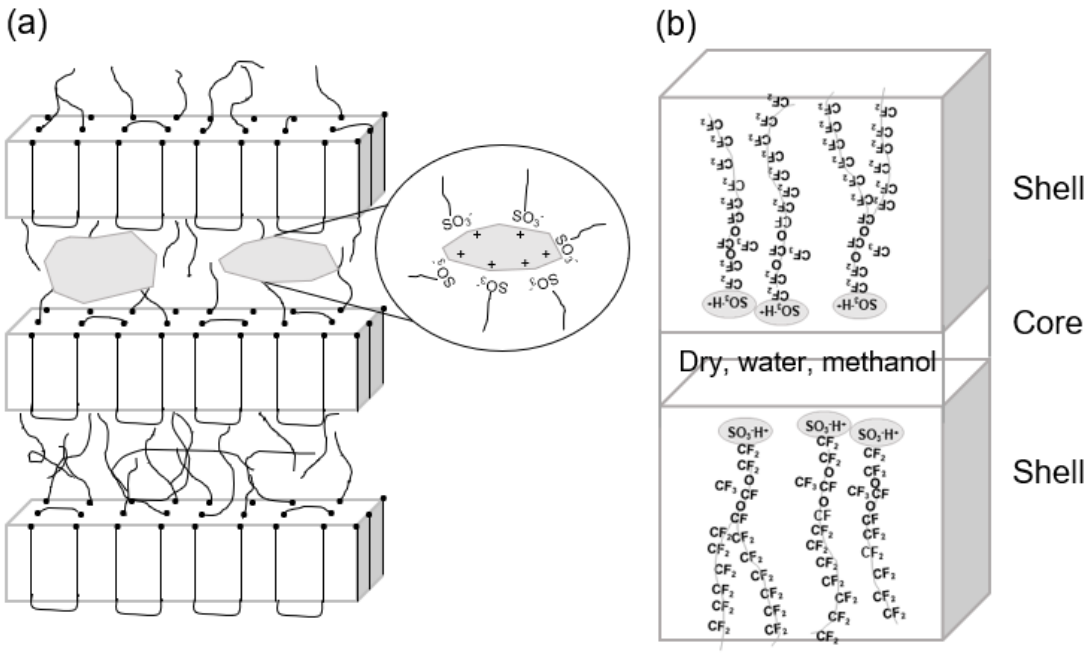

Figure 1-8. Comparison between the (a) lamellar model proposed by Litt,[75] and (b) sandwich model proposed by Haubold[76] for the morphology of Nafion. Adapted with permission from Elsevier.[76]

Utilizing scattering and microscopy techniques, Gebel and coworkers suggested a new structural evolution model that described the morphology of Nafion from dispersion to membrane.[77-79] In this model, the morphology of Nafion in the dry membrane state consists of small spherical ionic aggregates with diameters of ca. 1.5 nm and an average spacing between aggregates of ca. 2.7 nm. As water is added to the membrane, the aggregates begin to swell bringing exchange groups to the surface of the polymer-water interface. Upon hydration to 0.5 volume fraction water, a structural reorganization occurs and percolation pathways are formed within the membrane connecting the water-swollen spherical aggregates. Above 0.5 water volume fraction, inversion occurs such that the morphology is now a network of connected rods dispersed in water. Upon complete dissolution, the morphology is characteristic of a dispersion of isolated rods in solution. An illustration of this structural evolution model is presented in **Figure 1-9**.

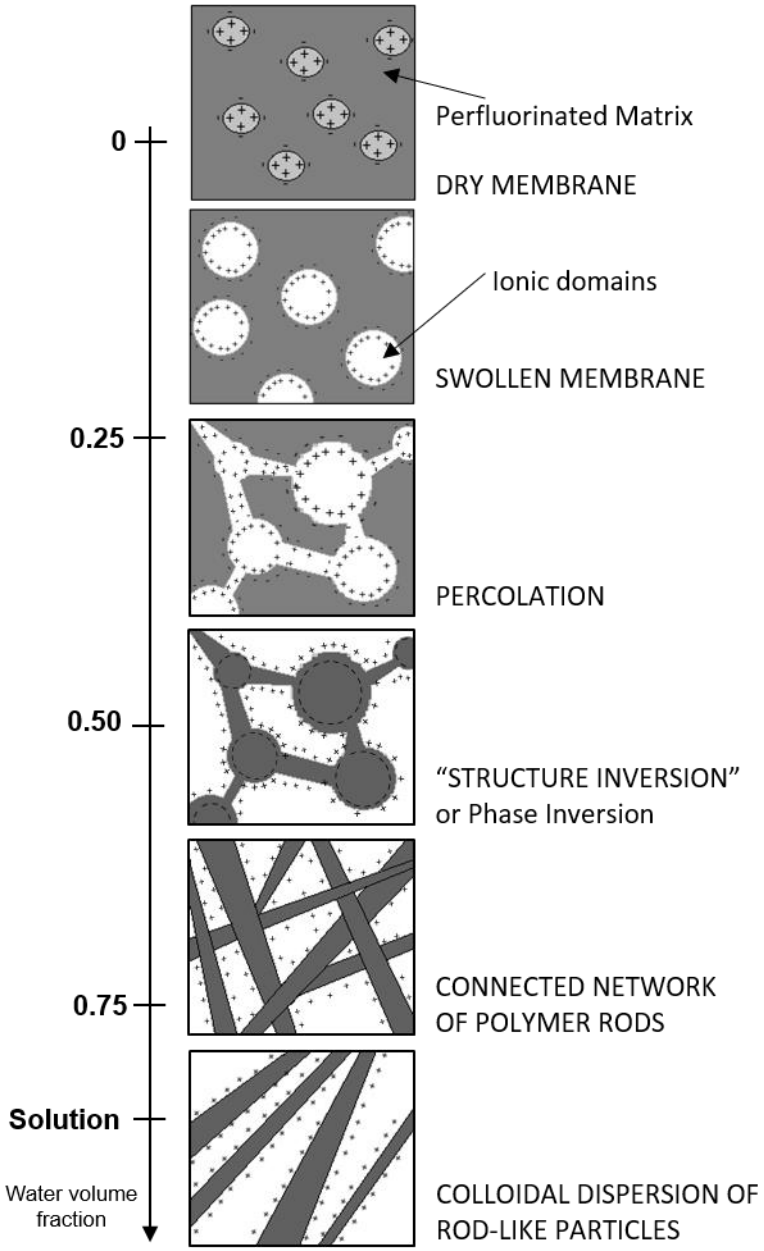

Figure 1-9. Structural evolution model proposed by Gebel et al. shows the evolution of morphology from dry membrane to dispersion. Adapted with permission from Elsevier.[78]

Rollet and coworkers investigated the structure of hydrated Nafion membranes neutralized with tetramethylammonium (TMA^+) counterions by SANS contrast matching with H_2O and D_2O.[80,81] The authors concluded that the TMA^+ counterions are located at the interface between

hydrophilic and hydrophobic domains based on the observation that the ionomer peak intensity varies as a function of scattering angle.[81] Furthermore, analysis of the SANS spectra obtained from contrast variation was conducted by assuming different scattering geometries including spherical or elongated cavities filled with electrolyte solution and spherical or rod-like aggregates of polymer surrounded by electrolyte solution. The SANS data was best fit to a model of polymer aggregates surrounded by solvent, however, the authors noted that it was impossible to distinguish between rod-like or spherical aggregates within this scattering range.

Rubatat, Rollet, Diat, and Gebel conducted a series of studies that led to the proposal of a model of rod-like aggregates for the morphology of Nafion.[82-85] By utilizing ultra-small angle X-ray scattering, they were able to probe the structure of water-swollen Li^+-form Nafion membranes over very large length scales, ranging from 10 to 1000 Å.[85] At ultra-small angles ($q<0.003$ Å^{-1}), Nafion exhibited a strong scattering upturn, which was attributed to large scale electron density inhomogeneities. At intermediate scattering angles, $0.01<q<0.1$ Å^{-1}, a less pronounced feature was observed for the water-swollen membrane, that was attributed to a supralamellar distance in the crystalline phase of the polymer, referred to as the "matrix knee," and becomes more pronounced with less water content. At higher scattering angles, $q>0.1$ Å^{-1}, the main scattering feature can be observed, which corresponds to local ordering between ionic clusters. The authors noted that the average intensity decay of q^{-1} power law at low scattering angles and q^{-4} power law at larger angles. While the q^{-4} power law in the Porod region represents a sharp interface between the scattering particles and the matrix, the q^{-1} power law is usually characteristic of a rod-like particle. Based on these experimental findings, the authors proposed a model of rod-like aggregates with a diameter of ca. 40 Å and a length larger than 1000 Å.

Rubatat, Gebel, and Diat expanded the aforementioned study to include hydrated Nafion membranes with lower water content than the previous studies.[84] Using both microscopy and small angle scattering, they investigated the structure of the ionic aggregates and spatial distribution in solution and solid-states. Scattering of Nafion dispersions show a q^{-4} power law at large angles and a q^{-1} power law in intermediate scattering angles, as observed previously, and attributed to the scattering of rod-like particles. Analysis of the scattering curve showed that a cylindrical form factor fit the data well except at very low scattering angles. Based on these results, the proposed structure of Nafion in dispersion is that of elongated particles consisting of packed hydrophobic backbone chains with pendant sulfonate groups located at the surface. Nafion membranes were then probed utilizing SANS with partially deuterated solvent and TMA^+ counterion. Investigation of the ultra-small angle upturn, associated with a large-scale characteristic length, led to the conclusion that ionic aggregates are elongated and exist in bundles of rod-like particles dispersed within the polymer matrix as illustrated in **Figure 1-10**. This fibrillar structure was further confirmed by a membrane deformation SAXS and SANS study.[82]

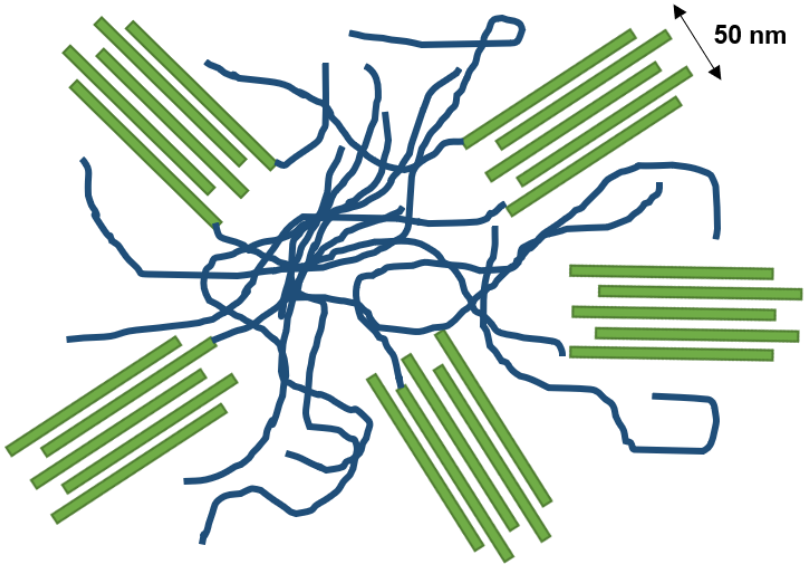

Figure 1-10. Illustration of elongated polymer aggregates proposed by Rubatat et al. Adapted with permission from American Chemical Society.[84]

In 2006, Kim, Glinka, Grot and Grot proposed a new fringed micelle structure for Nafion membranes based on a SANS study of the effects of water vapor sorption.[86] The observed sorption isotherms showed a correlation between the interaggregate distance and water uptake in the membranes. In addition, the authors found that the membrane morphology is dependent on membrane processing (extruded vs. cast), pretreatment (heated at 80 °C vs. as-received) and thickness. An observed SANS scattering power law of q^{-1} within the range of 0.009 and 0.1 $Å^{-1}$, also observed by Rubatat et al.,[83] led the authors to suggest the presence of a locally cylindrical structure. Ultimately, the authors introduce a fringed-micelle structure where hydrated ionic clusters form worm-like channels through the polymer matrix. In this structure, unlike the rod-like model proposed by Rubatat and Gebel, the crystallites are dispersed between the elongated domains as opposed to within them and the characteristic distance between crystallites spans the ionic domains. Despite the authors finding the fringed-micelle structure to be a probable model for

the morphology of Nafion, they do note that there is no physical evidence suggesting the validity of this model compared to a lamellar-type model.

In 2008, Schmidt-Rohr and Chen used a computer algorithm to quantitatively simulate the small angle scattering profile of hydrated Nafion.[87] The authors first attempted to simulate the SAXS profiles of Nafion utilizing some of the standing morphological models of the time. They noted that any model that did not suggest ordering between the ionic domains did not produce an ionomer peak and thus was eliminated as a possible model. The popular Gierke cluster-network model[37] was able to produce an ionomer peak but the simulated scattering curves did not match the experimental data. Other proposed models that were ruled out by this computer simulation method were the polymer bundles in a hydrated matrix,[80,81,83] ribbons made up of bilayers of chains,[85] models with alternating layers of polymer and water,[38,75,76] the wormlike or fringed-micelle model,[86] and a model proposed by Kreuer with a periodic cubic network of cylindrical channels.[88]

Ultimately, Schmidt-Rohr and Chen proposed a model of parallel water channels (inverted micellar structure) to explain the scattering data of oriented and unoriented Nafion films. In this model, the polymer backbone exists on the outside and the ionic groups line the inside of the channels. A cross-section of these channels is illustrated in **Figure 1-11**. The water channels have a diameter ranging from 1.8 to 3.5 nm but this value may vary along the length of the channel. The crystallites are presumed to be elongated and approximately cylindrical in agreement with previous findings by van der Heiden et al.[89] and Kim et al.[86] The parallel water-channel model accounts for the high proton conductivity and water permeability observed in Nafion and compared to previous models, seemed to more accurately describe the changes in SAXS data as a function of crystallinity, membrane thickness, and water content.

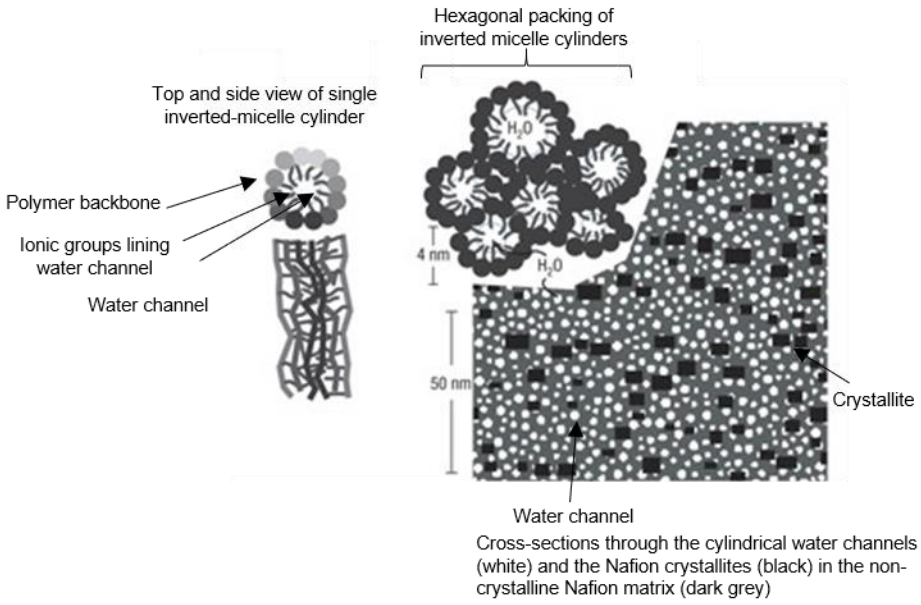

Figure 1-11. Parallel water-channel model proposed by Schmidt-Rohr and Chen. Adapted with permission from Springer Nature.[87]

In 2011, Elliot, Wu, Paddison, and Moore developed a theoretical method to gather model-independent structural information for Nafion utilizing statistical modelling of SAXS data and coarse-grained Dissipative Particle Dynamics (DPD) simulations.[90] These two theoretical methods showed that the ionic clustering in PFSAs is interconnected to but separate from the semicrystalline fluorocarbon backbone. The authors suggest that the fluorocarbon segments and ionic clusters each form a bicontinuous domain where the ionic clusters are embedded within the matrix of fluorocarbon chains as portrayed in **Figure 1-12**. The presented model was consistent with data for both unoriented and mechanically oriented membranes. In comparison with previous Nafion morphological models, this simulation confirmed the proposed network of ionic aggregates from the Gierke cluster-network model,[37] and rejected the extended parallel channels proposed by Schmidt-Rohr and Chen,[91] although it was not a direct match to either model.

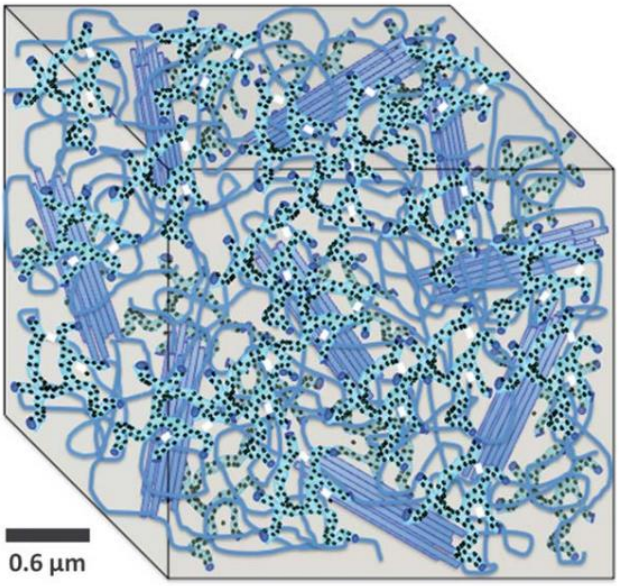

Figure 1-12. Schematic representation of the proposed morphology of hydrated Nafion. A continuous network of 3D channels (light blue) containing ionic clusters (black dots) are embedded in amorphous and crystalline fluorocarbon chains (dark blue). The scale bar represents the distance between ion clusters as observed by SAXS. Reprinted with permission from Royal Society of Chemistry.[90]

The existence of a continuous network of water-filled channels provides a good explanation for the high water-diffusion coefficient in Nafion. It also explains the nonlinear macroscopic swelling behavior by a facile redistribution of sulfonate groups between adjacent ionic aggregates with increasing hydration.

In 2013, Kreuer and Portale published a "critical revision" to the nano-morphology proposed for proton conducting ionomers.[92] In this study, they reexamined the vast amount of published experimental SAXS data for Nafion over a wide range of water fractions utilizing theoretical model simulations to reproduce experimental data. The authors vehemently rejected the Schmidt-Rohr parallel water-channel model,[91] citing a significant error in the experimentally calculated water volume fractions used to propose that model. In an attempt to reproduce the SAXS

data using a parallel water-channel model, it was found that the water contents required to replicate results were two times higher than the water content that was reported by Schmidt-Rohr and Chen. The basis for the parallel cylinder-model was that it was the only model that would fit the data at these reported low water volume fractions, whereas, Kreuer and Portale suggest that multiple models would fit the data at the actual water content in the membranes.

Upon rejecting the validity of the parallel water-channel model, Kreuer and Portale propose a locally flat ribbon-like model consisting of flat and narrow water domains of ca. 1 nm in size. Simulations of semi-disordered stacks of extended sheets were found to fit the experimental data well over a q-range of 1.5 to 5 nm^{-1}. At lower scattering angles, the simulated intensity was observed to have a q^{-2} power law dependency for stacks of sheets, in contrast to the experimentally observed q^{-1} dependency, suggesting that the structures are planar on a local scale only (< 4 nm). The driving force for these flattened hydrophilic domains results from the electrostatics within the highly dissociated ionic phase. Flattened structures allow the positively and negatively charged particles to stabilize each other by participating in ionic cross-links and avoids accumulation of positive charges that would occur in cylindrical structures. An illustration of the distribution of charges between these two types of structures is shown in **Figure 1-13**. While this model fit well to the experimental SAXS data and electrostatic energy theories, it is lacking a correlation between the microstructure and high proton conductivity at low water contents observed in Nafion.

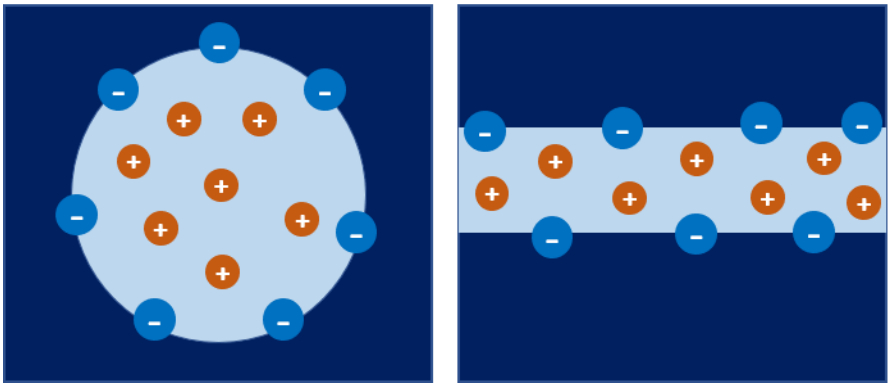

Figure 1-13. Illustration of the distribution of charges in a cylindrical model vs. locally flat ribbon model proposed by Kreuer and Portale. Adapted with permission from John Wiley and Sons.[92]

Feng, Savage and Voth utilized large-scale simulation models of realistic PFSA morphologies to examine the ion solvation and transport properties of these models.[93,94] In their simulation, they used morphologies that best match the scattering data as previously published by other groups, and compared which morphological model is the best fit to the dynamical properties.[94] The models used were a lamellar model to simulate the extreme version of the locally-flat model proposed by Kreuer,[92] rod-like polymer bundles, and a random morphology. Interestingly, upon building the polymer bundle model and allowing the molecular dynamics (MD) simulation to equilibrate, the bundle morphology was observed to immediately flatten into ribbons, much like the proposed locally-flat model. The lamellar model was rejected due to too low of a density and unrealistically fast diffusion properties. While the random model showed some agreement with the experimental data, the bundle model (that immediately flattened into a ribbon-like structure), had the best overall agreement further proposing the presence of a locally-flat morphology.[94]

A recent cryo electron tomography study of hydrated Nafion membranes provided the first 3D views of the nanoscale internal structure using a direct imaging approach.[95] Using advanced

electron-microscopy techniques, the authors observed two distinct morphologies for hydrated and dry Nafion. TEM results of the dry membranes indicate a structure of isolated nanoscale ionic clusters. Upon hydration, the isolated ionic clusters transform into a branched channel-type structure conducive to ion conductivity. A 3D rendering of the hydrophilic channels was constructed based on cryo TEM of frozen, hydrated Nafion membranes and is presented in **Figure 1-14**. This model supports a phase-separated bicontinuous network with domain spacings of ca. 5.1 nm that are in good agreement with SAXS measurements. A simulated SAXS profile based on this model agreed well with experimental results, however, lacking a matrix peak due to the suppression of crystallinity in these cast membranes. Nonetheless, the ability to obtain a 3D structure of hydrated Nafion directly, as opposed to relying on interpretations of broad scattering features, can be useful for refining structural models that provide information on the structure-property relationships of these ionomers.

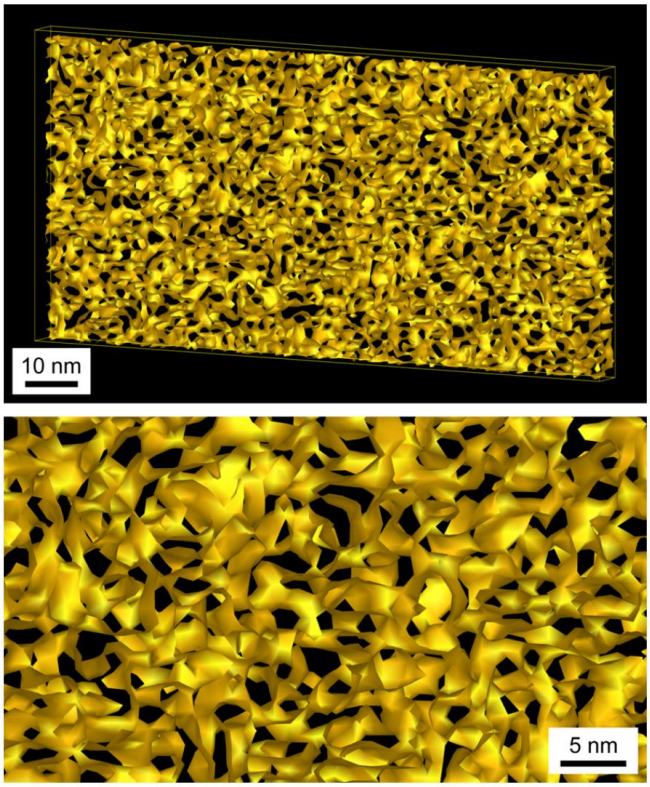

Figure 1-14. 3D reconstruction of the frozen, hydrated Nafion membrane as observed by cryo TEM. Reprinted with permission from American Chemical Society.[95] (https://pubs.acs.org/doi/10.1021/mz500606h)

Establishing an accurate description of the morphology of PFSAs is still a remaining challenge.[96] Based on the proposed models, it is suggested that hydrophilic domains of about 2 to 4 nm in dimension are separated by hydrophobic PTFE matrix of about 2 to 3 nm in dimension, but interconnected by secondary domains of 0.5 to 1 nm. However, these values all depend on a proposed shape of the ionic domains being either spherical or cylindrical, and direct evidence of the interconnected secondary domains is lacking. Nonetheless, these predicted dimensions agree with experimental data from porosimetry and cryoporometry, which predict that the water in hydrated PFSAs exist in domains of 1 to 3 nm in size.[97-100] Throughout the history of proposed PFSA models, the community has begun to gravitate toward either a rod-like or locally-flat

morphology. This morphology is further confirmed by the new direct imaging evidence that demonstrates a locally-flat and highly branched structure of the ionic domains in fully hydrated PFSAs.[95]

1.3 Development of PFSA Sidechain Structures

In PFSAs, equivalent weight (EW) is dictated by the ion content and molecular weight of the functional sidechain. Lower EW values correspond to increased proton conductivity across a range of temperatures and relative humidities.[16,101] However, molecular weight of the sidechain also determines the range of EWs for that polymer. As discussed in Section 1.1.1, EW is directly related to the average number of TFE units between sidechains, *m*, and the molecular weight of the sidechain. Therefore, for a specific EW value, the average number of TFE units between sidechains will be higher for a PFSA with a lower MW sidechain. Increased TFE units between sidechains allows for more crystallizability of the PTFE backbone that provides mechanical integrity to the membrane by reducing the water uptake and swelling that may cause pinholes and tears during the swelling-deswelling environment in a fuel cell.[16] For this reason, several PFSAs with different sidechain structures have been developed over the years to achieve lower EWs while maintaining the crystallizability necessary for good mechanical properties. In this section, the development of these different sidechains and some of their ensuing properties will be discussed.

1.3.1 Nafion Long Sidechain

Nafion® has been the benchmark PFSA since its creation in the late 1960s by Walther Grot of Dupont.[1] It was originally developed as a separator membrane for chlor-alkali cell industry but was later adapted for use as a proton exchange membrane in hydrogen fuel cells for portable energy

generation.[3] It has now become the most extensively studied material for use in PEMFC applications, and is widely recognized as the benchmark membrane in the PEMFC field.[1] Typical Nafion® membranes have an EW ranging from 1000 to 1100 g/eq (grams of polymer/moles equivalent proton exchange groups) and a chemical structure containing the typical PTFE backbone with "long" perfluoroether side chains containing pendant sulfonate groups.[1] Similar "long sidechain" (LSC) PFSAs that have been developed by other companies include Fumapem® (FuMA-Tech), Aciplex® (Asahi Chemical), Flemion® (Asahi Glass), and Gore-Select™ (Gore and Associates).[6] In 2019, The Chemours Company (a spinoff from DuPont that opened in 2015), announced its takeover and launch of a new Nafion™ membrane.[102]

The bulk of the PFSA characterization literature focuses on dynamic mechanical, dielectric, proton conductivity, water uptake, and morphological studies of Nafion. These numerous studies have provided a benchmark for proton conductivity, mechanical and chemical stability, and fuel cell performance to guide the synthesis of next-generation fuel cell membranes. While the exact morphology of Nafion is still under debate (discussed in Section 1.2.2.2), the presence of a continuous aqueous phase that allows for high proton conductivity is evident.[16] Nafion membranes are capable of taking up approximately 21 water molecules per sulfonic acid group when fully hydrated, which in turn allows it to reach proton conductivity values in excess of 0.1 S/cm.[103] However, at low water contents, the conductivity of Nafion drops extensively. For this reason, novel PFSAs with different sidechain chemistries have been developed and will be discussed along with their comparison to Nafion in the proceeding sections.

1.3.2 Dow Short Sidechain, Solvay Hyflon Ion/Aquivion

In the early 1980s, Dow Corporation filed a series of patents on the synthesis of a similar analog to Dupont's Nafion but with a shorter sidechain.[4,5,104-107] A series of characterization studies shortly followed to describe the physical properties of these short sidechain (SSC) ionomers. The first of these studies was conducted by Tant and coworkers in 1988 where they utilized differential scanning calorimetry (DSC), dynamic mechanical analysis (DMA), and wide angle X-ray diffraction (WAXD) to probe the physical properties and degree of crystallinity of the short sidechain ionomer.[108,109] This study provided the first evidence of increased degree of crystallinity with a lower MW sidechain PFSA. SSC ionomers were developed in EWs as low as 700 g/eq before complete loss of crystallinity was noticed. In comparison, Nafion loses crystallinity below 965 EW.[109] Moore and Martin also confirmed this finding in their study of the Dow SSC ionomer by X-ray scattering and DSC, noting that SSC membranes with EWs above 800 g/eq were crystalline.[110] Higher crystallinity in the SSC membranes was attributed to less disruption of crystallinity by the short sidechain as opposed to the long sidechain in Nafion. DSC experiments showed that despite the change in degree of crystallinity with varying EW values for the SSC, the melting temperature was unaffected by EW. Based on this finding, Moore and Martin proposed that the Dow SSC ionomers were more of a blocky copolymer structure than a truly random ionomer.[110] This study also showed the first evidence of an ionomer peak in the SAXS profiles for the SSC ionomer. The ionomer peak was observed to decrease in intensity with increasing EW, attributed to crystallinity acting as a barrier to water swelling.

In terms of fuel cell performance, the Dow SSC was shown to outperform Nafion in terms of power production and operating temperature range.[111,112] An 800 EW Dow SSC was observed to produce four times the current and power than a Nafion membrane at the same operating voltage. Additionally, an increase in the α-relaxation from 110 °C for Nafion to 160 °C for SSC meant that

the working temperature range of the fuel cell could be expanded. While the molecular motions associated with the α-relaxation in PFSAs will be discussed at length in **Chapter 2**, it is attributed to weakening of the physical crosslinks formed by ionic aggregates and is the dominant relaxation in these H^+-form PFSAs, above which, long-range motions of the polymer chains can occur.

When development of the Dow SSC ionomer was abandoned, Solvay developed an ionomer with the same structure under the tradename Hyflon Ion®, recently rebranded to Aquivion®. While the reason for abandonment of the SSC project by Dow is unknown, it is thought that it may have had to do with the complexity of synthesizing that short sidechain monomer. Solvay has developed their own, facile synthetic method (discussed in Section 1.4.1) that allows Aquivion to be produced on an industrial scale.[6]

Since its takeover by Solvay, there have been numerous studies on the mechanical, thermal, and chemical properties of Hyflon Ion/Aquivion.[6,113-115] In comparison with 1100 EW Nafion membranes, extruded Hyflon Ion membranes of 850 EW were shown to have similar mechanical properties in terms of tensile strength and resistance to tear initiation and propagation in both the dry and hydrated states.[115] This was attributed to a similar level of crystallinity in the Nafion and SSC membranes despite the difference in EW. Hyflon Ion also exhibited better fuel cell performance than Nafion, attributed to its lower EW (higher ion exchange capacity) and higher levels of hydration.[115] In terms of chemical stability within a fuel cell, Hyflon Ion showed good resistance to peroxide degradation over a working range of 70 to 90 °C, and the development of a chemically stabilized "S-grade" version of the ionomer membrane increased its resistance to chemical degradation and minimized hydrogen crossover.[113] DMA measurements of the Solvay SSC reconfirmed the high α-relaxation temperature at 160 °C, making it a promising material for high temperature fuel cell operations.[116]

In 2011, a comparison study on the fuel cell performance of Nafion versus Solvay SSC (Aquivion) membranes continued to highlight the benefits of a shorter sidechain PFSA.[117] A 790 EW Aquivion membrane was able to outperform 1100 EW Nafion of a similar thickness during high-temperature fuel cell operation at 130 °C. Fuel cell tests conducted with Aquivion as the proton exchange membrane showed lower ohmic resistance, less cross-over, and better electro-catalytic activity than Nafion under the same conditions. The authors attributed the enhanced properties to the presence of crystallinity in the low EW SSC sample, higher α-relaxation temperature, and lower EW than the Nafion comparison. Crystallinity enhances the mechanical properties of the membrane that reduces the amount of cross-over, while the high α-relaxation temperature ensures mechanical integrity at the temperatures necessary for high-temperature fuel cell operation. Additionally, the low EW values achievable for SSC compared to LSC Nafion result in higher conductivity and an increase in catalyst utilization.

1.3.3 3M PFSA Intermediate Sidechain

In 2003, 3M Company announced the development of their own version of the short sidechain PFSA.[16,118,119] With no trademarked nickname, it is referred to as 3M PFSA. Despite being considered a short sidechain PFSA, the structure of the 3M-PFSA sidechain is slightly longer than the Dow/Solvay version and thus will be referred to as an "intermediate" sidechain length. Similar to the SSC membranes, 3M PFSA is able to achieve low EW values while maintaining crystallinity. The 3M PFSA membranes demonstrate adequate crystallinity required for good mechanical properties in the hydrated state down to 800 EW. Above 800 EW, 3M PFSA membranes can withstand being boiled in water for extended lengths of time while maintaining strong films.[7,118] Membranes below 800 EW have also been created that are more fragile but still do not completely dissolve upon boiling in water as a similar EW LSC membrane would.

A study published by 3M in 2007, provided the first report of mechanical properties, chemical stability, and ion conductivity of the new 3M PFSAs.[7] A comparison of DMA results for 3M PFSA and Nafion membranes, both cast to the same thickness and with a nominal EW of 1000 g/eq, showed a higher α-relaxation temperature for 3M PFSA (at 125 °C, compared to 110 °C for Nafion). As with the SSC discussed previously, a higher α-relaxation temperature allows the membrane to be used in higher temperature fuel cell operations. The authors also noted that the storage modulus for 3M PFSA was higher before and after the α-relaxation compared to Nafion, which they proposed may provide improved mechanical stability against creep or membrane deformation and therefore extend the lifetime of a MEA. Fenton's tests for chemical stability yielded similar results for 3M PFSA to LSC Nafion membranes where the sidechain was observed to be cleaved from the backbone at the ether linkage.[7,120] With the addition of manganese ions to the membrane, they were able to reduce this chemical degradation by half.[7]

Fuel cell performance and proton conductivity studies showed an overall improvement for the intermediate sidechain 3M PFSA when compared to LSC Nafion.[7] Conductivity measurements were conducted over a temperature range of 80 to 120 °C and showed an overall trend of decreasing conductivity with increasing temperature, as expected for the reduction in water content at elevated temperatures. However, in comparing 3M PFSA of various EWs, lower EW membranes had higher proton conductivities across all temperature ranges. Proton conductivity values of low EW 3M PFSA (730 EW) were found to be 2.5 times higher than 1000 EW at 120 °C, demonstrating the importance of ionomers that can achieve low EW values for high-temperature fuel cell applications. Fuel cell testing showed that lower EW 3M PFSA membranes provided less cell resistance and an increase in performance at lower humidity levels than higher EW membranes and LSC Nafion.

In 2014, Maalouf and coworkers conducted an in-depth study combining NMR diffusion experiments and AC conductivity measurements at different water contents to describe the mechanism of increased proton transport in 3M PFSA ionomers.[121] The low EW membranes were observed to have higher conductivity than the high EW materials at every relative humidity (RH) value, in agreement with observations by Emery *et al*. from 3M.[7] Proton conductivity increased dramatically in EWs below 700 g/eq and this effect was most pronounced at low RH levels. By combining the observed conductivity data with NMR diffusion measurements (probing long-range motion of water molecules) and NMR relaxation data (molecular scale probe), the authors were able to provide additional information on the behavior of water and protons in the 3M PFSA membranes. At low water contents, the lowest EW PFSA (585 g/eq) had the fastest water diffusion over both long and short ranges. In addition, the NMR relaxation data revealed slower rates in 585 EW, characteristic of faster water motion and attributed to lower 'friction' between water molecules and sulfonate groups. Based on these experiments, the authors attributed the increase in proton conductivity of these low EW, intermediate sidechain PFSAs to the close proximity of the sulfonate groups to one another.[121] In low EW membranes, an estimated only two to four water molecules are able to bridge the sulfonate groups and create a connected pathway for proton and water transport.

Another study attempted to describe the increase in proton conductivity for the 3M PFSAs by performing theoretical simulations to investigate the morphology of these ionomers.[122] Dissipative particle dynamics (DPD) simulations were performed on 3M PFSA of varying EW, molecular weight, and water content. In this study, they found that in comparison to the SSC ionomers,[123] the longer sidechain in 3M PFSA actually provides more flexibility of the functional sidechains resulting in increased ability of the sidechains to aggregate into water clusters yielding

larger clusters. This finding was confirmed by a SAXS study comparing hydrated 3M PFSA to LSC Nafion and SSC Aquivion.[124] In 3M PFSA, decreasing EW causes the intensity of the matrix peak to decrease, indicating fewer crystalline domains in the membranes, also confirmed by wide angle X-ray studies. Additionally, the ionomer peak position was shown to be dependent on EW, and a plot of d-spacing vs. water content for various EW membranes showed consistency with the previous DPD study in that larger d-spacing was observed for longer sidechain PFSAs suggesting larger clusters possibly due to the flexibility of the sidechain and its ability to form aggregates.

1.3.4 3M Multi Acid Sidechain Ionomers

In 2010, 3M Company developed a new multi-acid sidechain perfluorinated ionomer based on the intermediate sidechain 3M PFSA.[125] The objective of this ionomer was to make a fuel cell membrane that could operate in high temperatures/low humidity in order to simplify cooling systems, facilitate heat rejection, and improve catalyst resistance to catalyst poisoning. 3M successfully synthesized a series of multi-acid ionomers that increase the number of proton exchange groups without altering the number of TFE units between sidechains, *n*. The design of these new sidechains incorporates a bis(sulfonyl)imide acid group in addition to the pendant sulfonic acid. The bis(sulfonyl)imide is considered an attractive proton exchange group because the proton is extremely acidic due to the strong electron withdrawing properties of the two sulfonyl groups and attached fluorocarbon segments. In fact, the sulfonyl imide is reported to have a higher gas-phase acidity than the traditional perfluorosulfonate group.[126]

3M first synthesized two different sidechain structures containing the sulfonyl imide and sulfonic acid groups.[125] One of which contained an aromatic sulfonic acid (Ortho Bis Acid) and the other was a completely perfluorinated sidechain (perfluoroimide acid, PFIA). The structure for

PFIA is shown in **Figure 1-15** where y=1. The Ortho Bis Acid ionomer contains an aromatic ring with a single sulfonic acid covalently attached to the sulfonyl imide group.

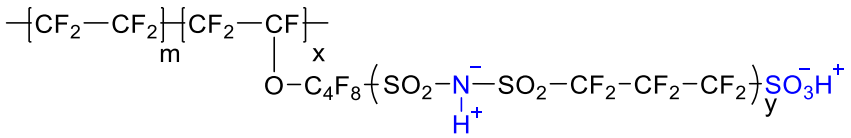

Figure 1-15. Chemical structure for 3M multi-acid ionomers, PFIA and PFICE.

In a subsequent publication, 3M introduced the perfluoro ionene chain extended (PFICE) ionomer with the same fully perfluorinated sidechain as in **Figure 1-15**, where y=2-3, referred to as PFICE-3 and PFICE-4 where the number indicates the total number of protogenic groups per sidechain including the sulfonic acid.[127] By adding multiple acidic groups per sidechain, they were able to achieve EWs as low as 438 g/eq while maintaining an adequate number of TFE units between sidechains for crystallinity to maintain mechanical integrity of the membranes. **Figure 1-16** shows the calculated average moles of TFE between sidechains as a function of EW for Nafion, Solvay SSC, 3M PFSA, and 3M PFIA (containing a single sulfonyl imide group and pendant sulfonic acid).[125] For a 3M PFIA with a certain number of average TFE units between sidechains, the EW values are lower than a 3M PFSA, SSC, or LSC of the same quantity *m*. A technical report published by 3M confirmed that introducing these longer sidechain structures with additional acidic sites did not disrupt the crystallizability of the ionomer.[128] WAXD data for the ortho bis acid multi-acid ionomer made from a 1000 EW $–SO_2F$ starting material, compared to the sulfonamide intermediate for that ionomer, and the 1000 EW PFSA version (same *m*) all showed a crystalline reflection at ca. 18° 2 θ, characteristic of PTFE crystallites.

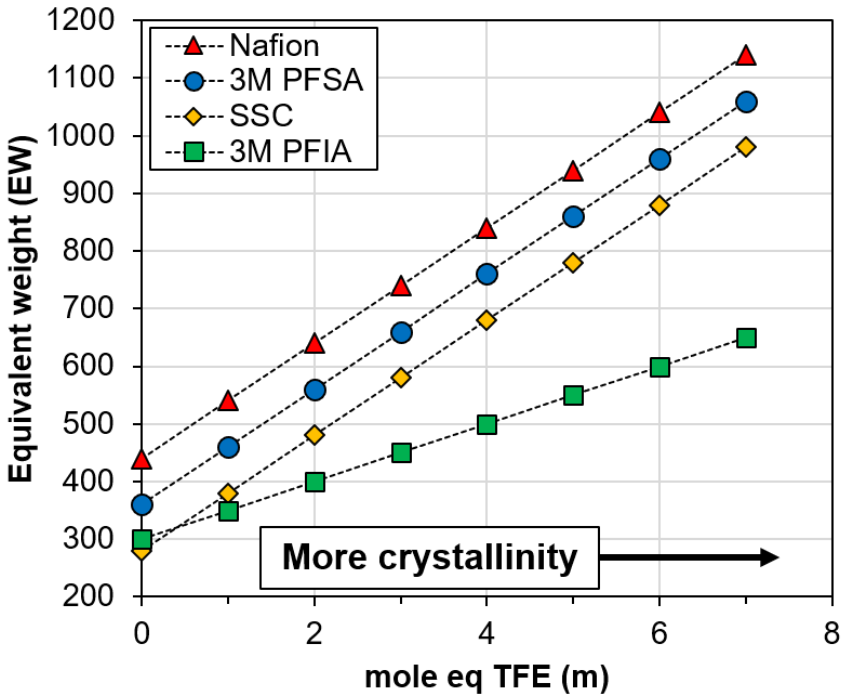

Figure 1-16. EW vs average moles of TFE between sidechains for Nafion, 3M PFSA, Solvay SSC and 3M PFIA. Adapted with permission from The Electrochemical Society.[125]

In terms of physical properties of these multi-acid ionomers, PFIA (containing one bis(sulfonyl)imide group) was shown to have a higher α-relaxation temperature (ca. 130 °C) than 3M PFSA or Nafion and a higher proton conductivity across a range of relative humidities.[125] The aromatic Ortho Bis Acid multi-acid ionomer did not perform as well in proton conductivity tests at low RH values as PFIA. This was attributed to the lower acidity of the aromatic sulfonic acid groups compared to the perfluorinated sulfonic acids.[16] PFIA and Ortho Bis Acid also had lower water uptake values than 3M PFSAs of the same EW, however, they had a higher water uptake than 3M PFSAs of the same TFE content.[125] Nonetheless, 3M PFSA single acid ionomers become soluble in boiling water below 700 EW whereas the 3M PFIA and ortho bis acid were able to withstand boiling water at an EW of 620 g/eq, showing the effectiveness of backbone crystallinity in maintaining the mechanical integrity of these multi-acid ionomers.

The introduction of PFICE ionomers with multiple bis(sulfonyl)imide groups per sidechain presented the possibility of creating ultra-low equivalent weight PFSAs for use in high-temperature fuel cell operations.[127] These PFICE ionomers showed the highest proton conductivity values compared to other PFSAs due to their increased quantity of ion exchange groups. At high relative humidities, the conductivity of PFIA was over two times as high as Nafion, and PFICE-4 (containing 3 bis(sulfonyl)imide groups) was over four times. In terms of fuel cell performance, these conductivities at high humidities were shown to not be as significant. However, at low relative humidities, the proton conductivities of PFIA and PFICE-4 were significantly improved such that a substantial improvement in voltage loss due to membrane resistance was to be expected for these multi-acid ionomers. A water solubility test showed that 625 EW PFIA with the same *m* value as an 800 EW PFSA had the same degree of solubility as the 800 EW PFSA. The same observation was made for PFICE-4 from a 700 EW PFSA backbone (which had the same degree of solubility as a 700 EW PFSA). However, it was noted that water swelling increased with decreasing EW regardless of the number of TFE units between sidechains in the backbone. The authors emphasize that this is the limitation of the PFICE approach because swelling and deswelling of the membrane can reduce the lifetime of a MEA.

While publications on these multi-acid ionomers are limited due their recent development, several studies (mostly focused on PFIA) have aimed to gain a better understanding on the role that the acidic bis(sulfonyl)imide group plays in hydration and proton transport compared to single acid PFSA ionomers.[129-136] Atomic force microscopy (AFM) studies and MD simulations have shown that PFIA has higher proton diffusion rates, more water content across all relative humidities, and larger hydrophilic domains compared to PFSAs.[131,132,134] A study conducted on interfacial and bulk water in ultrathin Nafion, 3M PFSA, and PFIA membranes using ellipsometry

and neutron reflectometry also showed much higher levels of hydration in the PFIA/platinum interface than observed for the PFSA counterparts.[130] More recently, a study was conducted to determine the chemical and morphological origins of improved conductivity in PFICE ionomers using advanced scattering techniques.[129] This study gave a glimpse into the different morphologies of the ionic aggregates in PFIA compared to its parent 3M PFSA ionomer, consisting of more ordered phase-separation and nanoscale transport pathways that facilitate proton transport.

Multi-acid ionomers have consistently shown exceptional proton conductivity and mechanical properties making them very promising for the future of fuel cell research. However, a recent extensive fuel cell durability study shed some light on the chemical stability of these multi-acid ionomers within the fuel cell environment.[137] Utilizing an open circuit voltage (OCV) test, which is the industry standard accelerated fuel cell test for studying the stability of membranes, PFIA showed some interesting and anomalous behaviors. The PFIA MEA showed a decay in OCV potential within the first 200 hours and an increase in cell resistance that rapidly grew near end of life of the MEA. Using liquid chromatography, the effluent water collected throughout the OCV cycle showed a variety of small molecule fragments that were attributed to cleavage of the PFIA sidechain. Additional studies on the membrane at the end of the OCV test also indicated that the PFIA sidechain was degrading during the test. While the authors could not provide a detailed mechanism of the degradation, they did point out that the sidechain was clearly cleaving from the backbone and further degrading at the sulfonyl imide linkage. Despite some of these issues with degradation, with the addition of a nanofiber support and stabilizing additives, PFIA was still able to withstand a 500-hour target set by the Department of Energy and the multi-acid sidechain concept remains a promising chemistry for the synthesis of next-generation fuel cell membranes.

1.4 Synthesis and Processing of Perfluorinated Ionomers

Perfluorinated ionomers are derived from a melt-processable $–SO_2F$ precursor form produced from the copolymerization of TFE and a perfluorovinyl ether with pendant sulfonyl fluoride group. After synthesis, the sulfonyl fluoride copolymer is then either melt-processed (extruded into sheets) and then hydrolyzed to the sulfonic acid to achieve a membrane, or directly hydrolyzed from the $–SO_2F$ "crumb" and dispersed into a solvent for solvent-casting the final membrane. In this section, the synthesis of each of the different PFSA sidechain structures is briefly discussed followed by the different processing methods required to make quality proton exchange membranes.

1.4.1 PFSA Synthesis

There are multiple manufacturers of perfluorinated ionomers as mentioned in Section 1.3, who synthesize variations of the three sidechain structures, referred to by their relative length: long, intermediate, and short. Synthesis of all of these PFSAs involves a copolymerization of TFE with a perfluorovinyl ether monomer. The ether linkage connecting the sidechains to the TFE backbone of these ionomers serves as a highly active group to allow for incorporation of a high weight percent of the functional comonomers.[3] Much of the difference between the synthesis of the various PFSA sidechains stems from the synthetic route to achieve each functional comonomer.

1.4.1.1 Synthesis of Nafion Functional Monomer

Synthesis of the functional monomer for Nafion is shown in Scheme 1.1.[3] It starts with the reaction of tetrafluoroethylene with sulfur trioxide at room temperature and atmospheric pressure to make TFE β-sultone. The sultone is catalyzed by fluoride ions then two equivalents of

hexafluoropropylene epoxide (HFPO) is added to make a di-adduct compound. Lastly, the di-adduct is reacted with sodium carbonate to make the final functional Nafion monomer in the sulfonyl fluoride form.

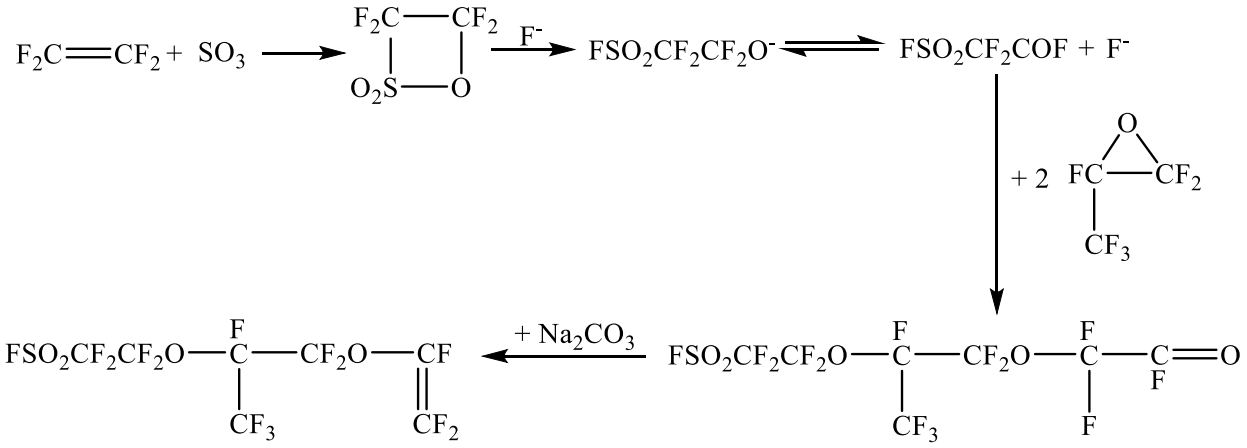

Nafion (Long Sidechain) Monomer

Scheme 1.1

1.4.1.2 Synthesis of Hyflon/Aquivion SSC Functional Monomer

The synthesis of short sidechain PFSAs was originally developed by Dow and then slightly altered when Solvay took over production of the SSC. Scheme 1.2 shows the original synthetic route for the Dow SSC functional monomer and Scheme 1.3 shows the new scheme for the Solvay Hyflon Ion/Aquivion monomer.[115] The synthesis of this SSC monomer also starts with the reaction of tetrafluoroethylene with sulfur trioxide to make TFE β-sulfone. Following this first step, the synthetic method deviates between the Dow and Solvay processes. The synthetic method developed by Dow involves multiple steps and the complexity of the steps most likely resulted in a high cost leading to the ultimate abandonment of industrial development. Solvay was able to apply their 'proprietary fluorovinyl ether process' to the production of the Hyflon Ion/Aquivion

monomer to combine the fluorination and fluoro-olefine addition steps into a single reaction step (Scheme 1.3).[115] This simplification of the synthetic process has allowed them to produce the SSC PFSA on an industrial scale.

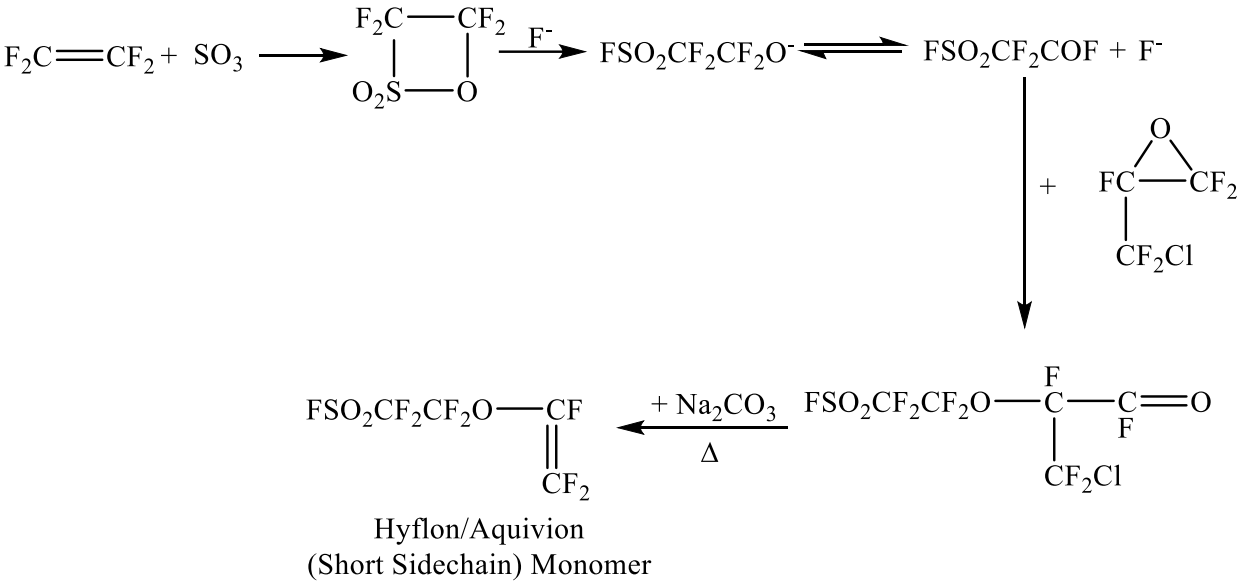

Scheme 1.2

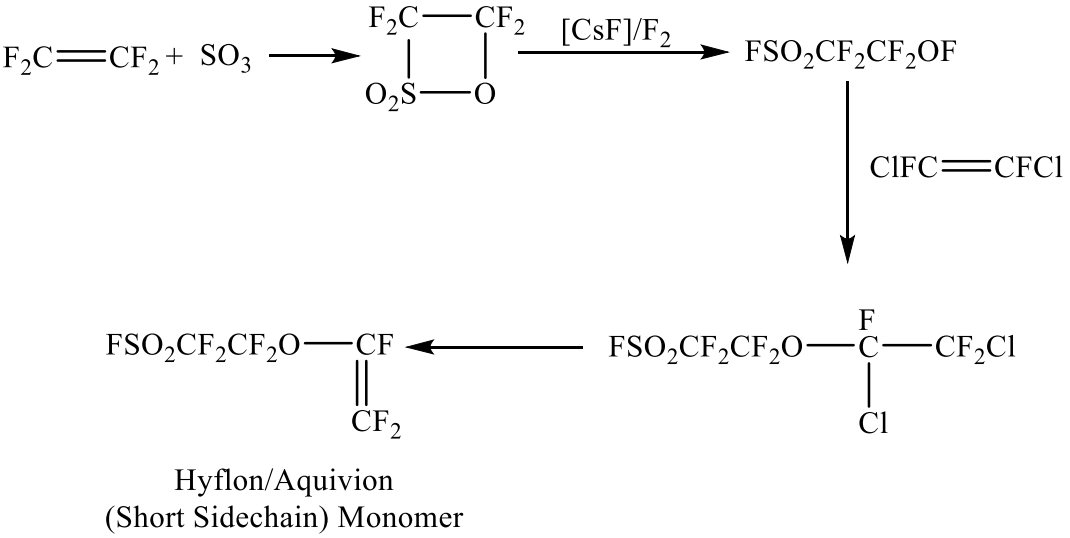

Scheme 1.3

1.4.1.3 Synthesis of 3M PFSA Functional Monomer

Synthesis of the 3M PFSA monomer is showed in Scheme 1.4.[7] The 3M PFSA monomer is synthesized starting with electrochemical fluorination (ECF) of 1,4-butane sulfone in hydrofluoric acid to yield 4-(fluorosulfonyl)hexafluorobutyryl fluoride. Coupling of 4-(fluorosulfonyl)hexafluorobutyryl fluoride with hexafluoropropylene epoxide (HFPO) gives perfluoro-4-(fluorosulfonyl)butoxypropionyl fluoride, which is then reacted with sodium carbonate to make the final monomer product.

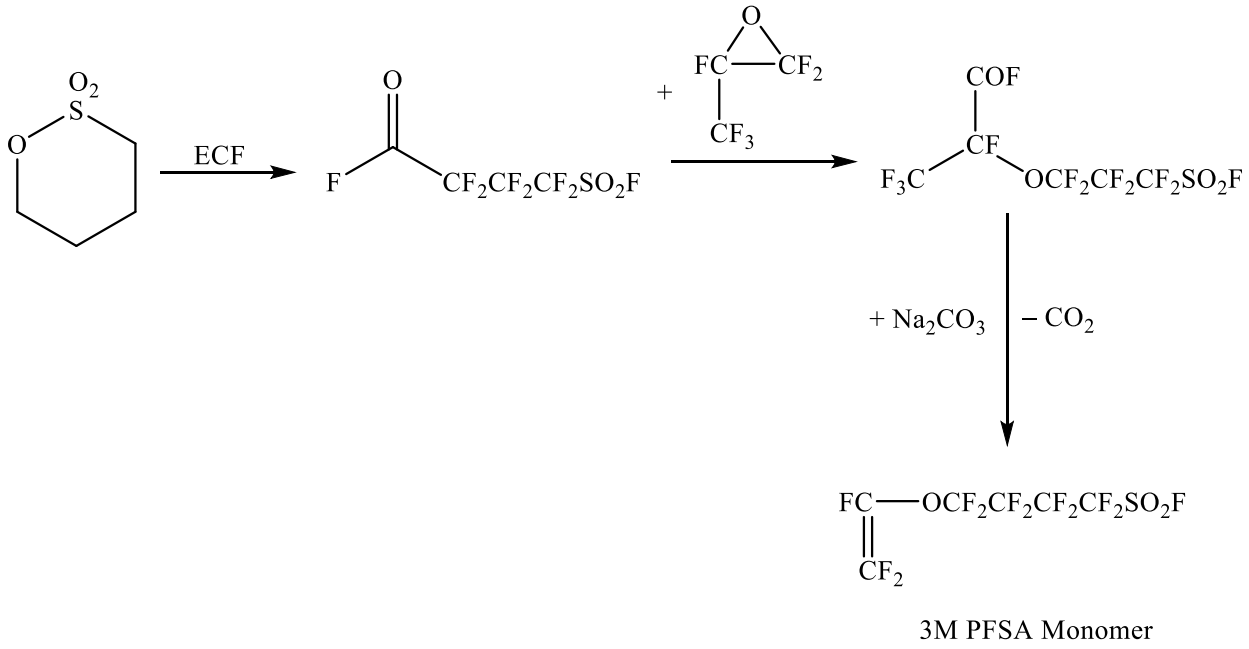

Scheme 1.4

1.4.1.4 Polymerization Reaction

PFSAs are generally produced by a free radical copolymerization of the functional monomer and tetrafluoroethylene. While multiple copolymerization methods have been reported

in literature, microemulsion polymerization appears to be the most commonly used method for producing PFSAs on an industrial scale.[6,7,138] A mixture of the functional monomer and lithium hydroxide are pre-emulsified into water using high shear and added to a high-pressure reactor.[7] Tetrafluoroethylene is fed into the reactor and the polymerization is initiated by a persulfate ion.

1.4.1.5 Synthesis of 3M Multi Acid Sidechain Ionomers

The synthesis of 3M's multi-acid ionomers starts with the already-polymerized 3M PFSA sulfonyl fluoride copolymer. The conversion of 3M PFSA into 3M PFIA or PFICE is shown in Scheme 1.5. Sulfonyl fluoride form 3M PFSA is converted to a sulfonamide by reaction with ammonia at high pressure and a temperature of −20 °C.[125] The resulting sulfonamide intermediate is dissolved in acetonitrile and perfluoropropoane disulfonyl fluoride is added to create the bis(sulfonyl)imide linkage. The polymer is then hydrolyzed with lithium hydroxide to achieve the final perfluoroimide acid ionomer (PFIA). To make perfluoro ionene chain extended (PFICE) ionomer, prior to hydrolysis, the addition of perfluoropropoane disulfonyl fluoride is repeated in subsequent reactions to add up to 3 bis(sulfonyl)imide groups to the sidechain prior to hydrolysis.

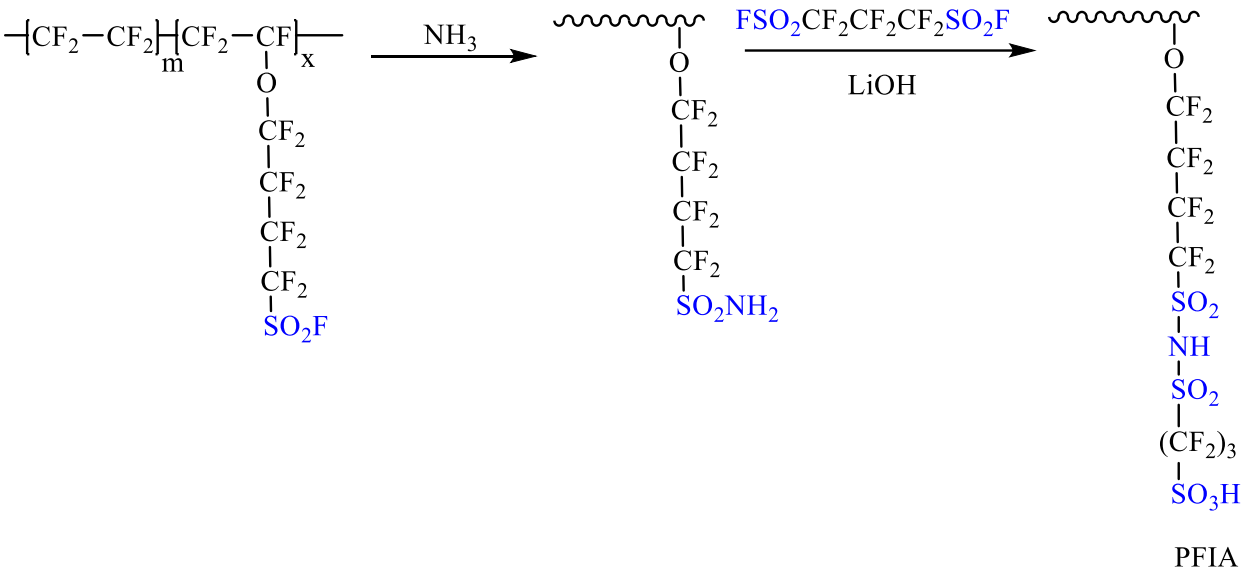

Scheme 1.5

1.4.2 Membrane Processing

After synthesis, the PFSAs are processed into membranes by either extrusion or solution casting. Both methods require the application of some type of elevated temperature, either during the process with extrusion, or after solution casting by drying and annealing steps. It is well documented that thermal history has a profound effect on the morphology and properties of PFSA membranes.[96] For this reason, it is important to understand the different membrane processing methods and how they may affect the structure and properties of the resulting membranes in order to guide synthesis and processing methods of next generation fuel cell membranes.

1.4.2.1 Extrusion/Melt-Processing

The original method for making Nafion membranes was by extrusion of the melt-processable sulfonyl fluoride precursor into sheets followed by hydrolysis of the $–SO_2F$ groups into sulfonic acid.[1,139] This method has been shown to result in microstructural orientation in the machine direction (as observed by X-ray scattering), which is undesirable because it causes anisotropic

swelling of the membrane that can be problematic in a fuel cell.[1] Orientation of the membrane can be eliminated only by biaxial stretching at a temperature above the α-relaxation temperature or by annealing above the melting temperature for longer 24-hour time periods.[140] Despite these orientation issues that arise from extrusion, extruded membranes are very mechanically stable, pliant, and insoluble in all solvents at temperatures below 200 °C.[141] Nafion 117 (extruded form of Nafion), that has an EW of 1100 g/eq and a thickness of 175 μm, is still produced today.

Solvay's Hyflon Ion/Aquivion SSC polymers have also been extruded into membranes following the same procedure in the sulfonyl fluoride form prior to hydrolysis to the sulfonic acid.[116] These SSC membranes are semicrystalline and can reach EW values of no less than 750 g/eq with thicknesses as low as 15 μm. Extruded SSC membranes have less water uptake than Nafion for a given EW, indicating that lower EW values can be made within an acceptable water uptake range. However, water uptake in the SSC membranes increases dramatically at lower EWs so they are only produced at EWs of 850 or higher. SSC extruded membranes that are 50 μm thick showed similar mechanical properties and better fuel cell performance than Nafion (1100 EW, 175 μm thick).[116]

Upon hydrolysis to the sulfonic acid form, PFSA membranes are no longer processable due to the coulombic interactions between the sulfonic acid groups and the presence of PTFE-like crystallites. The only way to melt-process the membrane after hydrolysis is to eliminate the crystallinity and weaken the strength of the electrostatic interactions between ionic aggregates. An example of this was done by Cable and Moore in 1992 by using bulky tetrabutylammonium (TBA^+) counterions to weaken the electrostatic network.[142] Using a method referred to as "steam stripping," the crystallites in the sample were eliminated by evaporating TBA^+-form Nafion solutions in boiling water, resulting in the TBA^+-form Nafion precipitating to the top due to the

hydrophobic nature of the counterion. Utilizing this steam stripping method, the authors were able to melt process the resulting amorphous TBA^+-Nafion powder into a pliable membrane.

1.4.2.2 Dispersion Casting

More recently, the PFSA community has shifted to dispersion casting methods instead of melt-processing in order to achieve thinner membranes. In the early 1980s, two publications reported a novel "dissolution" procedure for creating dispersions of Nafion into alcohol/water solvent mixtures using elevated temperature and pressure.[143,144] Based on work by Yeo *et al.* that proposed that PFSAs have two different solubility parameters resulting from both the hydrophobic and hydrophilic character of the polymer,[145] Martin, Rhoades, and Ferguson used a mixed solvent of alcohol and water to invoke maximum swelling of the ionomer and high temperatures to eliminate the PTFE-crystallites to allow ultimate dissolution of the Nafion membranes.[144] Another patent in 2001 outlined a new dissolution procedure for dispersing the Solvay Hyflon Ion SSC at low temperatures (between room temperature and 150 °C) with the addition of a small amount of a fluoropolyether in the solvent mixture.[146] The authors of this patent propose that the addition of the fluoropolyether serves to disrupt the ionic aggregates in dispersion leading to a reduction in the particle size.

Early studies on Nafion dispersions attempted to gain understanding on the structure of PFSA in these solutions. An early SANS study looked at a series of solutions containing different weight fractions of PFSA.[72] A scattering peak was observed that was attributed to the interference between scattering particles of nanometer-scale distributed homogeneously in solution. The authors observed that the spacing between scattering particles determined by the position of the scattering maximum ($d=2\pi q^{-1}$) varied linearly with polymer content, characteristic of a solution of charged particles repelling each other. It was ultimately proposed based on their SANS findings, that

Nafion dispersions consist of rod-like polymer in which the polymer is in contact with the solvent at the surface of the "micelle" as opposed to an open coil structure. A subsequent study further expanded this model, proposing that the center of the rod-like particles consist of a perfluorinated core while the charges are at the surface of the rod and the diameter of the particle is dependent on surface tension.[73]

In the late 1990s, an in-depth SAXS and SANS study of Nafion dispersions in the Li^+-form also confirmed the presence of rod-like particles.[147] The radius of the particle was calculated by the shape and intensity of scattering curves. For Nafion, the radius of the rod-like aggregate was calculated to be ca. 20 Å and the diameter was determined to be dependent on the solvent but typically over 300 Å in length. A subsequent study on dispersions of the Dow SSC PFSA also showed rod-like character with a radius of 17 Å.[148] In 2014, a study utilizing dynamic light scattering (DLS), SAXS and NMR experiments also observed rod-like character in PFSA dispersions in 1-propanol/water and ethanol/water mixtures.[149] The rod-like dispersion morphology has been widely accepted by the PFSA community even as characterization technology has advanced over the years, though the character of the rods has been shown to be affected by the type of solvent used in the dispersion. A SANS study of Nafion dispersed in various solvents indicated that particles of a well-defined cylindrical morphology with radii around 22 Å are formed in glycerol and ethylene glycol, while less-defined particles form in water/isopropanol mixtures.[150] The authors of this study originally proposed random-coil conformation characteristic of true solution behavior of Nafion in N-methylpyrrolidone (NMP), although that was rescinded in a later study that determined the particles in NMP are likely gelled to sizes too large to be detected by SANS.[151]

Initial films cast from PFSA dispersions were observed to have poor mechanical properties including brittleness, mud-cracks in the membrane, and high solubilities, that were undesirable for their use as fuel cell membranes.[1,147] The development of a new "solution processing" method for making cast Nafion membranes in the 1980s produced membranes that exhibited similar properties to the as-received extruded materials.[141,152] This solution processing method consisted of replacing the low boiling point alcohol/water mixtures in Nafion dispersions with a high boiling point solvent such as dimethyl sulfoxide (DMSO), ethylene glycol, or dimethylformamide (DMF). The high boiling point solvent is then evaporated off at elevated temperatures, leaving behind a "solution-processed" membrane that had low solubilities and developed some degree of crystallinity that was not observed in low temperature re-cast Nafion. A schematic of the solution-processing method is shown in **Figure 1-17**. The key to this process was a combination of the solvent that plasticizes the polymer aggregates and the high temperature that provides chain mobility necessary to allow reorganization of the polymer chains in solution and form an entangled network, therefore leading to a mechanically stable membrane. Crystalline lamella formed from the solution-processing method were also shown to increase and develop long-range order with additional annealing at elevated temperatures, further enhancing the mechanical properties of these membranes.[153]

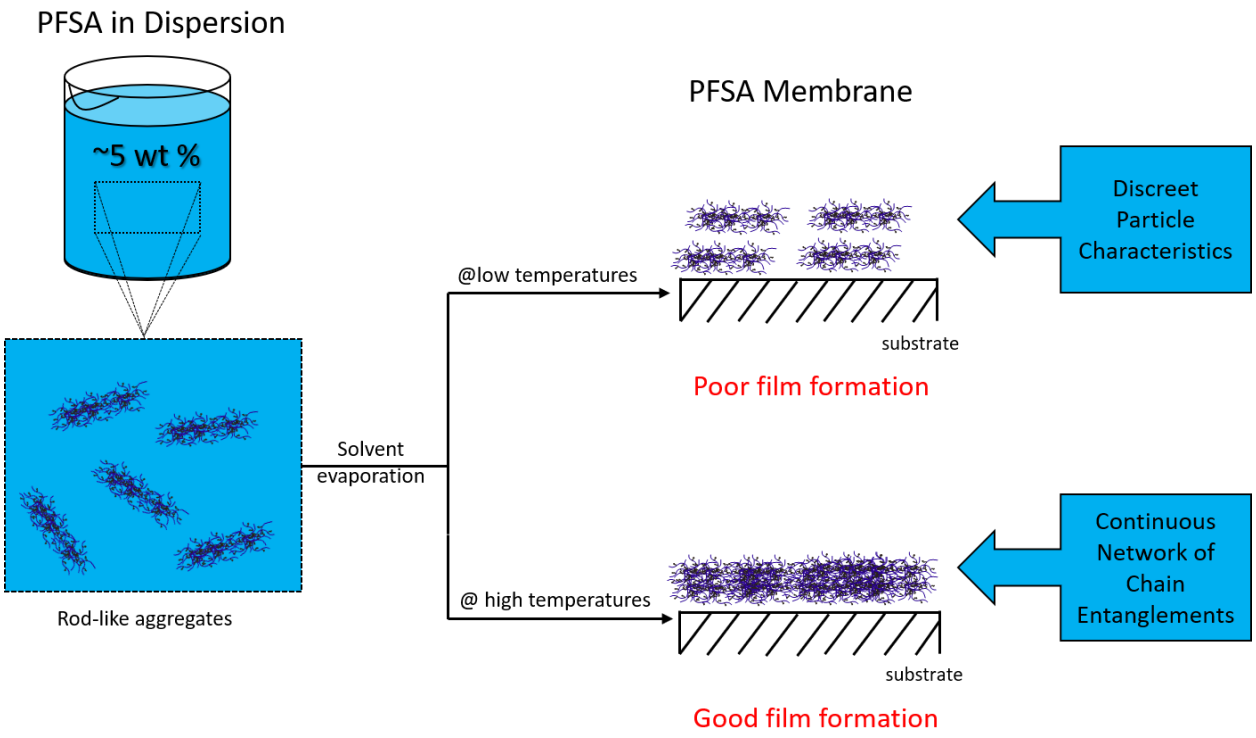

Figure 1-17. Solution processing method for filming membranes with good mechanical properties.

In 2015, Kim and coworkers conducted a large study on the origin of mechanical toughness in dispersion-cast (following the solution-processing method) Nafion, cast from a wide variety of solvents.[151] In this study, they were able to relate the critical gelation concentration of each solvent to the resulting toughness of a membrane cast from that solvent. Membrane toughness showed no correlation to degree of crystallinity. Based on these findings, it was determined that the origin of mechanical toughness in solution-cast membranes was related to the formation of chain entanglements as opposed to crystallinity.

1.4.2.3 Current Methods for Producing PFSA Membranes

PFSAs produced today are available both in extruded and solution-cast forms. Extruded Nafion 117 (1100 EW, 175 μm thickness) and solution-cast Nafion NR-211 (1100 EW, 25 μm thick) and NR-212 (1100 EW, 50 μm thick) are all available for purchase online. The methods used to produce the solution-cast membranes are not readily available to the public. Solvay's Aquivion is purchasable in the extruded form (870 and 980 EW in multiple thicknesses ≥ 50 μm) and the sulfonyl fluoride precursor form (870 and 980 EW pellets). Both Nafion and Aquivion can also be purchased as aqueous or alcohol-based dispersions.

The solution-casting method used to produce 3M PFSA membranes is published.[7] For these intermediate sidechain PFSAs, the raw sulfonyl fluoride precursor is hydrolyzed and dispersed in the same step by mixing with lithium hydroxide and water at elevated temperatures in a pressure vessel. The dispersion is then passed through an ion exchange column to convert the $–SO_3Li$ groups to $–SO_3H$. An alcohol cosolvent is either added directly to the dispersion or the dispersion can be evaporated down completely and re-dispersed into the solvent of interest separately. The 3M PFSA (and PFIA/PFICE) dispersions are then cast onto a substrate using a coating rod and dried in a force air oven at 80 °C followed by annealing above 150 °C for ten minutes.

1.4.2.4 Effect of Annealing

It is well understood that the morphology and properties of PFSA membranes are strongly affected by their thermal history.[1,96] This was briefly addressed in the previous sections where it was demonstrated that elevated temperatures are required to achieve membranes with good mechanical properties. Since the development of PFSAs, multiple studies have focused on the effect of annealing on membrane morphology and properties of solution-cast and extruded membranes.

One of the first studies that looked at the effect of annealing on extruded Nafion membraned was conducted by Gierke, Munn, and Wilson in 1981.[37] WAXD results for thermally annealed sulfonyl fluoride form Nafion showed a crystalline reflection at 18° 2θ that decreased in intensity as the sample annealing temperature was increased from 50 to 270 °C. However, a scattering feature was observed by SAXS at temperatures below the melting temperature of the precursor, clearly attributed to electron density differences between amorphous and crystalline phases in the precursor. The authors noted that this discrepancy had been observed in polyethylene due to chain folding, but did not attempt to prove whether that was the same case in the Nafion precursor. The decrease in the wide-angle scattering reflection at 18° 2θ with annealing temperature was also observed by Fujimura and coworkers.[70] The authors of this study noted that when the Nafion membrane was cooled back down to room temperature from 275 °C, the crystalline reflection reappeared, characteristic of melting and recrystallization of the polymer. The ionomer peak observed by SAXS was also shown to shift to larger scattering angles after increasing the temperature to 276 °C. The authors attributed this shift to decreasing inter-cluster distances.

In 2004, a study on the molecular origins of thermal transitions in Nafion showed the effect of annealing in Na^+ and Cs^+-counterion forms on crystallinity observed by DSC experiments.[154] In both counterion-forms, the initial heat showed a broad endotherm between 200 and 250 °C that disappeared upon reheat. This endotherm could be induced to reappear by annealing in the DSC at 200 °C for increasing lengths of time ranging from 0.5 to 24 hours. Based on the slow crystallization kinetics in semicrystalline polymers, this endotherm was assigned to the melting of PTFE-like crystallites. An additional, broad endotherm was observed in the first heat scan of Cs^+-form Nafion spanning ca. 100 to 150 °C. Upon annealing in the DSC for 2 hours at temperatures

ranging from 120 to 240 °C, this endotherm was observed to shift approximately 20-30 °C above the temperature at which it was annealed. Based on this finding, the low-temperature endotherm was assigned to the melting of small, imperfect crystals that develop in the sample due to annealing conditions.

Other studies observed an increase in relative degree of crystallinity in annealed Nafion membranes and related the increase in crystallinity to the conductivity of annealed membranes compared to unannealed. Li and coworkers looked at the effects of annealing Nafion NRE 211 (solution-cast membrane) in the H^+-form and the Na^+-form. Membranes were annealed at 160 °C in the H^+-form and 270 °C in the Na^+-form.[155] They observed an overall increase in relative degree of crystallinity based on WAXD measurements for both counterion-types after annealing, which led to an overall improvement in mechanical properties (determined from an increase in tensile strength). However, they noted that annealing the H^+-form reduced conductivity while annealing in the Na^+-form enhances conductivity. The authors attributed the increase in conductivity in the annealed Na^+-form membranes to the strong electrostatic interactions that become a driving force for cluster formation when activated at high temperatures. An additional study by Yin and coworkers in 2018 also showed an increase in degree of crystallinity with annealing of H^+-form solution-cast Nafion at different temperatures.[156] This increase in crystallinity led to increased mechanical properties (increased break stress values) but a decrease in overall conductivity.

In 1996, Sone, Ekdunge, and Simonsson performed proton conductivity measurements in a range of relative humidities on Nafion annealed at 80, 105, and 120 °C.[157] Proton conductivity values at 100% relative humidity decreased from 0.09 S/cm to 0.03 S/cm with increasing annealing temperature. The authors concluded that increasing the annealing temperature to close to the α-relaxation temperature of Nafion (110 °C) led to a reduction in both water uptake and conductivity.

In 2012, Maldonado and coworkers performed a systematic study on sorption and transport properties of extruded and solution-cast Nafion membranes dried at temperatures ranging from 60 to 110 °C.[158] In heat-treated membranes, they observed reduction in water uptake values that was attributed to shrinking of the polymer structure during drying. As a result of this, the water self-diffusion coefficient and proton conductivity were also reduced in the thermally treated samples.

While several of the aforementioned studies have shown a decrease in conductivity with annealing, some researchers have seen positive effects by annealing PFSAs in different counterion-forms or at high temperatures/extended annealing times. An example of this came from Thomas and coworkers in 2003, where an increase in conductivity was observed for Nafion membranes that were annealed at 140 °C in different alkylammonium counterion forms (ranging from tetramethylammonium to tetrapentylammonium).[159] The authors attributed the increase in conductivity to a restructuring of the membrane above the α-relaxation temperature based on fluorescence data that showed evidence that the alkylammonium salts changed the physical characteristic of the conducting channels. Contrary to findings by other annealing studies that showed a decrease in conductivity after annealing in the H^+-form, DeLuca and Elabd observed maximum proton conductivity values for Nafion membranes that were annealed in the H^+-form at 210 °C for ten minutes,[160] and Hensley and coworkers also observed an increase in conductivity after annealing H^+-form Nafion at 165 °C for three hours.[161]

In 2012, a SAXS study was conducted to look at the development of morphology in PFSA membranes during and after annealing above the α-relaxation temperature.[162] Unified fits from scattering data were used to quantify the sizes of the crystalline and ionic cluster phases in 3M PFSA membranes annealed 180, 190, and 200 °C. The authors observed an increase in the size of both the crystalline and cluster regions when annealed at 180 and 190 °C, but at 200 °C observed

a decrease in size of the ionomer phase at certain relative humidities. This finding suggested that there is a maximum annealing temperature that exists for these PFSA membranes.[128] From this study, it was proposed that annealing at 200 °C increases the degree of crystallinity to such an extent that reduces the mobility of the polymer chains and prevents the ionic clusters from swelling upon hydration.[162]

Clearly, there is discrepancy on the best thermal treatment method for PFSA membranes in order to improve both mechanical properties and proton conductivity/fuel cell performance. The properties of PFSAs are undoubtedly very sensitive to thermal history and thus it is hard to make direct comparisons across multiple studies that have used different counterions, annealing temperatures, annealing times, and pretreatment methods.

1.5 Conclusions

This review provides a summary of the history of PFSA membranes, their complex morphologies, and the current understanding of the effect of sidechain structure and processing conditions on membrane properties for use as PEMs in hydrogen fuel cells. There is a clear correlation between the structure, morphology, processing conditions, and resulting properties of these polymers. While the literature is densely packed with studies on these complicated PFSA systems, it is sometimes hard to compare results from different studies because of the use of different thermal treatments and membrane pretreatment conditions. One thing that is evident is that the water uptake, proton conductivity, fuel cell performance and mechanical integrity of these membranes can be tailored with a fundamental understanding of the effect of sidechain structure and thermal treatment on membrane morphology. In order to gain this information, it requires us

to know what temperatures are required to "make chains move" within the polymer. A large portion of this dissertation will focus on the thermal properties of these PFSAs, and how different sidechain structures may affect the thermal transitions, mechanical relaxations, and ultimately the morphology and properties developed by thermal treatment around those relaxation temperatures.

1.6 References

1. Mauritz, K. A.; Moore, R. B., State of Understanding of Nafion. *Chem. Rev.* **2004**, *104*, 4535.
2. Cable, K. M.; Mauritz, K. A.; Moore, R. B., Effects of hydrophilic and hydrophobic counterions on the Coulombic interactions in perfluorosulfonate ionomers. *J. Polym. Sci. Part B Polym. Phys.* **1995**, *33*, 1065.
3. Grot, W. G., Perfluorinated ion exchange polymers and their use in research and industry. *Macromol. Symp.* **1994**, *82*, 161.
4. Ezzell, B. R.; Carl, W. P.; Mod, W. A.; Google Patents: 1982.
5. Ezzell, B. R.; Carl, W. P.; Mod, W. A.; Google Patents: 1982.
6. Arcella, V.; Ghielmi, A.; Tommasi, G., High performance perfluoropolymer films and membranes. *Ann. N. Y. Acad. Sci* **2003**, *984*, 226.
7. Emery, M.; Frey, M.; Guerra, M.; Haugen, G.; Hintzer, K.; Kai; Lochhaas, H.; Pham, P.; Pierpont, D.; Schaberg, M.; Thaler, A.; Yandrasits, M.; Hamrock, S., The Development of New Membranes for Proton Exchange Membrane Fuel Cells *J. Electrochem. Soc.* **2007**, *11*, 3.
8. Heitner-Wirguin, C., Recent advances in perfluorinated ionomer membranes: structure, properties and applications. *J. Membr. Sci.* **1996**, *120*, 1.

9. Gronowski, A. A.; Yeager, H. L., Factors Which Affect the Permselectivity of Nafion® Membranes in Chlor-Alkali Electrolysis, I. *J. Electrochem. Soc.* **1991**, *138*, 2690.

10. Chandran, R. R.; Chin, D.-T., Reactor analysis of a chlor—alkali membrane cell. *Electrochim. Acta* **1986**, *31*, 39.

11. Yeager, H.; Kipling, B.; Dotson, R., Sodium ion diffusion in Nafion® ion exchange membranes. *J. Electrochem. Soc.* **1980**, *127*, 303.

12. Jorné, J., The Anolyte Diffusion Layer and Its Effect on Hydroxyl Transport Through Nafion Membrane in Chlor-Alkali Cell. *J. Electrochem. Soc.* **1982**, *129*, 722.

13. Yeo, R. S., Ion clustering and proton transport in Nafion membranes and its applications as solid polymer electrolyte. *J. Electrochem. Soc.* **1983**, *130*, 533.

14. Barbir, F. *PEM fuel cells: theory and practice*; Academic Press, 2013.

15. Danilczuk, M.; Lancucki, L.; Schlick, S.; Hamrock, S. J.; Haugen, G. M., In-Depth Profiling of Degradation Processes in a Fuel Cell: 2D Spectral-Spatial FTIR Spectra of Nafion Membranes. *ACS Macro Lett.* **2012**, *1*, 280.

16. Hamrock, S. J.; Yandrasits, M. A., Proton Exchange Membranes for Fuel Cell Applications. *J. Macromol. Sci., Rev. Macromol. Chem. Phys.* **2006**, *46*, 219.

17. Smitha, B.; Sridhar, S.; Khan, A. A., Solid polymer electrolyte membranes for fuel cell applications—a review. *J. Membr. Sci.* **2005**, *259*, 10.

18. Steele, B. C. H.; Heinzel, A., Materials for fuel-cell technologies. *Nature* **2001**, *414*, 345.

19. Vishnyakov, V. M., Proton exchange membrane fuel cells. *Vacuum* **2006**, *80*, 1053.

20. Cheng, H.; Scott, K., Improving performance of rechargeable Li-air batteries from using Li-Nafion® binder. *Electrochim. Acta* **2014**, *116*, 51.

21. Xi, J.; Wu, Z.; Teng, X.; Zhao, Y.; Chen, L.; Qiu, X., Self-assembled polyelectrolyte multilayer modified Nafion membrane with suppressed vanadium ion crossover for vanadium redox flow batteries. *J. Mater. Chem.* **2008**, *18*, 1232.

22. Kikuchi, K.; Tsuchitani, S., Nafion®-based polymer actuators with ionic liquids as solvent incorporated at room temperature. *J. Appl. Phys.* **2009**, *106*, 053519.

23. Landi, B. J.; Raffaelle, R. P.; Heben, M. J.; Alleman, J. L.; VanDerveer, W.; Gennett, T., Single wall carbon nanotube-Nafion composite actuators. *Nano Letters* **2002**, *2*, 1329.

24. Jung, J.-H.; Jeon, J.-H.; Sridhar, V.; Oh, I.-K., Electro-active graphene–Nafion actuators. *Carbon* **2011**, *49*, 1279.

25. Wang, P.; Zakeeruddin, S. M.; Comte, P.; Exnar, I.; Grätzel, M., Gelation of ionic liquid-based electrolytes with silica nanoparticles for quasi-solid-state dye-sensitized solar cells. *J. Am. Chem. Soc.* **2003**, *125*, 1166.

26. Sun, Q.; Harmer, M. A.; Farneth, W. E., An Extremely Active Solid Acid Catalyst, Nafion Resin/Silica Composite, for the Friedel−Crafts Benzylation of Benzene and p-Xylene with Benzyl Alcohol. *Ind. Eng. Chem. Res.* **1997**, *36*, 5541.

27. Espenscheid, M. W.; Ghatak-Roy, A. R.; Moore, R. B.; Penner, R. M.; Szentirmay, M. N.; Martin, C. R., Sensors from polymer modified electrodes. *J. Chem. Soc., Faraday Trans. 1* **1986**, *82*, 1051.

28. Rubinstein, I.; Bard, A. J., Polymer films on electrodes. 4. Nafion-coated electrodes and electrogenerated chemiluminescence of surface-attached tris (2, 2'-bipyridine) ruthenium (2+). *J. Am. Chem. Soc.* **1980**, *102*, 6641.

29. Rubinstein, I.; Bard, A. J., Polymer films on electrodes. 5. Electrochemistry and chemiluminescence at Nafion-coated electrodes. *J. Am. Chem. Soc.* **1981**, *103*, 5007.

30. Gerhardt, G. A.; Oke, A. F.; Nagy, G.; Moghaddam, B.; Adams, R. N., Nafion-coated electrodes with high selectivity for CNS electrochemistry. *Brain research* **1984**, *290*, 390.

31. Hydrogen & Fuel Cells Program. https://www.hydrogen.energy.gov/ (accessed August 8th, 2020).

32. DOE Technical Targets for Polymer Electrolyte Membrane Fuel Cell Components. https://www.energy.gov/eere/fuelcells/doe-technical-targets-polymer-electrolyte-membrane-fuel-cell-components (accessed August 8th, 2020).

33. Wycisk, R.; Pintauro, P. N.; Park, J. W., New developments in proton conducting membranes for fuel cells. *Curr. Opin. Chem. Eng.* **2014**, *4*, 71.

34. MacKnight, W. J.; Earnest, T. R., The structure and properties of ionomers. *J. Polymer Sci. Macromol. Rev.* **1981**, *16*, 41.

35. Orler, E. B.; Moore, R. B., Influence of Ionic Interactions on the Crystallization of Lightly Sulfonated Syndiotactic Polystyrene Ionomers. *Macromolecules* **1994**, *27*, 4774.

36. Marx, C. L.; Cooper, S. L., The crystallinity of ionomers. *J. Macromol. Sci., Phys.* **1974**, *9*, 19.

37. Gierke, T. D.; Munn, G. E.; Wilson, F. C., The morphology in nafion perfluorinated membrane products, as determined by wide- and small-angle x-ray studies. *J. Polym. Sci., Part B: Polym. Phys.* **1981**, *19*, 1687.

38. Starkweather, H. W., Crystallinity in perfluorosulfonic acid ionomers and related polymers. *Macromolecules* **1982**, *15*, 320.

39. Fujimura, M.; Hashimoto, T.; Kawai, H., Small-angle x-ray scattering study of perfluorinated ionomer membranes. 2. Models for ionic scattering maximum. *Macromolecules* **1982**, *15*, 136.

40. Brown, E. N.; Rae, P. J.; Orler, E. B.; Gray III, G. T.; Dattelbaum, D. M., The effect of crystallinity on the fracture of polytetrafluoroethylene (PTFE). *Materials Science and Engineering: C* **2006**, *26*, 1338.

41. Brown, E.; Rae, P.; Dattelbaum, D.; Clausen, B.; Brown, D., In-situ measurement of crystalline lattice strains in polytetrafluoroethylene. *Experimental mechanics* **2008**, *48*, 119.

42. Eisenberg, A.; Hird, B.; Moore, R. B., A new multiplet-cluster model for the morphology of random ionomers. *Macromolecules* **1990**, *23*, 4098.

43. Marx, C. L.; Caulfield, D. F.; Cooper, S. L., Morphology of ionomers. *Macromolecules* **1973**, *6*, 344.

44. Bonotto, S.; Bonner, E. F., Effect of ion valency on the bulk physical properties of salts of ethylene-acrylic acid copolymers. *Macromolecules* **1968**, *1*, 510.

45. Longworth, R.; Vaughan, D. J., Physical structure of ionomers. *Nature* **1968**, *218*, 85.

46. Eisenberg, A., Clustering of ions in organic polymers. A theoretical approach. *Macromolecules* **1970**, *3*, 147.

47. Mauritz, K. A. In *Ionomers*, Morphological theories; Springer: 1997, p 95.

48. Squires, E.; Painter, P.; Howe, S., Cluster formation and chain extension in ionomers. *Macromolecules* **1987**, *20*, 1740.

49. Forsman, W. C., Effect of segment-segment association on chain dimensions. *Macromolecules* **1982**, *15*, 1032.

50. Dreyfus, B., Model for the clustering of multiplets in ionomers. *Macromolecules* **1985**, *18*, 284.

51. Datye, V. K.; Taylor, P. L., Electrostatic contributions to the free energy of clustering of an ionomer. *Macromolecules* **1985**, *18*, 1479.

52. Binsbergen, F.; Kroon, G., Domain Size in Ionomers. *Macromolecules* **1973**, *6*, 145.

53. Macknight, W. J.; Taggart, W. P.; Stein, R. S., A model for the structure of ionomers. *J. Polym. Sci. C* **1974**, *45*, 113.

54. Roche, E.; Stein, R.; Russell, T.; MacKnight, W., Small-angle x-ray scattering study of ionomer deformation. *J. Polym. Sci., Part B: Polym. Phys.* **1980**, *18*, 1497.

55. Yarusso, D. J.; Cooper, S. L., Microstructure of ionomers: interpretation of small-angle x-ray scattering data. *Macromolecules* **1983**, *16*, 1871.

56. Yarusso, D.; Cooper, S. L., Analysis of SAXS data from ionomer systems. *Polymer* **1985**, *26*, 371.

57. Register, R. A., Morphology and Structure–Property Relationships in Random Ionomers: Two Foundational Articles from Macromolecules. *Macromolecules* **2020**, *53*, 1523.

58. Ding, Y. S.; Hubbard, S. R.; Hodgson, K. O.; Register, R. A.; Cooper, S. L., Anomalous small-angle X-ray scattering from a sulfonated polystyrene ionomer. *Macromolecules* **1988**, *21*, 1698.

59. Moore, R. B.; Bittencourt, D.; Gauthier, M.; Williams, C. E.; Eisenberg, A., Small-angle x-ray scattering investigations of ionomers with variable-length side chains. *Macromolecules* **1991**, *24*, 1376.

60. Hird, B.; Eisenberg, A., Phase dominance, multiple glass transitions, and apparent activation energies in some poly (styrene-co-alkali methacrylate) ionomers. *J. Polym. Sci. Part B Polym. Phys.* **1990**, *28*, 1665.

61. Gao, Z.; Zhong, X. F.; Eisenberg, A., Chain dynamics in coronas of ionomer aggregates. *Macromolecules* **1994**, *27*, 794.

62. Vanhoorne, P.; Jérôme, R.; Teyssié, P.; Laupretre, F., Direct NMR evidence for a local restriction in the segmental chain mobility of a model ionomer. *Macromolecules* **1994**, *27*, 2548.

63. Hsu, W. Y.; Gierke, T. D., Ion transport and clustering in nafion perfluorinated membranes. *J. Membr. Sci.* **1983**, *13*, 307.

64. Hsu, W. Y.; Gierke, T. D., Elastic theory for ionic clustering in perfluorinated ionomers. *Macromolecules* **1982**, *15*, 101.

65. Yeager, H.; Steck, A., Cation and water diffusion in Nafion ion exchange membranes: influence of polymer structure. *J. Electrochem. Soc.* **1981**, *128*, 1880.

66. Lee, P. C.; Meisel, D., Luminescence quenching in the cluster network of perfluorosulfonate membrane. *J. Am. Chem. Soc.* **1980**, *102*, 5477.

67. Falk, M., An infrared study of water in perfluorosulfonate (Nafion) membranes. *Can. J. Chem.* **1980**, *58*, 1495.

68. Roche, E. J.; Pineri, M.; Duplessix, R.; Levelut, A. M., Small-angle scattering studies of nafion membranes. *J. Polym. Sci., Part B: Polym. Phys.* **1981**, *19*, 1.

69. Roche, E. J.; Pineri, M.; Duplessix, R., Phase separation in perfluorosulfonate ionomer membranes. *J. Polym. Sci., Part B: Polym. Phys.* **1982**, *20*, 107.

70. Fujimura, M.; Hashimoto, T.; Kawai, H., Small-angle X-ray scattering study of perfluorinated ionomer membranes. 1. Origin of two scattering maxima. *Macromolecules* **1981**, *14*, 1309.

71. Miura, Y.; Yoshlda, H., Effects of water and alcohols on molecular motion of perfluorinated ionomer membranes. *Thermochim. Acta* **1990**, *163*, 161.

72. Aldebert, P.; Dreyfus, B.; Pineri, M., Small-angle neutron scattering of perfluorosulfonated ionomers in solution. *Macromolecules* **1986**, *19*, 2651.

73. Aldebert, P.; Dreyfus, B.; Gebel, G.; Nakamura, N.; Pineri, M.; Volino, F., Rod like micellar structures in perfluorinated ionomer solutions. *J. Phys.* **1988**, *49*, 2101.

74. Kumar, S.; Pineri, M., Interpretation of small-angle x-ray and neutron scattering data for perfluorosulfonated ionomer membranes. *J. Polym. Sci. Part B Polym. Phys.* **1986**, *24*, 1767.

75. Litt, M. In *Abstracts of Papers of the American Chemical Society*; AMER CHEMICAL SOC 1155 16TH ST, NW, WASHINGTON, DC 20036: 1997; Vol. 213, p 33.

76. Haubold, H. G.; Vad, T.; Jungbluth, H.; Hiller, P., Nano structure of NAFION: a SAXS study. *Electrochim. Acta* **2001**, *46*, 1559.

77. Gebel, G.; Lambard, J., Small-Angle Scattering Study of Water-Swollen Perfluorinated Ionomer Membranes. *Macromolecules* **1997**, *30*, 7914.

78. Gebel, G., Structural evolution of water swollen perfluorosulfonated ionomers from dry membrane to solution. *Polymer* **2000**, *41*, 5829.

79. Gebel, G.; Diat, O., Neutron and X-ray Scattering: Suitable Tools for Studying Ionomer Membranes. *Fuel Cells* **2005**, *5*, 261.

80. Rollet, A. L.; Gebel, G.; Simonin, J. P.; Turq, P., A SANS determination of the influence of external conditions on the nanostructure of nafion membrane. *J. Polym. Sci. Part B Polym. Phys.* **2001**, *39*, 548.

81. Rollet, A.-L.; Diat, O.; Gebel, G., A new insight into Nafion structure. *J. Phys. Chem. B* **2002**, *106*, 3033.

82. Rubatat, L.; Diat, O., Stretching effect on Nafion fibrillar nanostructure. *Macromolecules* **2007**, *40*, 9455.

83. Rubatat, L.; Rollet, A.; Diat, O.; Gebel, G., Characterization of ionomer membrane structure (NAFION) by small-angle X-ray scattering. *J. Phys. IV* **2002**, *12*, 197.

84. Rubatat, L.; Gebel, G.; Diat, O., Fibrillar Structure of Nafion: Matching Fourier and Real Space Studies of Corresponding Films and Solutions. *Macromolecules* **2004**, *37*, 7772.

85. Rubatat, L.; Rollet, A. L.; Gebel, G.; Diat, O., Evidence of Elongated Polymeric Aggregates in Nafion. *Macromolecules* **2002**, *35*, 4050.

86. Kim, M.-H.; Glinka, C. J.; Grot, S. A.; Grot, W. G., SANS Study of the Effects of Water Vapor Sorption on the Nanoscale Structure of Perfluorinated Sulfonic Acid (NAFION) Membranes. *Macromolecules* **2006**, *39*, 4775.

87. Schmidt-Rohr, K.; Chen, Q., Parallel cylindrical water nanochannels in Nafion fuel-cell membranes. *Nat. Mater.* **2008**, *7*, 75.

88. Kreuer, K. D., On the development of proton conducting polymer membranes for hydrogen and methanol fuel cells. *J. Membr. Sci.* **2001**, *185*, 29.

89. Van der Heijden, P.; Rubatat, L.; Diat, O., Orientation of drawn Nafion at molecular and mesoscopic scales. *Macromolecules* **2004**, *37*, 5327.

90. Elliott, J. A.; Wu, D.; Paddison, S. J.; Moore, R. B., A unified morphological description of Nafion membranes from SAXS and mesoscale simulations. *Soft Matter* **2011**, *7*, 6820.

91. Chen, Q.; Schmidt-Rohr, K., 19F and 13C NMR signal assignment and analysis in a perfluorinated ionomer (Nafion) by two-dimensional solid-state NMR. *Macromolecules* **2004**, *37*, 5995.

92. Kreuer, K. D.; Portale, G., A critical revision of the nano-morphology of proton conducting ionomers and polyelectrolytes for fuel cell applications. *Adv. Funct. Mater.* **2013**, *23*, 5390.

93. Feng, S.; Savage, J.; Voth, G. A., Effects of polymer morphology on proton solvation and transport in proton-exchange membranes. *J. Phys. Chem. C* **2012**, *116*, 19104.

94. Savage, J.; Voth, G. A., Proton solvation and transport in realistic proton exchange membrane morphologies. *J. Phys. Chem. C* **2016**, *120*, 3176.

95. Allen, F. I.; Comolli, L. R.; Kusoglu, A.; Modestino, M. A.; Minor, A. M.; Weber, A. Z., Morphology of hydrated as-cast nafion revealed through cryo electron tomography. *ACS Macro Lett.* **2015**, *4*, 1.

96. Kusoglu, A.; Weber, A. Z., New Insights into Perfluorinated Sulfonic-Acid Ionomers. *Chem. Rev.* **2017**, *117*, 987.

97. Divisek, J.; Eikerling, M.; Mazin, V.; Schmitz, H.; Stimming, U.; Volfkovich, Y. M., A Study of Capillary Porous Structure and Sorption Properties of Nafion Proton-Exchange Membranes Swollen in Water. *J. Electrochem. Soc.* **1998**, *145*, 2677.

98. Kononenko, N.; Fomenko, M.; Volfkovich, Y. M., Structure of perfluorinated membranes investigated by method of standard contact porosimetry. *Adv. Colloid Interface Sci.* **2015**, *222*, 425.

99. Koter, S., The equivalent pore radius of charged membranes from electroosmotic flow. *J. Membr. Sci.* **2000**, *166*, 127.

100. von Kraemer, S.; Sagidullin, A. I.; Lindbergh, G.; Furó, I.; Persson, E.; Jannasch, P., Pore Size Distribution and Water Uptake in Hydrocarbon and Perfluorinated Proton-Exchange Membranes as Studied by NMR Cryoporometry. *Fuel Cells* **2008**, *8*, 262.

101. Mathias, M. F.; Makharia, R.; Gasteiger, H. A.; Conley, J. J.; Fuller, T. J.; Gittleman, C. J.; Kocha, S. S.; Miller, D. P.; Mittelsteadt, C. K.; Xie, T., Two fuel cell cars in every garage? *Electrochem. Soc. Interface* **2005**, *14*, 24.

102. Chemours unveils new Nafion™ membrane for mobility fuel cells. *Fuel Cells Bulletin* **2019**, *2019*, 14.

103. Zawodzinski, T. A.; Springer, T. E.; Davey, J.; Jestel, R.; Lopez, C.; Valerio, J.; Gottesfeld, S., A comparative study of water uptake by and transport through ionomeric fuel cell membranes. *J. Electrochem. Soc.* **1993**, *140*, 1981.

104. Ezzell, B. R.; Carl, W. P.; Mod, W. A.; Google Patents: 1983.

105. Ezzell, B. R.; Carl, W. P.; Mod, W. A.; Google Patents: 1986.

106. Ezzell, B. R.; Carl, W. P.; Mod, W. A.; Google Patents: 1984.

107. Ezzell, B. R.; Carl, W. P.; Mod, W. A.; Google Patents: 1984.

108. Tant, M.; Lee, K.; Darst, K.; Martin, C., Effect of side-chain length on the properties of perfluorocarbon ionomers. *Polym. Mater. Sci. Eng* **1988**, *58*, 1074.

109. Tant, M. R.; Darst, K. P.; Lee, K. D.; Martin, C. W. In *Multiphase Polymers: Blends and Ionomers*, Structure and Properties of Short-Side-Chain Perfluorosulfonate Ionomers; American Chemical Society: 1989; Vol. 395, p 370.

110. Moore, R. B.; Martin, C. R., Morphology and chemical properties of the Dow perfluorosulfonate ionomers. *Macromolecules* **1989**, *22*, 3594.

111. Prater, K., The renaissance of the solid polymer fuel cell. *JPS* **1990**, *29*, 239.

112. Eisman, G., The application of a new perfluorosulfonic acid ionomer in proton-exchange membrane fuel cells: new ultra-high current density capabilities. *Fuel Cell Technology and Applications, PED Management Office for Energy Research, the Netherlands* **1987**, 287.

113. Merlo, L.; Ghielmi, A.; Cirillo, L.; Gebert, M.; Arcella, V., Resistance to peroxide degradation of Hyflon® Ion membranes. *J. Power Sources* **2007**, *171*, 140.

114. Arcella, V.; Ghielmi, A.; Merlo, L.; Gebert, M., Membrane electrode assemblies based on perfluorosulfonic ionomers for an evolving fuel cell technology. *Desalination* **2006**, *199*, 6.

115. Arcella, V.; Troglia, C.; Ghielmi, A., Hyflon ion membranes for fuel cells. *Ind. Eng. Chem. Res.* **2005**, *44*, 7646.

116. Ghielmi, A.; Vaccarono, P.; Troglia, C.; Arcella, V., Proton exchange membranes based on the short-side-chain perfluorinated ionomer. *J. Power Sources* **2005**, *145*, 108.

117. Stassi, A.; Gatto, I.; Passalacqua, E.; Antonucci, V.; Arico, A.; Merlo, L.; Oldani, C.; Pagano, E., Performance comparison of long and short-side chain perfluorosulfonic membranes for high temperature polymer electrolyte membrane fuel cell operation. *J. Power Sources* **2011**, *196*, 8925.

118. Guerra, M. A.; Google Patents: 2003.

119. Rivard, L.; Pierpont, D.; Freemeyer, H.; Thaler, A.; Hamrock, S. In *Fuel cell seminar, Miami Beach* 2003.

120. Healy, J.; Hayden, C.; Xie, T.; Olson, K.; Waldo, R.; Brundage, M.; Gasteiger, H.; Abbott, J., Aspects of the chemical degradation of PFSA ionomers used in PEM fuel cells. *Fuel cells* **2005**, *5*, 302.

121. Maalouf, M.; Sun, C.-N.; Pyle, B.; Emery, M.; Haugen, G. M.; Hamrock, S. J.; Zawodzinski Jr, T. A., Factors enabling high mobility of protons and water in perfluorosulfonate membranes under low hydration conditions. *Int. J. Hydrog. Energy* **2014**, *39*, 2795.

122. Wu, D.; Paddison, S. J.; Elliott, J. A.; Hamrock, S. J., Mesoscale modeling of hydrated morphologies of 3M perfluorosulfonic acid-based fuel cell electrolytes. *Langmuir* **2010**, *26*, 14308.

123. Wu, D.; Paddison, S. J.; Elliott, J. A., Effect of molecular weight on hydrated morphologies of the short-side-chain perfluorosulfonic acid membrane. *Macromolecules* **2009**, *42*, 3358.

124. Kusoglu, A.; Dursch, T. J.; Weber, A. Z., Nanostructure/Swelling Relationships of Bulk and Thin-Film PFSA Ionomers. *Adv. Funct. Mater.* **2016**, *26*, 4961.

125. Schaberg, M. S.; Abulu, J. E.; Haugen, G. M.; Emery, M. A.; O'Conner, S. J.; Xiong, P. N.; Hamrock, S., New Multi Acid Side-Chain Ionomers for Proton Exchange Membrane Fuel Cells. *ECS Trans.* **2010**, *33*, 627.

126. Koppel, I. A.; Taft, R. W.; Anvia, F.; Zhu, S.-Z.; Hu, L.-Q.; Sung, K.-S.; DesMarteau, D. D.; Yagupolskii, L. M.; Yagupolskii, Y. L., The gas-phase acidities of very strong neutral Bronsted acids. *J. Am. Chem. Soc.* **1994**, *116*, 3047.

127. Yandrasits, M.; Lindell, M.; Schaberg, M.; Kurkowski, M., Increasing fuel cell efficiency by using ultra-low equivalent weight ionomers. *Electrochem. Soc. Interface* **2017**, *26*, 49.

128. Hamrock, S. J. *Membranes and MEA's for Dry, Hot Operating Conditions*, 3M Company, 2011.

129. Su, G. M.; Cordova, I. A.; Yandrasits, M. A.; Lindell, M.; Feng, J.; Wang, C.; Kusoglu, A., Chemical and Morphological Origins of Improved Ion Conductivity in Perfluoro Ionene Chain Extended Ionomers. *J. Am. Chem. Soc.* **2019**.

130. Shrivastava, U. N.; Fritzsche, H.; Karan, K., Interfacial and Bulk Water in Ultrathin Films of Nafion, 3M PFSA, and 3M PFIA Ionomers on a Polycrystalline Platinum Surface. *Macromolecules* **2018**, *51*, 9839.

131. Atrazhev, V. V.; Astakhova, T. Y.; Sultanov, V. I.; Perry, M. L.; Burlatsky, S. F., Molecular Dynamic Study of Water-Cluster Structure in PFSA and PFIA Ionomers. *J. Electrochem. Soc.* **2017**, *164*, F1265.

132. Clark II, J. K.; Paddison, S. J., Proton dissociation and transfer in proton exchange membrane ionomers with multiple and distinct pendant acid groups: An ab initio study. *Electrochim. Acta* **2013**, *101*, 279.

133. Sengupta, S.; Pant, R.; Komarov, P.; Venkatnathan, A.; Lyulin, A. V., Atomistic simulation study of the hydrated structure and transport dynamics of a novel multi acid side chain polyelectrolyte membrane. *Int. J. Hydrog. Energy* **2017**, *42*, 27254.

134. Economou, N. J.; Barnes, A. M.; Wheat, A. J.; Schaberg, M. S.; Hamrock, S. J.; Buratto, S. K., Investigation of Humidity Dependent Surface Morphology and Proton Conduction in Multi-Acid Side Chain Membranes by Conductive Probe Atomic Force Microscopy. *J. Phys. Chem. B* **2015**, *119*, 14280.

135. Puskar, L.; Ritter, E.; Schade, U.; Yandrasits, M.; Hamrock, S.; Schaberg, M.; Aziz, E. F., Infrared dynamics study of thermally treated perfluoroimide acid proton exchange membranes. *Phys. Chem. Chem. Phys.* **2017**, *19*, 626.

136. Bawagan, A. D. O.; Hamrock, S. J.; Schaberg, M.; Yousef, I.; Ritter, E.; Schade, U., Far-infrared studies on Nafion and perfluoroimide acid (PFIA) and their alkali salts. *Vib. Spectrosc.* **2014**, *75*, 213.

137. Yandrasits, M.; Lindell, M.; Peppin, D.; Komlev, A.; Hamrock, S.; Haugen, G.; Fort, E.; Kalstabakken, K., Chemical Stability of Perfluorobis (sulfonyl) imide-Acid (PFIA) Ionomers in Open Circuit Voltage (OCV) Accelerated Test Conditions. *J. Electrochem. Soc.* **2018**, *165*, F3261.

138. Apostolo, M.; Arcella, V.; Google Patents: 2003.

139. Doyle, M.; Rajendran, G., Perfluorinated membranes. *Handbook of fuel cells* **2010**.

140. Elliott, J.; Hanna, S.; Newton, J.; Elliott, A.; Cooley, G., Elimination of orientation in perfluorinated ionomer membranes. *Polym. Eng. Sci.* **2006**, *46*, 228.

141. Moore, R. B.; Martin, C. R., Chemical and morphological properties of solution-cast perfluorosulfonate ionomers. *Macromolecules* **1988**, *21*, 1334.

142. Moore, R. B.; Cable, K. M.; Croley, T. L., Barriers to flow in semicrystalline ionomers. A procedure for preparing melt-processed perfluorosulfonate ionomer films and membranes. *J. Membr. Sci.* **1992**, *75*, 7.

143. Grot, W. G.; Google Patents: 1984.

144. Martin, C. R.; Rhoades, T. A.; Ferguson, J. A., Dissolution of perfluorinated ion-containing polymers. *Anal. Chem.* **1982**, *54*, 1639.

145. Yeo, R. S., Dual cohesive energy densities of perfluorosulphonic acid (Nafion) membrane. *Polymer* **1980**, *21*, 432.

146. Maccone, P.; Zompatori, A.; Google Patents: 2001.

147. Gebel, G.; Loppinet, B., Colloidal structure of ionomer solutions in polar solvents. *J. Mol. Struct.* **1996**, *383*, 43.

148. Loppinet, B.; Gebel, G., Rodlike Colloidal Structure of Short Pendant Chain Perfluorinated Ionomer Solutions. *Langmuir* **1998**, *14*, 1977.

149. Yamaguchi, M.; Matsunaga, T.; Amemiya, K.; Ohira, A.; Hasegawa, N.; Shinohara, K.; Ando, M.; Yoshida, T., Dispersion of rod-like particles of nafion in salt-free water/1-propanol and water/ethanol solutions. *J. Phys. Chem. B* **2014**, *118*, 14922.

150. Welch, C.; Labouriau, A.; Hjelm, R.; Orler, B.; Johnston, C.; Kim, Y. S., Nafion in dilute solvent systems: Dispersion or solution? *ACS Macro Lett.* **2012**, *1*, 1403.

151. Kim, Y. S.; Welch, C. F.; Hjelm, R. P.; Mack, N. H.; Labouriau, A.; Orler, E. B., Origin of Toughness in Dispersion-Cast Nafion Membranes. *Macromolecules* **2015**, *48*, 2161.

152. Moore, R. B.; Martin, C. R., Procedure for preparing solution-cast perfluorosulfonate ionomer films and membranes. *Anal. Chem.* **1986**, *58*, 2569.

153. Gebel, G.; Aldebert, P.; Pineri, M., Structure and related properties of solution-cast perfluorosulfonated ionomer films. *Macromolecules* **1987**, *20*, 1425.

154. Page, K. A.; Cable, K. M.; Moore, R. B., Molecular Origins of the Thermal Transitions and Dynamic Mechanical Relaxations in Perfluorosulfonate Ionomers. *Macromolecules* **2005**, *38*, 6472.

155. Li, J.; Yang, X.; Tang, H.; Pan, M., Durable and high performance Nafion membrane prepared through high-temperature annealing methodology. *J. Membr. Sci.* **2010**, *361*, 38.

156. Yin, C.; Wang, Z.; Luo, Y.; Li, J.; Zhou, Y.; Zhang, X.; Zhang, H.; Fang, P.; He, C., Thermal annealing on free volumes, crystallinity and proton conductivity of Nafion membranes. *J. Phys. Chem. Solids* **2018**, *120*, 71.

157. Sone, Y.; Ekdunge, P.; Simonsson, D., Proton conductivity of Nafion 117 as measured by a four-electrode AC impedance method. *J. Electrochem. Soc.* **1996**, *143*, 1254.

158. Maldonado, L.; Perrin, J.-C.; Dillet, J.; Lottin, O., Characterization of polymer electrolyte Nafion membranes: Influence of temperature, heat treatment and drying protocol on sorption and transport properties. *J. Membr. Sci.* **2012**, *389*, 43.

159. Thomas, T. J.; Ponnusamy, K. E.; Chang, N. M.; Galmore, K.; Minteer, S. D., Effects of annealing on mixture-cast membranes of Nafion® and quaternary ammonium bromide salts. *J. Membr. Sci.* **2003**, *213*, 55.

160. DeLuca, N. W.; Elabd, Y. A., Nafion®/poly (vinyl alcohol) blends: effect of composition and annealing temperature on transport properties. *J. Membr. Sci.* **2006**, *282*, 217.

161. Hensley, J. E.; Way, J. D., The relationship between proton conductivity and water permeability in composite carboxylate/sulfonate perfluorinated ionomer membranes. *J. Power Sources* **2007**, *172*, 57.

162. Liu, Y.; Horan, J. L.; Schlichting, G. J.; Caire, B. R.; Liberatore, M. W.; Hamrock, S. J.; Haugen, G. M.; Yandrasits, M. A.; Seifert, S.; Herring, A. M., Small-Angle X-ray Scattering Study of the Development of Morphology in Films Formed from the 3M Perfluorinated Sulfonic Acid Ionomer. *Macromolecules (Washington, DC, U. S.)* **2012**, *45*, 7495.

Chapter 2.

Thermal Transitions and Mechanical Relaxations in Perfluorinated Ionomers

(*Published in Fluoropolymers: Synthesis and Characterization*)

Christina M. Orsino[a] and Robert B. Moore[a]*

[a] *Department of Chemistry, Macromolecules Innovation Institute, Virginia Tech, Blacksburg, VA 24060*

**To whom correspondence should be addressed: rbmoore3@vt.edu*

2.1 Introduction to Perfluorinated Ionomers

Perfluorosulfonic acid ionomers (PFSAs) are a class of ionic fluoropolymers that consist of runs of tetrafluoroethylene containing up to ca. 22 mol percent perfluorovinyl ether sidechains terminated with pendant sulfonic acid groups.[1,2] The polar sidechains have been shown to assemble into aggregates, leading to a phase-separated "cluster" morphology where the polar ionic domains are dispersed and interconnected throughout the nonpolar poly(tetrafluoroethylene) (PTFE) matrix.[3] This phase separation between the polar and nonpolar domains provides pathways for proton conduction through the percolating ionic domains, facilitated by uptake of water into the membrane. In addition, sufficient runs of PTFE in the polymer backbone allow for crystallizability (unit cell dimensions identical to pure PTFE[4,5]) that provides mechanical integrity to the membranes and limits water swelling.[6,7]

PFSAs are used in a wide range of applications including chlor-alkali cells,[8-12] fuel cells,[13-18] batteries,[19,20] actuators,[21-23] solar cell electrolytes,[24] and in solid acid catalysis.[25] Nafion (now a product of Chemours) has been the benchmark PFSA since its creation in the late 1960s by Walther Grot of Dupont.[1] It has been the most widely studied material for use in proton exchange

membrane fuel cell (PEMFC) applications, and is widely recognized as the benchmark membrane in the PEMFC field.[1] While Nafion dominates in the literature, alternative perfluorinated ionomers continue to be developed with differing sidechain chemistries and higher ion exchange capacities (IECs) in an attempt to optimize functionality, transport properties, and electrochemical performance while maintaining mechanical stability. These alternative PFSAs include 3M's perfluorosulfonic acid (3M PFSA) and perfluoroimide acid (3M PFIA) ionomers, Solvay's Aquivion (formerly Dow SSC), and Asahi Glass' Flemion, (**Figure 2-1**) and are of increasing interest due to their desirable transport properties and application performance.[15,26]

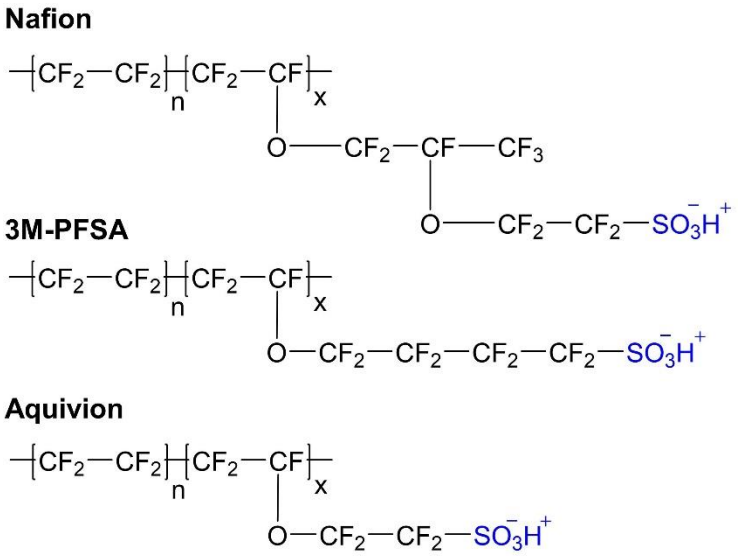

Figure 2-1. Chemical structure for common PFSAs.

In addition to varying sidechain structure, morphology and properties of PFSAs can be systematically manipulated by changing the length of TFE units between sidechains, or equivalent weight (EW). EW is defined as the grams of polymer per mol of ion exchange groups, which is inversely proportional to ion exchange capacity (IEC). EW is directly related to the average number of TFE units per side chain, *n*, by the equation $EW = 100n + MW_{sidechain}$ (mass of one TFE

unit is ca. 100 g/mol). Since the TFE units are crystallizable, and the PFSA copolymers are presumed to be random, it is recognized that crystallizability decreases significantly with decreasing TFE content (i.e., increasing sidechain content). By this relationship, for a given EW value, PFSAs containing shorter sidechains (lower $MW_{sidechain}$) will contain longer lengths of TFE units and thus have higher crystallizability.

Since the first report of glass transition data for Nafion back in 1977,[27] numerous studies have been conducted in an attempt to assign the underlying origins of the multiple thermal transitions and mechanical relaxations for these materials. Because of the high temperatures encountered in membrane processing and in application as proton exchange membranes in PEMFCs, it is necessary to have accurate assignments of the thermomechanical properties for PFSAs. Fundamental understanding of the underlying molecular-level and morphological origins of the thermomechanical relaxations is crucial to developing a full picture of the structure-property relationships for these materials. By combining multiple techniques to measure the thermal, viscoelastic, and dielectric properties of these ionomers, a general consensus is emerging within the last 20 years on the assignment of these relaxations. However, with the continuing development of new PFSAs with various sidechain structures and EWs, it is more important now than ever to have a clear understanding of the effect of ionomer structure and processing conditions on the thermomechanical properties for these complex materials.

This review serves as a historical perspective on the assignment of the thermal transitions and mechanical relaxations in PFSAs, in addition to a summary of the current perspectives and continuing work being done. Polymer characterization techniques including differential scanning calorimetry (DSC), dynamic mechanical analysis (DMA), and dielectric spectroscopy have been correlated with data from complementary techniques to provide fundamental information on the

molecular-level and morphological origins of the transition temperatures in PFSAs. This provides valuable information on the effect of sidechain structure, degree of hydration, EW, and processing conditions on the thermal properties of these ionomers.

2.2 Thermomechanical Characterization

2.2.1 Differential Scanning Calorimetry

Differential scanning calorimetry (DSC) has been used to investigate the thermal behavior of PFSAs including melting temperature (T_m), crystallization temperature (T_c), and T_g. Early DSC studies conducted on H^+-form and Na^+ neutralized PFSA materials reported two endothermic peaks below 300°C in the first heat as shown in **Figure 2-2**.[5,27-30] These two endothermic peaks were initially correlated to two thermomechanical relaxations that were observed around the same temperature, T_α and T_β, by dynamic mechanical analysis. Kyu, Hashiyama, and Eisenberg[31] assigned the two endothermic events observed by DMA and DSC to the glass transition of the matrix ($T_{g,m}$ ~ 140°C) and the glass transition of the ionic clusters ($T_{g,c}$ ~ 240°C). This assignment was further confirmed by Moore and Martin[5] when upon changing the counterion associated with the ionic clusters, the high temperature endotherm shifted dramatically. In these studies, the high temperature endotherm was shown to shift in temperature as a result of counterion type and processing conditions, leading to the assignment of this endotherm to the glass transition temperature of the ionic clusters, $T_{g,c}$.

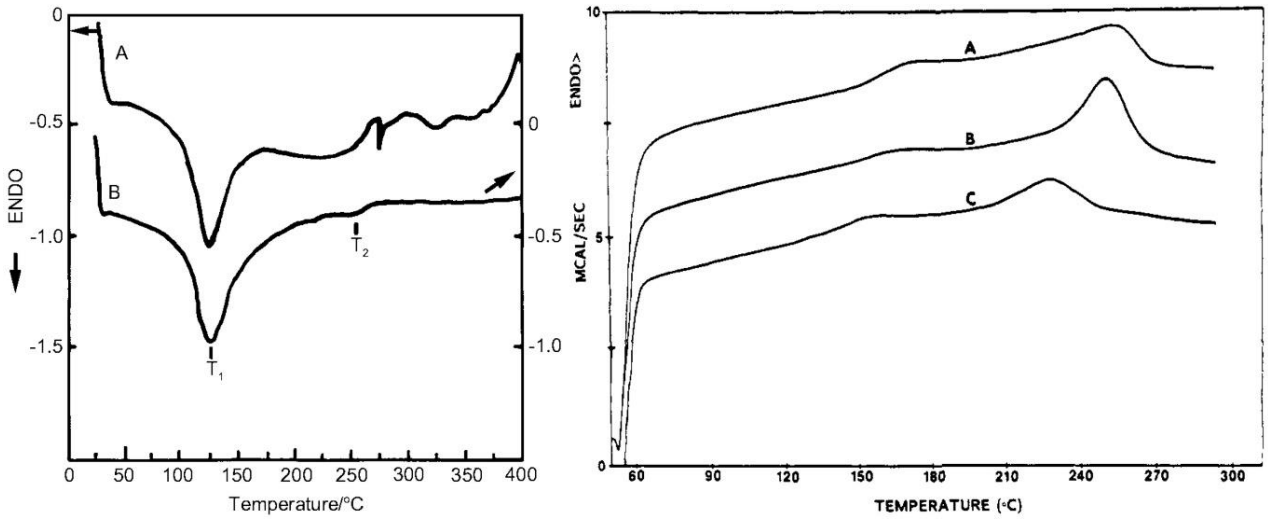

Figure 2-2. Example DSC thermograms for Nafion. Thermogram on left is from de Almeida's paper showing H+-form Nafion (A) first heat and Na+-form Nafion (B) first heat. Thermograms on right are from Moore & Martin 1988 showing Na+-form extruded Nafion (A), solution cast Nafion (B) and recast Nafion (C). The two endotherms appearing in both thermograms were initially attributed to the glass transition of the matrix and the ionic clusters at low and high temperatures, respectively. (Left) Reprinted by permission from Springer Nature.[28] (Right) Reprinted with permission from American Chemical Society.[5]

In a study conducted on the Dow short sidechain ionomer (Dow SSC, now Solvay Aquivion) membranes, Moore and Martin[32] observed two or three endotherms depending on EW. The first (ca. 150-180ºC) and second (ca. 270-300ºC) endotherms were assigned to the matrix glass transition and the ionic cluster glass transition, respectively following previous assignments. The third endotherm (ca. 335ºC) was only observed in SSC polymers above 635 EW and was assigned to the melting of the PTFE crystallites. This peak was unique to the SSC membranes, occurred at nearly the same temperature as the T_m for pure PTFE, and remained relatively constant with EW, leading to the conclusion that the SSC membranes produced at that time were rather blocky as opposed to purely random in their sequences of TFE units along the chains.[32] Mauritz and Su[30] studied the effect of annealing on the Dow SSC membranes, which also showed three endothermic peaks in agreement with the study by Moore and Martin. Annealing at different temperatures

revealed changes in the DSC peaks that were attributed to increased order and structural cohesion in the matrix. Their studies showed that with increasing temperature and/or time of annealing, the matrix becomes more homogeneous and tightly packed while the sidechains become more disordered. It was also found that decreasing equivalent weight leads to an increase in the T_g of the matrix, which was previously attributed to the formation of electrostatic crosslinks hindering long-range mobility of the backbone.

In a later DSC study by de Almeida and Kawano,[28] two endothermic events were also reported for neutralized Nafion at 122°C and 230°C. The lower temperature endotherm was observed in the first heating scan, but did not reappear upon immediate second heat. After some time, the endotherm at 122°C began to gradually reappear and shift to higher temperatures with increasing aging time. Since this endotherm appeared to be directly related to counterion and degree of hydration, the authors attributed it to a transition into ionic clusters as opposed to dissociation of aggregates. Furthermore, the high temperature endotherm at ca. 230-250°C was attributed to melting of PTFE crystallites due to a loss of crystalline peak observed by WAXS after heating the samples up to 275°C.

Following the findings of the de Almeida study where the low temperature endotherm was not reproducible upon second heat, Page, Cable, and Moore[33] investigated the thermal behavior of Nafion as a function of annealing times and temperatures. The initial heat of Na^+ neutralized Nafion membranes showed a broad endotherm between 200 and 250ºC that disappeared upon reheat, confirming the observation reported by de Almeida and Kawano.[28] This endotherm could be induced to reappear by annealing at 200ºC for various lengths of time, with increasing heat of fusion (ΔH) as the annealing time increased. Semicrystalline polymers with slow crystallization kinetics exhibit this same annealing/melting behavior and thus the high temperature endothermic

peak was attributed to the melting of PTFE crystallites in the presence of an electrostatic network.[33] An additional endothermic peak was observed in the Cs^+-form at ca. 100°C that also disappeared upon second heat. Upon annealing for 2 hours at increasing temperatures, this endotherm was observed to shift to ca. 20-30°C above the respective annealing temperature while the high temperature endotherm remained constant. These observations led to the conclusion that the lower temperature endotherm is due to melting of crystallites formed in the sample due to annealing conditions rather than the Tg of the fluorocarbon matrix as previously assigned.[33]

Despite conflicting assignments of the endothermic events, DSC is still used as a technique to characterize the thermal transitions in PFSAs. In a study published in 2013, Giffin and coworkers[34] used modulated DSC to investigate the effect of hydration on the thermal transitions in 3M-PFSA. In the total heat flow thermogram, they reported one endothermic event between −40 and −55 °C, and a second between 15 and 40 °C. They assigned the lower temperature transition as β and associated it with the ether moiety in the sidechain due to its similarity in temperature to the glass transition temperature of poly(oxatetrafluoroethylene). The endotherm between 15 and 40 °C, α, was attributed to $13_6 \rightarrow 15_7$ helical and conformational transformations in the PTFE domains, or segmental motions of the motion of the polymer backbone. In addition to the α and β-transitions, they noted a broad third transition, α_{pc}, between 50 and 100 °C that was assigned to long-range motions of the polymer backbone and sidechains upon weakening of the electrostatic crosslinks between sulfonate groups.

Given the vastly different interpretations over the years of the origins of thermal events in DSC data from PFSAs, it is important to note that first scan thermograms of any polymer are often plagued by artifacts. This is particularly true for H^+-form PFSAs, where residual water (tightly associated with the polar sulfonic acid groups) in even “dry” samples can dissociate/evaporate

over a wide range of temperatures (e.g., 50 to 200 °C) resulting in a broad endothermic event that is not observed upon second heat. Thus, careful consideration of the sample drying conditions prior to analysis must be given to eliminate the water artifact in these materials.

2.2.2 Dynamic Mechanical Analysis

The thermomechanical relaxations in Nafion have been extensively studied by dynamic mechanical analysis (DMA), which provides detailed information on thermomechanical relaxations with respect to the storage modulus (E'), loss modulus (E"), and loss tangent (tanδ). This method is known to be more sensitive to phase behavior of the ionic domains relative to DSC. DMA has often been utilized to determine the glass transition temperatures of perfluorinated ionomers by applying an oscillating force to the sample and measuring the ionomers' response to that force as it is heated over a temperature range.[35]

Dynamic mechanical relaxations in PFSAs and their sulfonyl fluoride precursors have been the subject of a many investigations since 1977.[7,15,26,27,29,31,33,35-50] The precursor to PFSAs contains a nonionic pendant SO_2F group that is then hydrolyzed to form the SO_3H ionomer. In an in-depth study by Hodge and Eisenberg conducted on the sulfonyl fluoride precursor to Nafion, three major dynamic mechanical relaxations were observed.[29] The lowest relaxation, γ, at ca. −190°C was attributed to rotations of the SO_2F group, while the β relaxation observed in the temperature range −100 to −20°C was attributed to backbone and sidechain motions. The dominant α relaxation at ca. 20°C was assigned as the glass transition temperature of the polymer.

The physical properties of the sulfonyl fluoride precursor are altered drastically upon hydrolysis to the SO_3H form as shown in **Figure 2-3**. In the tanδ data for H^+-form Nafion, three relaxations are observed over the temperature range of −160 to 150°C, assigned as α, β, and γ relaxations. An α-relaxation occurs at ca. 100°C, small β-relaxation at ca. 20°C that shifts to lower

temperatures with increasing water content,[27] and a γ-transition around -100°C. The α- and β-relaxation temperatures increase by over 100°C when counterion-exchanged from SO_3H to SO_3X ($X=Na^+$) but the γ relaxation remains the same,[31] indicating that the low temperature transition is due to short-range molecular motions in the PTFE backbone.[1]

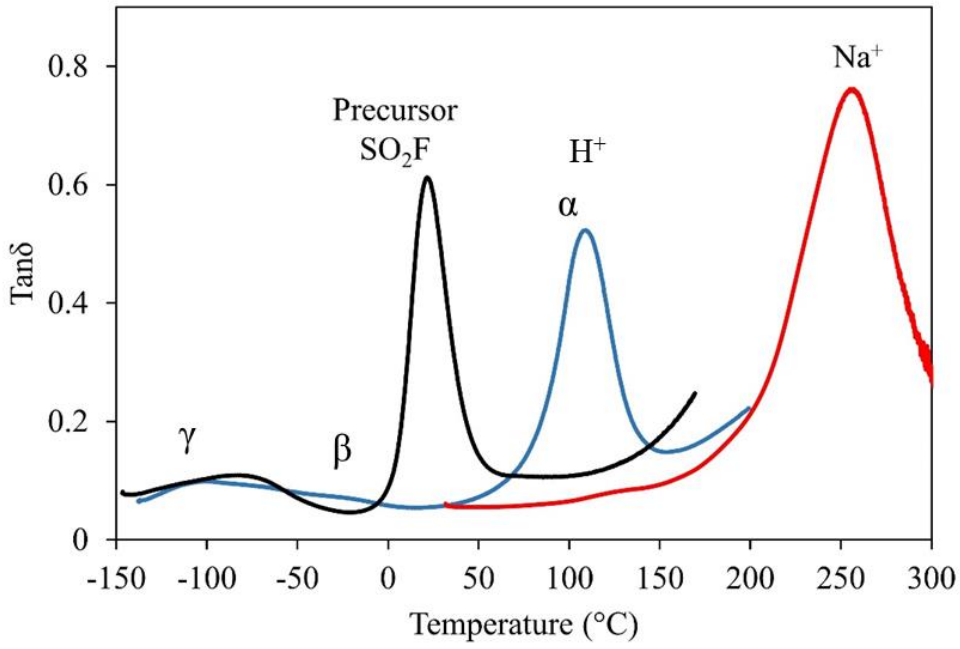

Figure 2-3. Dynamic mechanical analysis tanδ data for Nafion 117 in the precursor SO_2F form, H^+ ionomer-form and neutralized with Na^+ counterion.

Assignment of the molecular origins of the α- and β-relaxations in Nafion has been the subject of a large debate over the years while the assignment of the γ-relaxation to short-range motions of the polymer backbone has remained uncontested. In an early study by Yeo and Eisenberg, the β-relaxation was attributed to the relaxation of ionic domains due to its strong dependence on water content, and the α-relaxation was attributed to the glass transition of the fluorocarbon matrix.[27] In a later study by Kyu and Eisenberg conducted on partially ionized and neutralized Nafion, those assignments were reversed.[31] Tant and coworkers observed a thermomechanical relaxation at 100

°C, but did not observe a secondary relaxation at 0 °C as described by the earlier studies.[51] They assigned the 100 °C relaxation to main chain motions that are restricted by ionic crosslinks since the same transition was observed in the sulfonyl fluoride form at lower temperatures. Miura and Yoshida conducted a study that looked at the effect of solvents and different counterions on the molecular motions in Nafion and confirmed Kyu and Eisenberg's earlier assignment of the α-relaxation to motions within the polar clusters.[52]

Page, Cable, and Moore[33] conducted an in-depth study on various Nafion membranes including acid-form, sodium and cesium-form, and different alkylammonium counterions to study the effect of counterion on the thermomechanical properties of Nafion in attempt to assign the molecular origins of these transitions. It was concluded that the α-relaxation was due to chain motions near or in the ionic domains, and the β-relaxation was due to amorphous PTFE chains further from the aggregates.[33] The results of this study also showed that when Nafion is neutralized with large alkylammonium ions, the α- and β-relaxations shift to lower temperatures, indicating a plasticizing effect of the larger organic counterions. Page, Cable, and Moore correlated DMA data with solid state ^{19}F NMR and SAXS experiments to conclude that the α-relaxation is attributed to the onset of long-range mobility of chains/sidechains as a result of destabilization of the electrostatic network (i.e., chain motions within a dynamic electrostatic network) while the β-relaxation is attributed to the onset of segmental motions of the polymer chains within a static electrostatic network.[33] These assignments were also confirmed in a separate study by performing partial neutralization of Nafion with TBA^+ and Na^+ counterions.[53]

While previous assignments of the mechanical relaxations in Nafion were made on neutralized membranes, Osborn and coworkers[50] worked to assign the β-transition in H^+-form Nafion to the true T_g by conducting a study evaluating the peak dependence on degree of neutralization. It was

observed that the α- and β-relaxations of Nafion neutralized with tetrabutylammonium (TBA^+) counterions were at 115 °C and 75 °C, respectively. H^+-form Nafion displayed an α-relaxation at 100 °C and a weak peak near −20 °C. While the peak at −20 °C was assigned as the β-relaxation by convention, it was unclear whether it had the same molecular origins as the β-relaxation observed in neutralized Nafion. Invoking rule-of-mixture concepts, Osborn and coworkers conducted DMA studies on a series of H^+-form Nafion membranes partially neutralized with TBA^+ counterions. The β-relaxation temperature was shown to be compositionally dependent on the degree of neutralization with TBA^+, while the α-relaxation temperature remained independent. This behavior suggested that the molecular origin of the β-relaxation is the same in H^+-form as it is in TBA^+-form and was therefore assigned as the genuine T_g of Nafion.[50]

DMA appears to be the most sensitive technique for detecting all three thermal relaxations in PFSA membranes. At this time, a general consensus has been made about the assignments of the α-, β-, and γ-relaxations observed by DMA. This provides a very valuable tool for investigating the effect of structure, morphology, and processing on the mechanical relaxations in these materials. Further work on the effect of sidechain structure, EW, processing methods, and hydration has been done and is discussed further in Section 3. Current Perspectives on the Glass Transition Temperature in Perfluorinated Ionomers.

2.2.3 Dielectric Spectroscopy

Dielectric spectroscopy (DES) is a technique used to investigate the dielectric properties of PFSAs for determination of dielectric relaxations, which provides information that is complementary to that of dynamic mechanical analysis.[30,34,50,54-56] Many of the studies mentioned above correlate dielectric loss tanδ data to the dynamic mechanical tanδ data and will be discussed briefly here.

In an early dielectric study by Hodge and Eisenberg[29] on the Nafion sulfonyl fluoride precursor, the dielectric loss ε" at different frequencies was investigated. Three distinct peaks were observed and labeled γ, β, and α in order of increasing temperature. The α-transition was assigned to the glass transition temperature of the polymer due to its high activation energy in DES and decrease in mechanical modulus observed by DMA. The β-transition was associated with the fluorocarbon backbone and sidechains due to its high mechanical intensity observed by DMA and low dielectric strength. Lastly, the γ-relaxation was observed to be the most intense dielectric relaxation but a very weak mechanical relaxation as observed by DMA and was ultimately assigned to SO_2F group motions. Initial studies by Yeo and Eisenberg[27] on H^+-form Nafion displayed only two dielectric peaks, both in the β-relaxation temperature region.[27] The γ-relaxation was said to be dielectrically inactive and the α-relaxation difficult to observe due to fast desorption rate of water above room temperature. Due to the dielectric β-relaxation dependence on water content, it was assigned as the glass transition of the polar regions. The observation of β-relaxation by dielectric spectroscopy and its assignment to the glass transition of the aqueous domains was also confirmed by Starkweather and Chang[57] and Chen, Jayakody, and Greenbaum.[58]

In a series of studies conducted by Di Noto and coworkers,[34,59,60] dielectric broadband spectroscopy was used to investigate conductivity in terms of dielectric relaxations in Nafion and 3M-PFSA membranes. In these studies, a low-frequency relaxation peak was assigned as the α-relaxation mode and a peak at higher frequencies was assigned as the β-relaxation mode. The dielectric α-relaxation mode was defined as the "dynamic glass transition" attributed to segmental motions of PTFE backbone and correlated to the dynamic mechanical β-relaxation. The high frequency dielectric β-relaxation was thus associated with the dynamic mechanical α-relaxation and attributed to relaxations within the polar sulfonate crosslinks in Nafion.[59,60] In a later study

conducted on 3M-PFSA of different EWs, all three relaxations were observed in the dielectric tanδ data.[34] The lowest temperature relaxation, γ-relaxation, was attributed to local fluctuations of the TFE backbone while the β- and α-relaxations were assigned to conformational transitions of the sidechain and polymer segmental motion upon diffusion of conformational states in the TFE backbone, respectively. Further, both dielectric relaxation modes were said to be strongly coupled together.

Dielectric spectroscopy was also used by Osborn and coworkers[61] to confirm the assignment of the β-transition in acid-form Nafion to the genuine glass transition. A dielectric relaxation was observed at −20 °C in H^+-form Nafion that was also observed in the dynamic mechanical spectra. The Vogel-Fulcher-Tammann (VFT) equation, which fits well to data for glassy polymers above the dynamic glass transition, was found to be a good fit to the data over the range of temperatures encompassing the β-transition further confirming the β-transition as the genuine glass transition in Nafion. Because dielectric spectroscopy provides complementary information to DMA, it will continue to be a useful secondary technique for probing and confirming the assignment of the thermal transitions and mechanical relaxations in PFSAs.

2.2.4 Complementary Tools to Characterize Thermal Transitions

Many different techniques have been utilized over the years to help complement and explain the origins of the thermomechanical relaxations in PFSAs. These complementary tools employ techniques that probe molecular motions and morphology over temperature ranges that encompass the α-, β-, and γ-relaxations in order to provide insight on the molecular and morphological origins of these transitions.

In a study by Page, Cable, and Moore, variable temperature small angle X-ray scattering was used as a technique to confirm the assignment of the β-relaxation in neutralized Nafion as the true

glass transition of the polymer.[33] A representative small-angle X-ray scattering pattern for PFSAs displays a maximum at ca. $q = 1 – 2\ nm^{-1}$ that is termed the "ionomer peak" consistent with inter-aggregate correlations arising from contrast in electron density between the ionic domains and the PTFE matrix.[33] A second peak is observed at lower scattering vectors (ca. $q = 0.5\ nm^{-1}$) that is attributed to scattering from ordered crystallites developed from crystallization of the PTFE runs between sidechains.[3,62] This study focused on the intensity of the crystalline peak with increasing temperature. The crystalline peak in SAXS arises from electron density contrast between the crystalline and noncrystalline domains. Below T_m, the density of the crystalline component is relatively constant, while the amorphous component expands with temperature (i.e., its electron density decreases relative to the crystalline component). As contrast increases, the crystalline peak intensity increases. Based on the work of Fischer et al., this leads to a relationship between intensity of the crystalline peak and the thermal expansion coefficient of a semicrystalline polymer.[63] For glass-forming polymers, the thermal expansion coefficient increases linearly with temperature and has an abrupt change in slope when passing through the glass transition. By plotting the intensity of the crystalline peak vs. temperature, the authors observed two linear regions with an abrupt change in slope at the same temperature as the β-transition, confirming their conclusion that the β-transition is the glass transition for Nafion.[33]

Neutron scattering has also been a useful tool for analyzing the ion-hopping phenomenon that occurs above the α-transition in Nafion. Quasielastic neutron scattering (QENS) has been used to probe the molecular dynamics of counterions in PFSAs.[64] QENS is able to directly measure counterion dynamics of alkylammonium counterions, which was used as a direct analysis of ion hopping associated with the α-transition in Nafion. This studied showed that the α-relaxation is linked to the onset of mobility of the counterions on the length-scale of 20-30 Å. At temperatures

below the α-relaxation, movement of the counterions is very local, but at temperatures above T_α, the counterion motions were observed to increase in length scale attributed to a common ionomer phenomenon known as ion-hopping (i.e., a thermally-stimulated hopping of ion-pairs between aggregates).

NMR has been a valuable technique utilized in multiple studies for assigning the molecular origins of the thermomechanical transitions in PFSAs.[33,58,65] In one study, deuteron NMR was used to look at the effect of water content on low temperature Nafion relaxations.[58] Although a glass transition was not apparent by DSC, glassy behavior at low temperatures was inferred from deuteron NMR line shape. Variable temperature fluorine-19 NMR studies have provided fundamental insight on the molecular motions of the main chain and sidechains in Nafion.[33,66-69] First, comparing line width of a single signal in ^{19}F NMR spectrum for Nafion compared to Teflon provides insight into the effect of sulfonate pendant chains on mobility at different temperatures.[66] When line widths are plotted on an Arrhenius plot, there is an apparent break in motional regimes for Nafion at ca. 112 °C, corresponding to the α-transition temperature where long range motions begin to occur. Assignment of the ^{19}F peaks for Nafion was done using two dimensional ^{13}C-^{19}F NMR heteronuclear correlation under magic-angle spinning.[69] Separate peaks are observed for the $-OCF_2$ and $-CF_3$ nuclei in the sidechain and the $-CF_3$'s in the backbone. Using these peak assignments, a later study looked at variable temperature solid state ^{19}F NMR to probe the motions of the perfluoroether sidechains with spin-diffusion and sideband analysis.[33] The authors were able to attribute changes in spin-diffusion times to changes in the mobility of the polymer by assuming that the distance between side-chain and main-chain nuclei is essentially constant. They found that with increasing counterion size, the temperature dependence of the spin diffusion time increases. The increase in spin diffusion time at a particular temperature for TMA^+ and TBA^+

form Nafion were attributed to the onset of molecular motions, in agreement with SAXS and DMA data. They also observed the appearance of sidebands due to dipolar coupling that decrease in intensity as the mobility of polymer chains increases. The sidebands were found to decrease in intensity with increasing temperature and counterion size, leading to the conclusion that there is more mobility of the polymer chains at higher temperature and with larger counterions.

Recent interest in ultrathin films of Nafion have led to new techniques for characterizing the thermomechanical transitions in films only tens to hundreds of nanometers thick.[70,71] Variable temperature ATR-FTIR of Nafion films on SiO_2/Si substrates displayed a dramatic increase of the intensity of a CF_2 wagging vibrational mode at ca. 110 °C, which was attributed to the same α-transition temperature observed in bulk Nafion.[70] Another study on Nafion thin films utilized ellipsometry to determine the coefficient of thermal expansion and the change in rate of thermal expansion, T_T.[71] It was observed that for Nafion thin films in the H^+-form, T_T had the same molecular origin as the α-transition in the bulk ionomer. Interestingly, in the neutralized Na^+- and Cs^+-form, T_T is attributed to the β-transition temperature of the bulk ionomer. This study highlighted the interplay between the surface and the electrostatic interactions controlling the ionomer thin films.

2.3 Current perspectives on the Glass Transition in Perfluorinated Ionomers

Despite the debate over the assignments of the thermomechanical relaxations in PFSAs through the years, a general consensus has been reached in the community as to the underlying origins of these relaxations. In summary, the low temperature γ-relaxation is associated with local fluctuations of the $-CF_2-$ backbone and remains independent from the α- and β-relaxations. At temperatures around the α-relaxation, significant ion hopping occurs leading to destabilization of

the electrostatic network and facilitating the onset of long-range mobility of the chains/sidechains. In contrast, the β-relaxation is attributed to the onset of segmental motions of the polymer chains within a *static* electrostatic network and is assigned as the genuine T_g of PFSAs.[33] These assignments have been made by correlating multiple techniques (discussed above) as demonstrated in **Figure 2-4**. Variable temperature SAXS data provides information on the state of ionic aggregation as a function of temperature and gives insight into the relationship between the strength of the electrostatic network and the relaxations observed by DMA. Variable temperature ^{19}F solid-state NMR then provides insight on the molecular motions that are linked to these relaxations and morphological changes. From these experiments, it was observed that the α-relaxation in DMA correlates with the drop off of ionomer peak intensity in SAXS and a large increase in NMR spin-diffusion time (i.e., an increase in molecular mobility). This led to the conclusion that the α-relaxation is attributed to long-range motions associated with destabilization of the electrostatic network facilitated by ion-hopping. Additionally, SAXS provided evidence of ionic aggregation that persists through the β-relaxation temperature observed by DMA and no abrupt changes in sidechain mobility by NMR and thus it was concluded that these motions occur within a static network of physically crosslinked chains.[33]

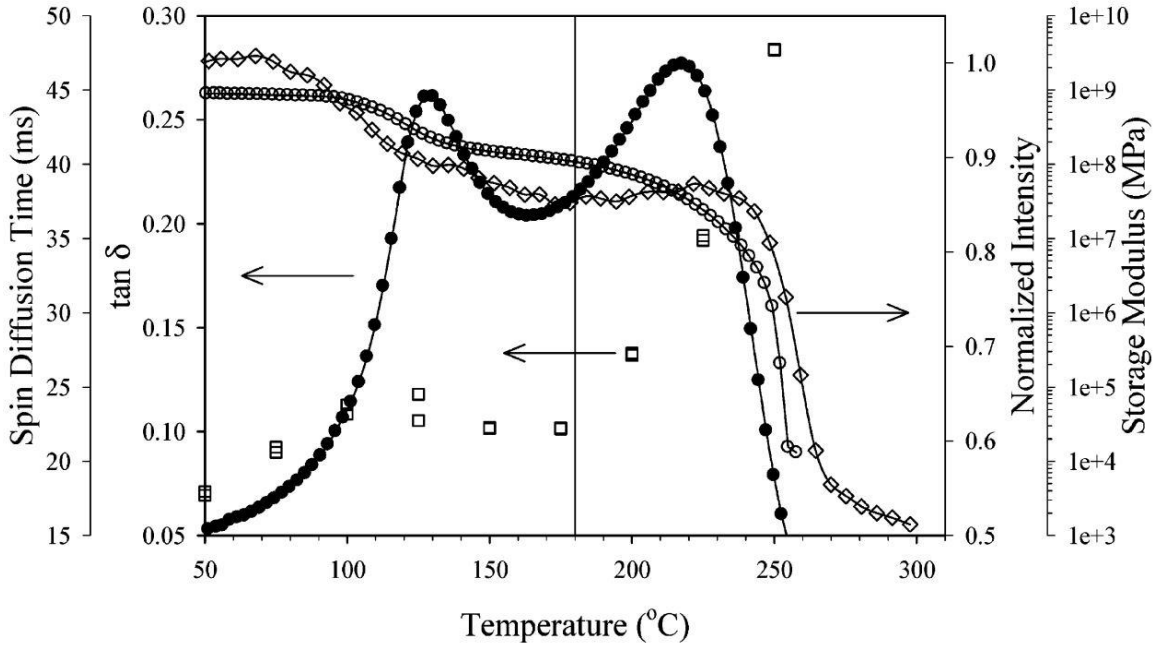

Figure 2-4. Correlations between (●) DMA Tanδ, (○) DMA storage modulus, (□) NMR spin diffusion time, and (◊) variable temperature SAXS lead to the assignments of the α- and β-relaxations in TMA^+-form Nafion. Reprinted with permission from American Chemical Society.[33]

Continuing work is being done to investigate the effect of structure, morphology, and processing on the thermomechanical transitions in PFSAs. The α- and β-relaxations are sensitive to EW, side-chain composition, annealing temperature, degree of hydration, and cation type due to their association with the motions of the sidechains, while the γ-relaxation remains relatively constant.[26,32,38,42,51,54] The α-relaxation decreases with added water content due to water plasticizing the sulfonate groups and facilitating the onset of ion hopping at lower temperatures.[27,28,59,72,73] Li, Pan, and Tang found that increasing the EW increases the temperature of the α-transition due to greater packing efficiency and restricted mobility from the longer PTFE segments between sidechains.[38] Results of this study also showed that the observed T_α for Nafion, SSC, and 3M-PFSA decreases with increasing length of sidechain (Nafion < 3M-PFSA < SSC) displayed in **Table 2-1**. Moukheiber and coworkers observed a similar trend of the α-relaxation

temperature decreasing with increasing sidechain length and attributed it to longer sidechains acting as plasticizers.[26] However, in long sidechain perfluoroimide acid ionomers (3M-PFIA, chemical structure shown in **Figure 2-5**), Schaberg and coworkers observed the α-relaxation temperature to be higher than any of the other membranes, which disagrees with the previous findings that increasing sidechain length leads to decrease in α-transition temperature.[42] It is to be noted that 3M-PFIA contains two ionic groups per sidechain that further restricts mobility.

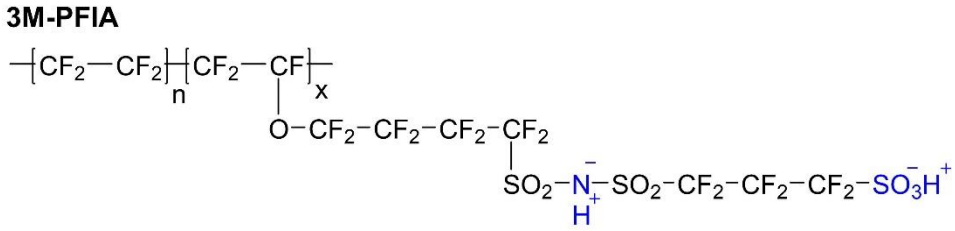

Figure 2-5. Chemical structure of 3M-PFIA containing acidic bis(sulfonyl)imide group in addition to a sulfonic acid group on each sidechain.

Table 2-1. Published relaxation temperatures for various PFSA membranes observed by dynamic mechanical analysis.

	T_α (°C)	T_β (°C)	T_γ (°C)
H^+-Nafion (1100 EW)[47,50]	100	-20 – 20	-100
H^+-SSC (850 EW)[38,47]	127	1	-98
H^+-3M-PFSA (1000 EW)[7]	125	N/A	N/A
H^+-3M-PFIA (625 EW)[42,74]	130	65	N/A

The genuine glass transition, β-relaxation, is also sensitive to water content and sidechain structure. Multiple studies have shown that the β-relaxation in H^+-form membranes is very sensitive to water and shifts to lower temperature with increasing water content due to plasticization.[27,75-77] This, of course, needs to be taken into consideration when determining the β-relaxation in new PFSAs. Lower EW PFSAs (in the H^+-form) will have a higher water content and

contain significant levels of residual water even after a drying step.[78] With some of these low EW PFSAs, the β-relaxation is very small and may be plasticized by water to low enough temperatures to overlap with the γ-transition, leading to one broad transition at temperatures around −100 °C making them difficult to assign.

The new multi-acid 3M-PFIA (**Figure 2-5**) provides a novel material for studying the effect of additional acidic sites per sidechain on the thermomechanical relaxations of PFSAs. Although they have been shown to have similar morphologies,[78] 3M-PFIA has a much more prominent relaxation in neutralized counterion forms than its "parent" 3M-PFSA ionomer.[74] Upon probing this relaxation, 3M-PFIA was found to exhibit behavior much more typical of a conventional glass forming polymer (i.e., reversible step-change in heat capacity and enthalpic recovery due to physical aging) and this thermal transition was assigned as a glass transition for 3M-PFIA. This finding leads to new questions regarding the role of the acidic bis(sulfonyl)imide group in creating a physically crosslinked network that affects backbone mobility.[74]

As cautioned above, residual water content can profoundly affect the DSC thermograms for PFSAs as shown in **Figure 2-6**. As received H^+-form Nafion 117 displays a large endotherm with a possible smaller endothermic shoulder on the first heat. However, upon equilibrating the Nafion 117 membrane at 50% relative humidity (RH) overnight, those endotherms increase in intensity. After drying the membranes thoroughly either under vacuum at 70 °C overnight, or in the DSC at 120 °C for two hours, those large endothermic events disappear suggesting that those endotherms are likely due to evaporation of water in the membranes. In membranes that were heat treated for water removal prior to running, there is a small endotherm that appears at ca. 30 °C above the temperature at which it was pretreated that disappears on second heat. As discussed in Section 2.2.1 on DSC, this is the same phenomenon was observed by Page, Cable and Moore that was

attributed to melting of small crystallites that form in the sample due to annealing conditions.[33] This data demonstrates the importance of not overinterpreting DSC thermograms for these ionomers, as the slightest change in water content or pretreatment conditions can have a drastic effect on the data.

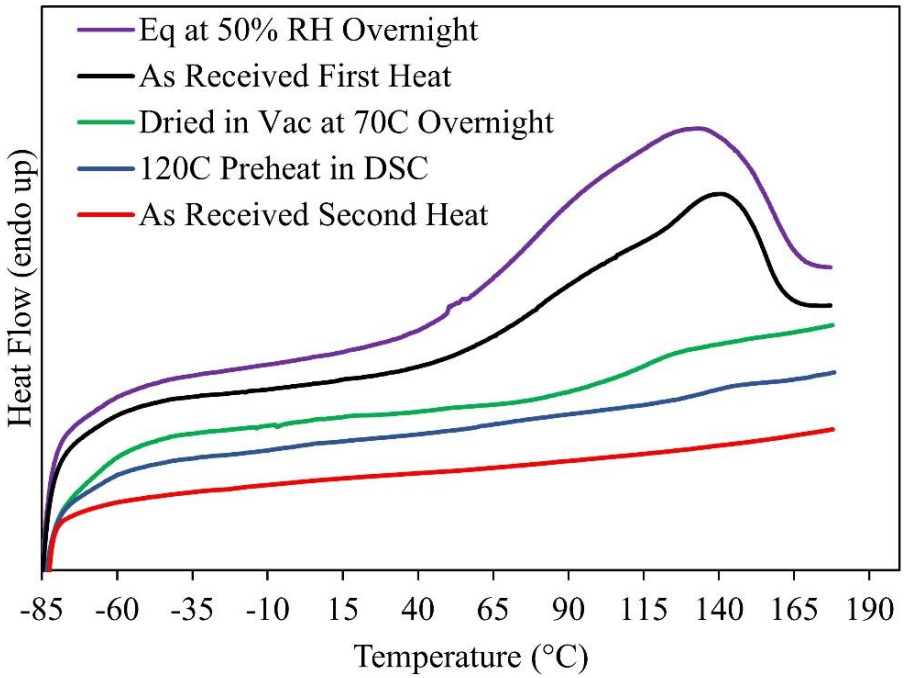

Figure 2-6. Effect of pretreatment conditions on the DSC thermogram for H^+-form Nafion 117.

While much of the PFSA scientific community has put great effort into the assignment of all of the thermomechanical relaxations in PFSAs, the insignificance of the γ- and β-relaxations when compared to the α-relaxation is of importance when considering processing and application of these ionomers at different temperatures. It is evident that the dominant relaxation in PFSAs stems from the physically crosslinked network that forms from aggregation of the sulfonate groups. Below the α-transition temperature, any molecular movements are going to be short-range, and very local segmental motions. Temperatures near or above the α-transition temperature are

required to facilitate ion hopping between sulfonate groups and ultimately destabilization of the physically crosslinked network allowing for long-range chain mobility. This means that one can expect no significant morphological reorganization at temperatures below the T_α, despite the other two thermomechanical relaxations that occur at lower temperatures.

2.4 Conclusions

This review provides a historical overview of the assignments of the thermal transition and mechanical relaxations in perfluorosulfonic acid ionomers. Although there have been multiple reviews in the area of PFSA research, the aim of this review is to provide a specific understanding of how the thermal transitions were assigned in PFSAs and how they can be related to the structure, morphology, and processing of these ionomers. In summary, three relaxations are observed in PFSAs over the temperature range of −120 °C to 120 °C in the H^+-form. The lowest temperature γ-relaxation is associated with local fluctuations of the $-CF_2-$ backbone while the β-relaxation is attributed to the onset of segmental motions of the polymer chains within a *static* electrostatic network and is assigned as the genuine T_g of PFSAs. Finally, the α-relaxation is attributed to the onset of long-range mobility of chains/sidechains as a result of destabilization of the electrostatic network. DMA and DES are sensitive and complementary techniques for probing the relaxations in these materials while DSC provides conflicting data depending on the pretreatment conditions. In addition, multiple complementary techniques including variable temperature SAXS, ^{19}F solid-state NMR, QENS, ATR-FTIR, and ellipsometry are valuable techniques utilized to help assign the molecular-level and morphological origins of thermal transitions and mechanical relaxations in these materials.

The thermally-induced onset of segmental motions is of great interest to the fuel cell community who look to process these ionomers over a range of temperatures to produce durable PEMs in fuel cells with morphologies designed to yield high thermal and chemical stability as well as high proton and water transport properties. Through this review, it is clear that the thermal properties of PFSAs can be tuned by changing sidechain structure, equivalent weight, annealing conditions, and degree of hydration. This information will be valuable moving forward in guiding the synthesis of next generation fuel cell membranes.

2.5 References

1. Mauritz, K. A.; Moore, R. B., State of Understanding of Nafion. *Chem. Rev.* **2004**, *104*, 4535.
2. Kusoglu, A.; Weber, A. Z., New Insights into Perfluorinated Sulfonic-Acid Ionomers. *Chem. Rev.* **2017**, *117*, 987.
3. Gierke, T. D.; Munn, G. E.; Wilson, F. C., The morphology in nafion perfluorinated membrane products, as determined by wide- and small-angle x-ray studies. *J. Polym. Sci., Part B: Polym. Phys.* **1981**, *19*, 1687.
4. Starkweather, H. W., Crystallinity in perfluorosulfonic acid ionomers and related polymers. *Macromolecules* **1982**, *15*, 320.
5. Moore, R. B.; Martin, C. R., Chemical and morphological properties of solution-cast perfluorosulfonate ionomers. *Macromolecules* **1988**, *21*, 1334.
6. Lai, Y.-H.; Mittelsteadt, C. K.; Gittleman, C. S.; Dillard, D. A., Viscoelastic stress analysis of constrained proton exchange membranes under humidity cycling. *J. Fuel Cell Sci. Tech.* **2009**, *6*, 021002.
7. Emery, M.; Frey, M.; Guerra, M.; Haugen, G.; Hintzer, K.; Kai; Lochhaas, H.; Pham, P.; Pierpont, D.; Schaberg, M.; Thaler, A.; Yandrasits, M.; Hamrock, S., The Development of New Membranes for Proton Exchange Membrane Fuel Cells *J. Electrochem. Soc.* **2007**, *11*, 3.
8. Gronowski, A. A.; Yeager, H. L., Factors Which Affect the Permselectivity of Nafion Membranes in Chlor-Alkali Electrolysis, I. *J. Electrochem. Soc.* **1991**, *138*, 2690.
9. Chandran, R. R.; Chin, D.-T., Reactor analysis of a chlor—alkali membrane cell. *Electrochim. Acta* **1986**, *31*, 39.
10. Yeager, H.; Kipling, B.; Dotson, R., Sodium ion diffusion in Nafion ion exchange membranes. *J. Electrochem. Soc.* **1980**, *127*, 303.

11. Jorné, J., The Anolyte Diffusion Layer and Its Effect on Hydroxyl Transport Through Nafion Membrane in Chlor-Alkali Cell. *J. Electrochem. Soc.* **1982**, *129*, 722.
12. Yeo, R. S., Ion clustering and proton transport in Nafion membranes and its applications as solid polymer electrolyte. *J. Electrochem. Soc.* **1983**, *130*, 533.
13. Barbir, F. *PEM fuel cells: theory and practice*; Academic Press, 2013.
14. Danilczuk, M.; Lancucki, L.; Schlick, S.; Hamrock, S. J.; Haugen, G. M., In-Depth Profiling of Degradation Processes in a Fuel Cell: 2D Spectral-Spatial FTIR Spectra of Nafion Membranes. *ACS Macro Lett.* **2012**, *1*, 280.
15. Hamrock, S. J.; Yandrasits, M. A., Proton Exchange Membranes for Fuel Cell Applications. *J. Macromol. Sci., Rev. Macromol. Chem. Phys.* **2006**, *46*, 219.
16. Smitha, B.; Sridhar, S.; Khan, A. A., Solid polymer electrolyte membranes for fuel cell applications—a review. *J. Membr. Sci.* **2005**, *259*, 10.
17. Steele, B. C. H.; Heinzel, A., Materials for fuel-cell technologies. *Nature* **2001**, *414*, 345.
18. Vishnyakov, V. M., Proton exchange membrane fuel cells. *Vacuum* **2006**, *80*, 1053.
19. Cheng, H.; Scott, K., Improving performance of rechargeable Li-air batteries from using Li-Nafion binder. *Electrochim. Acta* **2014**, *116*, 51.
20. Xi, J.; Wu, Z.; Teng, X.; Zhao, Y.; Chen, L.; Qiu, X., Self-assembled polyelectrolyte multilayer modified Nafion membrane with suppressed vanadium ion crossover for vanadium redox flow batteries. *J. Mater. Chem.* **2008**, *18*, 1232.
21. Kikuchi, K.; Tsuchitani, S., Nafion-based polymer actuators with ionic liquids as solvent incorporated at room temperature. *J. Appl. Phys.* **2009**, *106*, 053519.
22. Landi, B. J.; Raffaelle, R. P.; Heben, M. J.; Alleman, J. L.; VanDerveer, W.; Gennett, T., Single wall carbon nanotube-Nafion composite actuators. *Nano Letters* **2002**, *2*, 1329.

23. Jung, J.-H.; Jeon, J.-H.; Sridhar, V.; Oh, I.-K., Electro-active graphene–Nafion actuators. *Carbon* **2011**, *49*, 1279.
24. Wang, P.; Zakeeruddin, S. M.; Comte, P.; Exnar, I.; Grätzel, M., Gelation of ionic liquid-based electrolytes with silica nanoparticles for quasi-solid-state dye-sensitized solar cells. *J. Am. Chem. Soc.* **2003**, *125*, 1166.
25. Sun, Q.; Harmer, M. A.; Farneth, W. E., An Extremely Active Solid Acid Catalyst, Nafion Resin/Silica Composite, for the Friedel−Crafts Benzylation of Benzene and p-Xylene with Benzyl Alcohol. *Ind. Eng. Chem. Res.* **1997**, *36*, 5541.
26. Moukheiber, E.; De Moor, G.; Flandin, L.; Bas, C., Investigation of ionomer structure through its dependence on ion exchange capacity (IEC). *J. Membr. Sci.* **2012**, *389*, 294.
27. Yeo, S. C.; Eisenberg, A., Physical properties and supermolecular structure of perfluorinated ion-containing (nafion) polymers. *J. Appl. Polym. Sci.* **1977**, *21*, 875.
28. De Almeida, S.; Kawano, Y., Thermal behavior of Nafion membranes. *J. Therm. Anal. Calorim* **1999**, *58*, 569.
29. Hodge, I.; Eisenberg, A., Dielectric and mechanical relaxations in a Nafion precursor. *Macromolecules* **1978**, *11*, 289.
30. Su, S.; Mauritz, K. A., Dielectric Relaxation Studies of Annealed Short Side Chain Perfluorosulfonate Ionomers. *Macromolecules* **1994**, *27*, 2079.
31. Kyu, T.; Hashiyama, M.; Eisenberg, A., Dynamic mechanical studies of partially ionized and neutralized Nafion polymers. *Can. J. Chem.* **1983**, *61*, 680.
32. Moore, R. B.; Martin, C. R., Morphology and chemical properties of the Dow perfluorosulfonate ionomers. *Macromolecules* **1989**, *22*, 3594.

33. Page, K. A.; Cable, K. M.; Moore, R. B., Molecular Origins of the Thermal Transitions and Dynamic Mechanical Relaxations in Perfluorosulfonate Ionomers. *Macromolecules* **2005**, *38*, 6472.
34. Giffin, G. A.; Haugen, G. M.; Hamrock, S. J.; Di Noto, V., Interplay between Structure and Relaxations in Perfluorosulfonic Acid Proton Conducting Membranes. *J. Am. Chem. Soc.* **2013**, *135*, 822.
35. Menard, K. P. *Dynamic mechanical analysis: a practical introduction*; CRC press, 2008.
36. Zawodzinski, T. A.; Springer, T. E.; Davey, J.; Jestel, R.; Lopez, C.; Valerio, J.; Gottesfeld, S., A comparative study of water uptake by and transport through ionomeric fuel cell membranes. *J. Electrochem. Soc.* **1993**, *140*, 1981.
37. Zundel, G., Hydration Structure and Intermolecular Interaction in Polyelectrolytes. *Angew. Chem. Int. Ed. Engl.* **1969**, *8*, 499.
38. Li, J.; Pan, M.; Tang, H., Understanding short-side-chain perfluorinated sulfonic acid and its application for high temperature polymer electrolyte membrane fuel cells. *RSC Adv.* **2014**, *4*, 3944.
39. Kim, M.-H.; Glinka, C. J.; Grot, S. A.; Grot, W. G., SANS Study of the Effects of Water Vapor Sorption on the Nanoscale Structure of Perfluorinated Sulfonic Acid (NAFION) Membranes. *Macromolecules* **2006**, *39*, 4775.
40. Gebel, G.; Diat, O., Neutron and X-ray Scattering: Suitable Tools for Studying Ionomer Membranes. *Fuel Cells* **2005**, *5*, 261.
41. Tant, M. R.; Darst, K. P.; Lee, K. D.; Martin, C. W. In *Multiphase Polymers: Blends and Ionomers*, Structure and Properties of Short-Side-Chain Perfluorosulfonate Ionomers; American Chemical Society: 1989; Vol. 395, p 370.

42. Schaberg, M. S.; Abulu, J. E.; Haugen, G. M.; Emery, M. A.; O'Conner, S. J.; Xiong, P. N.; Hamrock, S., New Multi Acid Side-Chain Ionomers for Proton Exchange Membrane Fuel Cells. *ECS Trans.* **2010**, *33*, 627.

43. Kreuer, K. D.; Schuster, M.; Obliers, B.; Diat, O.; Traub, U.; Fuchs, A.; Klock, U.; Paddison, S. J.; Maier, J., Short-side-chain proton conducting perfluorosulfonic acid ionomers: Why they perform better in PEM fuel cells. *J. Power Sources* **2008**, *178*, 499.

44. Roche, E. J.; Pineri, M.; Duplessix, R.; Levelut, A. M., Small-angle scattering studies of nafion membranes. *J. Polym. Sci., Part B: Polym. Phys.* **1981**, *19*, 1.

45. Moore, R. B.; Martin, C. R., Procedure for preparing solution-cast perfluorosulfonate ionomer films and membranes. *Anal. Chem.* **1986**, *58*, 2569.

46. Heitner-Wirguin, C., Recent advances in perfluorinated ionomer membranes: structure, properties and applications. *J. Membr. Sci.* **1996**, *120*, 1.

47. Ghielmi, A.; Vaccarono, P.; Troglia, C.; Arcella, V., Proton exchange membranes based on the short-side-chain perfluorinated ionomer. *J. Power Sources* **2005**, *145*, 108.

48. Grot, W. G., Perfluorinated ion exchange polymers and their use in research and industry. *Macromol. Symp.* **1994**, *82*, 161.

49. Divoux, G. M.; Finlay, K. A.; Park, J. K.; Song, J.-M.; Yan, B.; Zhang, M.; Dillard, D. A.; Moore, R. B., Morphological Factors Affecting the Behavior of Water in Proton Exchange Membrane Materials. *ECS Trans.* **2011**, *41*, 87.

50. Osborn, S. J.; Hassan, M. K.; Divoux, G. M.; Rhoades, D. W.; Mauritz, K. A.; Moore, R. B., Glass Transition Temperature of Perfluorosulfonic Acid Ionomers. *Macromolecules (Washington, DC, U. S.)* **2007**, *40*, 3886.

51. Tant, M. R.; Darst, K. P.; Lee, K. D.; Martin, C. W., Structure and properties of short-side-chain perfluorosulfonate ionomers; ACS Publications: 1989.
52. Yoshida, H.; Miura, Y., Behavior of water in perfluorinated ionomer membranes containing various monovalent cations. *J. Membr. Sci.* **1992**, *68*, 1.
53. Phillips, A. K.; Moore, R. B., Mechanical and transport property modifications of perfluorosulfonate ionomer membranes prepared with mixed organic and inorganic counterions. *J. Polym. Sci. Part B Polym. Phys.* **2006**, *44*, 2267.
54. Hassan, M. K.; Abukmail, A.; Mauritz, K. A., Broadband dielectric spectroscopic studies of molecular motions in a Nafion membrane vs. annealing time and temperature. *Eur. Polym. J.* **2012**, *48*, 789.
55. Deng, Z.; Mauritz, K. A., Dielectric relaxation studies of water-containing short side chain perfluorosulfonic acid membranes. *Macromolecules* **1992**, *25*, 2739.
56. Deng, Z.; Mauritz, K. A., Dielectric relaxation studies of acid-containing short-side-chain perfluorosulfonate ionomer membranes. *Macromolecules* **1992**, *25*, 2369.
57. Starkweather Jr, H. W.; Chang, J. J., Water relaxation in perfluorosulfonate ionomers. *Macromolecules* **1982**, *15*, 752.
58. Chen, R.; Jayakody, J.; Greenbaum, S.; Pak, Y.; Xu, G.; McLin, M.; Fontanella, J., Studies of Water in Nafion Membranes Using Deuteron and Oxygen-17 Nuclear Magnetic Resonance, and Dielectric Relaxation Techniques. *J. Electrochem. Soc.* **1993**, *140*, 889.
59. Di Noto, V.; Lavina, S.; Negro, E.; Vittadello, M.; Conti, F.; Piga, M.; Pace, G., Hybrid inorganic–organic proton conducting membranes based on Nafion and 5 wt% of MxOy (M= Ti, Zr, Hf, Ta and W). Part II: relaxation phenomena and conductivity mechanism. *J. Power Sources* **2009**, *187*, 57.

60. Di Noto, V.; Gliubizzi, R.; Negro, E.; Pace, G., Effect of SiO2 on relaxation phenomena and mechanism of ion conductivity of [Nafion/(SiO2) x] composite membranes. *J. Phys. Chem. B* **2006**, *110*, 24972.

61. Osborn, S. J.; Hassan, M. K.; Divoux, G. M.; Rhoades, D. W.; Mauritz, K. A.; Moore, R. B., Glass Transition Temperature of Perfluorosulfonic Acid Ionomers. *Macromolecules* **2007**, *40*, 3886.

62. Fujimura, M.; Hashimoto, T.; Kawai, H., Small-angle x-ray scattering study of perfluorinated ionomer membranes. 2. Models for ionic scattering maximum. *Macromolecules* **1982**, *15*, 136.

63. Fischer, E.; Kloos, F.; Lieser, G., Direct evidence for glass transition taking place in the surface layers of solution grown crystals of polybutene-1. *J. Polym. Sci. Part C* **1969**, *7*, 845.

64. Page, K. A.; Park, J. K.; Moore, R. B.; Garcia Sakai, V., Direct analysis of the ion-hopping process associated with the α-relaxation in perfluorosulfonate ionomers using quasielastic neutron scattering. *Macromolecules* **2009**, *42*, 2729.

65. Page, K. A.; Jarrett, W.; Moore, R. B., Variable temperature 19F solid-state NMR study of the effect of electrostatic interactions on thermally-stimulated molecular motions in perfluorosulfonate ionomers. *J. Polym. Sci. Part B Polym. Phys.* **2007**, *45*, 2177.

66. Schlick, S.; Gebel, G.; Pineri, M.; Volino, F., Fluorine-19 NMR spectroscopy of acid Nafion membranes and solutions. *Macromolecules* **1991**, *24*, 3517.

67. Liu, S.-F.; Schmidt-Rohr, K., High-resolution solid-state 13C NMR of fluoropolymers. *Macromolecules* **2001**, *34*, 8416.

68. Boyle, N. G.; McBrierty, V. J.; Eisenberg, A., NMR investigation of molecular motion in Nafion membranes. *Macromolecules* **1983**, *16*, 80.

69. Chen, Q.; Schmidt-Rohr, K., 19F and 13C NMR signal assignment and analysis in a perfluorinated ionomer (Nafion) by two-dimensional solid-state NMR. *Macromolecules* **2004**, *37*, 5995.
70. Kollath, V. O.; Karan, K., New molecular scale insights into the α-transition of Nafion thin films from variable temperature ATR-FTIR spectroscopy. *Phys. Chem. Chem. Phys.* **2016**, *18*, 26144.
71. Tesfaye, M.; Kushner, D. I.; McCloskey, B. D.; Weber, A. Z.; Kusoglu, A., Thermal Transitions in Perfluorosulfonated Ionomer Thin-Films. *ACS Macro Lett.* **2018**, *7*, 1237.
72. Bauer, F.; Denneler, S.; Willert-Porada, M., Influence of temperature and humidity on the mechanical properties of Nafion 117 polymer electrolyte membrane. *J. Polym. Sci. Part B Polym. Phys.* **2005**, *43*, 786.
73. Kundu, S.; Simon, L. C.; Fowler, M.; Grot, S., Mechanical properties of Nafion™ electrolyte membranes under hydrated conditions. *Polymer* **2005**, *46*, 11707.
74. Orsino, C. M.; Lindell, M.; Yandrasits, M.; Hamrock, S.; Moore, R. B., Anomalous Appearance of a Distinct Glass Transition in Perfluoroimide Acid Ionomers. *ECS Trans.* **2019**, *92*, 455.
75. Matos, B.; Dresch, M.; Santiago, E.; Linardi, M.; De Florio, D.; Fonseca, F., Nafion β-relaxation dependence on temperature and relative humidity studied by dielectric spectroscopy. *J. Electrochem. Soc.* **2013**, *160*, F43.
76. Kyu, T.; Eisenberg, A. In *J. Polym. Sci. C*; Wiley Online Library: 1984; Vol. 71, p 203.
77. Page, K. A.; Rowe, B. W.; Masser, K. A.; Faraone, A., The effect of water content on chain dynamics in nafion membranes measured by neutron spin echo and dielectric spectroscopy. *J. Polym. Sci. Part B Polym. Phys.* **2014**, *52*, 624.

78. Su, G. M.; Cordova, I. A.; Yandrasits, M. A.; Lindell, M.; Feng, J.; Wang, C.; Kusoglu, A., Chemical and Morphological Origins of Improved Ion Conductivity in Perfluoro Ionene Chain Extended Ionomers. *J. Am. Chem. Soc.* **2019**.

Chapter 3.

Thermomechanical Relaxations in Short C2 and C4 Sidechain 3M Perfluorosulfonic Acid Ionomers

Christina M. Orsino, Denis Duchesne, Gregg Dahlke, Lisa Chen, and Robert B. Moore

3.1 Introduction

Perfluorosulfonic acid (PFSA) ionomers consisting of a polytetrafluoroethylene (PTFE) backbone and perfluoroether sidechains of various lengths containing sulfonated end groups are the current benchmark materials used in proton exchange membrane fuel cells (PEMFCs). Nafion® has been the most widely studied PFSA since its creation in the late 1960s by Walther Grot of Dupont.[1] While Nafion® dominates the PFSA literature, other perfluorinated ionomers continue to be developed with differing sidechain chemistries and higher ion exchange capacities (IECs) in an attempt to optimize performance and durability.[2] These ionomers consist of 3M's C4 perfluorosulfonic acid (3M-PFSA) and Solvay Specialty Polymer's short sidechain C2 Aquivion (**Figure 3-1**). Different PFSAs are commonly identified by their tradename (e.g. Nafion, 3M-PFSA, Aquivion) and their equivalent weight (EW), in grams of polymer per moles of sulfonic acid groups, which is inversely related to ion exchange capacity (IEC).[3]

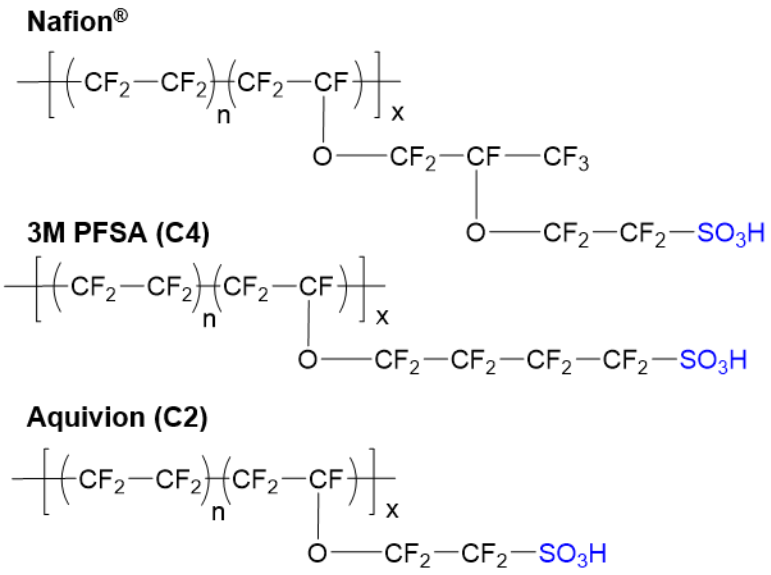

Figure 3-1. Chemical structures of Nafion, 3M-PFSA, and Aquivion.

The chemical and mechanical properties of PFSAs are governed by their phase-separated morphology.[1,3] The link between phase-separation and physical properties in ionomeric systems was originally established in hydrocarbon-based ionomers and provides a basis for the morphological and physical property characterization of PFSAs.[4] Ionomers are known to phase separate into hydrophilic and hydrophobic phases where the hydrophilic domains are established from aggregation of ions, while the hydrophobic domain is composed of the nonpolar backbone.[5] This phase separation leads to interesting physical properties in ionomers including a two-phase, dual glass transition behavior.[6,7] In hydrocarbon-based ionomers at low ion contents, small multiplets formed from interactions between the ions create physical crosslinks throughout the polymer matrix that effectively reduce the mobility of the polymer chains and increase the glass transition temperature.[4,6,8,9] The matrix glass transition temperature continues to increase with increasing ion content as a result of the introduction of more physical crosslinks. Above a certain ion content (the exact ion content depends on the chemical structure of the ionomer), a separate

relaxation appears at higher temperatures, indicating the development of a second phase in the material. This second relaxation is attributed to the "cluster" phase of the ionomer where there is overlap between regions of polymer chains with restricted mobility that are large enough to form their own phase.[4] Additionally, at high enough ion contents, the high temperature "cluster" α-relaxation even becomes dominant suggesting that the clusters form a contiguous phase.[9]

PFSAs also demonstrate two-phase glass transition behavior, although the definitions used to describe the molecular motions underlying their thermomechanical relaxations vary slightly from the classic ionomer assignments. First, the lowest temperature relaxation observed at temperatures below −100 °C, labeled as the γ-relaxation is observed in all PFSAs in both the sulfonyl fluoride precursor form, sulfonic acid form and neutralized forms. This relaxation is attributed to short-range molecular motions of the PTFE backbone and its assignment remains undisputed in the literature.[1,10] The assignments of the underlying molecular motions of two other relaxations observed for Nafion at higher temperatures, β- and α-, were the subject of debate in PFSA literature for quite some time.[1,3,11] In 2004, Page, Cable, and Moore conducted an in-depth study on various Nafion membranes neutralized with sodium, cesium, and different alkylammonium counterions to investigate the effect of counterion type on the thermomechanical properties of Nafion in attempt to assign the molecular origins of these two transitions.[11] In the sulfonic acid (H^+-form) and Na^+-form, the α-relaxation is the dominant relaxation in these PFSA materials. In the Na^+-form, both the α- and β-relaxations were observed to shift to much higher temperatures relative to the H^+-form. The authors then neutralized the sulfonic acid groups in Nafion with a series of alkylammonium counterions of different sizes. The smallest counterion, tetramethylammonium (TMA^+) had similar relaxation temperatures to Na^+-form. Increasing counterion size caused both the α- and β-relaxations to shift to lower temperatures, while the β-relaxation also increased in

intensity. The β-relaxation decreased in temperature with increasing counterion size toward the relaxation temperature of the sulfonyl fluoride precursor of Nafion (e.g., temperature at which long-range segmental motion of the polymer chains occurs with no electrostatic crosslinks). This finding was attributed to the large counterions decreasing the strength of electrostatic interactions, while the larger bulky counterions (tetrabutylammonium and larger) also effectively plasticized the material. The authors suggested that as the counterion size increases, the association between ion pairs is weakened and allows larger populations of chains to activate motion at lower temperatures, the extreme extension of this being the sulfonyl fluoride precursor (with no ion pair association).

Ultimately, a combination of DMA, variable temperature small angle X-ray scattering (SAXS), and variable temperature solid-state ^{19}F NMR led to the assignments of the α- and β-relaxations in Nafion in the neutralized (ionomer) form.[11] The α-relaxation was attributed to the onset of long-range mobility of the polymer chains facilitated by a weakening of the electrostatic interactions within the ionic aggregates (i.e., motions within a dynamic electrostatic network). The β-relaxation was attributed to the onset of thermally activated segmental polymer chain motions within the framework of a static electrostatic network. These assignments were also confirmed in a separate study by performing partial neutralization of Nafion® with TBA^+ and Na^+ counterions,[12] and are widely accepted by the PFSA community.[3] The difference between these assignments and those made for the hydrocarbon-based ionomers has to do with the assignment of the β-relaxation. In hydrocarbon ionomers, the β-relaxation is simply attributed to the glass transition of the matrix well-removed from the ionic aggregates and is therefore, minimally affected by a change in counterion type.[13] In Nafion, however, the β-relaxation was found to be strongly coupled to the strength of the electrostatic network and was thus assigned not specifically as a matrix T_g, but as

the onset of thermally activated main chain motions facilitated through sidechain mobility within a static physical network.[11] This β-relaxation was assigned as the genuine glass transition of Nafion.[11]

While previous assignments of the thermomechanical relaxations in Nafion were made on neutralized (ionomer) membranes, Osborn and coworkers worked to assign the β-transition in H^+-form Nafion by conducting a study evaluating the DMA tanδ peak temperature dependence on degree of neutralization.[14] It was observed that the α- and β-relaxations of Nafion neutralized with tetrabutylammonium (TBA^+) counterions were at 115 °C and 75 °C respectively. H^+-form Nafion displayed an α-relaxation at 100 °C and a weak peak near −20 °C. While the peak at −20 °C was assigned as the β-relaxation by convention, it was unclear whether it had the same molecular-level origins as the β-relaxation observed in neutralized Nafion. Invoking rule-of-mixture concepts, Osborn and coworkers conducted DMA studies on a series of H^+-form Nafion membranes partially neutralized with TBA^+ counterions. The β-relaxation temperature was shown to be dependent on the degree of neutralization with TBA^+ while the α-relaxation temperature remained mostly independent, suggesting that the molecular origin of the β-relaxation is the same in H^+-form as it is in TBA^+-form and was therefore assigned as the genuine T_g of Nafion.[14]

While a general agreement has been met in the literature for the molecular origins of thermal transitions in Nafion®, newer PFSA ionomers have yet to be fully explored. In 2012, Moukheiber and coworkers investigated the dependence of physical properties on the chemical structure of Nafion and Aquivion.[15] In this study, low temperature (−140 to 0°C) DMA data showed distinct γ- and β-relaxation temperatures for Aquivion and Nafion ionomers, but the β-relaxation was shown to be dependent on degree of crystallinity in the membranes for the Aquivion PFSA and decreased in temperature with increasing EW. In 2013, Giffin and coworkers published a study on

the interplay between structure and relaxations in PFSA membranes, where they looked at 3M PFSA of three different equivalent weights.[16] Utilizing broadband dielectric spectroscopy, they were able to observe the dielectric tanδ data over the temperature range of −155 to 155°C. They saw the opposite trend from Moukheiber that the dielectric β-relaxation temperature decreased with decreasing EW and attributed that to an increase in sidechain density and therefore interactions between the sidechains. Tesfaye and coworkers recently conducted a study on the thermal transitions in perfluorinated ionomer thin films.[17] In this work, they looked at the thermal transitions of thin films vs. bulk films of Nafion and 3M's PFSA of 825 EW. By using ellipsometry to determine the thermal expansion coefficients of PFSA thin films and comparing to literature bulk-membrane values, they were able to determine that the single thermal transition observed in H^+-form thin films was likely related to the bulk-film α-relaxation, while the transition in cation-exchanged thin films was related to the bulk-film β-relaxation. It is evident from these recent studies that these new sidechain chemistries can affect the inherent mechanical properties and that there is a lack of understanding in how different sidechain lengths and EWs affect the molecular mobility of these PFSAs.

Although numerous studies have been published on the morphology, transport properties, and fuel cell performance of 3M-PFSA and Solvay's short sidechain Aquivion, the literature is lacking full temperature-range DMA data spanning all three relaxations directly comparing the different sidechains structures in the H^+-form. While it is generally assumed that these new ionomers with only minor differences in sidechain structures will have the same mechanical properties as Nafion, it is important to fully investigate the effect of sidechain structures on these relaxations for the continuing development of processing conditions and fuel cell application temperatures. The purpose of this investigation is to advance the previous work on Nafion to

determine the true glass transition temperature of two other PFSA ionomers including 3M-PFSA of two EWs and Solvay's Aquivion. In this work, the term "true glass transition" is considered to be the onset of thermally activated main chain motions facilitated through sidechain mobility within a static physical network.[11] To this end, the glass transition temperature of the sulfonic acid-form ionomer can be compared directly to the glass transition temperature of the nonionic sulfonyl fluoride form precursors (the onset of long-range segmental motions of the main chains of the nonionic polymer). In addition, partial neutralization with TBA^+ counterion in combination with the Fox equation of copolymers provides fundamental information on the molecular origin of the β-transition temperature. By comparing three PFSA ionomers with differing sidechains, we are now able to present some insight on the effect of shorter sidechains and higher ion contents on the thermomechanical relaxations in PFSAs.

3.2 Experimental

3.2.1 Materials

3M-Perfluorosulfonic acid (3M-PFSA) ionomer and perfluorosulfonyl fluoride (3M-PFSF) precursors of 725 and 825 g/mol equivalent weight were provided by 3M. Nafion® 117 (1100 EW) membrane was purchased DuPont. Aquivion 870 EW membrane (E87-05S) and 870 EW precursor (P87F-SO_2F) were purchased from Sigma Aldrich. Tetrabutylammonium hydroxide (TBAOH), 1.5 M in water, and sodium hydroxide were obtained from Fisher Scientific and used without further purification.

3.2.2 Sulfonic acid membrane preparation and partial neutralization

3M PFSA films were prepared by casting a dispersion from alcohol and water onto polyimide film. The dispersions were dried in an oven with the temperature of 80°C followed by annealing for 10 minutes at 200°C. Membranes were removed from the polyimide film by soaking in water. Aquivion and Nafion membranes were used as-received. To remove impurities, the membranes were soaked in 8 M HNO_3 for 16 hours then rinsed thoroughly with deionized water. Ion exchange to 100% TBA^+-form was carried out by stirring the pretreated membranes in 1 M TBAOH in water for 24 hours, followed by repetitive washing with DI water. Partial neutralization of pretreated membranes was done by stirring each membrane in TBAOH/water solutions containing specified quantities of TBAOH (relative to the moles of sulfonic acid groups in the membranes) for 24 hours. TBAOH quantities ranging from 5 to 90 mol % for each membrane were calculated on the basis of equivalent weight of dry membranes. All prepared membranes were thoroughly rinsed with water before drying under vacuum at 70°C overnight.

3.2.3 Sulfonyl fluoride membrane preparation and partial hydrolysis

Sulfonyl fluoride precursors of Aquivion 870 EW and 3M PFSA 800 EW were vacuum dried prior to melt pressing at 250 °C for 2 minutes under 6 kPa pressure to achieve a film thickness of ca. 100 μm. After removing from the press, the membranes were allowed to cool under ambient conditions and removed from the Kapton film. Prior to partial hydrolysis, the melt pressed films were cut to size for DMA experiments (6.35 mm wide, 8 mm long, 0.1 mm thick) and annealed under vacuum at 120 °C for 6 hours then weighed. Following the partial hydrolysis method reported by Kyu, Hashiyama, and Eisenberg,[10] the films were then stirred in a 10% NaOH solution in water at 75 °C for varying lengths of time ranging from 1 minute to 24 hours. Upon removing from the NaOH solution, the membranes were immediately rinsed well with water then analyzed by ATR-FTIR to determine the extent of hydrolysis. These partially hydrolyzed samples in the

Na^+-form were then dried overnight under vacuum at 70 °C, weighed again for gravimetric determination of degree of hydrolysis, and converted to the sulfonic acid form by submerging in 8 M HNO_3 for 72 hours. This acidification procedure was also performed on an unhydrolyzed sample as a control to confirm that it has no effect on the SO_2F groups, and only acidifies the Na^+-sulfonates. Finally, the samples were removed from the HNO_3, rinsed well with water, and dried again under vacuum at 70 °C prior to DMA analysis.

3.2.4 Dynamic Mechanical Analysis

Dynamic mechanical analysis was performed on a TA Instruments DMA Q800 analyzer in tensile mode using clamps for thin film samples. All samples were cut from vacuum dried membranes with a width of 6.35 mm. The membranes were analyzed at a frequency of 1 Hz from −120 to 200°C for the partially neutralized samples and −140 to 200°C for the partially hydrolyzed samples with a heating ramp of 2°C/min, 1 Hz frequency, 15 μm oscillatory amplitude, a static force of 0.05 N, and a force track of 125%.

3.2.5 ATR FTIR

Attenuated total reflectance (ATR) FTIR was used to gain qualitative information about the degree of hydrolysis of partially hydrolyzed samples. Hydrated samples were blotted dry with Kimwipe and analyzed on a Varian 670-IR spectrometer equipped with a PIKE Technologies GladiATR™ attachment with a diamond crystal.

3.2.6 Extended Sidechain Length Calculations

The extended sidechain lengths for C2 Aquivion, C4 3M PFSA, and Nafion were calculated using Chem3D software. The sidechains were drawn as fully extended and the distance

between the sulfur group of the SO_3H and the oxygen group of the sidechain-backbone ether linkage was measured through space.

3.3 Results and Discussion

3.3.1 Dynamic Mechanical Analysis of H^+-Form PFSA Ionomers

Figure 3-2 shows the dynamic mechanical tanδ versus temperature data for H^+-form Aquivion, 3M PFSA, and Nafion 1100 EW. All three PFSAs have a dominant peak in the tanδ near 110 °C, assigned as the α-relaxation. As mentioned previously, the α-relaxation is attributed to the onset of long-range mobility of the ionomer main chains and sidechains via destabilization of the physically crosslinked (in H^+-form, hydrogen-bonded) network.[11] This α-relaxation appears to increase in temperature with decreasing sidechain length, Nafion < PFSA < Aquivion. While there is not concrete evidence as to why the sidechain length affects the α-relaxation in the literature, there are a couple of studies that propose that the longer sidechains may plasticize the polymer chains and thus reduce the α-relaxation temperature.[15,18] However, it is difficult to make a direct comparison between sidechain length as these PFSAs have varying ion contents as well, which will affect the temperature of the α-relaxation.[2,19,20] As expected, though, for all three sidechain lengths and ion contents, the α-relaxation is the principle relaxation (relaxation with the highest tanδ intensity) in these sulfonic acid ionomers.

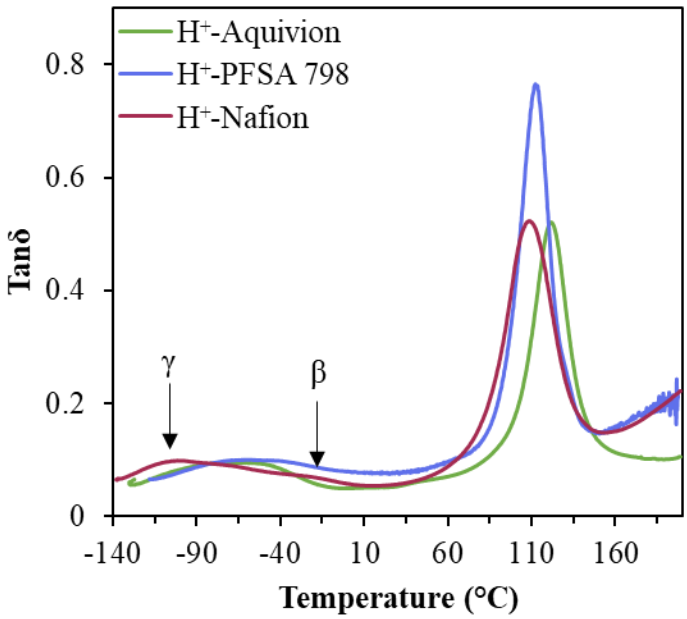

Figure 3-2. Dynamic mechanical tan delta vs temperature of H^+-form Aquivion 870 EW, 3M PFSA 800 EW, and Nafion 1100 EW.

At low temperatures, a very small bump in the tanδ is observed in H^+-form Nafion at ca. −20 °C in addition to the γ-relaxation peak at ca. −100 °C. This small β-relaxation has also been observed in previous literature and assigned as the onset of thermally activated main chain motions facilitated through sidechain mobility within a static physical network through a combination of the two thermomechanical relaxation studies mentioned previously.[11,14] Interestingly, it is hard to distinguish two different low temperature relaxations in the shorter sidechain Aquivion and 3M PFSA ionomers. Instead, these two ionomers appear to just have a large α-relaxation and one broad relaxation below 0 °C. Based on the assignment of the β-relaxation to molecular motions induced by *sidechain* mobility within a physically-crosslinked network, it is possible that in these short sidechain ionomers, there is not enough mobility of the sidechains to clearly observe this specific relaxation. In order to probe this possibility, we can use counterions to manipulate the strength of the physically crosslinked network.

3.3.2 *Partial Neutralization with TBA^+ Counterion.*

Figure 3-3 compares DMA data of H^+-form 800 EW 3M PFSA to the TBA^+-neutralized form. Distinct α- and β-transition temperatures are observed at ca. 110°C and ca. 80°C in the TBA^+-form, respectively. The H^+-form shows one distinct α-transition at ca. 110°C and one broad transition around the same temperature range as the γ-transition. To gain insight into how the β-transition translates from the TBA^+- to the H^+-form, we invoke rule of mixture concepts following previous work done by Osborn *et al* in their assignment of the β-relaxation in H^+-form Nafion.[14] We assume that TBA^+ counterions are homogeneously distributed among the pendant sulfonate groups in order to investigate the compositional dependence of the β-relaxation. By partially neutralizing the ionomers with increasing quantities of TBA^+ we can track the shift of the β-relaxation systematically with ion content. TBA^+ works well for all three sidechain structures (3M-PFSA, Aquivion, Nafion) due to its prominent β-peak that is easy to track with varying degrees of neutralization.

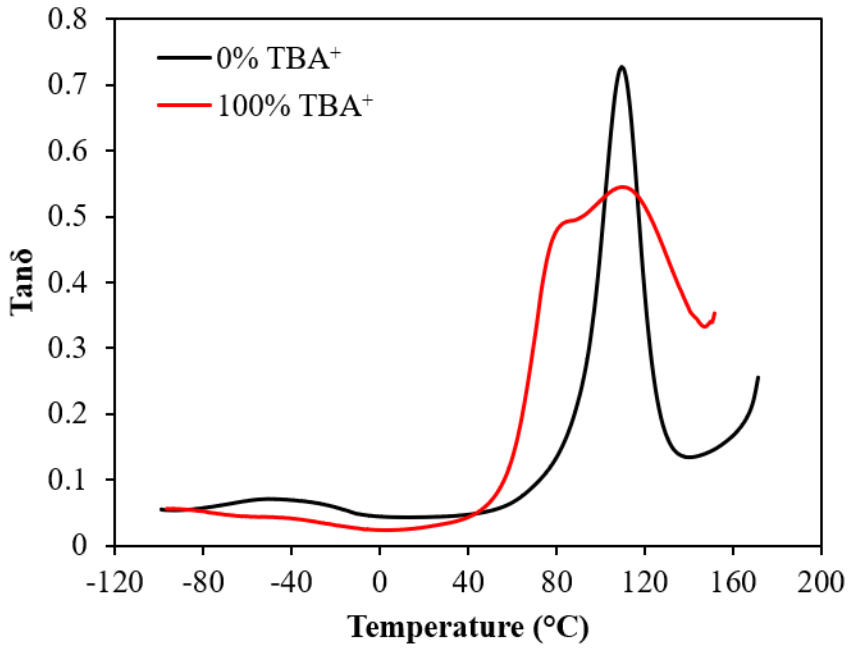

Figure 3-3. Dynamic mechanical tanδ vs temperature data for 3M PFSA 800 EW in the H^+-form and TBA^+-form.

Figure 3-4A shows the dynamic mechanical tanδ data for PFSA 800 EW neutralized with different TBA^+ counterion compositions. The prominent α-relaxation is observed at around the same temperature for all samples, while the β-relaxation shifts to lower temperatures and decreases in intensity with decreasing TBA^+ content. Unlike what was seen for Nafion previously,[14] the β-relaxation observed in the TBA^+-form does not track all of the way down to the broad transition at ca. −40°C seen in the H^+-form. In fact, when looking at the plot of α- and β-transition peak maxima vs. TBA^+ composition (**Figure 3-4B**), the β-relaxation steadily decreases in a seemingly linear fashion with decreasing TBA^+ content. The same trend is seen for 725 EW 3M PFSA (higher ion content than the 800 EW PFSA) and Aquivion as observed in **Figure 3-5**. However, in Aquivion, the β-relaxation does not appear to decrease to as low of temperatures as the two 3M PFSA ionomers. The plot of β-relaxation temperature versus TBA^+ content can be extrapolated to 0 %

TBA^+ content for all three PFSAs to predict where the β-relaxation would be expected in the H^+-form . In the 800 EW 3M PFSA, it extrapolates to 35 °C, while in Aquivion it extrapolates to 50 °C. Interestingly, these two temperatures are around the same temperature as the glass transition of the sulfonyl fluoride precursor (containing no ionic or hydrogen bonding interaction) for both of these PFSAs, further indicating that perhaps the "glass transition" (β-relaxation) in these ionomers is completely suppressed by the physically crosslinked network.

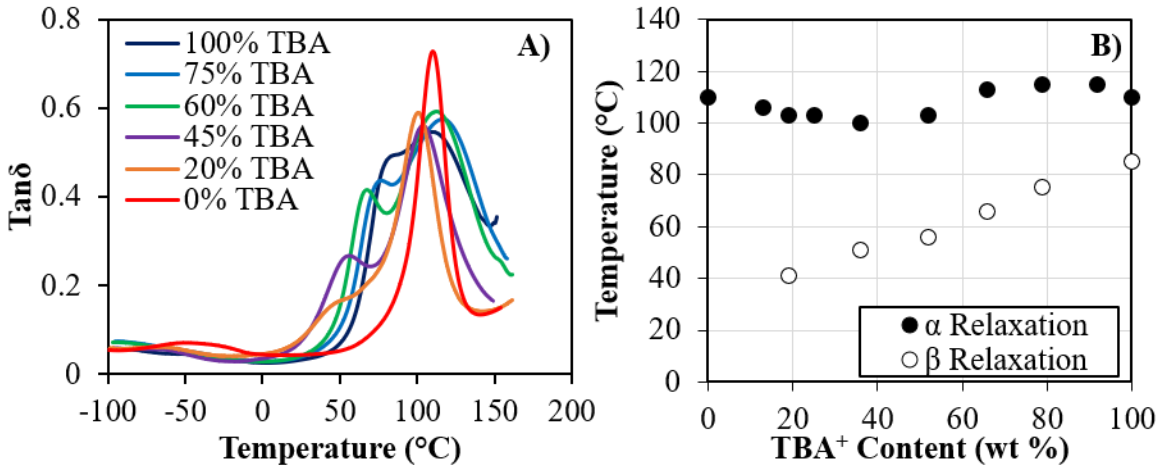

Figure 3-4. A) Tanδ data for the partial neutralization of 800 EW 3M PFSA with 100, 75, 60, 45, 20, and 0% TBA counterion compositions and B) Dynamic mechanical α- and β-relaxation temperatures vs. TBA^+ content for PFSA 800 EW.

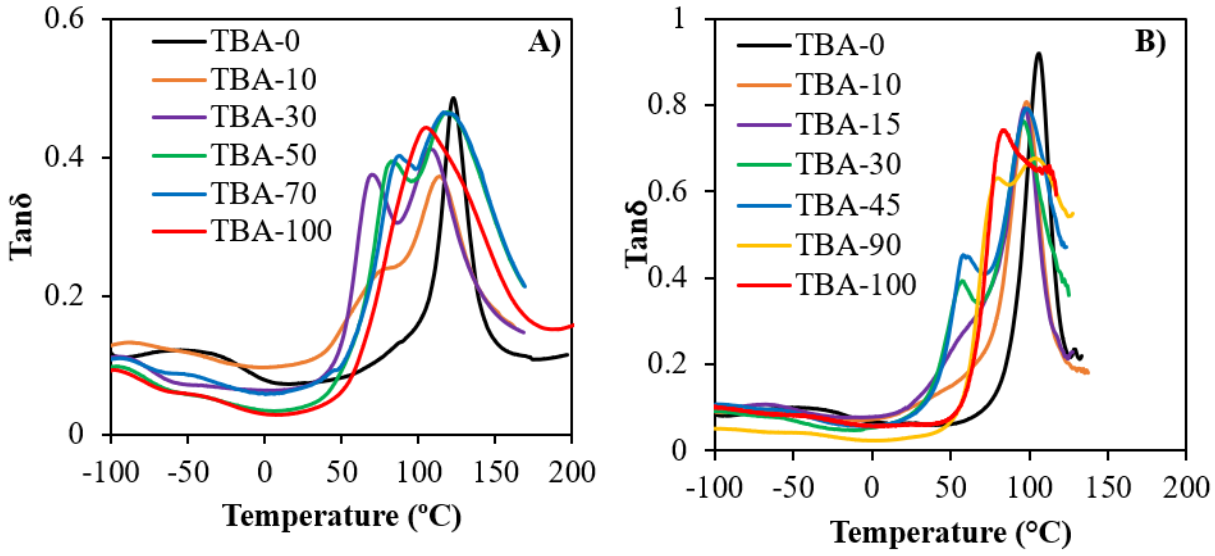

Figure 3-5. Tanδ vs. temperature for partially neutralized A) Aquivion 870 EW membranes and B) 3M PFSA 725 EW membrane with TBA^+ counterions.

Very low ion contents of TBA^+ were examined to observe the drop-off in the β-relaxation peak in the H^+-form . Dynamic mechanical tanδ data for 800 EW 3M PFSA at low TBA^+ counterion contents (< 30 weight percent) are shown in **Figure 3-6**. It is apparent from this low ion-content data that the β-relaxation "grows in" with increasing counterion content: increasing in magnitude and ultimately increasing in temperature. This finding further confirms the prediction that this relaxation is completely suppressed in H^+-form 3M PFSA and Aquivion due to their shorter sidechains and increased sidechain content compared to Nafion, but begins to appear when a large, bulky counterion is introduced to the system. In fact, it has been shown that bulky TBA^+ counterions may effectively function as internal plasticizers.[12,21,22] In the aforementioned study on Nafion neutralized with alkylammonium counterions of various sizes, the β-relaxation was observed to increase in intensity with increasing counterion size.[11] This was attributed to a weakening of the electrostatic network that allows a larger population of chains to exhibit activated motion at the lower relaxation temperature. In these shorter sidechain PFSAs, it is likely that at

low TBA^+ content, lone ion pairs are formed on isolated sidechains that provide the mobility for some mainchains to begin segmental motion at the lower glass transition temperature. With increasing TBA^+ content, an electrostatic network begins to take the place of the hydrogen-bonded network which causes this β-relaxation to increase in temperature with increasing ion content.

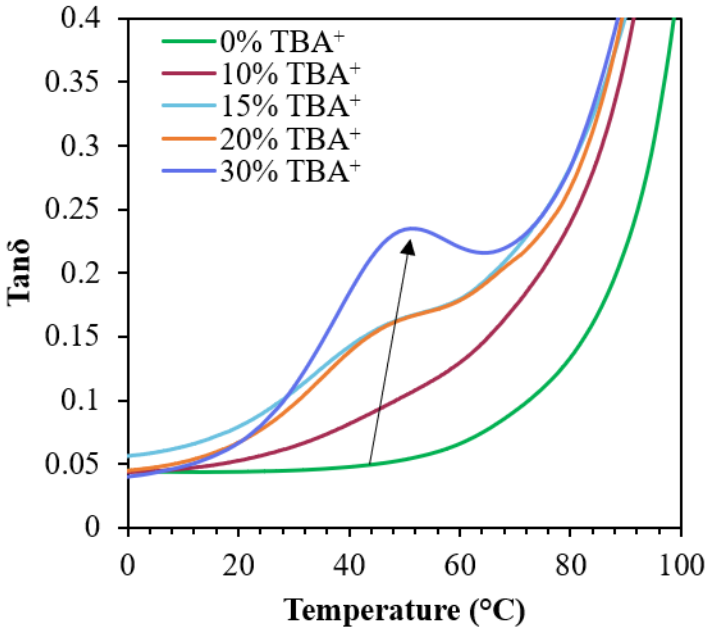

Figure 3-6. Tanδ data of 3M PFSA 800 EW with low degrees of TBA content.

An additional interesting observation is that the β-relaxation temperature trends linearly to the glass transition temperature of the precursor with decreasing TBA^+-content. If the β-relaxation is of the same origin as the glass transition in the precursor (segmental motions of the polymer backbone), then it makes sense that when the physically-crosslinked network is weakened, this relaxation would be observed at the same temperature as the glass transition of the nonionic precursor. However, the linearity of the relationship between the β-relaxation of the TBA^+-counterion form and sulfonyl fluoride precursor with ion content requires further explanation. To

explain this relationship, we apply the Fox equation for polymer blends and copolymers.[23] In this case, we assume that the TBA^+ counterions are homogeneously distributed among the sulfonic acid groups and thus the polymer can be considered a copolymer of TBA^+- and H^+-form PFSA. The Fox equation predicts the glass transition temperature for a copolymer based on the weight percent of each comonomer fraction and the glass transition temperature of that pure comonomer. The glass transition of the copolymer, T_g, is calculated from

$$\frac{1}{T_g} = \frac{\omega_1}{T_{g,1}} + \frac{\omega_2}{T_{g,2}} \quad (1)$$

Where ω_1 and $T_{g,1}$ are the weight fraction and glass transition temperature of polymer 1, respectively, and ω_1 and $T_{g,1}$ are the weight fraction and glass transition temperature of polymer 2. In implementing the Fox equation to this TBA^+ neutralization system, $T_{g,1}$ is taken to be the β-relaxation temperature of the pure TBA^+-form ionomer. The weight fraction (ω_1) of the TBA^+ component is calculated by the factoring in the mol percent TBA^+ counterion, mass of TBA^+ counterion, sidechain mass, and average number of TFE units between sidechains for each ionomer based on EW. The glass transition temperature of the sulfonyl fluoride precursor is utilized as $T_{g,2}$ where ω_2 is the weight fraction of H^+-form ionomer calculated from $1-\omega_1=\omega_2$.

The calculated Fox equation for each system is plotted in **Figure 3-7** for 800 EW and 725 EW 3M PFSA, and Aquivion. Each of the three systems investigated follow the theoretical Fox equation data well. Considering that this equation factors in the different sidechain structures and equivalent weights that vary between ionomers, this Fox equation relationship showing a linear decrease in the β-relaxation of the TBA^+-form PFSA to the glass transition temperature of the sulfonyl fluoride precursor with decreasing ion content appears to confirm that the β-relaxation of the TBA^+-form PFSA and the precursor are of the same molecular origin.

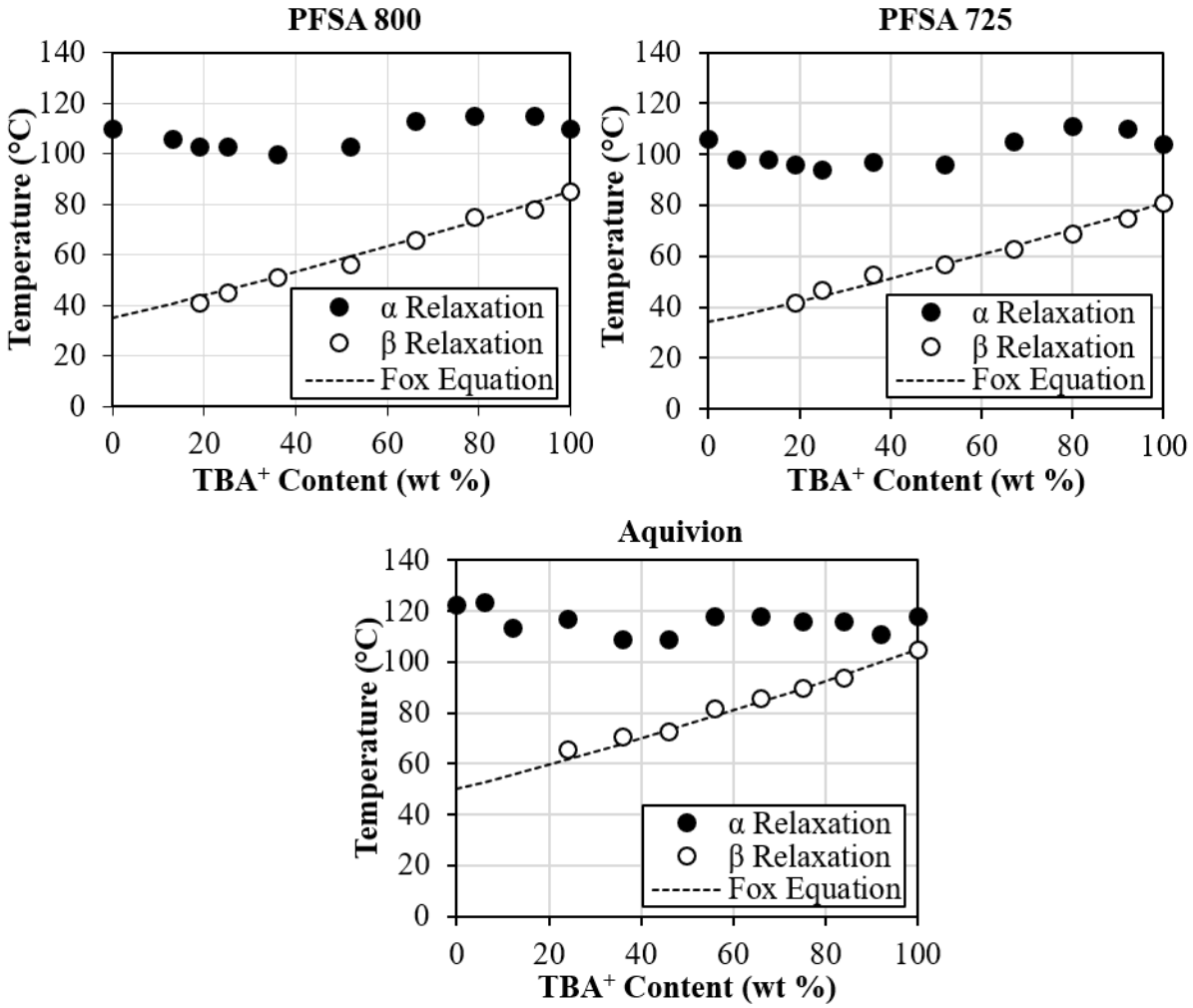

Figure 3-7. Transition temperature vs. TBA^+ counterion content overlaid with the theoretical Fox equation data represented by dashed lines for A) 800 EW 3M, B) 725 EW 3M PFSA, and C) Aquivion.

3.3.3 Partial Hydrolysis from Sulfonyl Fluoride Precursor to Sulfonic Acid.

In PFSAs, the prominent relaxation observed in the $-SO_2F$ precursor form is attributed to a classic glass transition of an amorphous polymer, defined as the onset of long-range segmental motion of the polymer chains. The addition of ion content to the nonionic polymer (by hydrolyzing

the nonionic $-SO_2F$ groups to $-SO_3^-X^+$ ion pairs) yields electrostatic interactions that creates the physically crosslinked network that restricts chain mobility. Since the sulfonyl fluoride precursor is one extreme with no hydrogen-bonding or ionic interactions, and the sulfonic acid form is another extreme with significant hydrogen-bonding interactions that these segmental motions are no longer observed, a partial hydrolysis of the precursor can be performed to systematically track the changes in the glass transition temperature and observe the formation of the α-relaxation at higher conversions.

The dynamic mechanical tanδ versus temperature for Aquivion, Nafion, 725 and 800 EW 3M PFSA are shown in **Figure 3-8**. The glass transitions of these sulfonyl fluoride precursors occur at ca. 20 °C for Nafion, 35 °C for both 3M PFSAs, and 45 °C for Aquivion. These are the temperatures that the TBA^+ neutralization experiment extrapolated to at 0% TBA^+ content. Although the TBA^+ neutralization experiment provided some indirect observations for the suppression of the β-relaxation in the H^+-form shorter sidechain ionomers, partial hydrolysis of the sulfonyl fluoride groups should show this suppression more directly. Since the sulfonyl fluoride precursors are melt processable, they can be melt-pressed into membranes prior to hydrolysis in sodium hydroxide for varying periods of time to create a series of partially hydrolyzed membranes following a method by Kyu, Hashiyama, and Eisenberg.[10] The $-SO_2F$ groups that were hydrolyzed to $-SO_3Na$ groups are then converted to $-SO_3H$ groups by submersing in 8 M nitric acid to create a series of $-SO_2F/-SO_3H$ membranes. This provides a means to systematically track the glass transition temperature of a 100% nonionic polymer, to the hydrogen-bonded form and provide fundamental information about the suppression of the glass transition and dominance of the α-relaxation in these short sidechain ionomers.

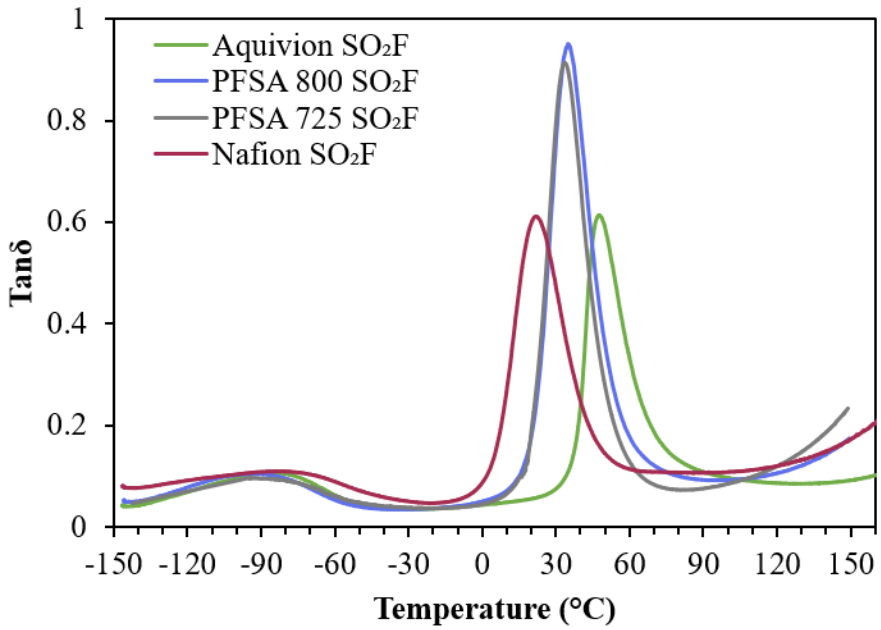

Figure 3-8. DMA tanδ vs temperature for nonionic sulfonyl fluoride precursors of Aquivion 870 EW, PFSA 800 EW, PFSA 725 EW, and Nafion 1100 EW.

A series of partially hydrolyzed membranes were prepared following the procedure in the experimental section.[10] FTIR was used to estimate an extent of hydrolysis for each sample as shown in **Figure 3-9**. Attenuated Total Reflectance (ATR) FTIR was used as a facile method for analyzing membrane samples, however it is important to note that this technique only probes approximately 1 to 2 μm into the surface of the sample. It is expected that hydrolysis of these membranes will occur starting on the outside and continuing inward with increasing hydrolysis time,[10] so ATR FTIR may show complete hydrolysis within the 1 to 2 μm penetration depth but that does not mean the bulk sample is hydrolyzed. Regardless of its limitations, the FTIR spectra for these hydrolyzed samples show evidence of partial hydrolysis. A peak at ca. 1469 cm^{-1} in the sulfonyl fluoride precursor has been attributed to S-F stretching of the SO_2F functional group.[24] With increasing hydrolysis time, the S-F band decreases in intensity to extinction, indicating that there are no longer S-F vibrations as expected for hydrolyzed samples. In the Na^+-sulfonate form,

a strong S-O symmetric stretch of the sulfonate group is observed at ca. 1060 cm^{-1}.[25] This molecular motion is not observed in the precursor, but appears to grow in with increasing hydrolysis time before reaching a maximum intensity after 15 minutes of hydrolysis.

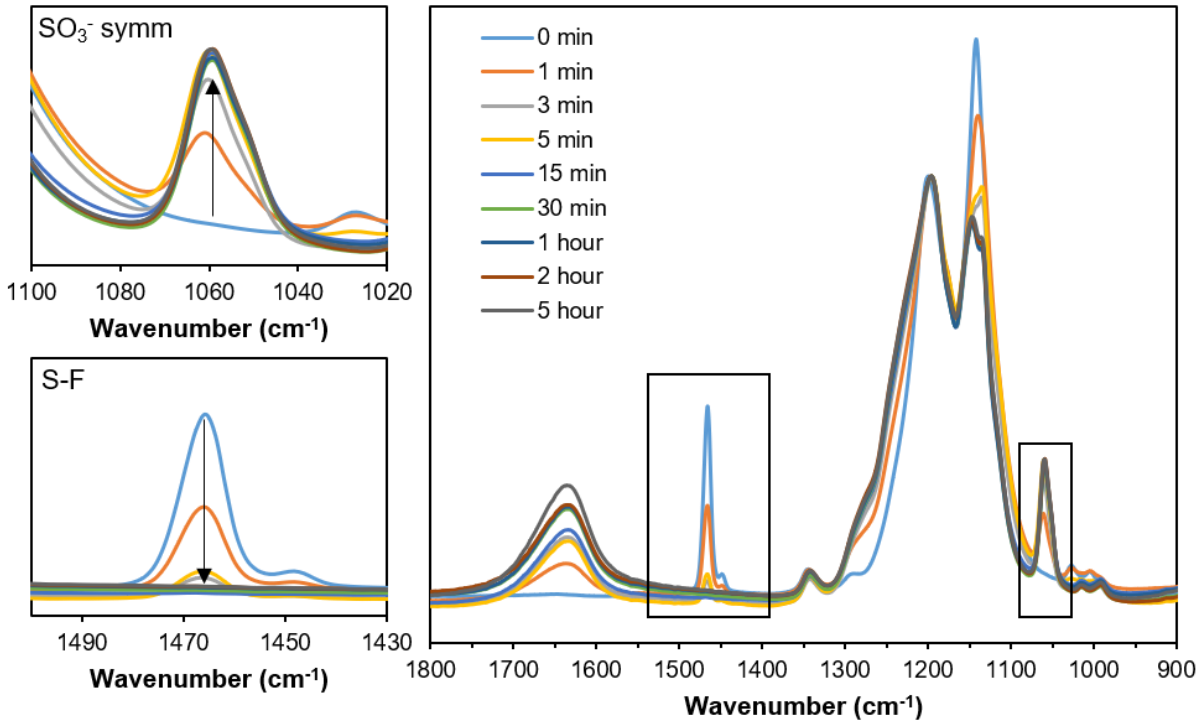

Figure 3-9. ATR FTIR data of sulfonyl fluoride form 3M PFSA 800 EW membranes hydrolyzed for varying lengths of time ranging from 0 minutes to 5 hours.

As an alternative method, the degree of conversion from the sulfonyl fluoride to the Na^+-sulfonate form was quantitatively determined by gravimetric analysis. Percent conversion as a function of hydrolysis time in 10 % NaOH solution at 75 °C is displayed in **Figure 3-10**. Some of the limitations of gravimetric analysis are evident from this figure. First, each membrane was cut down to size (6.35 x 9 x 0.1 mm) for the DMA analysis prior to being hydrolyzed, leading to low sample masses that make it difficult to detect very low percent conversions due the limit of detection of the analytical balance. Because of this, samples that were hydrolyzed for less than 15

minutes appear as 0 % conversion, when it is clear from the FTIR (and DMA data in the following section) that some hydrolysis has occurred. Additionally, Na^+-form PFSAs are known to uptake water rapidly even under ambient conditions. That is apparent in the 350- and 630-minute samples where the measured percent conversion is above 100%, likely due to the addition of water molecules in the final mass analysis. However, even with these limitations, a combination of gravimetric analysis, ATR FTIR, and DMA show that partial hydrolysis of sulfonyl fluoride membranes is easily achieved through this established 10% NaOH method.[10] FTIR shows that hydrolysis begins to occur even within one minute, and gravimetric analysis shows that full hydrolysis is achieved somewhere between 120 and 360 minutes for membranes of this size and EW.

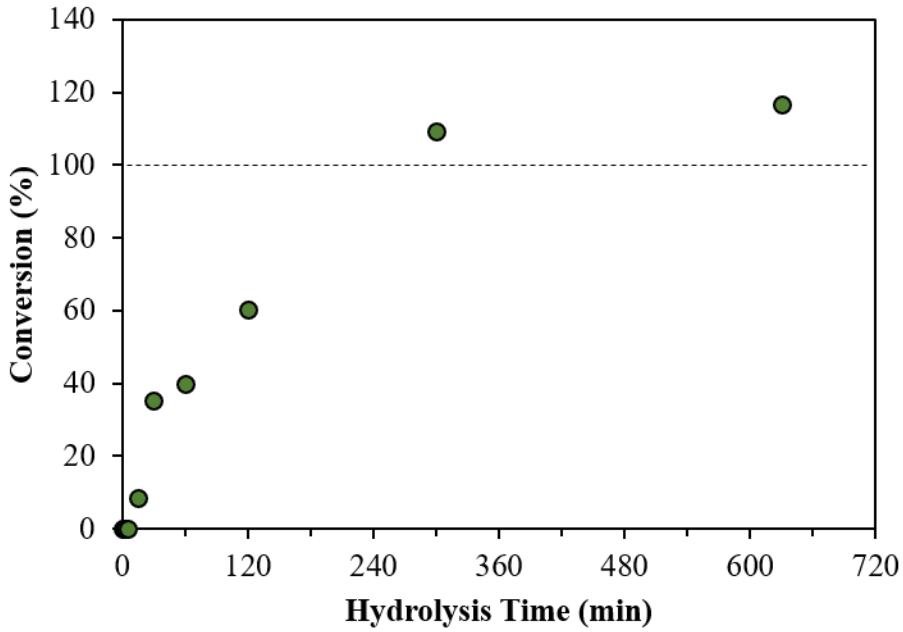

Figure 3-10. Percent conversion from the sulfonyl fluoride precursor into partially hydrolyzed Na^+-sulfonate 3M PFSA 800 EW in 10% NaOH solution at 75 °C as a function of hydrolysis time. The dashed line serves to point out where 100 % conversion is achieved and values above this are likely due to water uptake from ambient humidity by the highly hydroscopic sulfonate groups.

Dynamic mechanical analysis of the partially hydrolyzed and acidified 800 EW 3M PFSA membranes is shown in **Figure 3-11**. In the nonionic sulfonyl fluoride form (0 min hydrolysis), there are two observable peaks in the tanδ, as shown previously in **Figure 3-8**, that are attributed to local short-range motions of the PTFE backbone at low temperatures and the glass transition at ca. 35 °C. Similarly, a small drop in storage modulus occurs at low temperatures followed by a drop of three orders in magnitude through the glass transition. With increasing hydrolysis time, the peak in tanδ at 35 °C decreases in intensity while the large drop in storage modulus through that glass transition also decreases. At five minutes of hydrolysis (less than 9 % conversion based on gravimetric data), a second peak in the tanδ begins to appear at ca. 100 °C that increases in magnitude and temperature with increasing hydrolysis time. At 630 minutes of hydrolysis, the relaxation at 35 °C is completely suppressed and only the α-relaxation near 110 °C is observed, similar to the DMA tanδ profiles in H^+-form PFSA, indicating that full hydrolysis is likely achieved at that point.

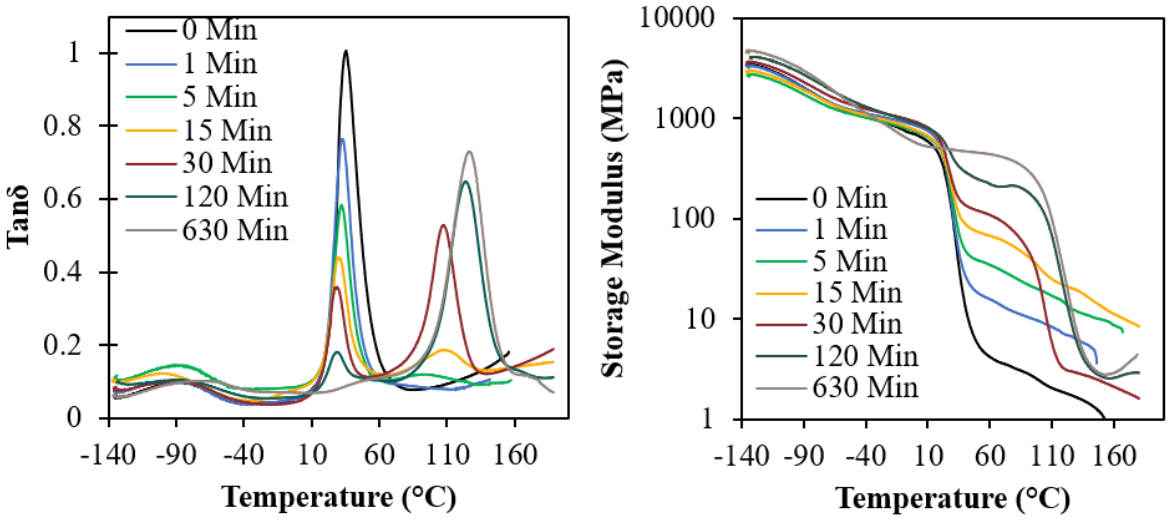

Figure 3-11. DMA tanδ and storage modulus data of sulfonyl fluoride form 800 EW 3M PFSA membranes hydrolyzed for various lengths of time.

The same study was conducted on Aquivion membranes. The degree of hydrolysis was determined by gravimetric analysis as shown in **Figure 3-12**. Again, the values at low hydrolysis time are limited by the low sample mass and the values at high hydrolysis time are exaggerated, likely due to water uptake in the membranes. However, a similar series of partially hydrolyzed membranes to the 3M PFSA were obtained for Aquivion where close to 100% conversion from SO_2F to SO_3H was achieved at hydrolysis times longer than 120 minutes.

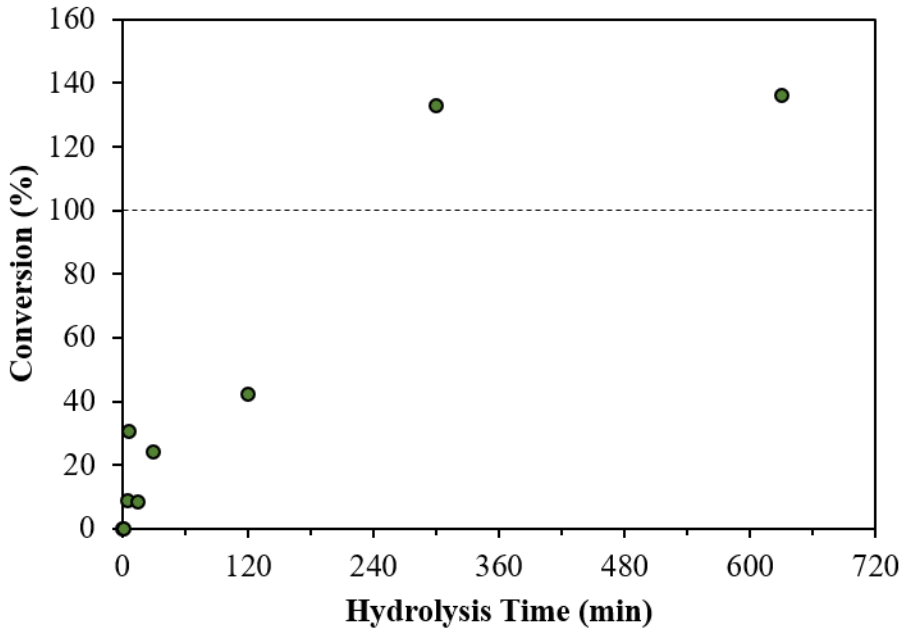

Figure 3-12. Percent conversion from the sulfonyl fluoride precursor into partially hydrolyzed Na^+-sulfonate Aquivion 870 EW in 10% NaOH solution at 75 °C as a function of hydrolysis time. The dashed line serves as a guide to point out where 100 % conversion is achieved.

DMA data for the partially hydrolyzed Aquivion membranes is shown in **Figure 3-13**. The same results are observed in Aquivion as were observed in the 3M PFSA. With increasing hydrolysis time, the peak in tanδ representative of segmental motions of the precursor polymer chains decreases in intensity while the large drop in storage modulus through that glass transition also decreases. After five minutes of hydrolysis, a second peak in the tanδ begins to appear above

100 °C that increases in magnitude and temperature with increasing hydrolysis time. At 630 minutes of hydrolysis, the precursor T_g is completely suppressed and only the α-relaxation of the H^+-form PFSA is observed, similar to the DMA tanδ profiles in H^+-form PFSA, indicating that full hydrolysis is likely achieved at that point.

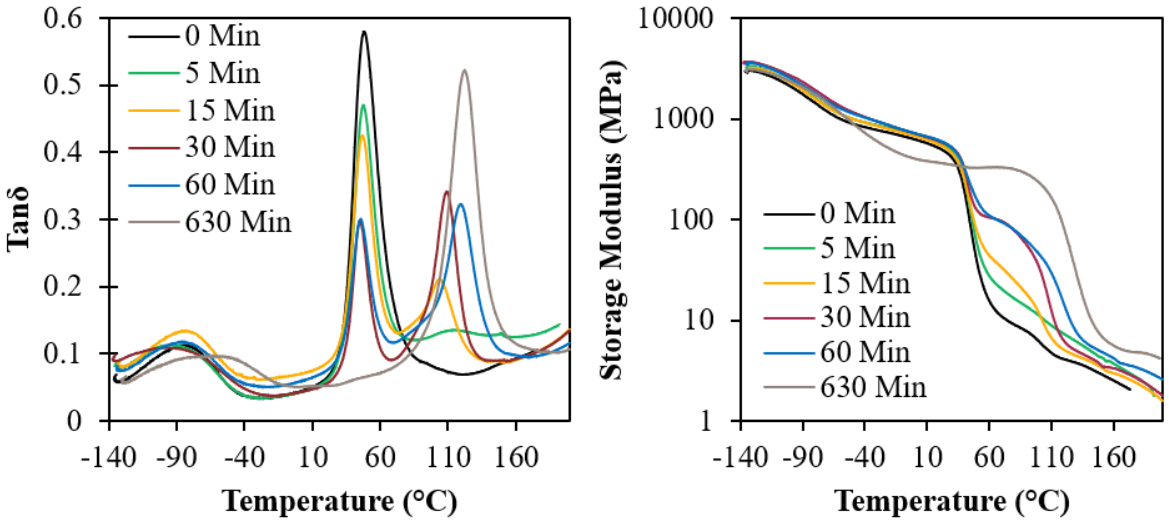

Figure 3-13. DMA tanδ and storage modulus data of sulfonyl fluoride form Aquivion 870 EW membranes hydrolyzed for various lengths of time.[9]

The trends that are observed in these partially hydrolyzed sample mimic what has been reported in the classic hydrocarbon ionomer literature. In a series of styrene-sodium methacrylate ionomers of different ion contents, the intensity of the "matrix" glass transition temperature (akin to the β-relaxation in PFSAs) was shown to decrease with increasing ion content.[6] This is attributed to the addition of multiplets to the matrix that restrict mobility of the surround polymer chains through physical crosslinks. In addition to the decrease in tanδ peak height with increasing ion content, a second peak was also observed at higher temperatures that increased in intensity and temperature with increasing ion content. This peak was attributed to the ionic cluster phase.[6] At

ion contents above 6 mol % in these polystyrene-methacrylate ionomers, the cluster glass transition becomes dominant over the matrix glass transition, suggesting that the cluster phase coalesces into a continuous network.[9] An analogous interpretation can be made in these PFSA systems with partial hydrolysis. A plot of tanδ peak height versus percent conversion of the sulfonyl fluorides into sulfonic acids (**Figure 3-14**) shows a crossover point where the α-relaxation becomes the dominant relaxation. The crossover point occurs at 20% conversion for 3M PFSA (ca. 3.8 mol % ion content based on 800 EW) and 23% conversion for Aquivion (ca. 3.3 mol % ion content based on 870 EW). In these short sidechain ionomers with relatively high functional sidechain contents, the α-relaxation becomes the principle relaxation at very low ion contents. Additionally, the complete decrease to extinction of the glass transition upon hydrolysis provides further evidence that the dominance of the hydrogen-bonded physical crosslinks that are anchored to the polymer main chains by a short sidechain effectively prevent the chain mobility necessary to observe the β-relaxation in H^+-form 3M PFSA and Aquivion membranes.

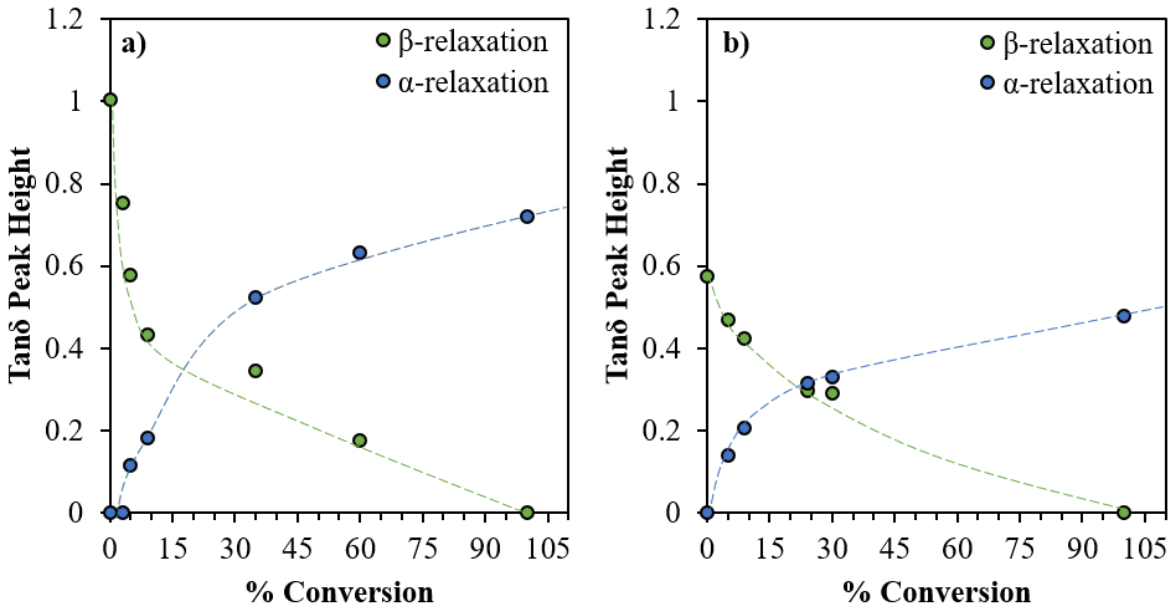

Figure 3-14. Dynamic mechanical tanδ peak height as a function of percent conversion of the sulfonyl fluoride groups to sulfonic acid groups for (a) 800 EW 3M PFSA and (b) Aquivion membranes.

3.3.4 Reconciling the Glass Transition Temperature for H^+-Nafion.

Figure 3-15 shows the α- and β-transition temperatures vs. TBA^+ content for Nafion® as previously published from our group in 2007.[14] The β-transition temperature observed for H^+-form Nafion was at ca. −26°C, which was inferred from the small peak observed in the tanδ around that temperature. The β-transition for pure TBA^+-form Nafion was observed at 86°C. Partial neutralization showed a steady decrease of the β-transition temperature with decreasing TBA^+ content and therefore the −26°C transition for the H^+-form was concluded to be of the same origin as the 86°C transition for the TBA^+-form and thus the true glass transition of Nafion.

Following the approach used above for the 3M PFSA and Aquivion, the same Fox formalism method can be applied to the Nafion system to determine the theoretical glass transition

temperature with intermediate TBA^+ contents utilizing both the β-relaxation temperature observed in the H^+-form (T_β = -26 °C) as the value for $T_{g,2}$ and the sulfonyl fluoride precursor glass transition temperature (T_g = 20 °C) as $T_{g,2}$ to determine which is a better fit to the observed data. In the case of $T_{g,2}$ = −26 °C, the neutralization data clearly does not fit the theoretical prediction. However, using $T_{g,2}$ = 20 °C in the Fox equation appears to fit the data better and only deviates at low TBA^+ ion content. Thus, the broader perspective of common behavior among PFSAs of different sidechain length suggests that the "true T_g" of Nafion is more reasonably in the vicinity of 20 °C. Moreover, the true T_g of PFSAs in their acid forms, in general, are likely more associated with segmental motions characteristic of their respective nonionic sulfonyl fluoride precursors (i.e., segmental motions of chains free of restrictions from strongly associating sidechains). However, in the pure acid forms, it is likely that water (and the complex array of hydrogen bonding interactions and water plasticization) can significantly perturb the observed relaxations.

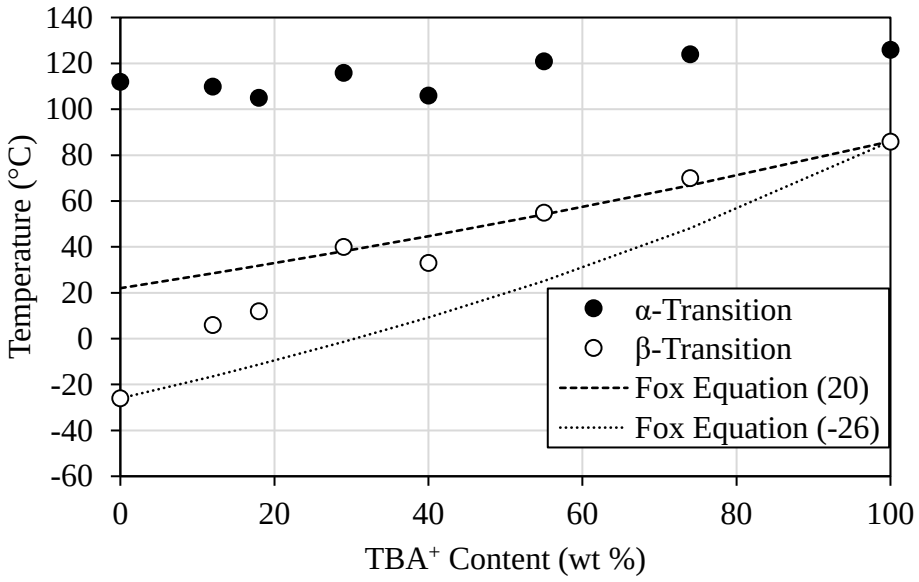

Figure 3-15. Transition temperature vs. TBA+ counterion content fit adapted from Osborn et. al.[14] overlaid with calculated Fox Equation using the original assumed Tg ($T_{g,1}$= −26°C) and the T_g of the precursor ($T_{g,2}$= 20°C).

The β-transition in Nafion has been reported in a range of temperatures from −62°C to 23°C in the literature demonstrating that this lower temperature relaxation subject to wide variability depending on test method and sample conditions.[3] This transition has also been shown to be very sensitive to water content as discussed in the previous section. While it is likely that the β-transition of H^+-form Nafion is the true glass transition temperature (onset of segmental motions within a static physically crosslinked network), it is reasonable to assume that these motions are strongly affected by water content. The glass transition temperature of completely dry H^+-form membranes, based on the findings of this investigation, is predicted to occur in the range of the sulfonyl fluoride precursor T_g, between 0 and 20°C. Deviation of the β-transition temperature from the theoretical Fox equation data begins to occur at low TBA^+ content when there is less of the bulky, hydrophobic counterion and higher sulfonic acid content that adsorbs water and leads to higher water content under ambient conditions thus decreasing the glass transition temperature.

Figure 3-16 shows dynamic mechanical tanδ versus temperature data for dry and hydrated Nafion 117. The "dry" Nafion was dried under vacuum overnight at 70°C prior to running. Hydrated Nafion was prepared by stirring in boiling water for 1 hour and blotted with a Kimwipe to remove excess water before running. In this experiment, the dry Nafion shows two distinct low temperature transitions at ca. −100°C and ca. −20°C. When hydrated, two separate γ- and β-relaxations are no longer observable. Even in a Nafion membrane that was equilibrated in 85 % relative humidity for 6 hours prior to running DMA, the resolution of the β-relaxation has started to decrease. While these findings require further investigation, it is apparent that the appearance of the β-relaxation in H^+-form Nafion is very susceptible to water content in the membrane.

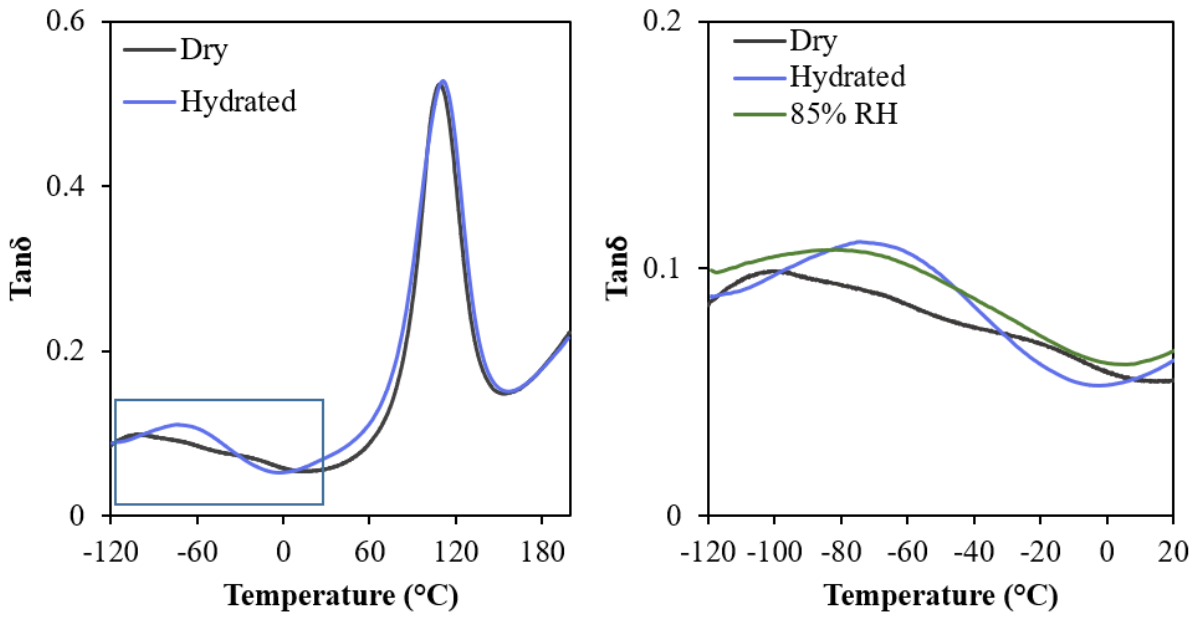

Figure 3-16. Tanδ vs. temperature for Nafion after drying under vacuum, boiling in water for 6 hours, and hydrating in 85% relative humidity chamber prior to running. On the right, the data is zoomed in to focus on the low temperature relaxations.

A schematic of the molecular dynamics for Nafion, C2, and C4 PFSAs is shown in **Figure 3-17**. The 3M PFSA (C4) has a high ion content (19 mol % for 800 EW and 22.5 mol % for 725 EW), which serves to increase the overall collective interactions of the ionic aggregates, leading to a stronger physical crosslink. These strong physical crosslinks then pull the backbone within a region of restricted mobility, where the mobility of the polymer chains within close proximity to the sulfonic acid sites is restricted due to the hydrogen-bonded interactions.[4] Similarly, the 870 EW C2 Aquivion contains an intermediate ion content (15 mol %) above that of 1100 EW Nafion (13 mol %) and below that of 3M PFSA. This finding is similar to what is observed in classic ionomer literature, where at elevated ion contents, the mobility of the matrix phase is restricted and the high-temperature cluster glass transition is the principle relaxation.[4,6]

In Nafion, it is important to note that the ion content is the lowest compared to the C2 and C4 PFSAs, but also the sidechain is longer and more flexible due to two ether linkages. The extended sidechain lengths in 3M PFSA, Aquivion, and Nafion (6.4 Å, 4.0 Å, and 8.2 Å, respectively) are well below the persistence length for PTFE (ca. 11.4 nm),[26] indicating that these sidechain structures are likely not very flexible. However, the incorporation of two ether linkages in the Nafion sidechain likely adds some provided mobility that allows for segmental motions of the backbone to occur within a static hydrogen-bonded network.

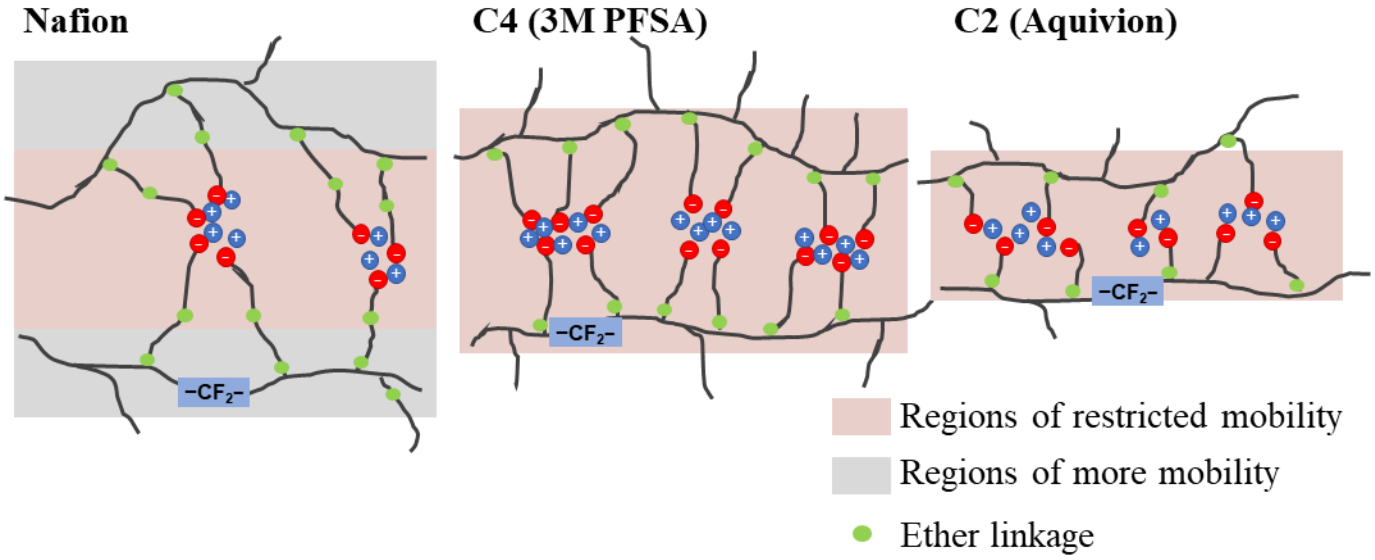

Figure 3-17. Schematic of the regions of restricted mobility around the ionic aggregates in Nafion, C4 3M PFSA, and C2 Aquivion.

3.4 Conclusions

This work provides a detailed analysis of the β-relaxation in shorter sidechain PFSAs that have yet to be investigated. Preliminary DMA data for 3M PFSA and Aquivion membranes in the H^+-form showed only two dynamic mechanical relaxations compared to the three observed in Nafion. Upon neutralization to TBA^+-form, all three relaxations are observed in these shorter

sidechain ionomers. Membranes that were partially neutralized with TBA^+ counterion showed a linear decrease in the β-relaxation temperature with decreasing counterion content. Interestingly, when extrapolated to 0 % TBA^+ content, the β-relaxation was predicted to occur at the same temperature as the glass transition in the nonionic sulfonyl fluoride precursor form of these ionomers, indicating that the underlying molecular motions of the nonionic glass transition do not occur in the H^+-form. This linear dependence was reconciled by using the Fox equation of polymer blends. At low TBA^+ contents, the β-relaxation was observed to "grow in" and increase in intensity with increasing ion content. This finding suggests that perhaps this relaxation that is associated with segmental motions of the mainchains *induced by sidechain mobility*, is completely suppressed in H^+-form 3M PFSA and Aquivion due to their high ion (sidechain) content but begins to appear when a large, bulky counterion is introduced to the system.

Partial hydrolysis of the sulfonyl fluoride precursor for 3M PFSA and Aquivion showed a decrease in peak intensity of the glass transition with increasing ion content. At less than 8% conversion of the SO_2F groups to SO_3H groups, the α-relaxation begins to appear and increases in magnitude and temperature with increasing ion content. A crossover point between dominance of the β- and the α-relaxations is observed for both Aquivion and 3M PFSA at ca. 3 mol % ion content, indicating that the hydrogen-bonded network becomes the principle phase in these PFSAs at very low ion contents. Upon complete conversion to the H^+-form, the β-relaxation is completely suppressed, confirming the conclusions from the TBA^+ neutralization experiments, that the mobility of the polymer chains is completely restricted by the physically crosslinked network in 3M PFSA and Aquivion. This behavior is reminiscent of classic ionomer systems where the matrix glass transition decreases in intensity while the cluster glass transition increases in intensity with increasing ion content.

The original assignment of the glass transition temperature for Nafion was at ca. −26°C based on a small peak in the DMA tanδ at that temperature. This same β-transition in the H^+-form has been reported to span a wide range of temperatures from −62 to 23°C.[3] Based on this work, predicted onset of segmental motions for dry H^+-Nafion is more likely to be in the range of 0 to 20°C, based on the T_g of the precursor and our new insights from this study of multiple sidechains and equivalent weights. Nafion has longer sidechain containing two flexible ether linkages that allow for more backbone mobility, particularly at lower ion contents. Additionally, it is likely that water appears to play a role in the appearance of the β-transition at lower temperatures in Nafion.

3.5 Acknowledgments

The authors acknowledge 3M for providing PFSA materials for this study and for funding this research.

3.6 References

1. Mauritz, K. A.; Moore, R. B., State of Understanding of Nafion. *Chem. Rev.* **2004**, *104*, 4535.
2. Hamrock, S. J.; Yandrasits, M. A., Proton Exchange Membranes for Fuel Cell Applications. *J. Macromol. Sci., Rev. Macromol. Chem. Phys.* **2006**, *46*, 219.
3. Kusoglu, A.; Weber, A. Z., New Insights into Perfluorinated Sulfonic-Acid Ionomers. *Chem. Rev.* **2017**, *117*, 987.
4. Eisenberg, A.; Hird, B.; Moore, R. B., A new multiplet-cluster model for the morphology of random ionomers. *Macromolecules* **1990**, *23*, 4098.

5. MacKnight, W. J.; Earnest, T. R., The structure and properties of ionomers. *J. Polymer Sci. Macromol. Rev.* **1981**, *16*, 41.

6. Kim, J.-S.; Jackman, R. J.; Eisenberg, A., Filler and Percolation Behavior of Ionic Aggregates in Styrene-Sodium Methacrylate Ionomers. *Macromolecules* **1994**, *27*, 2789.

7. Kim, J. S.; Wu, G.; Eisenberg, A., Viscoelastic properties of poly (styrene-co-acrylate) and poly (vinylcyclohexane-co-acrylate) ionomers. *Macromolecules* **1994**, *27*, 814.

8. Rigdahl, M.; Eisenberg, A., Viscoelastic properties of sulfonated styrene ionomers. *J. Polym. Sci., Part B: Polym. Phys.* **1981**, *19*, 1641.

9. Hird, B.; Eisenberg, A., Phase dominance, multiple glass transitions, and apparent activation energies in some poly (styrene-co-alkali methacrylate) ionomers. *J. Polym. Sci. Part B Polym. Phys.* **1990**, *28*, 1665.

10. Kyu, T.; Hashiyama, M.; Eisenberg, A., Dynamic mechanical studies of partially ionized and neutralized Nafion polymers. *Can. J. Chem.* **1983**, *61*, 680.

11. Page, K. A.; Cable, K. M.; Moore, R. B., Molecular Origins of the Thermal Transitions and Dynamic Mechanical Relaxations in Perfluorosulfonate Ionomers. *Macromolecules* **2005**, *38*, 6472.

12. Phillips, A. K.; Moore, R. B., Mechanical and transport property modifications of perfluorosulfonate ionomer membranes prepared with mixed organic and inorganic counterions. *J. Polym. Sci. Part B Polym. Phys.* **2006**, *44*, 2267.

13. Kim, J. S.; Roberts, S. B.; Eisenberg, A.; Moore, R. B., Preferential cluster-phase plasticization of ionomers containing surfactant molecules. *Macromolecules* **1993**, *26*, 5256.

14. Osborn, S. J.; Hassan, M. K.; Divoux, G. M.; Rhoades, D. W.; Mauritz, K. A.; Moore, R. B., Glass Transition Temperature of Perfluorosulfonic Acid Ionomers. *Macromolecules (Washington, DC, U. S.)* **2007**, *40*, 3886.

15. Moukheiber, E.; De Moor, G.; Flandin, L.; Bas, C., Investigation of ionomer structure through its dependence on ion exchange capacity (IEC). *J. Membr. Sci.* **2012**, *389*, 294.

16. Giffin, G. A.; Haugen, G. M.; Hamrock, S. J.; Di Noto, V., Interplay between Structure and Relaxations in Perfluorosulfonic Acid Proton Conducting Membranes. *J. Am. Chem. Soc.* **2013**, *135*, 822.

17. Tesfaye, M.; Kushner, D. I.; McCloskey, B. D.; Weber, A. Z.; Kusoglu, A., Thermal Transitions in Perfluorosulfonated Ionomer Thin-Films. *ACS Macro Lett.* **2018**, *7*, 1237.

18. Li, J.; Pan, M.; Tang, H., Understanding short-side-chain perfluorinated sulfonic acid and its application for high temperature polymer electrolyte membrane fuel cells. *RSC Adv.* **2014**, *4*, 3944.

19. Hamrock, S. J. *Membranes and MEA's for Dry, Hot Operating Conditions*, 3M Company, 2011.

20. Emery, M.; Frey, M.; Guerra, M.; Haugen, G.; Hintzer, K.; Kai; Lochhaas, H.; Pham, P.; Pierpont, D.; Schaberg, M.; Thaler, A.; Yandrasits, M.; Hamrock, S., The Development of New Membranes for Proton Exchange Membrane Fuel Cells *J. Electrochem. Soc.* **2007**, *11*, 3.

21. Moore, R. B.; Cable, K. M.; Croley, T. L., Barriers to flow in semicrystalline ionomers. A procedure for preparing melt-processed perfluorosulfonate ionomer films and membranes. *J. Membr. Sci.* **1992**, *75*, 7.

22. Weiss, R. A.; Agarwal, P. K.; Lundberg, R. D., Control of ionic interactions in sulfonated polystyrene ionomers by the use of alkyl-substituted ammonium counterions. *J. Appl. Polym. Sci.* **1984**, *29*, 2719.

23. Fox, T. G., Influence of Diluent and of Copolymer Composition on the Glass Temperature of a Poly-mer System. *Bull. Am. Phys. Soc.* **1956**, *1*, 123.

24. Perusich, S. A., FTIR equivalent weight determination of perfluorosulfonate polymers. *J. Appl. Polym. Sci.* **2011**, *120*, 165.

25. Heitner-Wirguin, C., Infra-red spectra of perfluorinated cation-exchanged membranes. *Polymer* **1979**, *20*, 371.

26. Salerno, K. M.; Bernstein, N., Persistence Length, End-to-End Distance, and Structure of Coarse-Grained Polymers. *J. Chem. Theory Comput.* **2018**, *14*, 2219.

Chapter 4.

Probing the Morphological Origins of Thermomechanical Behavior in Perfluoroimide Acid Ionomer Membranes

(Published in ECS Transactions)

(Expanded)

Christina M. Orsino,[a] Matthew Lindell,[b] Michael Yandrasits,[b] Steven Hamrock,[b] Melissa Novy,[a] and Robert B. Moore[a]*

[a] *Department of Chemistry, Macromolecules Innovation Institute, Virginia Tech, Blacksburg, VA 24060*

[2]*3M Company, St. Paul, MN, 55144, USA*

**To whom correspondence should be addressed: rbmoore3@vt.edu*

4.1 Introduction

Perfluorosulfonic acid ionomers (PFSAs) are a class of random ionomers containing runs of tetrafluoroethylene and up to ca. 22 mol percent perfluorinated sidechains with pendant sulfonic acid groups.[1,2] These ionomers are the most commonly used polymers for membranes in proton exchange membrane (PEM) fuel cells due to their exceptional proton conductivity and chemical and physical durability.[3] The polar sidechains on PFSAs have been shown to organize into aggregates, leading to a nanophase separated morphology where the ionic domains are dispersed in a percolated network throughout the nonpolar poly(tetrafluoroethylene) (PTFE) matrix. This

complex, phase separated morphology between the nonpolar backbone and polar sidechains leads to remarkable proton conductivity and mechanical properties. While the sulfonic acid groups facilitate proton exchange through the membrane, runs of pure PTFE between sidechains allow for crystallizability that leads to high mechanical stability and limited water uptake, thus reducing the likelihood of swelling-induced thinning and pinholes in the membranes.[4,5] These properties are necessary for the stress and lifetime requirements of a PEM fuel cell.

PFSAs are characterized by their equivalent weight (EW) that relates the number (*n*) of TFE units (molar mass = 100 g/mol) in the backbone between sidechains to the molar mass of the sidechain structure ($MW_{sidechain}$) and ion exchange capacity (IEC, milliequivalents/g) through the following equation:

$$EW = \frac{g\ polymer}{equivalents\ PEG} = \frac{1000}{IEC} = 100n + MW_{side\ chain} \quad (1)$$

Where the nominal EW value is considered in terms of grams of polymer per mol equivalent of proton exchange groups (PEG). For use in the harsh conditions of a PEM fuel cell, PFSAs must have a balance of crystallizable TFE backbone units (*n*) for mechanical stability and high IEC for proton conductivity.

Several PFSA ionomers have been developed with differing sidechain chemistries in order to optimize functionality for critical proton transport, while maintaining desirable mechanical properties as thin membranes. As the first PFSA, and consequently the benchmark membrane, Nafion® (**Figure 4-1**) has been the most widely studied PFSA for use in PEM fuel cells.[1] It has the conventional perfluorinated ionomer structure consisting of a PTFE backbone with sidechains bearing a single pendant sulfonic acid group, and typically has an EW of 1000 to 1100 g/eq. In 2007, 3M developed a version of the PFSA ionomer, named 3M PFSA (**Figure 4-1**), with a shorter

sidechain that allows for EW values as low as 800 g/eq while maintaining good mechanical properties.[5] Additional short sidechain structure PFSAs have been developed by Solvay, named Aquivion, achieving EW values as low as 870 g/eq in their commercial membranes. An obvious tradeoff of these single sulfonic acid PFSA structures is that the only way to improve IEC is to sacrifice the average number of crystallizable TFE units in the backbone, which tends to adversely increase water uptake and decrease mechanical stability.[5,6]

In 2010, 3M first reported their development of a new multi-acid sidechain ionomer, named perfluoroimide acid ionomer (3M PFIA) (**Figure 4-1**), for use in high temperature fuel cells.[7,8] The 3M PFIA contains an acidic bis(sulfonyl)imide group on each sidechain in addition to a terminal sulfonic acid group. These two acidic sites per sidechain offers a decreased EW while maintaining long runs of PTFE in the backbone for sufficient crystallizability and, thus, maintained mechanical properties. Starting with the same sulfonyl fluoride precursor material as an 825 EW PFSA, the sidechain extended PFIA has an EW of 625 g/eq with the same number of TFE units between sidechains (n = 4) as the 825 EW PFSA. For example, WAXS data comparing a 1,000 EW precursor and the generated 700 EW PFIA analog membranes has shown that the extra length on the sidechain from additional acidic sites does not affect the backbone crystallinity.[9] Additionally, the PFIA ionomer has been shown to have higher proton conductivity than its parent PFSA ionomer across a range of humidity levels and temperatures.[7,9-11] This demonstrates its promise for its use in fuel cells operated at higher temperatures and lower humidity, although with possible durability issues stemming from chemical degradation of the sidechain.[8] Despite these stability issues, the PFIA multi-acid sidechain concept has been shown to be a promising new technology for the advancement of proton conducting membranes.

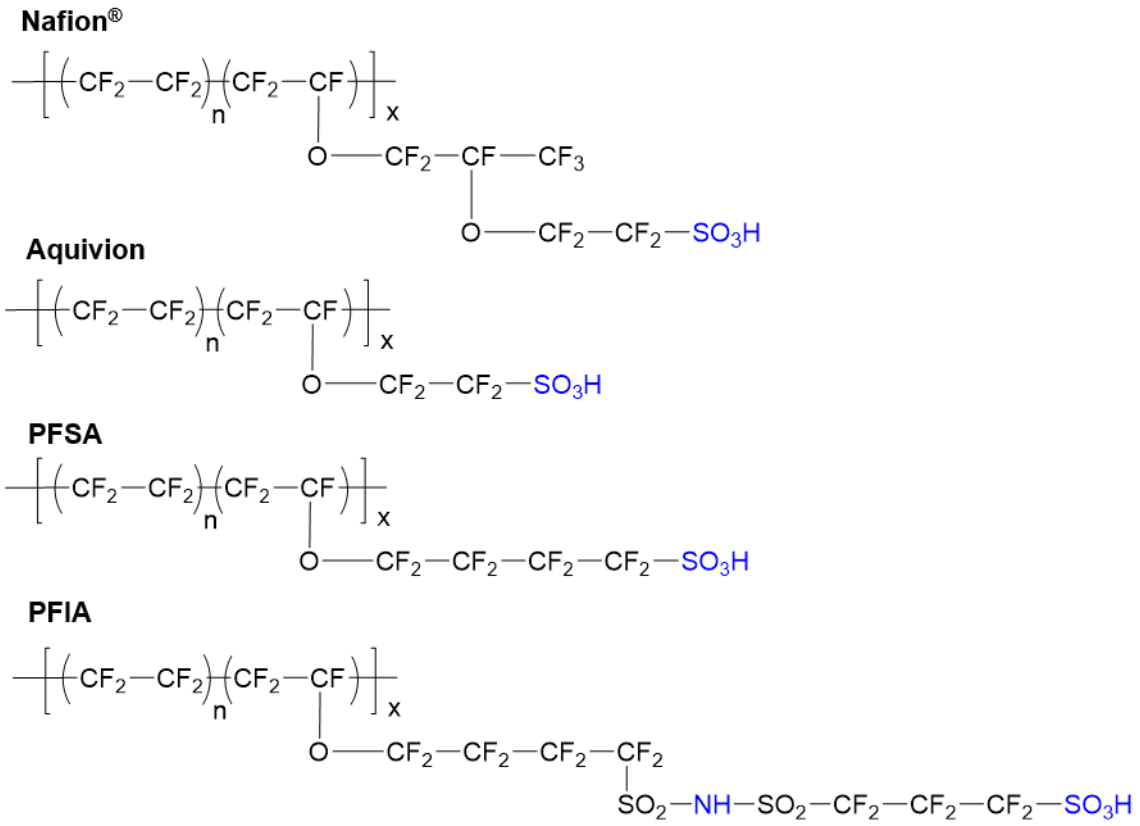

Figure 4-1. Chemical structures for Nafion, Aquivion, 3M PFSA and 3M PFIA.

Recent studies on PFIA have aimed to gain a better understanding of the role that the acidic bis(sulfonyl)imide group plays in hydration and proton transport compared to single acid PFSA ionomers.[11-18] Atomic force microscopy (AFM) studies and MD simulations have shown that the PFIA has higher proton diffusion rates, elevated water content across all relative humidities, and larger hydrophilic domains compared to PFSAs.[14,15,17] A study conducted on interfacial and bulk water in ultrathin Nafion, 3M PFSA, and PFIA membranes using ellipsometry and neutron reflectometry also showed much higher levels of hydration in the PFIA/platinum interface than observed for the PFSA counterparts.[13] More recently, advanced scattering techniques were used to determine the chemical and morphological origins of improved conductivity in PFIA ionomers bearing multiple imide units per sidechain.[12] This study gave a glimpse into the unique

morphologies of the ionic aggregates in PFIA compared to its parent 3M PFSA ionomer, consisting of more ordered phase-separation and nanoscale transport pathways that facilitate proton transport.

Currently, the majority of studies performed on PFIA ionomers have focused on how the addition of a bis(sulfonyl)imide group in the sidechain leads to increased hydration and proton conductivity. These studies are certainly important for the fuel cell community in attempt to find new membranes for increased performance at higher temperatures. However, in contrast to the wealth of information available for PFSAs, little is known about the morphological contributions to the thermomechanical properties of PFIAs. Such information is critical to understanding the fundamental structure-processing-property relationships of these materials for use in high temperature fuel cell operations and high temperature processing conditions.

Multiple PFSA reviews, including a recent review from our group specifically on the thermal transitions and mechanical relaxations in PFSAs,[19] have summarized the historical perspective on the morphology and molecular-level assignments of thermomechanical relaxations in PFSAs.[1,2,20]. Three thermomechanical relaxations have been observed in PFSAs, two of which (the high temperature α-relaxation and lower temperature β-relaxation) are coupled to the physical crosslinks that form due to aggregation of the sulfonate groups terminating each sidechain. In terms of thermal and mechanical properties of PFSAs, these ionic aggregates are generally accepted to constitute the electrostatic networks and thus control segmental mobility. Because thermomechanical relaxations in PFSAs are coupled to their ionic aggregate structures, small angle x-ray scattering studies have been utilized to characterize the underlying morphological origins of these relaxations.

In order to accelerate the development of next generation fuel cell membranes such as 3M PFIA, it is necessary to gain fundamental insight into the effect of a multi-acid sidechain on the

morphology and thermomechanical properties of these unique perfluorinated ionomers. This work presents the first in-depth study of the thermomechanical properties and aggregate morphology of 3M PFIA compared to its parent ionomer, 3M PFSA. By utilizing a 3M PFSA that contains the same value of *n* in the backbone as a comparison, the effect of the differing sidechain chemistries on the thermal transitions in 3M PFIA can be elucidated. Dynamic mechanical analysis (DMA) is utilized to determine the thermomechanical relaxations of 3M PFIA in the acid-form (H^+-form) as well as the neutralized Na^+-form. Differential scanning calorimetry (DSC) is then employed to further confirm the transitions observed by DMA and to investigate the appearance of a distinct glass transition temperature that is observed in 3M PFIA. Modeling of SAXS data for PFIA and PFSA reveal significant distinctions between the aggregate structures that can account for the underlying differences in thermomechanical relaxations between PFIA and PFSA.

4.2 Experimental

4.2.1 Materials

3M Perfluoroimide acid (PFIA) of 625 EW and 3M perfluorosulfonic acid (PFSA) of 825 and 1000 EW powders were provided by 3M. Nafion® 117 (1100 EW) membrane was purchased DuPont and Aquivion® E87-05S (870 EW) membrane was purchased from Sigma Aldrich. All other reagents and solvents were obtained from Sigma-Aldrich and used without further purification.

4.2.2 Membrane preparation

PFIA and PFSA membranes were prepared by casting a concentrated dispersion from ethanol and water onto a polyimide film utilizing an Elcometer motorized film applicator with a

casting knife set to a wet thickness of 200 μm. The cast films were dried in an oven at 80 °C, followed by annealing for 10 minutes at 200 °C. Membranes of approximately 25-40 μm in thickness were removed from the polyimide film by soaking in water. To remove impurities, the membranes were soaked in 8 M HNO_3 for 16 hours then rinsed five times with deionized water. The Na^+-, K^+-, Rb^+-, and Cs^+-form membranes were prepared by soaking the HNO_3-treated membranes in 1 M solutions of the appropriate group 1A hydroxide in water, while the Mg^{2+}-form was prepared by soaking in 0.5 M solution of $MgSO_4$ in water. After treatment, all membranes were thoroughly rinsed with water before drying under vacuum at 70 °C overnight. Extruded Nafion and Aquivion membranes for supplemental experiments were used as received and treated following the same procedure as the cast PFIA and PFSA membranes.

Partial neutralization of the 3M PFIA samples with Na^+ counterion was performed by stirring the membranes in NaOH solutions containing specified quantities of NaOH for 24 hours followed by rinsing with water. On the basis of equivalent weight of dry PFIA, the following ratios of H^+-form to Na^+-form membranes were prepared: 100/0, 75/25, 50/50, 25/75, 0/100. All membranes were rinsed thoroughly with water and dried under vacuum overnight at 70 °C after neutralization.

4.2.3 Thermomechanical Characterization

Dynamic mechanical analysis was performed on a TA Instruments DMA Q800 analyzer in tensile mode using clamps for thin film samples. All samples were cut from vacuum dried membranes with a width of 6.35 mm. The membranes were analyzed at a frequency of 1 Hz from 20 to 200 °C in the acid-form, 50 to 400 °C for the monovalent cation neutralized membranes, and 50 to 500 °C for the Mg^{2+}-form membranes with a heating ramp of 2 °C/min.

DSC data were collected for the neutralized ionomers on a TA Instruments Q2000 at 20 °C/min ramp rate under nitrogen purge. Initial DSC thermograms were obtained after thoroughly drying the samples in the DSC at 120 °C for 2 hours. The thermograms described as "slow cooled" were dried for 2 hours at 120 °C, cooled to 0 °C, ramped from 0 to 350 °C at 20 °C/min, then slow cooled back to 0 °C at 20 °C/min. Thermograms described as "second heat" were then ramped again from 0 to 350 °C at 20 °C/min after following the previous steps. For annealing experiments, samples were annealed in the DSC at 120, 150, 180, 210, and 240 °C for two hours prior to being cooled to 50 °C then ramped from 50 °C to 350 °C at 20 °C/min. For the physical aging study, 3M PFIA and 3M PFSA samples were held at 150 °C for 0, 0.5, 2, 6 and 12 hours in the DSC prior to being cooled to 50 °C then ramped from 50 °C to 350 °C at 20 °C/min.

4.2.4 Small Angle X-Ray Scattering and Model Fitting

Small angle X-ray scattering (SAXS) experiments were performed on dry membranes in the H^+-, Na^+-, and Cs^+-forms using a Rigaku S-Max 3000 3 pinhole SAXS system, equipped with a rotating anode emitting X-ray with a wavelength of 0.154 nm (Cu Kα). The sample-to-detector distance was 1603 mm and the q-range was calibrated using a silver behenate standard. Two-dimensional SAXS patterns were obtained using a 2D multiwire, proportional counting, gas-filled detector, with an exposure time of 2 hours. All the SAXS data were analyzed using the SAXSGUI software package to obtain radially integrated SAXS and WAXD intensity versus the scattering vector q, where $q = (4\pi/\lambda)\sin(\theta)$, θ is one half of the scattering angle and λ is the X-ray wavelength. The SAXS data were corrected for sample thickness and transmission and fit with the Kinning Thomas modified hard sphere model,[21] and a modified hard cylinder model.[22]

4.3 Results & Discussion

4.3.1 Dynamic Mechanical Analysis

The thermomechanical properties of PFSAs have been well studied by dynamic mechanical analysis (DMA) since 1977.[20,23-28] In the dynamic mechanical spectrum for Nafion®, there are three apparent relaxations assigned as α, β, and γ. The lowest temperature relaxation T_{γ}, occurs at ca. −100 °C and has been attributed to the local motions of the PTFE backbone. A second relaxation, T_{β}, has been observed at temperatures ranging between −62 and 23 °C, depending on the study. This relaxation has been assigned as the true glass transition temperature of Nafion® and, more specifically, the onset of segmental motions within a static electrostatic network.[20,29] Lastly, the high temperature relaxation, T_{α}, is observed at ca. 100 °C and is attributed to the onset of long-range motions of both the main and side chains facilitated by a weakening of the electrostatic interactions within the ionic aggregates due to ion-hopping (i.e., the ion pairs "hop" from one aggregate to another in order to relieve local stress).[20] The temperatures at which these relaxations occur can be varied upon neutralization of the H^+ to other counterions. For example, T_{α} at 100 °C for H^+-form Nafion® increases to 200 °C upon conversion to the Na^+-form, a shift that is attributed to the increase in network strength when converting from a weak hydrogen-bonded physically crosslinked network to a strong electrostatic network.[20] The chain motions associated with both α- and β-relaxations are coupled to the physical crosslinks within the ionic aggregates.[28] The origins of thermomechanical relaxations in perfluorinated ionomers can be elucidated by manipulating the strength of the physically crosslinked network with different counterions.

Figure 4-2A shows the results obtained from DMA for 625 EW 3M PFIA and its parent ionomer (same *n* value), 825 EW 3M PFSA, in the H^+-form. Both ionomers exhibit an α-relaxation at ca. 125 °C for 3M PFSA and 145 °C for 3M PFIA. In perfluorinated ionomers, the α-relaxation has been assigned to long range motions of both main and side chains through destabilization of the physical network (i.e., the hydrogen-bonded network in these acid-form PFSAs).[20] While 3M PFSA does not appear to have a β-transition in this temperature range, a small broad peak is observed for 3M PFIA in the range of ca. 50 to 90 °C.

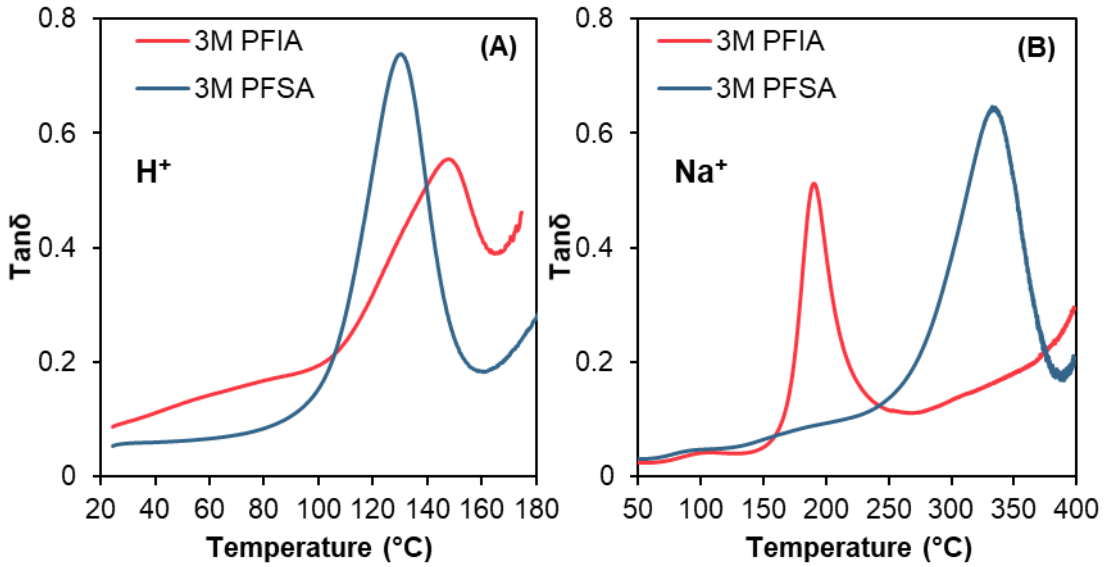

Figure 4-2. Dynamic mechanical tanδ versus temperature plots for 3M PFIA and 3M PFSA in the (A) H^+-form and (B) Na^+-form membranes.

In order to investigate the differences in the dynamic mechanical data, membranes were fully neutralized with sodium counterions (Na^+-form) to observe the effect of counterion type on the dynamic mechanical relaxations in 3M-PFIA. **Figure 4-2B** shows the DMA data for 3M PFIA and 3M PFSA in the Na^+-form. It is important to note here that the physical network in the neutralized ionomers is now an electrostatic network established through much stronger electrostatic dipole-dipole interactions, relative to the weaker hydrogen-bonded network in the H^+-

form materials. Upon complete neutralization, the T_α for the 3M PFSA shifts over 200 °C from 130 °C (H^+-form) to ca. 335 °C (Na^+-form). By comparison, the difference between T_α for Nafion® 1100 EW in the H^+ and Na^+-form is only 100 °C.[20] The increased shift observed for the 825 EW 3M PFSA is expected for an ionomer with lower EW (i.e., higher ion content) and attributed to enhanced chain immobilization by a more electrostatically crosslinked network. Similarly, short-sidechain Aquivion (containing two CF_2 groups and a pendant sulfonic acid) with an EW of 870 g/eq has an α-relaxation at 120°C in the H^+-form and increases to 350 °C in the Na^+-form (See **Figure S4-1**). The 3M PFIA, however, appears profoundly different than the 3M PFSA, Aquivion, and Nafion when fully neutralized to the Na^+-form. Considering that 3M PFIA has a low equivalent weight (625 g/eq) compared to 3M PFSA (825 g/eq) and a higher T_α in the H^+-form, one would expect the T_α to increase to a higher temperature than 3M PFSA when neutralized. Interestingly, the DMA data for Na^+-form 3M PFIA shows a prominent relaxation at ca. 190 °C, which is well below the T_α for 825 EW 3M, 870 EW Aquivion, and 1100 EW Nafion® in the Na^+-form. Based on the tanδ data alone, it is now unclear if the intense peak at 190 °C is of the same molecular origin as α-relaxation of 3M PFIA or an increase in the magnitude of the β-relaxation still within a physically crosslinked network.

The storage modulus versus temperature data for H^+- and Na^+-form 3M PFIA and 825 EW 3M PFSA membranes is shown in **Figure 4-3**. In the H^+-form, the 3M PFIA passes through a noticeable β-relaxation at ca. 60°C then a large α-relaxation at ca. 130°C, similar to the observed drops in storage modulus for both relaxations in TMA^+-form Nafion.[20] The 3M PFSA has an α-transition temperature slightly lower than 3M PFIA in the H^+-form. Both ionomers have a rubbery plateau above the α-transition that is observed in both Nafion and Aquivion H^+-form ionomers as

well (See **Figure S4-2**). For each of the ionomers, this high temperature plateau is likely attributed to physical crosslinks present with the semi-crystalline matrix.

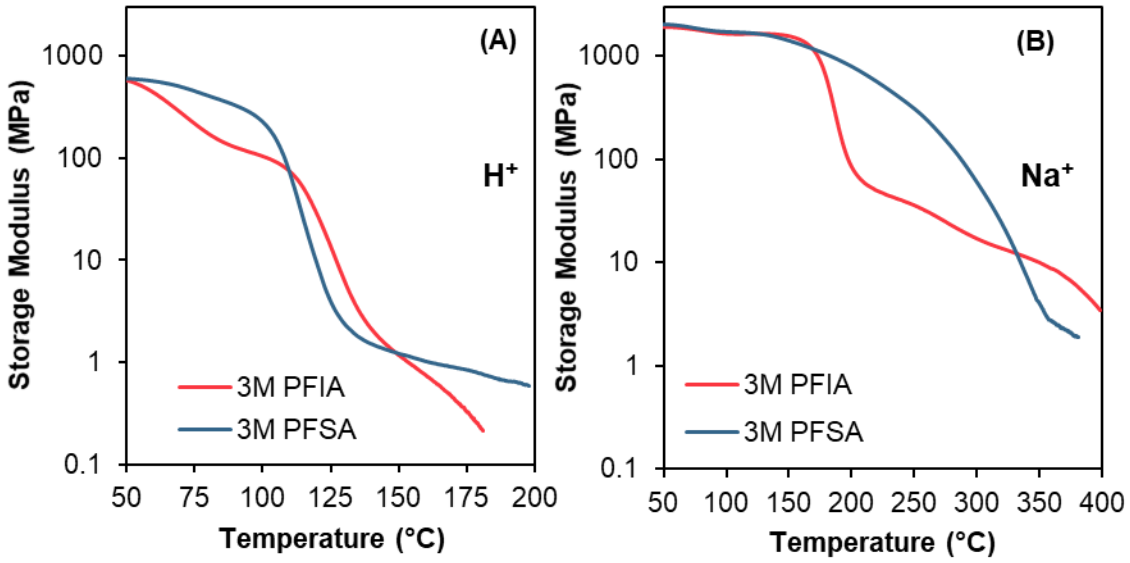

Figure 4-3. Dynamic mechanical storage modulus versus temperature for (A) H^+-form and (B) Na^+-form PFIA and PFSA.

Upon conversion to the Na^+-form, the observed storage modulus profile for 3M PFSA is typical of perfluorosulfonic acid ionomers neutralized with an alkali metal counterion.[20] The temperature at which the storage modulus drops several orders of magnitude is much higher in 3M PFSA than in 3M PFIA. The large modulus drop in Na^+-form 3M PFIA begins around 160 °C, although, interestingly, there is a distinct rubbery plateau for 3M PFIA that has not been observed in other perfluorinated ionomer systems in the Na^+-form. We originally attributed this rubbery plateau to mechanical integrity provided by an electrostatic network creating physical crosslinks, suggesting that the large peak in tanδ at 190 °C is the β-relaxation for PFIA.[30] In 3M PFIA, there appears to be a small drop in storage modulus between 200 and 250 °C, within the rubbery plateau region, that is likely due to melting of the PTFE-like crystallites. In 3M PFSA, the melting of

crystallites occurs simultaneously with the onset of ion-hopping, which leads to a very broad drop in storage modulus over a wide temperature range.

Partial neutralization of Nafion membranes has been used in the past to clarify the molecular origins of relaxations observed in DMA.[28,29] Because the α- and β-relaxations are both coupled to the strength of the physically crosslinked network, it is possible to systematically manipulate that network and track the shift in temperature of these relaxations. Dynamic mechanical tanδ data for a series of partially neutralized 3M PFIA and 3M PFSA membranes are shown in **Figure 4-4**. For both the PFSA and PFIA, it can be observed that the α-relaxation in the H^+-form systematically shifts to higher temperatures with increasing Na^+ incorporation. The systematic shift in α-relaxation temperature with counterion composition is akin to the characteristic behavior of miscible polymer blends (e.g., H^+ PFSA molecularly mixed with Na^+ PFSA).[28,29] Assuming that the Na^+ counterion is homogeneously distributed among acidic groups in the membranes, the clear compositional shift of the α-relaxation in the H^+-form to the dominant relaxation in the Na^+-form ionomers indicates that both relaxations are of the same molecular origin. Moreover, these data suggest that the dominant relaxation in the Na^+-form 3M PFIA is in fact an α-relaxation, which has the same molecular origin as the α-relaxation of the 3M PFSA.

Also notable in **Figure 4-4A** is that 3M PFIA has a clear β-relaxation in the H^+-form that appears to systematically shift to higher temperatures with increasing Na^+ content. This finding is similar to observations of classic ionomer systems where increasing ion content results in an increase in the matrix glass transition temperature due to the electrostatic interactions between ions that act as physical crosslinks.[31] Similarly, in TBA^+/Na^+ mixed counterion Nafion membranes, the β-relaxation was also shown to shift to increasing temperatures with increasing Na^+-counterion content.[28] This was attributed to the increased strength of the electrostatic network formed from

small Na^+ counterions, as opposed to bulky TBA^+ counterions, that restricted the mobility of the polymer chains and resulted in an increase in both the α- and β-relaxations. The α- and β-relaxations are both coupled to the electrostatic forces within the aggregates and thus both are expected to systematically shift with counterion composition. This is strong evidence that the large relaxation observed in Na^+-form 3M PFIA is the α-relaxation for that ionomer as opposed to the β-relaxation as previously attributed.[30]

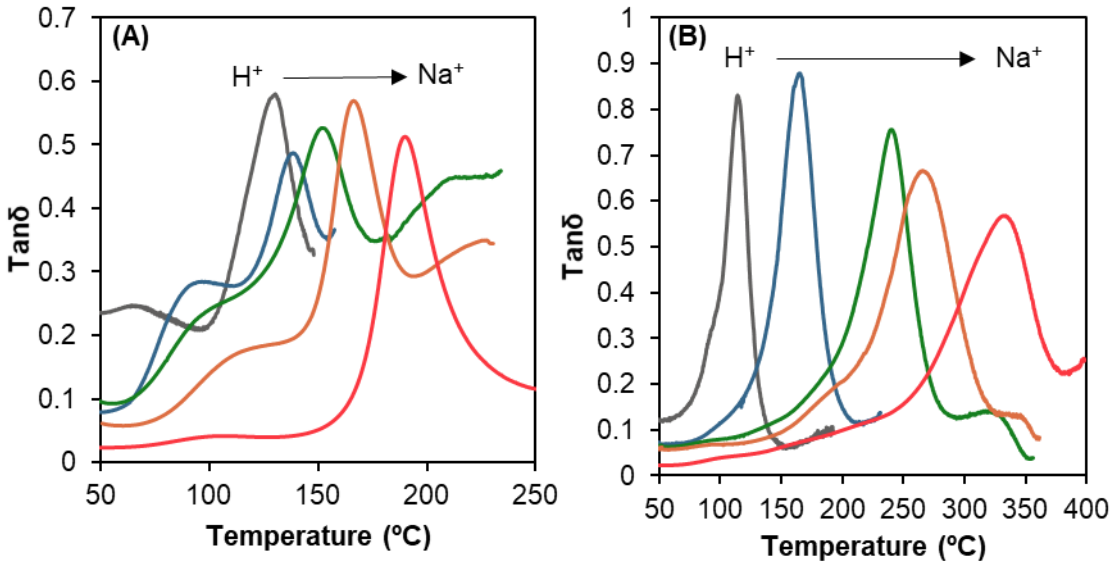

Figure 4-4. Dynamic mechanical tanδ versus temperature plots for partially neutralized (A) 3M PFIA and (B) 3M PFSA membranes. From left to right: 100/0, 75/25, 50/50, 25/75, and 0/100 H^+/Na^+-form membranes.

Shifts in the α-relaxation temperature with Na^+ counterion content for both 3M PFIA and 3M PFSA are plotted in **Figure 4-5**. For both ionomers, the α-relaxation temperature for the intermediate counterion contents occurs at temperatures in between the relaxation temperature for the two pure components. A similar study done on mixed counterion (TBA^+/Na^+) Nafion membranes showed the α-relaxation temperature dependence on counterion content follows the Fox formalism for polymer blends.[28] Since the α-relaxation is assigned to the onset of long-range

mobility of polymer chains resulting from destabilization of the electrostatic network, it was expected that this relaxation would track with counterion composition following the simple rule-of-mixtures concept. In **Figure 4-5**, the dominant relaxation temperatures for 3M PFIA and 3M PFSA were plotted along with the Fox equation[32] based on counterion composition

$$\frac{1}{T_r} = \frac{\omega_1}{T_{r1}} + \frac{\omega_2}{T_{r2}} \quad (2)$$

Where the observed relaxation temperature (T_r) depends on the weight fraction (ω_1 and ω_2) of the two pure components and their respective relaxation temperatures (T_{r1} and T_{r2}).[28] In the case of 3M PFIA and 3M PFSA, the observed relaxation temperature increases with increasing Na^+ counterion content following the rule-of-mixtures. This is strong evidence that the large relaxation observed in Na^+-form 3M PFIA is of the same molecular origin as the α-relaxation in the H^+-form. Thus, the principle relaxation in Na^+-form 3M PFIA at ca. 190 °C is attributed to the onset of long-range mobility of the chains/sidechains as a result of destabilization of the electrostatic network.[20] The underlying question that arises from these findings is why the α-relaxation in PFIA occurs 150 °C lower than that of its parent ionomer PFSA despite having a higher ion content. In order to address this, further information is necessary about the aggregate structure for each ionomer, which will be addressed in the following sections.

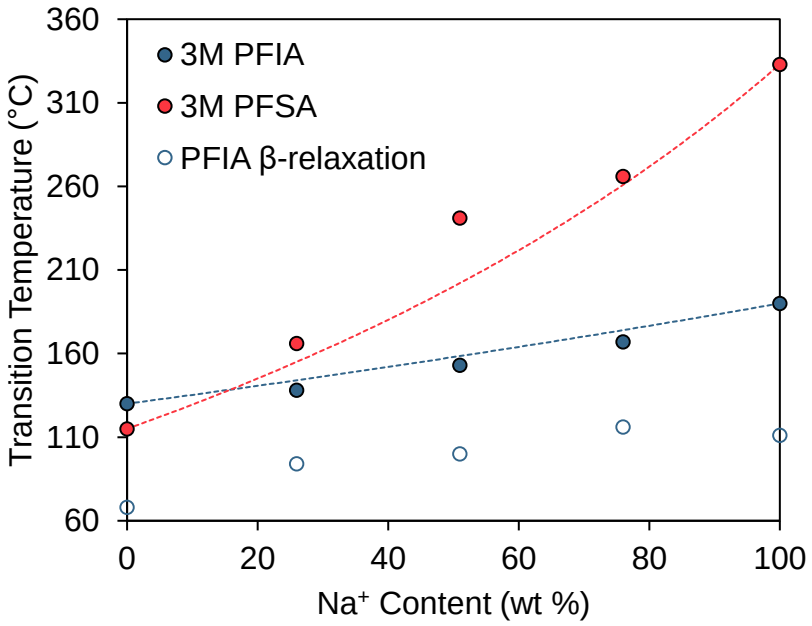

Figure 4-5. Relaxation temperature vs. Na^+ content for both 3M PFIA and 3M PFSA membranes partially neutralized with Na^+ counterion. The points are plotted along the theoretical Fox equation (dashed lines) for the two systems.

Now, to explain the rubbery plateau in the storage modulus data above this α-relaxation for Na^+-form 3M PFIA presented in **Figure 4-3**, the concept of ion-hopping must be considered. In the rheological behavior of ionomers, the terminal relaxation time is determined by the amount of time that an ion pair spends in an aggregate before "hopping" to another aggregate in a thermally activated process, called ion-hopping.[33] The "ion-hopping temperature" (cluster glass transition temperature) is characterized as the temperature at which the aggregates become thermodynamically unstable and elastic forces imposed on the polymer chains are balanced with the electrostatic forces of the aggregates.[34,35] This ion-hopping process is the same mechanism attributed to the α-relaxation in PFSAs.[20,35] At temperatures in the vicinity of the α-relaxation, the elastic forces imposed on the polymer chains results in ion-pairs hopping from one aggregate to another, resulting in a dynamic network. In 3M PFIA, however, the two ion pairs on each sidechain

each act as a physical crosslink that restricts mobility of the sidechains to which they are attached. Upon the onset of ion-hopping, the probability of both ion pairs on one sidechain hopping from one aggregate to another at the same time is low. For this reason, some mechanical integrity is still maintained even after the physically crosslinked network has transitioned into a dynamic network.

4.3.2 Differential Scanning Calorimetry

Figure 4-6 shows first heat, cool, and second heat DSC thermograms for Na^+-form 3M PFIA and parent 3M PFSA in the Na^+-form. Both ionomers display a small melting endotherm at 280 °C that disappears upon second heat. This thermal behavior is typical of semicrystalline ionomers (where electrostatic interactions profoundly slow recrystallization),[36,37] and is attributed to the melting of PTFE-like crystallites.[20] A noteworthy difference between the DSC thermograms of 3M PFIA and 3M PFSA is the endothermic event that appears at ca. 170 °C in all scans of 3M PFIA. This endotherm occurs at the same temperature as the large α-relaxation observed in the DMA data indicating that it is likely of the same molecular origin. Arrows in **Figure 4-6A** indicate the temperature at which a distinct and reversible change in heat capacity occurs, characteristic of a glass transition. In the 3M PFSA, there is a small, broad endotherm at a similar temperature in the first heat, but reversibility is lost upon subsequent cool and reheat.

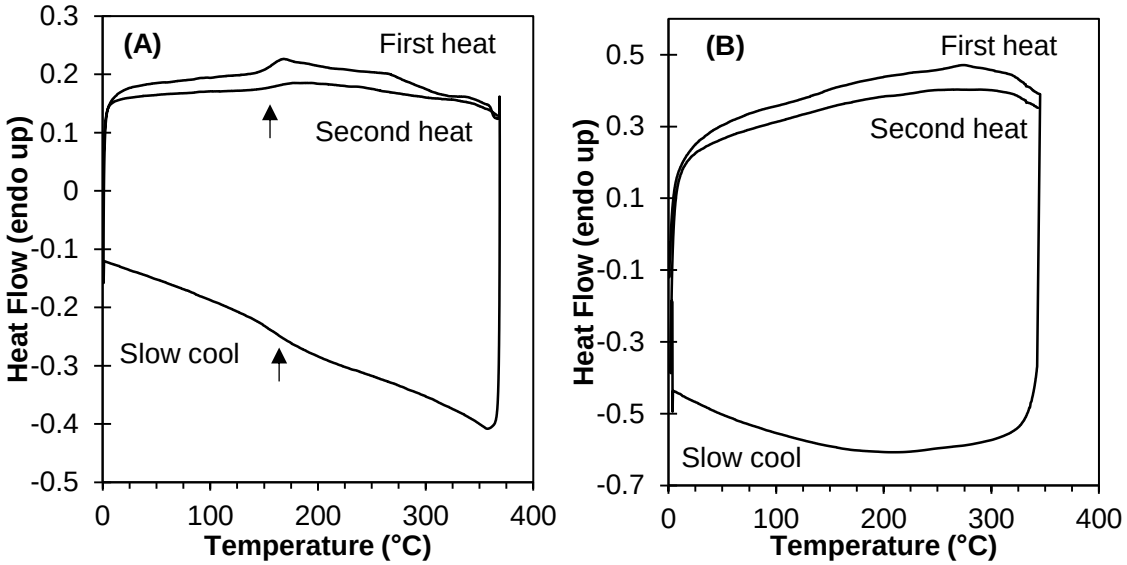

Figure 4-6. DSC thermograms of Na^+ form (A) 3M PFIA and (B) 825 EW 3M PFSA first heat, slow cool, and second heat at a ramp rate of 20 °C/min.

Multiple endothermic events have been well documented in the literature for perfluorinated ionomers.[23,24,38,39] Two endothermic events were originally thought to correlate to the β and α DMA relaxations and were initially attributed to the glass transition temperature of the matrix and the ionic domains.[38,40] Almeida and Kawano later attributed the high temperature endotherm at ca. 230 °C to melting of PTFE crystallites in Nafion® while the lower temperature endothermic event was attributed to an order-disorder transition within the ionic clusters.[39] Ultimately, Page, Cable, and Moore were able to assign both the low and high temperature endotherms to melting of small and large crystallites, respectively.[20] The low temperature endotherm was shown to be dependent on thermal history by annealing at different temperatures and observed to systematically shift to higher temperatures with increasing annealing temperature, as commonly observed in semi-crystalline polymers.[41-43]

To determine the origin of the low temperature endotherm in 3M PFIA, variable temperature annealing studies were conducted. **Figure 4-7** shows the DSC thermograms for Na^+-form 3M PFIA, 825 EW 3M PFSA, and 1000 EW 3M PFSA, each annealed at temperatures

ranging from 120 to 240 °C for two hours prior to ramping from 50 to 350 °C. For the three ionomers, two endotherms were observed under these experimental conditions. In both 3M PFSAs and 3M PFIA, the high temperature endotherm at ca. 280 °C remains relatively constant for all annealing temperatures and is attributed to melting of the PTFE crystallites. For the 3M PFSA, the low temperature endotherm is observed at ca. 20-30 °C above the temperature at which it was annealed and thus is dependent on thermal history. The shift in this low temperature endotherm is much more pronounced in 3M PFSA 1000 EW (**Figure 4-7C**) due to its relatively larger *n* value and higher crystallizability; it is included here for comparison. This is the same phenomenon observed for Nafion annealed at different temperatures and is, therefore, assigned to the melting of small, imperfect crystals that form based on thermal treatment for both 825 and 1000 EW 3M PFSAs.[20]

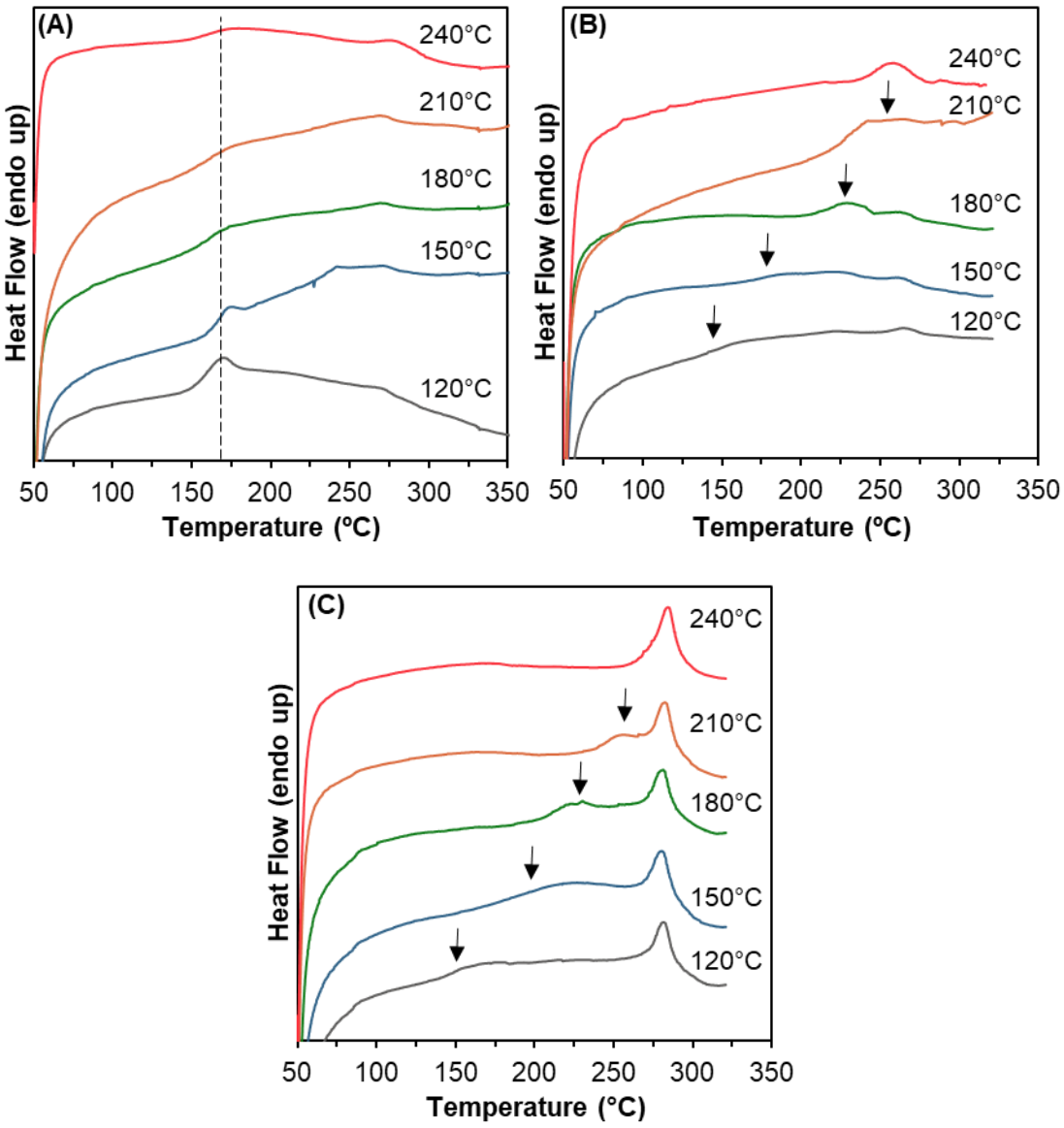

Figure 4-7. Effect of annealing temperature on DSC thermograms of Na^+-form (A) 3M PFIA, (B) 825 EW 3M PFSA and (C) 1000 EW 3M PFSA annealed for 2 hours. Thermograms are shifted along y-axis for comparison.

While a similar low-temperature enthalpic event is observed at ca. 170 °C in the 3M PFIA annealed at 120 °C for two hours (**Figure 4-7A**), this endotherm does not shift in temperature with increasing annealing temperature. In fact, when annealed at 180 °C and above, the endothermic event does not shift in temperature but rather changes in shape from an endothermic peak to a simple step change in heat capacity. Considering that the endothermic event at 170 °C in the PFIA

is not dependent on thermal history and that it remains upon subsequent cools and reheats, it appears reasonable to assign this event to a glass transition as opposed to a melt of small imperfect crystals.

In **Figure 4-7A**, it is also important to note that when PFIA is annealed at temperatures just below the temperature of the apparent T_g, a distinct endothermic peak appears upon reheating. For simple glass-forming polymers, an endothermic peak in the vicinity of the T_g is the signature of enthalpic recovery upon physical aging at a temperature just below the T_g.[44] Sub T_g physical aging of polymers generally involves a slow densification of the polymer, leading to increased enthalpic interactions between the chains as the system tends to achieve a more favorable thermodynamic state.[45] Densification of the chains increases with the amount of time that the polymer is held at the aging temperature. Upon reheating, the densified chains go through enthalpic recovery as the polymer passes through the glass transition causing an increase in enthalpy, which appears as a first-order peak superimposed upon the step change in heat capacity at the glass transition in DSC. For physical aging, a linear relationship has been observed between the area under the enthalpic recovery endotherm (ΔH) and the log of aging time.[46-48]

In the case of the 3M PFIA, the physical aging phenomenon can be used as a means to confirm that the apparent glass transition in PFIA is a true T_g by aging at a temperature just below the apparent T_g and observing whether enthalpic recovery occurs upon reheating. **Figure 4-8** shows the effect of aging 3M PFIA and 3M PFSA at 150 °C for times ranging from 0 to 12 hours. The 3M PFSA demonstrates a small endotherm that increases in magnitude with increasing annealing time at 150 °C. However, when compared to that of the 3M PFIA, the endotherm seen for 3M PFSA is much less pronounced. This endotherm observed for 3M PFSA appears to be the same melting endotherm that is observed in **Figure 4-7** that shifts with annealing temperature and

thus is attributed to the small crystallites that form upon annealing. Further confirmation of this is seen in **Figure 4-8C** by plotting the enthalpy of the small endotherm vs. log(aging time). The enthalpy of the small endotherm observed in 3M PFSA does not increase linearly with log(annealing time) as would be expected in the case of physical aging. Based on this, the endotherm observed in 3M PFSA can be definitively assigned to that of crystalline melting and not to a glass transition.

In **Figure 4-8B**, a very distinct enthalpic recovery peak is observed for the 3M PFIA aged at 150 °C, which also increases in magnitude with increased aging time. When plotted as enthalpy vs. log(aging time), as seen in **Figure 4-8D**, there is a clear linear dependence. These results confirm our conclusion that Na^+-form 3M PFIA has a glass transition at ca. 170 °C observed by both DMA and DSC. In addition to the Na^+-form, the 3M PFIA exhibits this glass transition behavior in K^+-, Rb^+-, and Cs^+-forms (monovalent cations) shown in **Figure S4-3**. With increasing counterion size, the glass transition decreases in temperature and the melting temperature increases. These trends are typical of semicrystalline ionomers where larger counterions weaken the dipole-dipole interactions and thus reduce the strength of the electrostatic crosslinks leading to more chain mobility.[20,36]

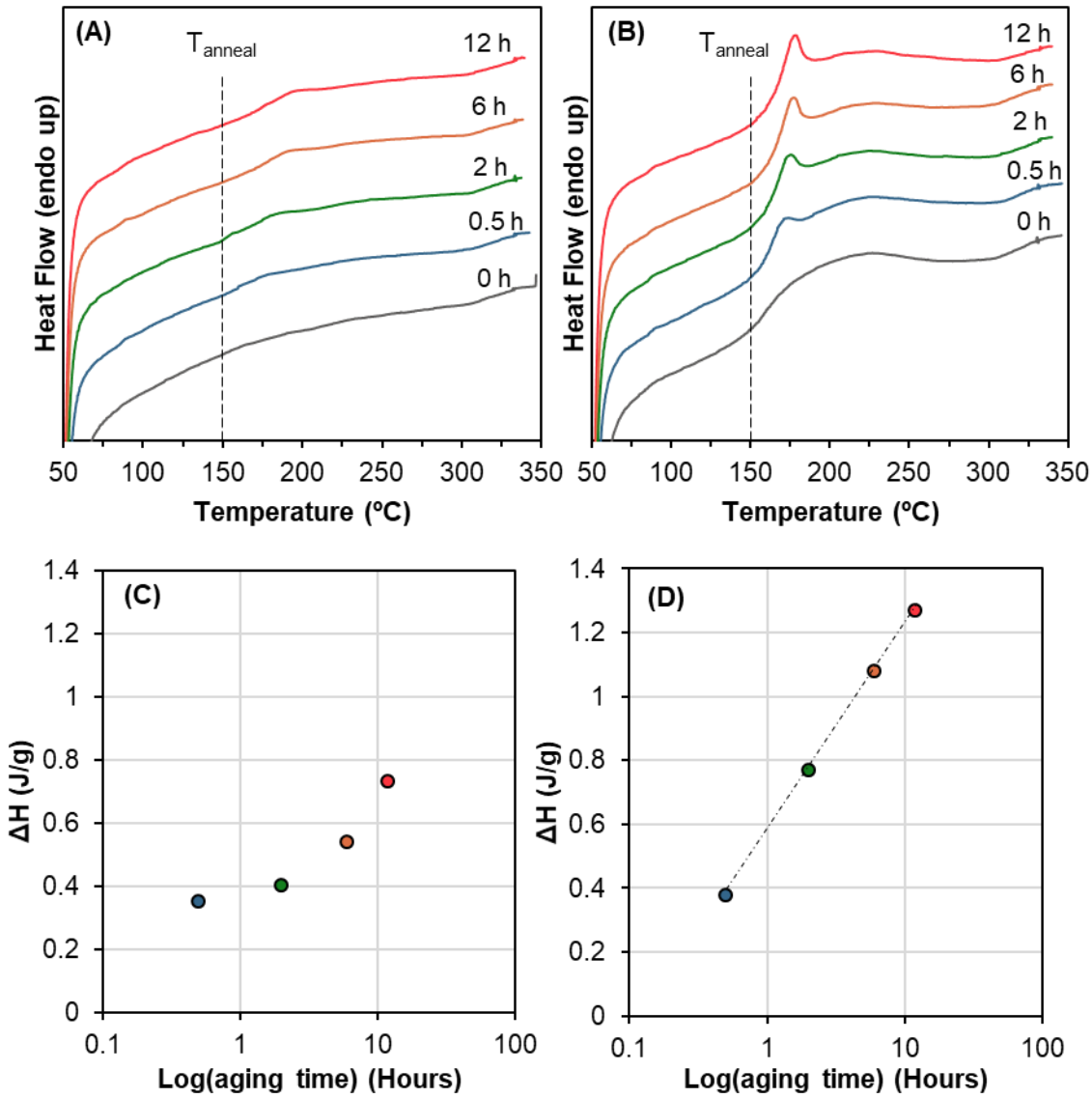

Figure 4-8. DSC thermograms of (A) 825 EW 3M PFSA and (B) 3M PFIA after physical aging at 150 °C for times ranging from 0 to 12 hours before ramping from 50 to 350 °C, (C) enthalpy vs. log(physical aging time) for the endotherm observed at ca. 175 °C in 825 EW 3M PSFA and (D) enthalpy vs. log(physical aging time) for the endotherm observed at ca. 175 °C in 3M PFIA.

It is interesting that in PFIA, the α-relaxation is observable by DSC and exhibits behavior of a true glass transition. In order to explain this anomalous behavior, we look back into classic ionomer literature. In noncrystalline ionomer systems where two-phase behavior is observed by DMA, there is only one glass transition observed by DSC. In the case of polystyrene-*co*-acrylate,

at low ion contents the matrix T_g is observed by DSC but not the cluster T_g.[49] This was attributed to the small heat capacity change over the cluster transition compared to the large change in heat capacity over the matrix transition. At higher ion contents (e.g. above 11 mol %), only the cluster T_g was observed by DSC. In these PS-*co*-AA systems, it was found that DSC only detected the dominant transition observed by DMA.[49-51] However, in polyvinylcyclohexane-*co*-acrylate ionomers, DSC only detected the matrix T_g despite the dominance of the cluster T_g at high ion contents.[49] A linear relationship was observed between the peak in the dynamic loss modulus and the glass transition observed by DSC for PV-*co*-AA, PS-*co*-AA, and MDI-based urethane ionomer systems.[49,52] In these studies, it was noted that while there were two peaks present in dynamic mechanical tanδ data attributed to the matrix and cluster T_gs, there was only one peak present in the loss modulus data, reflecting either the matrix or the cluster phase. It was determined that for ionomer systems that only have one peak in the loss modulus, only one transition was observed by DSC.

In the dynamic mechanical tanδ data for the Na^+-form PFIA, there are two peaks observed for the α- and β-relaxations. However, the loss modulus data presented in **Figure S4-4** shows only one peak for PFIA in the Na^+-form and a very broad peak for PFSA. In PFIA, this peak in the loss modulus is very sharp and distinct and occurs at ca. 180 °C, which corresponds well with the temperature at which this glass transition temperature is observed by DSC. This relationship between peak in the loss modulus and a single glass transition in DSC agrees well with what was observed in the aforementioned classic ionomer systems. While it is well understood that DSC only detects changes in enthalpy, DMA is capable of detecting molecular motions that are both enthalpic and entropic in nature as both contribute to the overall compliance of a sample.[53] Experimental evidence has shown that the molecular motions underlying the drop in storage

modulus and peak in loss modulus in DMA are attributed to local segmental motion (LSM) (i.e. a cooperative motion of chains), that is enthalpic in nature.[53] Rouse modes, which are entropic in nature, are observed as peaks in the tanδ data. DSC characterizes the enthalpy change induced by LSM, hence the correlation between observing a single peak in loss modulus and a single transition in DSC thermograms.

Enthalpy change induced by LSMs can be very small for complex systems with a broad glass transition and therefore may be undetectable by DSC.[54] In Na^+-form 3M PFSA, the α-relaxation observed by tanδ has a full width at half maximum (FWHM) of almost 70 °C whereas in PFIA, the relaxation occurs over a much narrower temperature range with a FWHM of 27 °C. Based on the information from this study, it is evident that the large peak in loss modulus at the α-relaxation temperature for PFIA is of the same molecular mechanism as the glass transition observed by DSC. In contrast, the α-relaxation in PFSA is very broad and has no distinct peak in the loss modulus data so there is no observable glass transition in the DSC thermograms.

4.3.3 Morphology via Small-Angle X-Ray Scattering

To provide more information on the strength of the physically crosslinked network formed in PFIA, it is necessary to probe the morphology of these ionomers using x-ray scattering and model fitting methods. SAXS profiles for PFSA ionomers are characterized by an intercrystalline peak and a broad ionomer peak. A representative small-angle X-ray scattering pattern for PFSAs displays a maximum at ca. $q = 1 – 2\ nm^{-1}$ that is termed the "ionomer peak" consistent with inter-aggregate correlations arising from contrast in electron density between the ionic domains and the PTFE matrix. A second peak is observed at lower scattering vectors (ca. $q = 0.5\ nm^{-1}$) that is attributed to scattering from ordered crystallites developed from crystallization of the PTFE runs between sidechains.[1] The intensities of these peaks have been shown to vary with the use of

different counterions due to changes in electron density contrast between phases by changing the electron density of the ionic phase with larger counterions.[55,56] **Figure 4-9** shows the SAXS profiles for 3M PFIA and 3M PFSA in dry H^+-, Na^+-, and Cs^+-forms. In the H^+-form, the intercrystalline and ionomer peaks are apparent in both ionomers, meaning that despite having an additional acid group per sidechain in PFIA, the two ionomers appear to have similar morphological features. Collecting SAXS profiles in different counterion forms offers the ability to vary the contrast of the ionomer and intercrystalline peaks by varying the electron density within the polar domains. This has been demonstrated before in Nafion, where increasing the electron density of the polar domains by increasing counterion size decreases the intensity of the intercrystalline peak and increases the intensity of the ionomer peak.[55,57] This contrast variation technique is the subject of a future publication, but for this investigation, we will focus on the Cs^+-form membranes where the ionomer peak is able to be isolated and better fit to a model to determine the aggregate morphology.

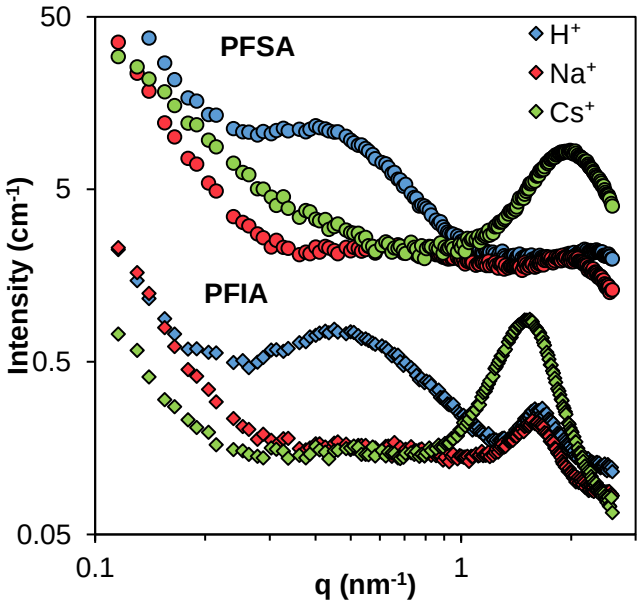

Figure 4-9. SAXS profiles of 3M PFIA and 3M PFSA in different alkali metal counterion forms shifted along the y-axis.

While 3M PFIA and 3M PFSA appear to have very similar morphologies, there is a marked difference between the two in the q_{max} and FWHM of the ionomer peak. In an in-depth study by Kusoglu and coworkers,[12] a combination of x-ray absorption spectroscopy and x-ray scattering were used to probe the hydrophilic domain spacing, ordering, and connectivity of 3M PFIA ionomers. In this work, the authors observed that the ionomer peak for 3M PFIA was at lower scattering vectors than 3M PFSA and also had a smaller FWHM. Lower q_{max} values correspond to larger hydrophilic domain separation (*d*-spacing) for 3M PFIA compared to 3M PFSA and Nafion and was attributed to the longer sidechain length of PFIA. In a molecular dynamics study on PFIA conducted by Atrazhev and coworkers, the water cluster size at the same water content was observed to be larger for PFIA than PFSA structures, indicative of both protonic sites on the PFIA sidechain binding with water molecules increasing the cluster size.[14] Additionally, a study on bulk water in ultrathin films of Nafion, 3M PFSA, and 3M PFIA ionomers by Shrivastava and coworkers, showed that PFIA exhibited five monolayers equivalent of interfacial water compared to one to two observed in PFSA ionomers.[13] This excess water observed in PFIA was attributed to larger sized hydrophilic domains in PFIA than PFSA, which instigates phase segregation. These three studies paint a picture of the PFIA aggregate structure that contains both the bis(sulfonyl)imide and sulfonic acid group incorporated within the aggregate to account for the larger water uptake of PFIA, as well as the increase in hydrophilic domain separation observed by SAXS. Additionally, the span of the ionomer peak correlates to the distribution of inter-aggregate spacings. Kusoglu and coworkers observed a smaller FWHM of the ionomer peak in PFIA than PFSA, which is indicative of a smaller distribution of domain spacings and thus a more ordered structure for PFIA relative to PFSA.[12]

Similar to the SAXS work done by Kusoglu and coworkers, the same observations can be made with 3M PFIA and 3M PFSA in different counterion forms. Noticeably, 3M-PFIA maintains a sharp, well-ordered ionomer peak throughout all counterion forms, while the ionomer peak in 3M PFSA becomes very small and broad in the Li^+- and H^+-form. This is further evidence of the homogeneous distribution of domain spacing in 3M PFIA compared to the broad distribution of domain spacings observed in 3M PFSA and Nafion. In addition, the q_{max} position of the ionomer peak is at lower values for PFIA, which as mentioned earlier, is indicative of larger domain spacings.

To provide more insight into the aggregate structure of PFIA and PFSA, the Cs^+-form data for each was first fit with the Kinning Thomas (K-T) model.[21] SAXS data in the Cs^+-form provided the best fit for the ionomer peak because it eliminates any contributions from the intercrystalline scattering feature. In addition, PFIA and PFSA in the Cs^+-form still exhibit the same thermomechanical behavior as in the Na^+-form as shown in **Figure S4-5**. The K-T model assumes aggregates of a spherical geometry in a liquid-like arrangement, based on the Percus-Yevick hard-sphere liquid theory.[58] This model consists of parameters for A, R_1, R_{ca}, and V_p; where A is a scaling factor that accounts for intensity, R_1 is the radius of the ionic aggregate, R_{ca} is the radius of closest approach ($2R_{ca}$ ~ interaggregate d-spacing), and V_p is the volume per particle. The raw scattering data for PFIA and PFSA is overlaid with the best K-T fit in **Figure 4-10**, and the corresponding parameters are shown in **Table 4-1.** Volume of the aggregate is calculated from the radius of the aggregate, R_1, determined from the K-T model using the equation for volume of a sphere. It is important to note that the perfluorinated ionomer field has come to a general consensus that the morphology of PFSAs are more rod-like as opposed to spherical.[59-61] We fully recognize that a majority of current literature attributes the form of the aggregates to be more rod-like. With

the use of this model we are not trying to make a statement as to the form of the aggregate but only as a tool to make quantitative comparisons. From the K-T model fits, it is observed that PFSA has a smaller aggregate volume and radius of closest approach than PFIA, as expected from the lower scattering angles observed for PFIA.

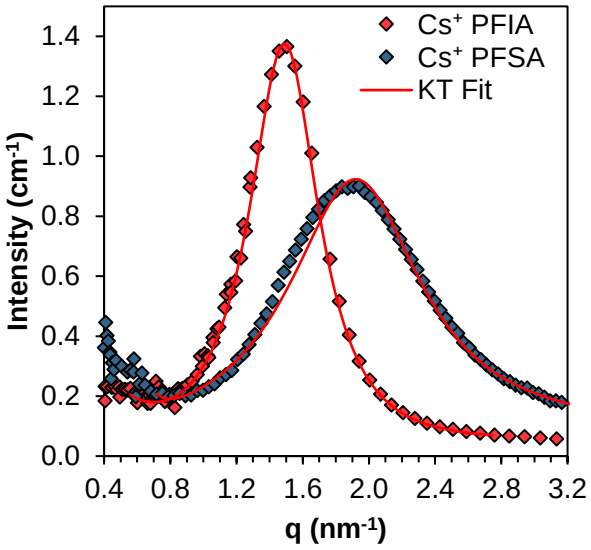

Figure 4-10. Experimental SAXS profiles of the ionomer peak and the theoretical K-T fit for Cs^+-form 3M PFIA and 3M PFSA.

Table 4-1. Parameters extracted from the K-T model for PFIA and PFSA.

	R_1 (nm)	**R_{ca} (nm)**	**V_p (nm^3)**	**Aggregate Volume (nm^3)**	**N_{agg}***
Cs^+-PFSA	0.96	1.56	55.43	3.71	23
Cs^+-PFIA	1.43	2.11	108.8	12.2	23

*Number of sidechains per aggregate. For PFIA, $2*N_{agg}$ = number of ion pairs per aggregate.

Simple space filling calculations were used to determine the approximate number of sidechains for both PFIA and PFSA that form the ionic aggregate structure (N_{agg}). For the number of ion pairs, or sidechains in the case of PFIA (1/2 number of ion pairs), N_{agg} is estimated by

dividing the aggregate volume by the molecular volume of model compounds.[62-64] For example, cesium triflate (CF_3SO_3Cs) has a MW of 282 g/mol and a density of 2.9 g/cm^3,[65] which yields a molecular volume of 162 Å^3. To estimate N_{agg} of PFSA, the aggregate volume is divided by the molecular volume of cesium triflate to yield ca. 23 sidechains per aggregate.

For PFIA, it is reasonable to assume that the aggregate volume includes both the bis(sulfonyl)imide moiety and the terminal sulfonate group within the same aggregate.[66] Additionally, the three intervening CF_2 groups covalently bonded between the two ionic functional groups are not long or flexible enough to form a loop outside of the aggregate and are considered to be packed within the aggregate structure as well. Based on these considerations, the number of sidechains per aggregate (N_{agg}) is calculated by dividing the aggregate volume by the molecular volume of cesium triflate as calculated for PFSA and bis(trifluoromethane)sulfonimide (TFSI) ($(CF_3SO_2)_2NH$). Because these two model compounds each contain a CF_3 group, the volume of those two CF_3 groups are considered to take up a similar volume to the $CF_2CF_2CF_2$ segment intervening between the ionic groups. Without a proper model compound for TFSI in the cesium form, we have to account for the large volume of a Cs^+ counterion by assuming the volume of a proton is negligible and adding the volume of a Cs^+ ion, based on its ionic radius (r_{ion}=1.81 Å).[67] Using this method, the molecular volume of cesium-TFSI is calculated to be 368 Å^3. Dividing the aggregate volume for PFIA in **Table 4-1** by the molecular volumes of cesium triflate and cesium-TFSI gives an estimate of 23 sidechains per aggregate (N_{agg}) for PFIA. The aggregate volume for PFIA as determined from the K-T model is over 3 times larger than that for the PFSA (**Table 4-1**) and is able to accommodate the same average number of sidechains per aggregate even when packing the cesium bis(sulfonyl)imide, cesium sulfonate, and intervening CF_2 groups within the aggregate.

While the K-T model gives a very basic estimate of aggregate structure and number of sidechains per aggregate for PFIA and PFSA, it is also important to remember that it assumes a spherical aggregate geometry, something that has been disputed in the literature for PFSAs. Instead, a better prediction of the aggregate structure could be made by assuming a cylindrical or rod-like aggregate morphology.[59,61,68,69] In order to estimate the aggregate structure from the SAXS data accounting for a cylindrical morphology, we implement a modified hard cylinder (MHC) model introduced by Winey and coworkers in 2015.[22] In this model, which is a variation of a modified hard sphere model,[21,70,71] the ionic aggregates are considered as cylindrical forms with a radius R and length L, separated by a distance defined as the radius of closest approach, R_{ca}. A cylindrical form factor is applied in addition to a structure factor for a liquid-like spatial arrangement of hard cylinders developed by Pederson and coworkers.[72] The MHC model ultimately has five parameters including R, L, R_{ca}, number density of rods, *n*, and overall magnitude of the intensity, A. While Winey and coworkers emphasize that the MHC model is an approximation, it serves as a valuable tool for comparing the aggregate structures of PFSA and PFIA.

Figure 4-11 shows Cs^+-form SAXS data for PFIA and PFSA overlaid with the MHC model fit for each. At first glance, the MHC model appears to fit the data for PFSA better than the K-T model, suggesting that PFSA aggregate structures are likely better fit with a cylindrical morphology. The MHC parameters are displayed in **Table 4-2**. The PFIA appears to have a larger aggregate radius but shorter cylinder length than PFSA meaning the cylindrical aggregates are shorter and wider in PFIA. While the MHC model provides values for the length of the cylinders (L), it is important to mention that the authors of this model emphasized that unique values for L, *n*, and A were not possible for their system as they found several sets of these parameters that fit

their data equally well. For our data, we were able to establish unique values for these parameters, addressed in **Figure S4-6**, that give reasonable dimensions for the aggregate cylinder sizes in PFIA and PFSA.

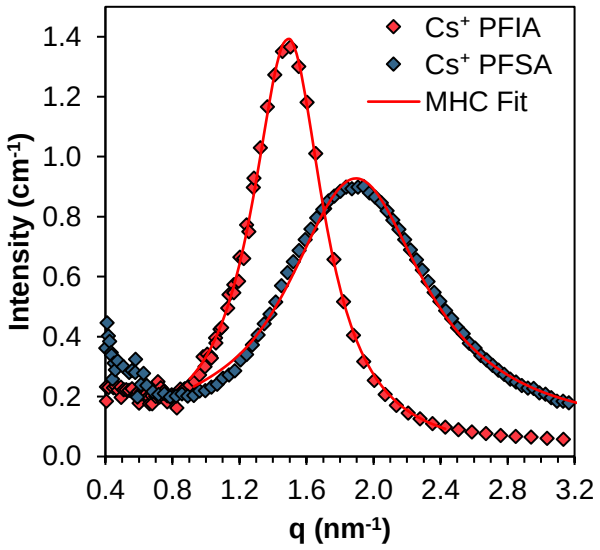

Figure 4-11. Experimental SAXS profiles of the ionomer peak and the theoretical Modified Hard Cylinder fit for Cs^+-form 3M PFIA and 3M PFSA.

Table 4-2. Parameters extracted from the Modified Hard Cylinder model for PFIA and PFSA.

	R_1 (nm)	**L (nm)**	**R_{ca} (nm)**	**V_p (nm^3)***	**Aggregate Volume (nm^3)**	**N_{agg}****	**Density of Ion Pairs**
Cs^+-PFSA	0.53	10.9	1.40	239.8	9.62	60	6
Cs^+-PFIA	0.99	8.88	1.82	354.6	27.3	52	3

*Calculated from the fit parameter *n* (number density of rods), where $V_p = 1/n$.

**Number of sidechains per aggregate. For 3M PFIA, $2*N_{agg}$ = number of ion pairs per aggregate.

Simple space filling calculations are again used to calculate N_{agg} for PFIA and PFSA assuming this cylindrical geometry. The volume of a cylinder is calculated from the R and L values extracted from the MHC model. N_{agg} is estimated by dividing the volume per aggregate by the

sample compound volumes for PFIA and PFSA sidechains. From the MHC model, the number of sidechains per aggregate is estimated as 52 for PFIA and 60 for PFSA. Considering that these two ionomers have the same number of sidechains and same length of TFE units between sidechains, it is not unreasonable that they would have a similar number of sidechains participating, on average, per aggregate. This is the result of both the KT model and the MHC model, where in both models, the calculated number of sidechains per aggregate are similar for PFIA and PFSA. Despite having a similar number of sidechains per aggregate, the density of ion pairs (calculated as number of ion pairs/aggregate volume) within each aggregate is lower for PFIA than it is for PFSA, indicating a more tightly packed aggregate for PFSA than PFIA.

To better visualize the packing of ions within aggregate structures for PFIA and PFSA, a 2D schematic representation based off the MHC model data is presented in **Figure 4-12**. This representation is a snapshot of the cross-sectional area of a cylindrical aggregate with radius, R_1, and radius of closest approach, R_{ca}, drawn to scale from the model fits. This schematic represents a cross-section view looking down ¼ the cylinder (for clarity), and thus there are 13 sidechains included in the PFIA schematic and 15 sidechains in the PFSA schematic. The large Cs^+ counterions are also included within R_1, 26 for PFIA and 15 for PFSA. From this demonstration, it is notable that the larger aggregate size for PFIA allows the accommodation of both ionic groups per sidechain, along with the three CF_2 groups covalently bonded in between those ionic groups. Although the PFSA packs much less molecular content within the aggregate structure with only one ion pair per sidechain, they appear to be more tightly packed together within the aggregate radius than the PFIA sidechains. In order to quantify this chain packing, the value of surface area of the aggregate can be estimated and compared to the number of sidechains penetrating that surface. Similar estimations have been used in ionomer micelle systems to determine the tightness

of packing of micelles by calculating surface area per aggregate and dividing it by the aggregation number, or number of chains in each aggregate, where a lower surface area per chain indicates more compact packing of the micellar spheres.[73,74]

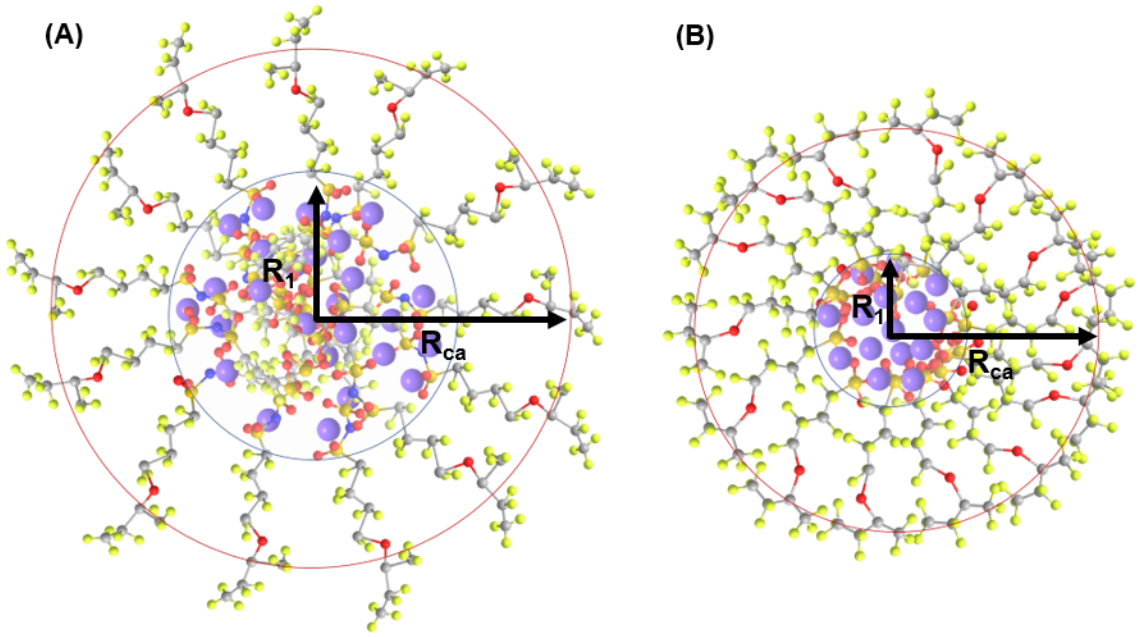

Figure 4-12. 2D schematic representation of the cross-sectional area of cylindrical (a) PFIA and (b) PFSA aggregates based on the Modified Hard Cylinder model fits and space-filling calculations.

In the KT model, surface area per aggregate (SA_{agg}) can be calculated using R_1 and the equation for surface area of a sphere. To determine the space around each sidechain penetrating that surface area, the calculated SA_{agg} is divided by the number of sidechains per aggregate. The values from these calculations are presented in **Table 4-3**. From the KT model, it is apparent that the surface area per sidechain is much higher in PFIA than PFSA, indicating reduced closeness of packing between sidechains for PFIA. The same calculations were performed from the MHC model, utilizing the values for R and L in the equation for surface area of a cylinder to attain SA_{agg}

values. SA_{agg} is then divided by the number of sidechains per aggregate determined from the MHC model and space filling calculations to get surface area per aggregate. These values are also presented in **Table 4-3**. The values for surface area per aggregate are much smaller from the MHC model than the KT model. They are also much more reasonable based on the estimated cross-sectional area of a CF_3 group, further explained in Supplemental Information. Despite the disparity in surface area per sidechain numbers between the two models, in both calculations it is observed that PFIA has a larger surface area per sidechain than PFSA. This clearly suggests that the sidechains are more tightly packed in their aggregate structures in PFSA than they are in PFIA. We attribute this to the addition of molecular bulk, from the intervening fluorocarbons between ion pairs in PFIA, which effectively space out the ion pairs within the multiplet. This results in a weakening of the physical crosslinks within the aggregate for PFIA compared to PFSA. Additionally, PFIA has a lower density of ion pairs in each aggregate than PFSA, which may also account for a weakened aggregate strength.

Table 4-3. Surface area per aggregate and per sidechain values from the KT and MHC models.

	SA_{agg} KT Model (nm^2)	**SA_{agg} MHC Model (nm^2)**	**Surface Area per sidechain (KT Model) (nm^2)**	**Surface Area per sidechain (MHC Model) (nm^2)**
Cs^+-PFSA	173	38.1	7.5	0.6
Cs^+-PFIA	1885	61.4	82	1.2

4.3.4 Correlation of morphology to thermomechanical properties

The link between dynamic mechanical relaxations and x-ray scattering studies has been reconciled in the amorphous random ionomer literature by the development of the multiplet-cluster model.[34,66] Ion pairs are recognized to aggregate together to form multiplets, which are stabilized

with increasing strength of electrostatic interactions between ion pairs. Small alkali metal counterions are known to result in stronger electrostatic interactions between ion pairs within the multiplet than larger counterions, which inhibit the onset of ion hopping.[36] Each ion pair acts a physical crosslink that immobilizes the polymer chain at that point, thus effectively reducing the mobility of the polymer chains within close vicinity of the aggregates (e.g., the region of restricted mobility).[66] At high ion contents, these regions of restricted mobility become close enough to overlap to establish large contiguous domains referred to as "clusters" that have their own glass transition temperature.

Perfluorinated ionomers have traditionally not been included in classic ionomer morphological models due to their semicrystalline nature.[66] However, extensive studies have shown that they contain large multiplets that are distributed throughout the matrix with some degree of heterogeneity.[20] These multiplets are generally accepted to constitute the physically crosslinked network within PFSAs that inhibit segmental mobility. The ionomer peak has been directly correlated to thermomechanical relaxations in Nafion by variable temperature SAXS experiments in different counterion forms that show a temperature dependence of the ionomer peak, which begins to decrease in intensity as the ionomer passes through the α-transition temperature.[20] While several structural models have been developed to explain the origin of the ionomer peak in PFSA SAXS data, the disordered nature of the ionomer that leads to a broad scattering feature without higher-order peaks has made it difficult to fit the data to specific scattering models.[1,2] However, more recent studies have begun to point to rod-like elongated polymer aggregates.[59,61,68,69] Based on the understanding that aggregate structures in PFIA and PFSA contribute to the restriction of chain mobility, we are able to use model estimates to explain some of the anomalous behavior of PFIA membranes.

Aggregate structures were modeled in the previous section using both spherical and cylindrical models. In both models, PFSA was found to have a smaller aggregate volume than PFIA, and model compounds were used to estimate the number of sidechains participating in each aggregate for both ionomers. Based on these calculations and further surface area per sidechain and ion pair density calculations, it was determined that the PFSA aggregates are likely more densely packed with ion pairs than PFIA aggregates. The long, bulky sidechain on PFIA leads to less dense packing within the aggregate structure, and the presence of three intervening hydrophobic CF_2 groups within the aggregate weakens the collective strength of the aggregate as an electrostatic crosslink. This leads to a lower α-relaxation temperature for PFIA than PFSA in the Na^+-form. However, in the H^+-form, PFIA has a higher α-relaxation temperature than PFSA. This is likely due to the difference between the type of interactions with the two different counterions. In Na^+-form, the interactions between ion pairs are the result of dipole-dipole interactions through space. Where PFIA has less dense packing of ions in each aggregate, these interactions are weaker than PFSA with closer packing between ions. In the H^+-form, the physical crosslinks are constituted by hydrogen-bonding, of which PFIA has twice the number of hydrogen-bond donors/acceptors than PFSA, leading to a higher α-relaxation temperature. While this concept is difficult to explain in the context of weak hydrogen bonding interactions compared to strong electrostatic interactions, we can support this argument by using divalent counterions to create ionic crosslinks between the functional groups. Dynamic mechanical tanδ versus temperature data for Mg^{2+}-PFIA and PFSA are shown in **Figure S4-7**, where the α-relaxation has increased to 415 °C for PFIA and 440 °C for PFSA. The divalent Mg^{2+} counterion acts as a physical crosslink by interacting with two sulfonate groups directly, as opposed to the ion-dipole to ion-dipole interactions between two monovalent Na^+-sulfonate groups, which are attracted to each other by

dipole-dipole forces. This direct electrostatic interaction from the divalent counterion serves to increase the strength of the collective forces within the ionic aggregates compared to monovalent Na^+ counterions. In both the H^+-form and Mg^{2+}-form, where both ion exchange groups on PFIA's sidechain are actively participating in the physical network, the α-relaxation occurs at a closer temperature to that of PFSA.

4.4 Conclusions

In this work, we have presented the first in-depth study probing the thermal properties of a multi-acid sidechain perfluorinated ionomer from 3M. DMA experiments immediately showed clear differences in the thermomechanical relaxations in 3M PFIA when compared to 3M PFSA. In the H^+-form, the α-relaxation temperature for 3M PFIA is slightly higher than 3M PFSA, as expected for an ionomer with higher ion content. Upon conversion to the Na^+-form, the α-relaxation in 3M PFIA was shown to occur at a lower temperature than the α-relaxation in 3M PFSA, Nafion®, and Aquivion®. This is the first indication that the physically crosslinked network of Na^+-form 3M PFIA has a significantly different effect on polymer chain mobility compared to that of the parent 825 EW 3M PFSA.

DSC experiments definitively confirmed the appearance of a true glass transition temperature in monovalent cation-form 3M PFIA that occurs at the same temperature as the α-relaxation observed in the dynamic mechanical loss modulus vs. temperature data. It was noted that the α-relaxation in 3M PFIA is a very sharp relaxation, likely due to the homogeneous distribution of aggregate sizes, and is enthalpic in nature. This prominent and narrow relaxation in PFIA gives rise to glass transition behavior typical of semicrystalline ionomers. In contrast, the

glass transition of Na^+-form 3M PFSA is not observed by DSC due to the very broad α-relaxation temperature likely due to the heterogeneous distribution of aggregate sizes in PFSA.

X-ray scattering data showed that PFIA and PFSA have similar morphologies, but different aggregate sizes. By fitting the SAXS data with a modified hard sphere and modified hard cylinder model, it was observed that PFIA has much larger aggregate sizes than PFSA, which allows for incorporation of the longer sidechain containing two ionic functionalities and the intervening CF_2 groups within the aggregate. Further space filling calculations showed that PFSA aggregates are likely more tightly packed than PFIA aggregates. In PFIA, the incorporation of hydrophobic CF_2 groups into the aggregate along with looser packing likely contributes to a weakening the collective strength of the dipole-dipole interactions.

Based on this work, the 3M PFIA exhibits behavior very similar to classic ionomer systems when in a monovalent ion form, which signals a remarkable new phenomenon for the 3M PFIA structure. While PFSAs generally have very broad thermomechanical relaxations owing to the distribution of aggregate sizes, PFIA has a very narrow distribution of aggregate sizes leading to sharp relaxations that mimic classic ionomer glass transitions. In addition, the PFIA aggregate structure was shown to be larger and less tightly packed, reducing the strength of the physically crosslinked network. This fundamental insight into the effect of additional acidic sites on the thermal and mechanical properties of these polymers contributes to guiding the synthesis of these next generation fuel cell membranes.

4.5 Acknowledgments

The authors acknowledge 3M Company for providing PFSA and PFIA materials. Support for this research was provided by 3M Company. MATLAB code for the modified hard cylinder model was provided by Karen Winey's research group at University of Pennsylvania.

4.6 Supporting Information

Expected shift from H^+-form to Na^+-form for PFSA ionomers

Figure S4-1 shows the DMA tanδ data for Aquivion with a short (C2) sidechain structure and pendant sulfonic acid. Aquivion used in this study has an EW of 870 g/mol which equates to ca. 14 mol % ion content (in comparison with 800 EW PFSA=19 mol % and 625 EW PFIA=38 mol %). Aquivion 848 has an α-relaxation at 125 °C in the H^+-form that shifts to 350 °C in the Na^+-form.

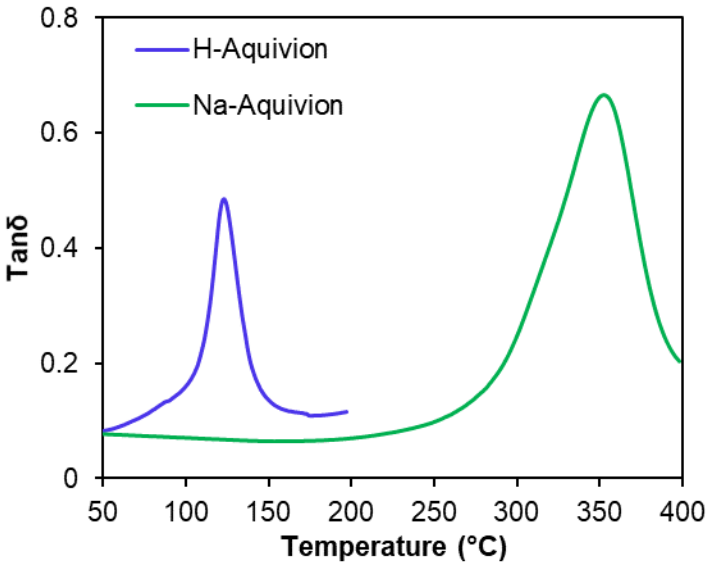

Figure S4-1. Short sidechain Aquivion DMA tanδ data in the H^+- and Na^+-form.

Rubbery Plateau above T_α in PFSAs

Figure S4-2 shows the DMA tanδ and storage modulus data for three PFSAs with different sidechain structures in the H^+-form. In all three PFSAs, an α-relaxation is observed in the vicinity of 100-120 °C that is characterized by a peak in the tanδ and a sharp drop in storage modulus. Above the α-relaxation drop in storage modulus, a rubbery plateau is observed due to maintained mechanical integrity below the melting temperature of these ionomers (at ca. 220 °C).

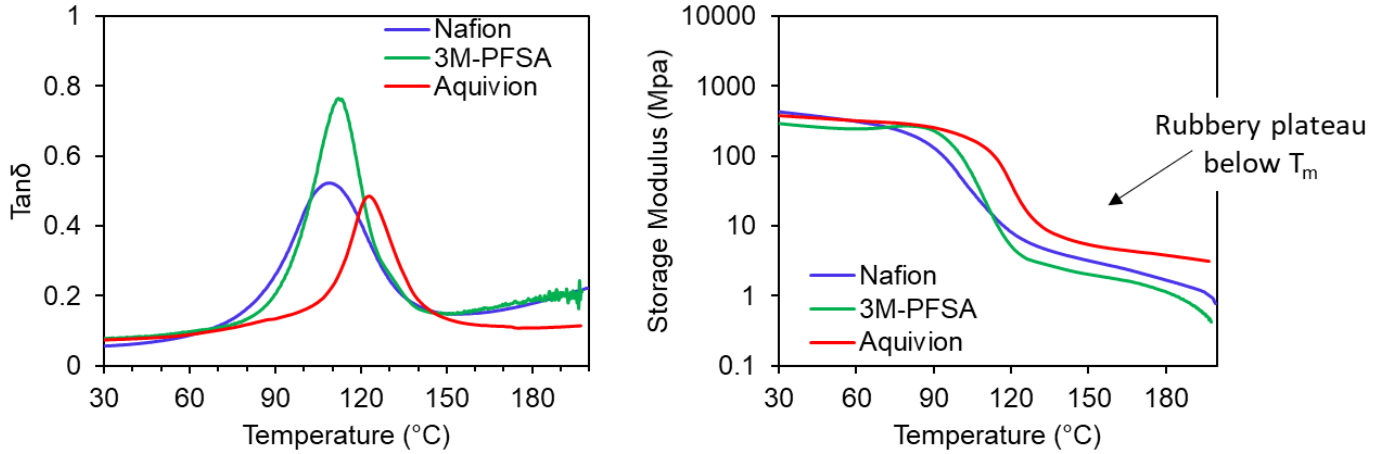

Figure S4-2. H^+-Form DMA Data for Nafion, 3M-PFSA, and short sidechain Aquivion.

DSC Thermograms of PFIA in Different Monovalent Counterion Forms.

The glass transition observed in the Na^+-counterion form PFIA presented in the bulk of this work, is also very clear for other monovalent counterions. **Figure S4-3** shows DSC thermograms for PFIA neutralized with different alkali metal counterions. After holding at 120 °C for 120 minutes for water removal for all samples, the glass transition temperature is very apparent with signs of physical aging. With increasing counterion size, the glass transition slightly decreases in temperature and the melting temperature increases. These trends are typical of semicrystalline

ionomers where larger counterions reduce the strength of the electrostatic crosslink leading to increased chain mobility.[20,36]

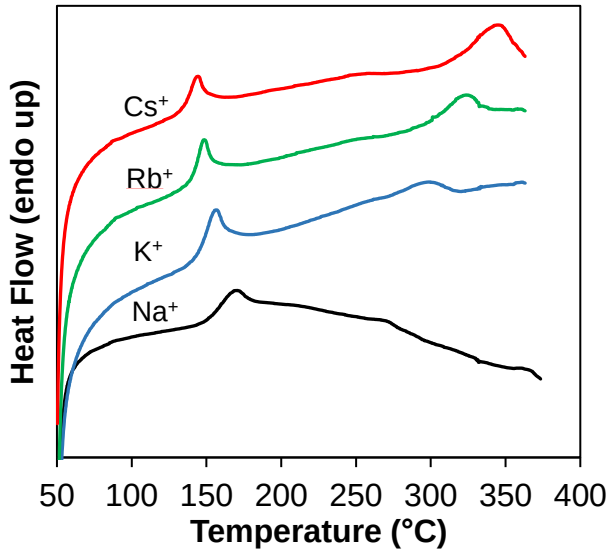

Figure S4-3. DSC thermograms of 3M PFIA neutralized with different alkali metal counterions.

Dynamic Mechanical Loss Modulus Data

While the tanδ data for PFIA and PFSA show multiple peaks corresponding to the α- and β-relaxations, the loss modulus shows only one peak for PFIA and a very broad peak for PFSA as shown in **Figure S4-4**. The peak in loss modulus for Na^+-form PFIA is at ca. 180 °C, the same temperature as the observed glass transition temperature in DSC. As discussed within the main portion of this manuscript, a peak in loss modulus data corresponds to local segmental motion that is enthalpic in nature.[53] DSC also measures change in enthalpy due to local segmental motion so it will only detect thermal transitions that are observed in the loss modulus data. Peaks in the tanδ are due to larger Rouse modes that are entropic in nature and thus not detectable by DSC. In Na^+-form PFSA, there is no glass transition observed by DSC because there is only a very broad peak

in the loss modulus therefore the change in enthalpy across that transition is likely very small and undectable.[54]

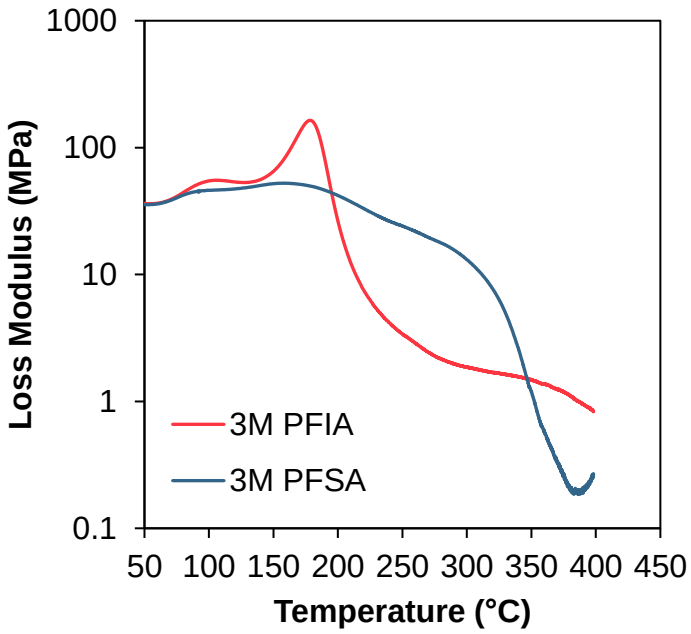

Figure S4-4. Dynamic mechanical loss modulus versus temperature for 3M PFIA and 3M PFSA in the Na^+-form.

Thermomechanical Relaxations of PFIA and PFSA in different Counterion forms

In order to achieve a good fit for the ionomer peak observed by SAXS for PFSA and PFIA, we chose to use the Cs^+ counterion form because it changes the electron density contrast of the polar domains such that the crystalline feature does not appear and does not interfere with the model fit. However, DMA data shows that the same trends are observed in the Cs^+-form as observed in the Na^+-form, so this SAXS data is still applicable. **Figure S4-5** shows the DMA tanδ for PFIA and PFSA in the Cs^+-counterion form. The α-relaxation in PFSA is observed at higher temperatures than PFIA and is much broader in PFSA than for PFIA. This is consistent with the

same dipole-dipole interactions as observed for Na^+ counterion being weaker in PFIA than in PFSA.

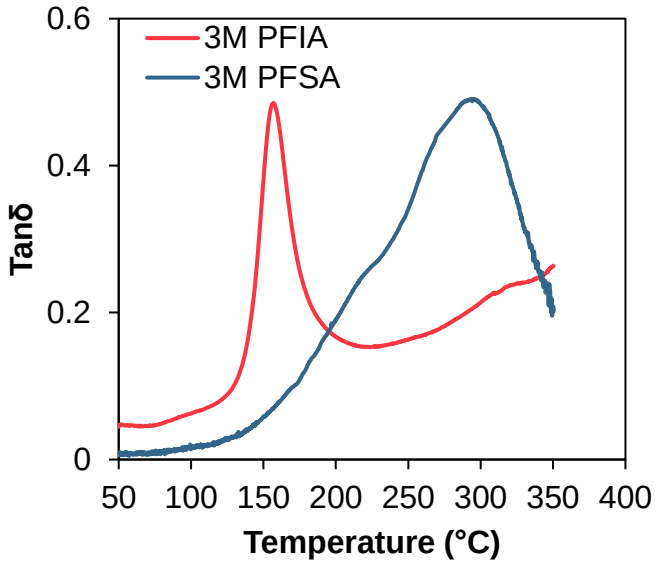

Figure S4-5. Cs^+-form DMA tanδ versus temperature data for 3M PFIA and 3M PFSA.

Modified Hard Cylinder Model Fitting

Authors of the MHC model indicated that unique values for length, *n*, and A were not attainable with their system, so they only presented data for the R and R_{ca} values.[22] In the PFIA/PFSA system, a unique length value is necessary in order to calculate an aggregate volume based on a cylindrical geometry. **Figure S4-6** shows Cs^+-form PFIA data fit with different, reasonable L and *n* values to show the difference of fit. In **Figure S4-6A**, the *n* value is held constant while the value for L is varied. It is apparent that a value of ca. 8.88 nm is the best fit where the values for 8 and 10 deviate from the data. In **Figure S4-6B**, the value for L is held at 8.88 nm while *n* is varied. Additionally, this shows us that the fit value of $n = 0.0028$ nm^{-3} fits the data the best.

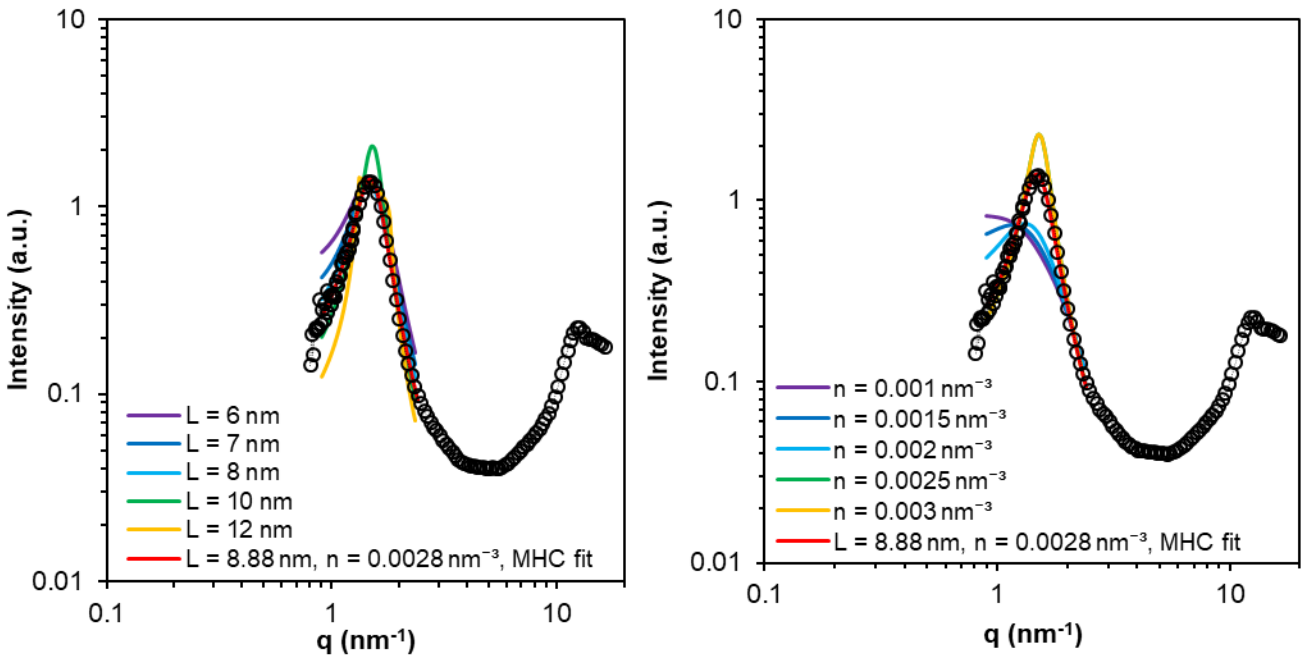

Figure S4-6. MHC Model fits overlaid over PFIA SAXS data with different values for (a) L and (b) *n* showing the best fits for both parameters.

The values for L from the MHC model are also confirmed to be reasonable from the surface area calculations done within the main text of this manuscript. Utilizing the R and L values from the MHC model for Cs^+-form PFIA and PFSA, the surface area per sidechain was calculated as 1.2 nm^2 and 0.6 nm^2 for PFIA and PFSA, respectively. To determine whether these values for are reasonable, we take into consideration the cross-sectional area of a perfluorinated sidechain. For both, PFIA and PFSA, it is assumed that the cross-sectional area of the sidechain can be estimated from the cross-sectional area of a CF_2 group. To estimate this, the cross-sectional area of a CF_3H molecule is calculated from the density and molecular weight of CF_3H to get the molecular volume. The radius is extrapolated from the molecular volume assuming a spherical geometry, and the area is calculated from that radius value to get a cross-sectional area of CF_3H of 1.5 nm^2.

Dynamic Mechanical Relaxations in Divalent Counterion Form

It was established in the bulk of the paper that in the monovalent counterion form, PFIA has weaker aggregate structures due to the less tight packing of ions within the aggregates from incorporation of CF_2 intervening segments. In the monovalent form, the driving force for aggregation is dipole-dipole interactions between sulfonate-cation contact pairs. When the cation is exchanged to a divalent counterion, the dipole-dipole interactions are then replaced by ionic bonds. Ionic bonds are much stronger in nature than electrostatic interactions and as a result, are able to strengthen the ionic aggregates in 3M-PFIA. This is shown in **Figure S4-7**, where the α-relaxation temperature for PFIA and PFSA both increase drastically to 415 °C and 440 °C, respectively.

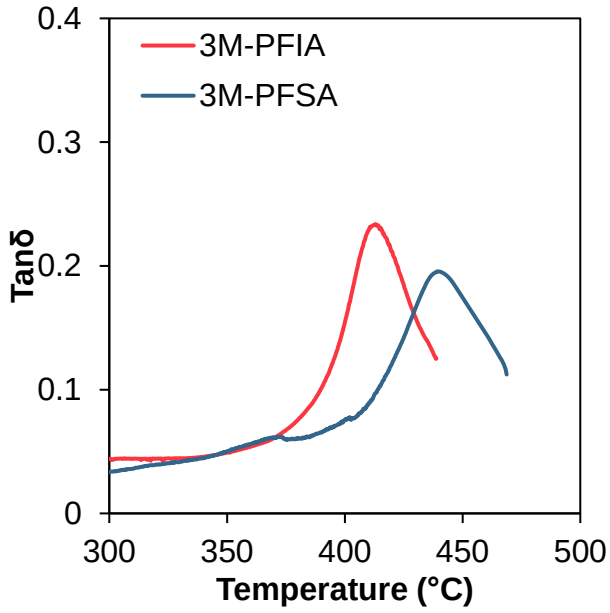

Figure S4-7. Dynamic mechanical tanδ versus temperature for Mg^{2+}-form 3M-PFIA and 3M-PFSA.

4.7 References

1. Mauritz, K. A.; Moore, R. B., State of Understanding of Nafion. *Chem. Rev.* **2004**, *104*, 4535.
2. Kusoglu, A.; Weber, A. Z., New Insights into Perfluorinated Sulfonic-Acid Ionomers. *Chem. Rev.* **2017**, *117*, 987.
3. Hamrock, S. J.; Yandrasits, M. A., Proton Exchange Membranes for Fuel Cell Applications. *J. Macromol. Sci., Rev. Macromol. Chem. Phys.* **2006**, *46*, 219.
4. Lai, Y.-H.; Mittelsteadt, C. K.; Gittleman, C. S.; Dillard, D. A., Viscoelastic stress analysis of constrained proton exchange membranes under humidity cycling. *J. Fuel Cell Sci. Tech.* **2009**, *6*, 021002.
5. Emery, M.; Frey, M.; Guerra, M.; Haugen, G.; Hintzer, K.; Kai; Lochhaas, H.; Pham, P.; Pierpont, D.; Schaberg, M.; Thaler, A.; Yandrasits, M.; Hamrock, S., The Development of New Membranes for Proton Exchange Membrane Fuel Cells *J. Electrochem. Soc.* **2007**, *11*, 3.
6. Divoux, G. M.; Finlay, K. A.; Park, J. K.; Song, J.-M.; Yan, B.; Zhang, M.; Dillard, D. A.; Moore, R. B., Morphological Factors Affecting the Behavior of Water in Proton Exchange Membrane Materials. *ECS Trans.* **2011**, *41*, 87.
7. Schaberg, M. S.; Abulu, J. E.; Haugen, G. M.; Emery, M. A.; O'Conner, S. J.; Xiong, P. N.; Hamrock, S., New Multi Acid Side-Chain Ionomers for Proton Exchange Membrane Fuel Cells. *ECS Trans.* **2010**, *33*, 627.
8. Yandrasits, M.; Lindell, M.; Peppin, D.; Komlev, A.; Hamrock, S.; Haugen, G.; Fort, E.; Kalstabakken, K., Chemical Stability of Perfluorobis (sulfonyl) imide-Acid (PFIA) Ionomers in Open Circuit Voltage (OCV) Accelerated Test Conditions. *J. Electrochem. Soc.* **2018**, *165*, F3261.

9. Hamrock, S. J. *Membranes and MEA's for Dry, Hot Operating Conditions*, 3M Company, 2011.

10. Hamrock, S. J.; Herring, A. M. In *Fuel Cells: Selected Entries from the Encyclopedia of Sustainability Science and Technology*, Proton Exchange Membrane Fuel Cells: High-Temperature, Low-Humidity Operation; Kreuer, K.-D., Ed.; Springer New York: New York, NY, 2013, p 577.

11. Puskar, L.; Ritter, E.; Schade, U.; Yandrasits, M.; Hamrock, S.; Schaberg, M.; Aziz, E. F., Infrared dynamics study of thermally treated perfluoroimide acid proton exchange membranes. *Phys. Chem. Chem. Phys.* **2017**, *19*, 626.

12. Su, G. M.; Cordova, I. A.; Yandrasits, M. A.; Lindell, M.; Feng, J.; Wang, C.; Kusoglu, A., Chemical and Morphological Origins of Improved Ion Conductivity in Perfluoro Ionene Chain Extended Ionomers. *J. Am. Chem. Soc.* **2019**.

13. Shrivastava, U. N.; Fritzsche, H.; Karan, K., Interfacial and Bulk Water in Ultrathin Films of Nafion, 3M PFSA, and 3M PFIA Ionomers on a Polycrystalline Platinum Surface. *Macromolecules* **2018**, *51*, 9839.

14. Atrazhev, V. V.; Astakhova, T. Y.; Sultanov, V. I.; Perry, M. L.; Burlatsky, S. F., Molecular Dynamic Study of Water-Cluster Structure in PFSA and PFIA Ionomers. *J. Electrochem. Soc.* **2017**, *164*, F1265.

15. Clark II, J. K.; Paddison, S. J., Proton dissociation and transfer in proton exchange membrane ionomers with multiple and distinct pendant acid groups: An ab initio study. *Electrochim. Acta* **2013**, *101*, 279.

16. Sengupta, S.; Pant, R.; Komarov, P.; Venkatnathan, A.; Lyulin, A. V., Atomistic simulation study of the hydrated structure and transport dynamics of a novel multi acid side chain polyelectrolyte membrane. *Int. J. Hydrog. Energy* **2017**, *42*, 27254.

17. Economou, N. J.; Barnes, A. M.; Wheat, A. J.; Schaberg, M. S.; Hamrock, S. J.; Buratto, S. K., Investigation of Humidity Dependent Surface Morphology and Proton Conduction in Multi-Acid Side Chain Membranes by Conductive Probe Atomic Force Microscopy. *J. Phys. Chem. B* **2015**, *119*, 14280.

18. Bawagan, A. D. O.; Hamrock, S. J.; Schaberg, M.; Yousef, I.; Ritter, E.; Schade, U., Far-infrared studies on Nafion and perfluoroimide acid (PFIA) and their alkali salts. *Vib. Spectrosc.* **2014**, *75*, 213.

19. Orsino, C. M. M., Robert B In *The Fascinating World of Fluoropolymers and their Applications*, Thermal transitions and mechanical relaxations in perfluorinated ionomers; Ameduri, B. F., S Ed.; Elsevier: 2020.

20. Page, K. A.; Cable, K. M.; Moore, R. B., Molecular Origins of the Thermal Transitions and Dynamic Mechanical Relaxations in Perfluorosulfonate Ionomers. *Macromolecules* **2005**, *38*, 6472.

21. Kinning, D. J.; Thomas, E. L., Hard-sphere interactions between spherical domains in diblock copolymers. *Macromolecules* **1984**, *17*, 1712.

22. Buitrago, C. F.; Bolintineanu, D. S.; Seitz, M. E.; Opper, K. L.; Wagener, K. B.; Stevens, M. J.; Frischknecht, A. L.; Winey, K. I., Direct comparisons of X-ray scattering and atomistic molecular dynamics simulations for precise acid copolymers and ionomers. *Macromolecules* **2015**, *48*, 1210.

23. Hodge, I.; Eisenberg, A., Dielectric and mechanical relaxations in a Nafion precursor. *Macromolecules* **1978**, *11*, 289.

24. Yeo, S. C.; Eisenberg, A., Physical properties and supermolecular structure of perfluorinated ion-containing (nafion) polymers. *J. Appl. Polym. Sci.* **1977**, *21*, 875.

25. Nakano, Y.; MacKnight, W. J., Dynamic mechanical properties of perfluorocarboxylate ionomers. *Macromolecules* **1984**, *17*, 1585.

26. Kyu, T.; Eisenberg, A. In *J. Polym. Sci. C*; Wiley Online Library: 1984; Vol. 71, p 203.

27. Moore, R. B.; Martin, C. R., Morphology and chemical properties of the Dow perfluorosulfonate ionomers. *Macromolecules* **1989**, *22*, 3594.

28. Phillips, A. K.; Moore, R. B., Mechanical and transport property modifications of perfluorosulfonate ionomer membranes prepared with mixed organic and inorganic counterions. *J. Polym. Sci. Part B Polym. Phys.* **2006**, *44*, 2267.

29. Osborn, S. J.; Hassan, M. K.; Divoux, G. M.; Rhoades, D. W.; Mauritz, K. A.; Moore, R. B., Glass Transition Temperature of Perfluorosulfonic Acid Ionomers. *Macromolecules (Washington, DC, U. S.)* **2007**, *40*, 3886.

30. Orsino, C. M.; Lindell, M.; Yandrasits, M.; Hamrock, S.; Moore, R. B., Anomalous Appearance of a Distinct Glass Transition in Perfluoroimide Acid Ionomers. *ECS Trans.* **2019**, *92*, 455.

31. Kim, J.-S.; Jackman, R. J.; Eisenberg, A., Filler and Percolation Behavior of Ionic Aggregates in Styrene-Sodium Methacrylate Ionomers. *Macromolecules* **1994**, *27*, 2789.

32. Fox, T. G., Influence of Diluent and of Copolymer Composition on the Glass Temperature of a Poly-mer System. *Bull. Am. Phys. Soc.* **1956**, *1*, 123.

33. Tierney, N. K.; Register, R. A., Ion hopping in ethylene− methacrylic acid ionomer melts as probed by rheometry and cation diffusion measurements. *Macromolecules* **2002**, *35*, 2358.

34. Eisenberg, A., Clustering of ions in organic polymers. A theoretical approach. *Macromolecules* **1970**, *3*, 147.

35. Page, K. A.; Park, J. K.; Moore, R. B.; Garcia Sakai, V., Direct analysis of the ion-hopping process associated with the α-relaxation in perfluorosulfonate ionomers using quasielastic neutron scattering. *Macromolecules* **2009**, *42*, 2729.

36. Orler, E. B.; Moore, R. B., Influence of Ionic Interactions on the Crystallization of Lightly Sulfonated Syndiotactic Polystyrene Ionomers. *Macromolecules* **1994**, *27*, 4774.

37. Orler, E. B.; Calhoun, B. H.; Moore, R. B., Crystallization kinetics as a probe of the dynamic network in lightly sulfonated syndiotactic polystyrene ionomers. *Macromolecules* **1996**, *29*, 5965.

38. Moore, R. B.; Martin, C. R., Chemical and morphological properties of solution-cast perfluorosulfonate ionomers. *Macromolecules* **1988**, *21*, 1334.

39. De Almeida, S.; Kawano, Y., Thermal behavior of Nafion membranes. *J. Therm. Anal. Calorim* **1999**, *58*, 569.

40. Kyu, T.; Hashiyama, M.; Eisenberg, A., Dynamic mechanical studies of partially ionized and neutralized Nafion polymers. *Can. J. Chem.* **1983**, *61*, 680.

41. Lemstra, P.; Kooistra, T.; Challa, G., Melting behavior of isotactic polystyrene. *Journal of Polymer Science Part A-2: Polymer Physics* **1972**, *10*, 823.

42. Kohzaki, M.; Tsujita, Y.; Takizawa, A.; Kinoshita, T., The crystallization and formation of cluster of ethylene ionomer during physical aging. *J. Appl. Polym. Sci.* **1987**, *33*, 2393.

43. Alizadeh, A.; Richardson, L.; Xu, J.; McCartney, S.; Marand, H.; Cheung, Y.; Chum, S., Influence of structural and topological constraints on the crystallization and melting behavior of polymers. 1. Ethylene/1-octene copolymers. *Macromolecules* **1999**, *32*, 6221.

44. Berens, A. R.; Hodge, I., Effects of annealing and prior history on enthalpy relaxation in glassy polymers. 1. Experimental study on poly (vinyl chloride). *Macromolecules* **1982**, *15*, 756.

45. Struik, L. C. E., Physical aging in plastics and other glassy materials. *Polym. Eng. Sci.* **1977**, *17*, 165.

46. Hutchinson, J. M.; Smith, S.; Horne, B.; Gourlay, G. M., Physical Aging of Polycarbonate: Enthalpy Relaxation, Creep Response, and Yielding Behavior. *Macromolecules* **1999**, *32*, 5046.

47. Echeverria, I.; Su, P. C.; Simon, S. L.; Plazek, D. J., Physical aging of a polyetherimide: Creep and DSC measurements. *J. Polym. Sci. Part B Polym. Phys.* **1995**, *33*, 2457.

48. Androsch, R.; Schick, C.; Schmelzer, J. W., Sequence of enthalpy relaxation, homogeneous crystal nucleation and crystal growth in glassy polyamide 6. *Eur. Polym. J.* **2014**, *53*, 100.

49. Kim, J. S.; Wu, G.; Eisenberg, A., Viscoelastic properties of poly (styrene-co-acrylate) and poly (vinylcyclohexane-co-acrylate) ionomers. *Macromolecules* **1994**, *27*, 814.

50. Suchocka-Galaś, K., Microphase separation in ionomers based on styrene-acrylic acid copolymers. *Eur. Polym. J.* **1989**, *25*, 1291.

51. Suchocka-Gałaś, K., The state of ion aggregation in ionomers based on copolymers of styrene and acrylic acid—I. Thermal studies. *Eur. Polym. J.* **1990**, *26*, 1203.

52. Lee, D.; Register, R. A.; Yang, C.; Cooper, S. L., MDI-based polyurethane ionomers. 2. Structure-property relationships. *Macromolecules* **1988**, *21*, 1005.

53. Lei, Z.; Xing, W.; Wu, J.; Huang, G.; Wang, X.; Zhao, L., The proper glass transition temperature of amorphous polymers on dynamic mechanical spectra. *J. Therm. Anal. Calorim* **2014**, *116*, 447.

54. Seyler, R. J. *Assignment of the glass transition*; Astm International, 1994; Vol. 1249.

55. Shi, S.; Weber, A. Z.; Kusoglu, A., Structure-Transport Relationship of Perfluorosulfonic-Acid Membranes in Different Cationic Forms. *Electrochim. Acta* **2016**, *220*, 517.

56. Zhang, M. Morphological Characterization and Analysis of Ion-Containing Polymers Using Small Angle X-ray Scattering . Ph.D. Dissertation, Virginia Tech, Blacksburg, VA, 2014.

57. Zhang, M. Morphological Characterization and Analysis of Ion-Containing Polymers Using Small Angle X-ray Scattering. PhD Thesis, Virginia Tech, Blacksburg, VA, 2014.

58. Percus, J. K.; Yevick, G. J., Analysis of classical statistical mechanics by means of collective coordinates. *Physical Review* **1958**, *110*, 1.

59. Rubatat, L.; Rollet, A. L.; Gebel, G.; Diat, O., Evidence of Elongated Polymeric Aggregates in Nafion. *Macromolecules* **2002**, *35*, 4050.

60. Gebel, G.; Loppinet, B., Colloidal structure of ionomer solutions in polar solvents. *J. Mol. Struct.* **1996**, *383*, 43.

61. Gebel, G., Structural evolution of water swollen perfluorosulfonated ionomers from dry membrane to solution. *Polymer* **2000**, *41*, 5829.

62. Moore, R. B.; Bittencourt, D.; Gauthier, M.; Williams, C. E.; Eisenberg, A., Small-angle x-ray scattering investigations of ionomers with variable-length side chains. *Macromolecules* **1991**, *24*, 1376.

63. Zhou, N. C.; Chan, C. D.; Winey, K. I., Reconciling STEM and X-ray scattering data to determine the nanoscale ionic aggregate morphology in sulfonated polystyrene ionomers. *Macromolecules* **2008**, *41*, 6134.

64. Enokida, J. S.; Hu, W.; Fang, H.; Morgan, B. F.; Beyer, F. L.; Winter, H. H.; Coughlin, E. B., Modifying the Structure and Dynamics of Ionomers through Counterion Sterics. *Macromolecules* **2020**.

65. Hildebrandt, L.; Dinnebier, R.; Jansen, M., Crystal structure and ionic conductivity of cesium trifluoromethyl sulfonate, CSSO3CF3. *Zeitschrift für anorganische und allgemeine Chemie* **2005**, *631*, 1660.

66. Eisenberg, A.; Hird, B.; Moore, R. B., A new multiplet-cluster model for the morphology of random ionomers. *Macromolecules* **1990**, *23*, 4098.

67. Shannon, R. D., Revised effective ionic radii and systematic studies of interatomic distances in halides and chalcogenides. *Acta Crystallogr. Sec. A* **1976**, *32*, 751.

68. Loppinet, B.; Gebel, G., Rodlike Colloidal Structure of Short Pendant Chain Perfluorinated Ionomer Solutions. *Langmuir* **1998**, *14*, 1977.

69. Rubatat, L.; Gebel, G.; Diat, O., Fibrillar Structure of Nafion: Matching Fourier and Real Space Studies of Corresponding Films and Solutions. *Macromolecules* **2004**, *37*, 7772.

70. Yarusso, D.; Cooper, S. L., Analysis of SAXS data from ionomer systems. *Polymer* **1985**, *26*, 371.

71. Yarusso, D. J.; Cooper, S. L., Microstructure of ionomers: interpretation of small-angle x-ray scattering data. *Macromolecules* **1983**, *16*, 1871.

72. Pedersen, J. S., Instrumentation for Small-Angle X-ray and Neutron Scattering and Instrumental Smearing Effects. *Neutrons, X-rays and Light: Scattering Methods Applied to Soft Condensed Matter* **2002**, 127.

73. Nguyen, D.; Zhong, X.-F.; Williams, C. E.; Eisenberg, A., Effect of ionic chain polydispersity on the size of spherical ionic microdomains in diblock ionomers. *Macromolecules* **1994**, *27*, 5173.

74. Nguyen, D.; Williams, C. E.; Eisenberg, A., Block ionomer micelles in solution. 1. Characterization of ionic cores by small-angle X-ray scattering. *Macromolecules* **1994**, *27*, 5090.

Chapter 5.

A New Method of Detecting Thermal Transitions in H^+-Form Perfluorosulfonic Acid Ionomers by Differential Scanning Calorimetry

Christina M. Orsino,[a] Denis Duchesne,[b] Gregg Dahlke,[b] Lisa Chen,[b] and Robert B. Moore[a]

[a]*Department of Chemistry, Macromolecules Innovation Institute, Virginia Tech, Blacksburg, VA, 24060, USA*

[b]*3M Company, St. Paul, MN, 55144, USA*

5.1 Introduction

Perfluorosulfonic acid ionomers (PFSAs) are copolymers of polytetrafluoroethylene (PTFE) and a perfluorovinyl ether sidechain containing pendant sulfonate groups.[1,2] In PFSAs, aggregation of the polar sidechains leads to a nanophase-separated "cluster" morphology where the polar ionic domains are dispersed and interconnected throughout the nonpolar PTFE matrix.[3] This phase separation between the polar and nonpolar domains provides pathways for proton conduction through the percolating ionic domains, facilitated by uptake of water into the membrane. In addition, sufficient runs of PTFE in the polymer backbone allow for crystallizability (unit cell dimensions identical to pure PTFE)[4,5] that provides mechanical integrity to the membranes and limits water swelling.[6,7]

PFSAs are most widely utilized as proton exchange membranes (PEMs) in PEM hydrogen fuel cells.[1,8] Structures for common PFSA materials are shown in **Figure 5-1**. Nafion®, now a product of Chemours, has been the benchmark PFSA since its creation in the late 1960s by Walther Grot of Dupont.[1] It has been the most well-studied material for use in proton exchange membrane fuel cell (PEMFC) applications, and is widely recognized as the benchmark membrane in the

PEMFC field.[1] While Nafion dominates in the literature, alternative perfluorinated ionomers continue to be developed with differing sidechain chemistries and higher ion exchange capacities (IECs) in an attempt to optimize functionality, transport properties, and electrochemical performance while maintaining mechanical stability. These alternative PFSAs with shorter sidechains than Nafion, include 3M's perfluorosulfonic acid (3M PFSA) and Solvay's Aquivion (short sidechain, SSC), and are of increasing interest due to their desirable transport properties and application performance.[9,10] In addition to differing sidechain chemistries, the physical properties of PFSAs are governed by their equivalent weight (EW). In short, EW is the ratio of grams of polymer to moles of ionic sidechain content. Higher EW PFSAs contain a larger number of crystallizable TFE units between sidechains and less ionic sidechain content.

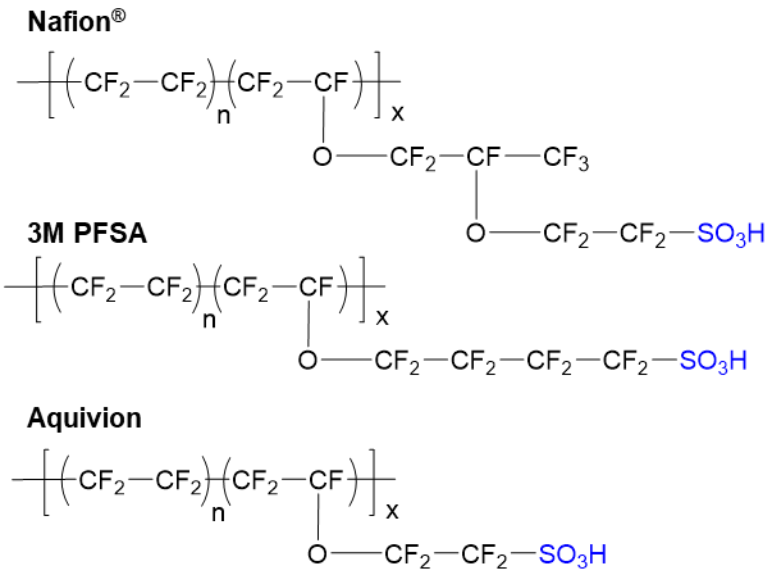

Figure 5-1. Chemical structures for Nafion, 3M PFSA and Aquivion (SSC) containing the same TFE backbone with slight differences in sidechain structure.

Since the first report of glass transition data for Nafion back in 1977,[11] numerous studies have been conducted in an effort to assign the underlying origins of the multiple thermal transitions

and mechanical relaxations for PFSA materials. It is necessary to have accurate assignments of the thermomechanical properties for these materials in order to develop processing conditions that result in optimal morphologies, consisting of well phase-separated nanodomains with developed crystallinity for mechanical stability and percolated ionic pathways for ion conduction. Fundamental understanding of the underlying molecular-level and morphological origins of the thermomechanical relaxations is crucial to developing a full picture of the structure-property relationships for these materials. By combining multiple techniques to measure the thermal, viscoelastic, and dielectric properties of these ionomers, a general consensus has emerged within the last 20 years on the assignment of these relaxations.[2] However, with the continuing development of new PFSAs with various sidechain structures and EWs, it has become increasingly important to have a clear understanding of the effect of ionomer structure on the morphology and thermomechanical properties for these complex materials.

Differential scanning calorimetry (DSC) has been used to investigate the thermal behavior of PFSAs including melting temperature (T_m) and glass transition temperature (T_g) . Early DSC studies conducted on H^+-form and Na^+-neutralized PFSA materials reported two endothermic peaks below 300°C in the first heat.[5,11-14] These two endothermic peaks were initially correlated to two thermomechanical relaxations that were observed around the same temperature, T_α and T_β, by dynamic mechanical analysis. Kyu, Hashiyama, and Eisenberg assigned the two endothermic events observed by DMA and DSC to the glass transition of the matrix ($T_{g,m}$ ~ 140°C) and the glass transition of the ionic clusters ($T_{g,c}$ ~ 240°C) in Na^+-form Nafion .[15] This assignment was further confirmed by Moore and Martin when upon changing the counterion associated with the ionic clusters, the high temperature endotherm shifted dramatically.[5] In these studies, the high temperature endotherm was shown to shift in temperature as a result of counterion type and

processing conditions, leading to the assignment of this endotherm to the glass transition temperature of the ionic clusters, $T_{g,c}$.

Since these original assignments, there have been numerous studies and some debate over the origins of the endotherms observed by DSC.[16] Ultimately, a study conducted by Page, Cable, and Moore in 2004 came to a different conclusion about the two endotherms observed in the DSC thermograms for Nafion membranes.[17] The lower temperature endotherm that was originally assigned as the glass transition of the matrix, was shown to disappear upon reheat and shift with annealing temperature, leading to its reassignment as melting of secondary crystallites due to thermal treatment. The high temperature endotherm originally attributed to the glass transition of the clusters, was also shown to disappear upon reheat, but could be induced to reappear by thermally annealing at a temperature below the endothermic event.[17] Based on this observation, and the disappearance of the crystalline WAXS reflection at temperatures above this endotherm,[12] the high temperature endotherm was ultimately assigned to the melting of PTFE crystallites.

The assignments of the morphological origins of these melting endotherms in PFSAs were determined using Nafion in the alkali metal salt form (e.g., the proton of the sulfonic acid group was exchanged with a Na^+ or Cs^+ counterion.) To this day, DSC is used as a complementary technique to describe glass transition behavior in PFSA membranes, despite conflicting assignments of various endotherms observed in thermograms reported in literature.[16] Given the vastly different interpretations over the years of the origins of thermal events in DSC data from PFSAs, it is important to note that first scan thermograms of any polymer are often plagued by artifacts. This is particularly true for H^+-form PFSAs, where residual water (tightly associated with the polar sulfonic acid groups) in even "dry" samples can dissociate/evaporate over a wide range

of temperatures (e.g., 50 to 200 ^{o}C) resulting in a broad endothermic event that is not observed upon second heat.

Despite the appearance of extraneous endothermic events within the first heat scan of PFSAs that have been overinterpreted over the years, the use of DSC as a complementary tool to probe thermal transitions in PFSAs should not be completely ruled out. The additional endotherms that are observed in the first heat are the result of either excess water in the membrane or melting of crystallites that form from thermal treatments. Both of these endothermic events are irreversible and should be easily removed from the thermogram following a precise DSC pretreatment protocol. In this work, the water content within H^{+}-form PFSA membranes of different sidechain structures and ion contents is determined and a drying protocol is developed to remove all residual water from membranes prior to the first heat. An initial heating scan is then used to melt any residual crystallinity within the membrane that may be artificially attributed as a thermal transition. Upon second heat, a single thermal transition is observed in all of the PFSAs investigated and DMA studies of partially neutralized membranes are used to correlate the DSC thermal transition to the previously assigned thermomechanical relaxations in PFSAs.

5.2 Experimental

5.2.1 Materials.

The 3M-Perfluorosulfonic acid (3M-PFSA) ionomer of 800 and 725 equivalent weight (EW, g polymer/mol sulfonate groups) were provided by 3M. Nafion® 117 (1100 EW) membrane was purchased DuPont and Aquivion 870 EW membrane (E87-05S) was purchased from Sigma Aldrich. A 720 EW SSC (Aquivion analog used in water uptake measurements) membrane,

Fumasep FS-720, was purchased from FuelCellStore. Tetrabutylammonium hydroxide (TBAOH), 1.5 M in water, was obtained from Fisher Scientific and used without further purification.

5.2.2 Membrane preparation

3M-PFSA membranes were prepared by casting a dispersion from alcohol and water onto polyimide film. The dispersions were dried in an oven with the temperature of 80°C followed by annealing for 10 minutes at 200°C. Membranes were removed from the polyimide film by soaking in water. Aquivion and Nafion membranes were used as-received. To remove impurities, all membranes were soaked in 8 M HNO_3 for 16 hours then rinsed thoroughly with deionized water. Ion exchange to 100% TBA^+-form was carried out by stirring the pretreated membranes in 1 M TBAOH in water for 24 hours. Partial neutralization of pretreated membranes was done by stirring each membrane in TBAOH/water solutions containing specified quantities of TBAOH for 24 hours. TBAOH quantities ranging from 5 to 90 mol % for each membrane were calculated on the basis of equivalent weight of dry membranes. All prepared membranes were thoroughly rinsed with water before drying under vacuum at 70°C overnight.

5.2.3 Differential Scanning Calorimetry

DSC data were collected for the H^+-form and partially neutralized ionomers on a TA Instruments Q2000 at 20 °C/min ramp rate under nitrogen purge. Initial DSC thermograms were obtained after thoroughly drying the samples in the DSC at 120 °C for 2 hours. After the initial drying step, the samples were cooled down to −85 °C, then ramped from −85 °C to 200 °C at 20 °C/min as the “first heat” scan to remove any thermal history from the sample. After the first heat, they were cooled from 200 °C to −85 °C at 20 °C/min, however the cooling rate for the Refrigerated Cooling System used with the TA Q2000 decreases at temperatures below 0 °C and

likely began cooling at a rate closer to 2 to 10 °C/min.[18] Second heat data was taken from −85 °C to 200 °C at 20 °C/min. For the physical aging study, 3M PFSA samples were held at 45 °C or 85 °C for 0, 0.5, 2, 6 and 12 hours in the DSC, cooled to −85 °C, then heated from −85 °C to 200 °C at 20 °C/min.

5.2.4 Dynamic Mechanical Analysis

Dynamic mechanical analysis was performed on a TA Instruments DMA Q800 analyzer in tensile mode using clamps for thin film samples. All samples were cut from vacuum dried membranes with a width of 6.35 mm. The membranes were analyzed at a frequency of 1 Hz from −120 to 200°C with a heating ramp of 2°C/min.

5.2.5 Dynamic Vapor Sorption

Dynamic vapor sorption (DVS) experiments were performed on a TA Instruments VTI-SA+ high performance sorption analyzer at 3M Company in St. Paul, MN. All samples were hydrated by soaking overnight in water and blotted dry prior to analysis. Upon loading into the instrument, the membranes were equilibrated at 60 °C for 1 hour then the temperature was set to 25 °C for water uptake experiments. The relative humidity (RH) level was stepped from 5% to 95% RH and back with 5% increments. At each RH step, the sample was held until the weight change was less than 0.001% in 5 minutes for a maximum equilibration time of 2 hours.

5.3 Results and Discussion

5.3.1 Water content effects on the DSC first heat of PFSAs

DSC thermograms for H^+-form Nafion with different pretreatment conditions are shown in **Figure 5-2**. As-received H^+-form Nafion displays a large endotherm with a possible smaller endothermic shoulder on the first heat. However, upon equilibrating the Nafion 117 membrane at 50% relative humidity (RH) overnight, those endotherms increase in intensity and overlap into one broad endotherm. After drying the membranes thoroughly either under vacuum at 70 °C overnight, or in the DSC at 120 °C for two hours, those large endothermic events disappear suggesting that those endotherms are likely due to evaporation of water in the membranes upon heating. In membranes that were heat treated for water removal prior to running, there is a small endotherm that appears ca. 30 °C above the temperature at which it was pretreated that disappears on second heat. This is the same phenomenon was observed by Page, Cable and Moore that was attributed to melting of small crystallites that form in the sample due to annealing conditions.[17] In the H^+-form, the sulfonic acid groups in PFSAs begin to decompose close to 200 °C.[2,19] For this reason, DSC studies cannot be performed up to temperatures high enough to capture the melting temperature of the PTFE-like crystallites formed from the crystallizable backbone segments in Nafion membranes in the H^+-form (ranging from 250 to 300 °C).[3,17] This data demonstrates the importance of not overinterpreting DSC thermograms for these ionomers, as the slightest change in water content or pretreatment conditions can have a drastic effect on the data. In order to interpret DSC data for PFSAs in the H^+-form, a precise pretreatment method is necessary for full removal of water in the membranes that can be used across PFSAs with differing sidechain structures and ion contents.

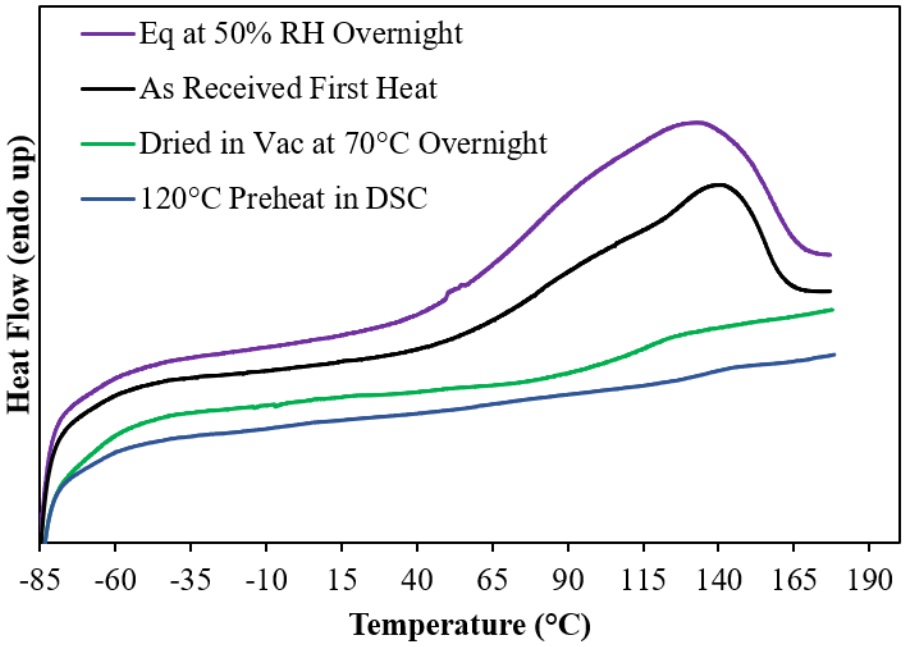

Figure 5-2. DSC first heat thermogram of Nafion after different pretreatment conditions.

Water uptake isotherms for PFSAs with different sidechain lengths and ion contents (EW values) are shown in **Figure 5-3**. Water content is represented as a ratio of water molecules to the number of sulfonate groups, λ.[20] Nonlinear water uptake isotherms are the result of initial solvation of the SO_3H groups with bound water up to 75% RH, followed by swelling of the hydrophilic domains with mobile water molecules at higher RH values.[21-24] During initial hydration, water molecules solvate the protons of the sulfonic acid groups and form hydration shells that compose the bound water in the membrane. An interconnected network of domains is believed to form after adsorption of only 2 or more water molecules per sulfonic acid group.[2] The hydration shells continue to increase in size with increasing water content up to 5 or 6 water molecules per sulfonic acid. In the bulk water regime at 75% RH and higher, the hydrophilic domains behave more like a bulk-water region where water molecules can move freely. In this regime, the effects of crystallinity and ion exchange capacity on water uptake are more pronounced, as observed in

Figure 5-3 where the isotherms for the different PFSAs appear to deviate more at RH values of 75% and higher.

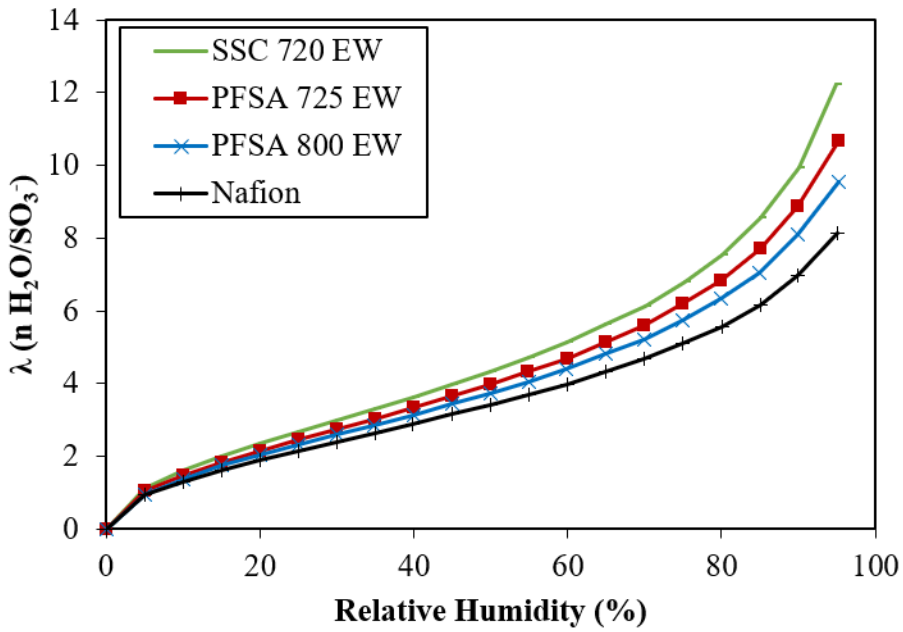

Figure 5-3. Water uptake isotherms at 25 °C for short sidechain (analog to Aquivion), PFSA 725 and 825 EW, and Nafion 1000 EW in the H-form.

Of importance to this DSC study is the bound water within PFSA membranes at ambient relative humidity levels. For all PFSAs investigated in **Figure 5-3**, there are ca. 2 to 5 water molecules per sulfonic acid group in the range of 30 to 60% RH. **Figure 5-4** shows the water content of each PFSA at 50 % RH based on EW. Membranes with higher EW values for a given sidechain typically contain more crystallinity, which limits the water uptake capacity by increasing the PTFE backbone's resistance to deformation.[2] Within this ambient RH regime, the water content within PFSA membranes are considered to be strongly bound water molecules that can only be removed at elevated temperatures. An FTIR study of water content in H^+-form Nafion membranes showed that complete water removal is only achieved after drying at temperatures near 95 °C under

vacuum.[25] It's even more difficult to remove bound water in Na^+-form Nafion, where temperatures in excess of 400 °C are necessary for complete dehydration.[25,26] In H^+-form 3M PFSA, a previous study investigated residual water content in membranes by drying them at 120 °C for 30 minutes.[27] An 825 EW 3M PFSA was shown to contain ca. 2.5 moles of water per moles of sulfonate groups that were removed after this drying method. Some studies have found that a small trace of water may remain in H^+-form PFSAs up to 200 °C, where the onset of sulfonic acid degradation occurs (in the range of 200 to 250 °C).[28]

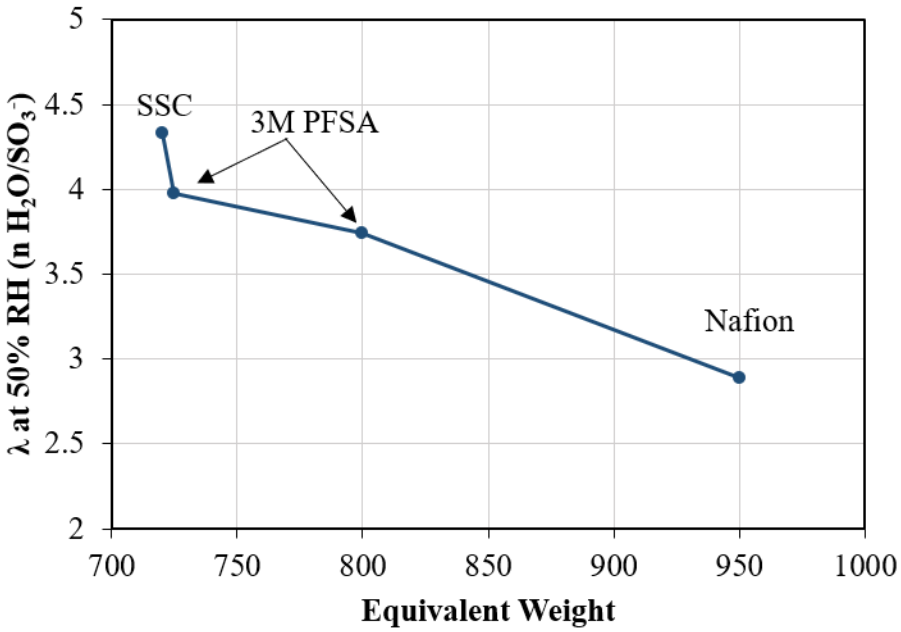

Figure 5-4. Water content vs. EW for H-form PFSAs of different sidechain structures at 50% relative humidity.

For the purpose of performing DSC experiments, a drying step at 120 °C for two hours *in* the DSC appears to remove enough water in PFSA membranes to create a linear baseline. This method was used by Page, Cable and Moore to thoroughly dry Nafion membranes in the DSC allowing for elucidation of two melting endotherms in the Cs^+- and Na^+-counterion forms that

were attributed to melting of PTFE-like crystallites.[17] Due to the high temperature of the thermomechanical relaxations in Na^+- and Cs^+-form Nafion that overlap with the melting endotherms, and the broad nature of these relaxations in these counterion forms, thermomechanical relaxations have not been observed by DSC. This DSC drying method, however, has not yet been used on H^+-form membranes to probe the glass transition behavior.

5.3.2 DSC Drying Method for Water Removal

A new method of performing DSC experiments on PFSAs in the H^+-form employs a drying step to remove any residual water from the membranes and a first heat scan to remove any thermal history that results from this drying step. In this method, the sample is cooled down to −85 °C after the drying step, then heated to 230 °C (first heat), cooled back to −85 °C (cool), and heated a second time to 230 °C (second heat) all at a rate of 20 °C/min. The relatively fast heating rate of 20 °C/min (typical scan rates for DSC are 10 °C/min) was chosen to improve the sensitivity of the instrument for detection of a broad glass transition with a likely small change in heat capacity across the transition.[29] The subzero starting temperature was chosen to allow enough linear baseline on either side of the observed transition to confirm the appearance of a small step-change in heat flow at this high heating rate.

The DSC thermograms for H^+-form Nafion after a two-hour hold at 120 °C for water removal is shown in **Figure 5-5**. In the first heat, two small endothermic events are observed at ca. 50 °C and 150 °C. Although it is hard to attribute these endotherms to anything because of their small and broad appearance that makes them difficult to distinguish from the baseline, it is likely that the endotherm at 150 °C is the result of small, imperfect crystals that formed during the 120 °C drying process.[17] During the cooling step, it is also difficult to distinguish any features in the thermogram due to the abrupt change in cooling rate below 0 °C, that is inherent to the limitations

of the cooling accessory attached to the DSC instrument.[18] The second heat, however, provides a relatively clear, linear baseline where a step change in the heat flow can be observed at ca. 50 °C for H^+-form Nafion. In this second heat, the higher temperature endotherm at 150 °C is no longer present, confirming that this endotherm was the result of crystallites formed from the drying step. By performing a second heat scan and removing that endotherm at higher temperatures, the baseline is much more linear making it easier to distinguish the clear step change at 50 °C.

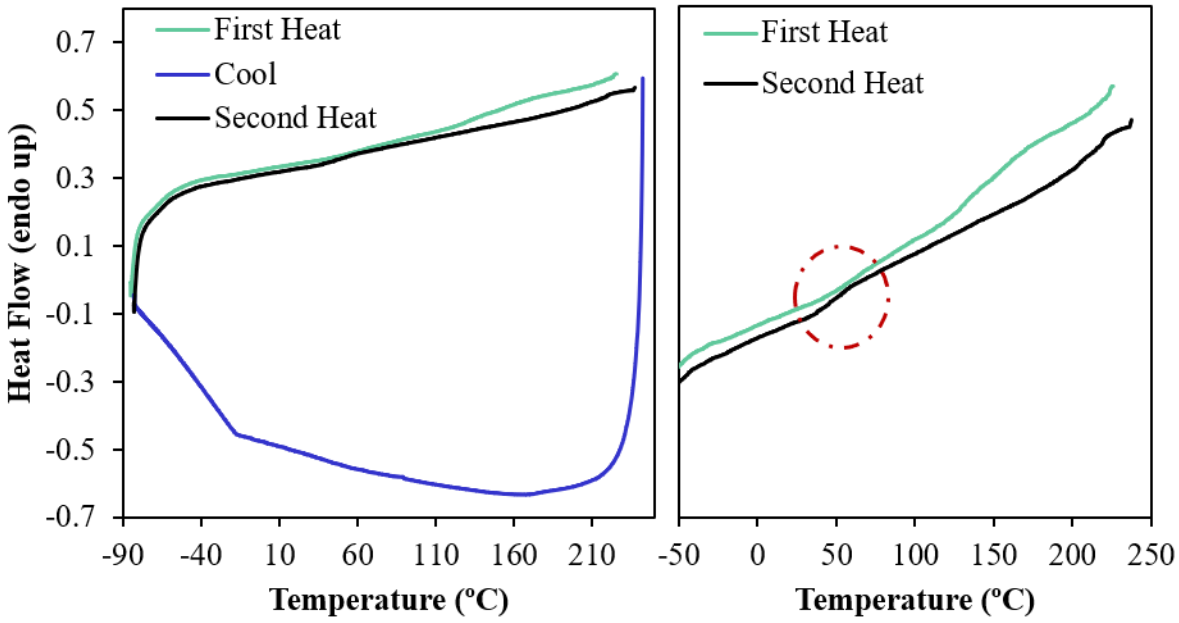

Figure 5-5. First heat, slow cool, and second heat thermograms of H^+-form Nafion after a 120-minute drying step at 120 °C in the DSC. Zooming in on the second heat on the right shows a small step change in heat flow around 50 °C.

While the initial appearance of this endothermic event in H^+-form Nafion looks like a second-order transition, it can be further confirmed by looking at several other H^+-form PFSAs that exhibit the same behavior following the new DSC pretreatment protocol. **Figure 5-6** shows the second heat for H^+-form Aquivion, Nafion, and 3M PFSA after this drying method was used.

In all three PFSAs, a step-change in the heat flow is observed upon the second heat. The temperature at which that step-change occurs is different between the samples, increasing in temperature with decreasing sidechain length. The step-change is more pronounced in 3M PFSA and Nafion, and very broad in Aquivion, making it harder to distinguish from the baseline.

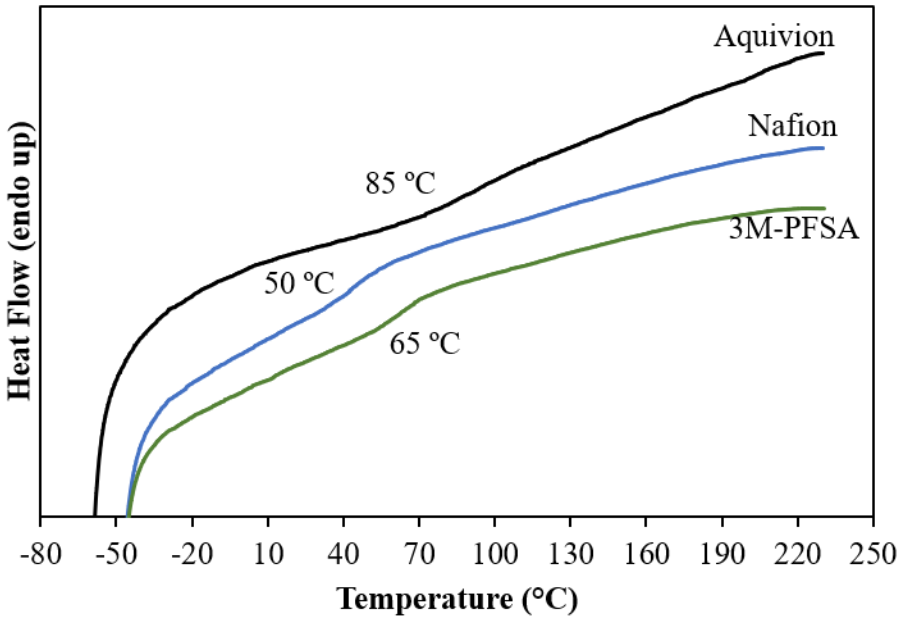

Figure 5-6. DSC thermograms of Aquivion, Nafion, and 3M-PFSA after 120-minute drying step at 120 °C.

Figure 5-7 shows the reproducibility of this method for detecting this thermal transition in H^+-form PFSAs. In this experiment, four different samples of 3M PFSA were prepared and run using the drying, second heat method. All four thermograms show a distinguishable step-change in the heat flow at ca. 65 °C. The transition is also observable in subsequent heats of the same sample, indicating reversibility. The reproducibility and reversibility of this endothermic event indicates that it is likely attributed to a second-order glass transition for these PFSAs. Ideally, this would be confirmed by looking at the cooling scan from 200 to below 0 °C for signs of a reversible step-

change upon cooling. However, due to the abrupt slope change in the baseline of the cooling scan, a small step-change in heat flow is not observable.

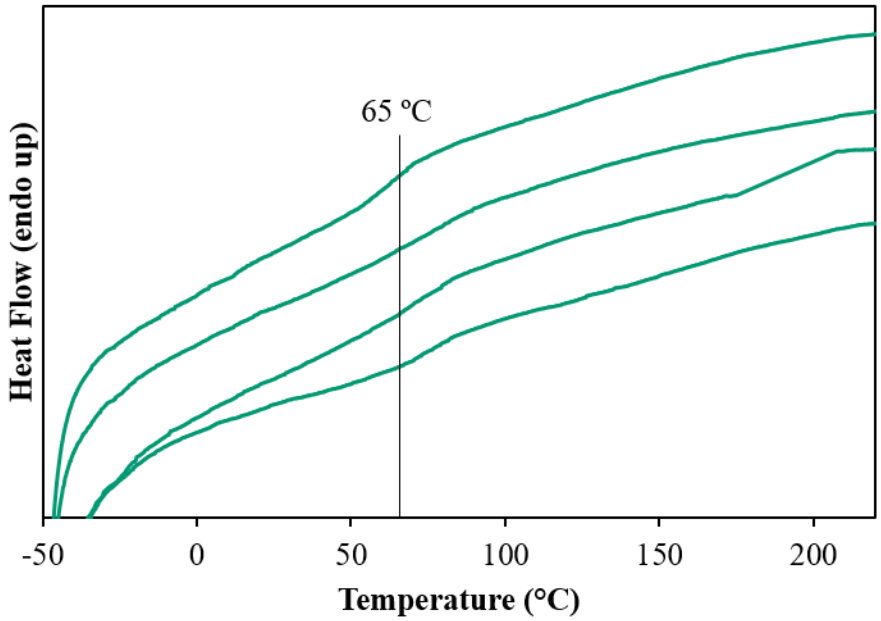

Figure 5-7. DSC thermograms of H-form 3M-PFSA 800 EW membrane repeated four times with the same method all show the same stepchange in heat flow around 65 °C, showing the reproducibility of this endothermic event with this new DSC method.

Another method for confirming glass transition behavior of this endothermic event is by utilizing the physical aging phenomenon as a tool to probe this transition. For simple glass-forming polymers, an endothermic peak in the vicinity of the T_g is the signature of enthalpic recovery upon physical aging at a temperature just below the T_g.[30] Sub T_g physical aging of polymers generally involves a slow densification of the polymer, leading to increased enthalpic interactions between the chains as the system tends to achieve a more favorable thermodynamic state.[31] Densification of the chains increases with the amount of time that the polymer is held at the aging temperature. Upon reheating, the densified chains go through enthalpic recovery as the polymer passes through the glass transition causing an increase in enthalpy, which appears as a first-order peak

superimposed upon the step change in heat capacity at the glass transition in DSC. For physical aging, a linear relationship has been observed between the area under the enthalpic recovery endotherm (ΔH) and the log of aging time.[32-34]

In the case of these H^+-form PFSAs, the physical aging phenomenon can be used as a means to confirm that the apparent glass transition is a true T_g by aging at a temperature just below the apparent T_g and observing whether enthalpic recovery occurs upon reheating. **Figure 5-8** shows the effect of aging 3M PFSA at 45 °C (20 °C below the apparent glass transition) and at 85 °C (20 °C above the apparent glass transition). The 3M PFSA annealed at 85 °C reveals a small endotherm that increases in magnitude with increasing annealing time. However, when compared to that of the sample annealed at 45 °C, the endotherm resulting from the 85 °C anneal is broader and less pronounced. This endotherm observed for the 85 °C anneal is likely due to melting of small crystallites that form upon annealing.[17] Further confirmation of this is seen in **Figure 5-8** by plotting the enthalpy of the small endotherm vs. log(aging time). The enthalpy of the small endotherm observed in 3M PFSA annealed at 85 °C does not increase linearly with log(annealing time) as would be expected in the case of physical aging, whereas the endotherm that appears with annealing at 45 °C behaves more like that observed in physical aging. While this experiment gives some indication of true glass transition behavior of this step-change in heat flow observed in H^+-form PFSAs, the aging-induced endotherm still does not appear as profound as a typical glass forming polymer. Further confirmation that this endotherm is not due to the formation of small crystallites in the sample is necessary to confirm that physical aging is occurring at 45 °C in these samples. Unfortunately, the small increase in crystallinity that may appear in these samples is not easily detectable by X-ray scattering methods where the PTFE crystallite peak is overlapping with a broad, amorphous halo for these ionomers.

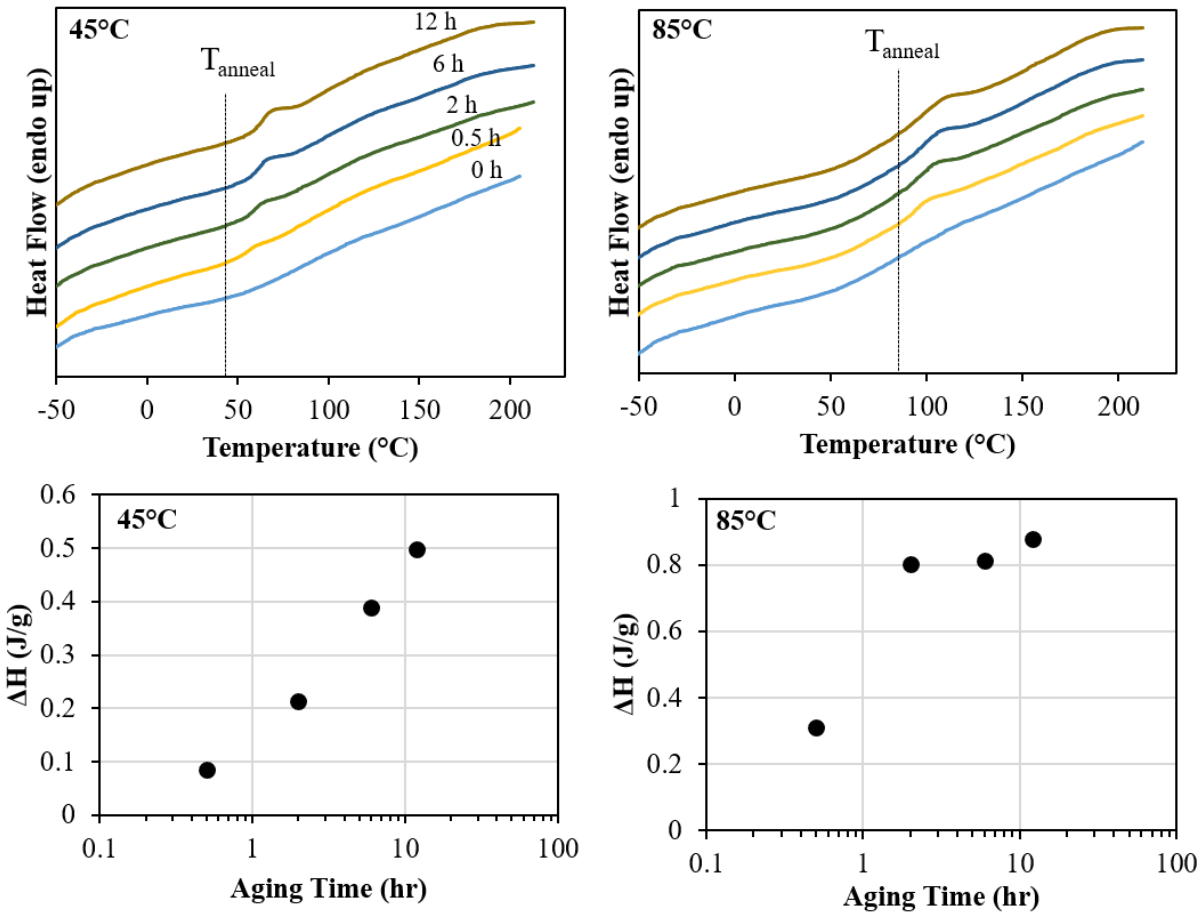

Figure 5-8. Physical aging experiment of 800 EW 3M PFSA annealed at 45 °C and 85 °C for various lengths of time. The enthalpy of each endotherm is plotted vs. log of aging time.

5.3.3 Determining the Thermomechanical Origin of the DSC Thermal Transition.

In the dynamic mechanical spectra for PFSAs, there are generally three observed thermomechanical relaxations.[11,13,17,35-38] The lowest temperature γ-relaxation (observed in the vicinity of −100 °C) has been attributed to the local motions of the PTFE backbone. A higher temperature β-relaxation has been observed in Nafion at temperatures ranging between −62 and 23 °C, depending on the study. This relaxation has been assigned as the true glass transition temperature of Nafion and, more specifically, the onset of segmental motions within a static electrostatic network.[17,39] Lastly, the high temperature α-relaxation is observed at ca. 100 °C and

is attributed to the onset of long-range motions of both the main and side chains facilitated by a weakening of the electrostatic interactions within the ionic aggregates.[17] The temperatures at which these relaxations occur can be varied upon exchange of the sulfonic acid proton to other counterions. For example, the α-relaxation at 100 °C for H^+-form Nafion increases to 200 °C upon conversion to the Na^+-form, a shift that is attributed to the increase in network strength when converting from a weak hydrogen-bonded physically crosslinked network to a strong electrostatic network.[17] The chain motions associated with both α- and β-relaxations are coupled to the physical crosslinks within the ionic aggregates.[38] The origins of thermomechanical relaxations in perfluorinated ionomers can be elucidated by manipulating the strength of the physically crosslinked network with different counterions.

While the dynamic mechanical spectra show three relaxations for PFSAs, it is interesting that only one thermal transition is observed in the DSC data presented above. In an attempt to assign the enthalpic transition temperature observed by DSC to one of the thermomechanical relaxations observed by DMA, we can manipulate the strength of the physically crosslinked network and systematically shift one of the relaxation temperatures and compare that with the DSC data. An example of this has been performed using partial neutralization of Nafion membranes with tetrabutylammonium (TBA^+) counterions.[39] In the TBA^+-form, Nafion (as well as Aquivion and 3M PFSA, explored in **Chapter 3**) have an α-relaxation occurring at the same temperature as the α-relaxation in the H^+-form. However, the β-relaxation in the TBA^+-form is at much higher temperatures than the H^+-form. By partially neutralizing the H^+-form ionomers with increasing quantities of TBA^+, the β-relaxation is observed to shift to increasing temperatures while the α-relaxation remains the same. Based on these observations, if the same partially neutralized samples are investigated by DSC, the transition temperature observed will either shift with TBA^+ content

if the transition is related to the β-relaxation, or remain at the same temperature if it is related to the α-relaxation.

DSC thermograms for partially neutralized 800 EW 3M PFSA are shown in **Figure 5-9**. In all of these experiments, the same 120 °C drying step was utilized and the data reported is the second heat. A clear step-change transition is observed in all samples. In the 20% TBA^+-form, the transition appears at ca. 33 °C and increases in temperature with increasing TBA^+ content to ca. 58 °C for the 100 % TBA^+-form. Interestingly, the H^+-form thermogram does not follow the trend observed for the partially neutralized membranes. This transition temperature is observed at ca. 65 °C and is much broader and indistinct compared to the partially neutralized samples.

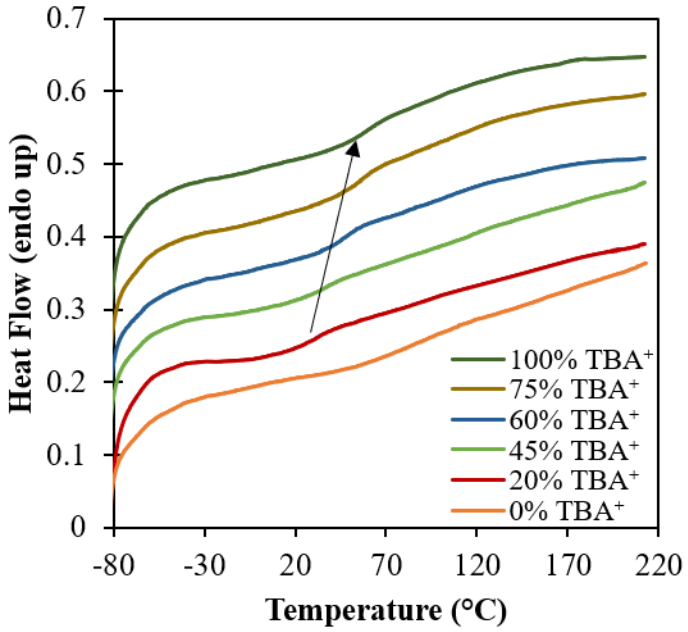

Figure 5-9. DSC thermograms for 800 EW 3M PFSA partially neutralized with TBA^+ counterions.

A better visual of the shift in transition temperature with TBA^+ content is displayed in **Figure 5-10**. In this plot, the corresponding α- and β-relaxation temperatures for partially

neutralized 3M PFSA (determined by dynamic mechanical tanδ peak maximum, data is presented in a later figure) are plotted along with the observed DSC transition for each sample. There is a clear relationship between the β-relaxation temperature and the transition observed by DSC. The DSC transition appears approximately 20 °C lower than the β-relaxation, but follows the same trend with TBA^+ content. The transition temperature observed for the H^+-form deviates from this trend and appears at a higher temperature.

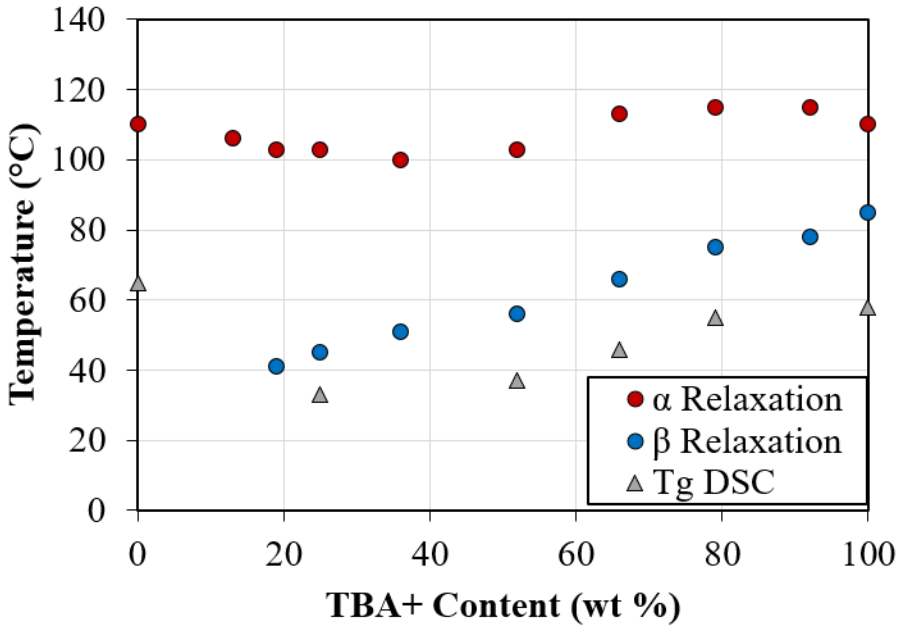

Figure 5-10. Plot of relaxation vs. TBA content for 800 EW 3M PFSA including the measured transition observed by DSC.

In DMA, there are three ways to report the glass transition temperature for a glassy polymer. It can either be taken from the inflection point in the decrease in storage modulus through the transition, the peak in the loss modulus, or the peak in tanδ.[40] Typically, the glass transition temperature is reported as the peak in the tanδ, as was reported in the data above. However, the peak in loss modulus is more representative of the onset of segmental molecular motions than the peak in tanδ. The peak in tanδ is usually observed several degrees higher than the peak in loss

modulus, well past the onset of softening of the material. In more complicated systems with broader transitions, such as the case of these semicrystalline ionomers, this difference in observed transition temperatures between the tanδ peak maximum and loss modulus peak maximum is more pronounced.[40]

A plot of loss modulus versus temperature for the series of partially neutralized 3M PFSA membranes is shown in **Figure 5-11**. What's most interesting from this data is the appearance of only one prominent peak in all of the samples despite there being two clear peaks in the tanδ, attributed to the α- and β-relaxations. For the partially neutralized samples, the peak in loss modulus corresponds to the temperature range of the β-relaxation observed in the tanδ data. However, in the H^+-form sample, the peak in loss modulus corresponds to the temperature range of the α-relaxation in the tanδ data. This observation is most evident in the 100% H^+-form and 100% TBA^+-form samples. As mentioned previously, both the H^+-form and TBA^+-form have α-relaxations at the same temperature (ca. 110 °C), observed in the tanδ data in **Figure 5-11**. However, when looking at the loss modulus peaks, the peak in TBA^+-form is lower than the peak in the H^+-form, closer to the β-relaxation temperature for the TBA^+-form. This may explain the single transition observed by DSC that appears at higher temperatures in the H^+-form and lower temperatures in the partially neutralized forms. DSC probes transitions that are enthalpic in nature, such as the onset of local segmental motion.[41] In DMA, a peak in the loss modulus has been attributed to the onset of local segmental motions of cooperative chains involving several repeat units, while the peak in tanδ has been attributed to larger Rouse modes, which are entropic in nature. Thus, a correlation has been made between the peak in loss modulus and transition temperature observed in DSC of glassy polymers. Since there is only one observed peak in the loss

modulus for these PFSA membranes, corresponding to either the α- or β-relaxation, there is only one transition observed by DSC.

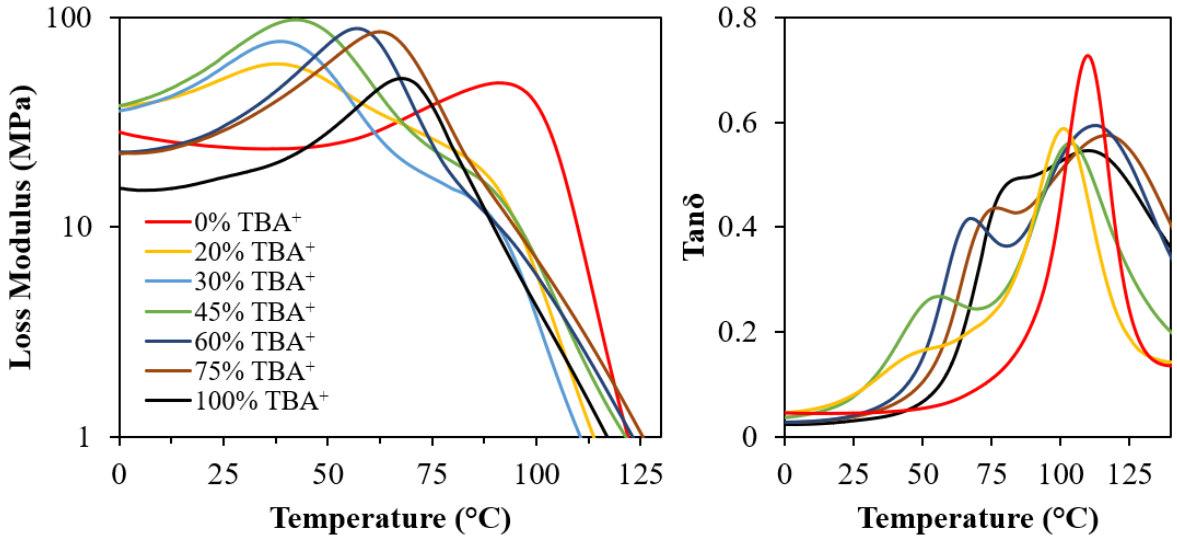

Figure 5-11. Dynamic mechanical loss modulus and tanδ vs temperature data for 800 EW 3M PFSA partially neutralized with TBA^+ counterions.

The loss modulus peak temperature and DSC transition temperature for the 3M PFSA partial neutralization series is shown in **Figure 5-12**. The transition temperature observed by DSC is clearly of the same molecular origin as the peak in loss modulus for all samples. This relationship between the peaks in the dynamic mechanical loss modulus and thermal transitions in DSC has also been observed in hydrocarbon-based ionomers.[42-44] In styrene-sodium methacrylate ionomers, a linear relationship was observed between two thermal transitions measured using DSC and two peaks in the loss modulus measured by DMA.[42] However, in a different study on poly(styrene-*co*-acrylate) and poly(vinylcyclohexane-*co*-acrylate) ionomers, only a single thermal transition was observed by DSC despite the presence of two maxima in the DMA tanδ.[43] In this case, only one

peak in the loss modulus was observed, related either to the matrix glass transition or the cluster glass transition depending on ion content, although a second shoulder appeared on the loss modulus plot instead of a fully developed peak, similar to the shoulder observed in the loss modulus data for the partially neutralized PFSA. A similar result was also observed for methylenebis (*p*-phenyl isocyanate)-based polyurethane ionomers.[44] For these materials where only a single peak appears in the loss modulus data, a single thermal transition is observed in the DSC thermograms as well.

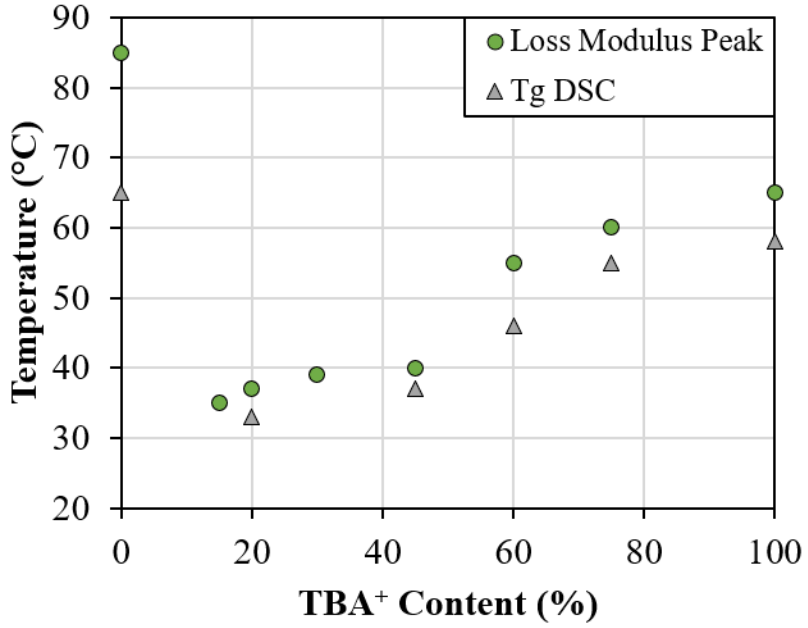

Figure 5-12. Loss modulus peak temperature and DSC transition temperature vs TBA^+ content for 800 EW 3M PFSA.

Although multiple studies on ionomers document the observation of two peaks in tanδ and only one peak in loss modulus,[43-45] there is yet to be a confirmed explanation for this behavior. Based on the data presented here, the β-relaxation appears to give rise to the peak in loss modulus and DSC thermal transition in PFSAs that contain TBA^+ counterions. However, the α-relaxation gives rise to the peak in loss modulus and thermal transition in the H^+-form. The α- and β-

relaxations in PFSAs are closely coupled, and both relaxations are observed to be affected by counterion size and composition.[17] To emphasize this point, the β-relaxation is attributed to the onset of segmental motions of the polymer chains *within* a static physically crosslinked network. The α-relaxation is attributed to the onset of long-range mobility of the polymer chains as a result of destabilization of the physically crosslinked network. So, both relaxations are affected by the strength of the crosslinked network formed by aggregation of the sulfonic acid/sulfonate groups. In the H^+-form, the β-relaxation is not easily observed in PFSAs with shorter sidechains and higher EWs (such as the 3M PFSA investigated here), as discussed in **Chapter 3**. In this case, the physical crosslinks restrict the mobility of the polymer chains such that segmental motion does not occur until enough thermal energy has been induced to begin destabilization of the hydrogen-bonded network. Hence, the peak in loss modulus and thermal transition are not observed until temperatures approach the α-relaxation. Upon introducing TBA^+ counterions, the physically crosslinked network is plasticized by the bulky counterions allowing for the onset of segmental mobility (still within a physically crosslinked network) at lower temperatures. For this reason, in the partially neutralized and fully neutralized forms, the peak in loss modulus and thermal transition are observed at temperatures in the vicinity of the β-relaxation.

Interestingly, a similar relationship between the α-relaxation and observed thermal transition in H^+-form, and the β-relaxation and observed thermal transition in the salt form for PFSAs has been observed before. In a study on thermal transitions in thin film PFSAs, thermal film expansion measurements were used to determine the transition temperatures of Nafion in the Cs^+-, Na^+-, and H^+-form in thin films compared to bulk film relaxations.[46] Ellipsometry was used to determine the film expansion rate with increasing temperature, and a single thermal transition (marked by a change in the slope of the expansion rate) was observed in each of the samples. In

this study, the thermal transition observed in H^+-form Nafion was attributed to the α-relaxation, while the thermal transition observed in Cs^+- and Na^+-form Nafion were attributed to the β-relaxation due to the temperature ranges at which these transitions were observed compared to the relaxations in the bulk ionomer. Since this study was the first to observe this relationship between the single thermal transition and the two different thermomechanical relaxations based on counterion form in PFSAs, it was tentatively attributed to differences in the interactions between the sulfonic acids and Cs^+-/Na^+-sulfonates with the substrate. However, based on the results of this work where the same relationship is observed in the bulk film by DSC measurements, it's evident that the thermomechanical and thermal behavior of PFSAs in the sulfonic acid form differ from that in the neutralized salt form.

5.4 Conclusions

This work demonstrates a new DSC protocol for removing artifacts in the thermograms of H^+-form PFSAs in order to resolve the appearance of a thermal transition. The purpose of this work was to determine whether DSC could be used as a complementary technique to DMA for determining thermal transitions in these ionomers. Despite numerous publications over the years that have attributed various endothermic events observed in DSC thermograms of Nafion to thermal transitions, there has been conflicting evidence based on the processing conditions used in each study. The development of a standard pretreatment method for investigating PFSAs of different sidechain content and length by DSC is necessary for future studies to make meaningful comparisons, and to prevent further overinterpretation of irreversible artifacts that have been mistakenly assigned as thermal transitions.

Water uptake data illustrated the amount of water that is absorbed into H^+-form PFSA membranes in ambient conditions. In order to fully remove that water for DSC measurements, a drying step at 120 °C for two hours in the DSC was proposed. After this drying step, an additional endothermic event appeared in the first heat that was attributed to the melting of small crystallites that form during the drying step. Upon melting those crystallites, cooling back to subzero temperatures, and reheating the sample, a reproducible linear thermogram was observed with a distinguishable step-change transition for H^+-form Nafion, Aquivion, and 3M PFSA. The temperature of this transition increased with decreasing sidechain length. In order to correlate this single thermal transition to one of the three previously assigned thermomechanical relaxations in PFSAs, partial neutralization with TBA^+ counterion was used to systematically manipulate the strength of the crosslinked network and vary the dynamic mechanical β-relaxation temperature. The single thermal transition was shown to be related to a single peak in the loss modulus for all samples, an observation that has been reported previously by hydrocarbon-ionomer studies. In the H^+-form, the peak in loss modulus and thermal transition result from molecular motions that occur within the α-relaxation. In the TBA^+-form and partially neutralized samples, the peak in loss modulus and thermal transition result from the molecular motions underlying the β-relaxation. This study is the first to document a clear, reproducible thermal transition in H^+-form PFSAs by DSC and correlate it to the thermomechanical relaxations. From this work, it is apparent that the thermomechanical and thermal properties of PFSAs in the H^+-form behave differently than PFSAs in the neutralized salt form.

5.5 Acknowledgments

The authors acknowledge 3M for providing PFSA materials for this study and for funding this research.

5.6 References

1. Mauritz, K. A.; Moore, R. B., State of Understanding of Nafion. *Chem. Rev.* **2004**, *104*, 4535.
2. Kusoglu, A.; Weber, A. Z., New Insights into Perfluorinated Sulfonic-Acid Ionomers. *Chem. Rev.* **2017**, *117*, 987.
3. Gierke, T. D.; Munn, G. E.; Wilson, F. C., The morphology in nafion perfluorinated membrane products, as determined by wide- and small-angle x-ray studies. *J. Polym. Sci., Part B: Polym. Phys.* **1981**, *19*, 1687.
4. Starkweather, H. W., Crystallinity in perfluorosulfonic acid ionomers and related polymers. *Macromolecules* **1982**, *15*, 320.
5. Moore, R. B.; Martin, C. R., Chemical and morphological properties of solution-cast perfluorosulfonate ionomers. *Macromolecules* **1988**, *21*, 1334.
6. Lai, Y.-H.; Mittelsteadt, C. K.; Gittleman, C. S.; Dillard, D. A., Viscoelastic stress analysis of constrained proton exchange membranes under humidity cycling. *J. Fuel Cell Sci. Tech.* **2009**, *6*, 021002.
7. Emery, M.; Frey, M.; Guerra, M.; Haugen, G.; Hintzer, K.; Kai; Lochhaas, H.; Pham, P.; Pierpont, D.; Schaberg, M.; Thaler, A.; Yandrasits, M.; Hamrock, S., The Development of New Membranes for Proton Exchange Membrane Fuel Cells *J. Electrochem. Soc.* **2007**, *11*, 3.
8. Hamrock, S. J.; Herring, A. M. In *Fuel Cells: Selected Entries from the Encyclopedia of Sustainability Science and Technology*, Proton Exchange Membrane Fuel Cells: High-Temperature, Low-Humidity Operation; Kreuer, K.-D., Ed.; Springer New York: New York, NY, 2013, p 577.

9. Hamrock, S. J.; Yandrasits, M. A., Proton Exchange Membranes for Fuel Cell Applications. *J. Macromol. Sci., Rev. Macromol. Chem. Phys.* **2006**, *46*, 219.

10. Moukheiber, E.; De Moor, G.; Flandin, L.; Bas, C., Investigation of ionomer structure through its dependence on ion exchange capacity (IEC). *J. Membr. Sci.* **2012**, *389*, 294.

11. Yeo, S. C.; Eisenberg, A., Physical properties and supermolecular structure of perfluorinated ion-containing (nafion) polymers. *J. Appl. Polym. Sci.* **1977**, *21*, 875.

12. De Almeida, S.; Kawano, Y., Thermal behavior of Nafion membranes. *J. Therm. Anal. Calorim* **1999**, *58*, 569.

13. Hodge, I.; Eisenberg, A., Dielectric and mechanical relaxations in a Nafion precursor. *Macromolecules* **1978**, *11*, 289.

14. Su, S.; Mauritz, K. A., Dielectric Relaxation Studies of Annealed Short Side Chain Perfluorosulfonate Ionomers. *Macromolecules* **1994**, *27*, 2079.

15. Kyu, T.; Hashiyama, M.; Eisenberg, A., Dynamic mechanical studies of partially ionized and neutralized Nafion polymers. *Can. J. Chem.* **1983**, *61*, 680.

16. Orsino, C. M.; Moore, R. B., Thermal transitions and mechanical relaxations in perfluorinated ionomers. *Fascinating Fluoropolymers and Their Applications* **2020**, 205.

17. Page, K. A.; Cable, K. M.; Moore, R. B., Molecular Origins of the Thermal Transitions and Dynamic Mechanical Relaxations in Perfluorosulfonate Ionomers. *Macromolecules* **2005**, *38*, 6472.

18. Dallas, G.; Aubuchon, S., TA Instruments DSC Cooling Accessories.

19. Feng, M.; Qu, R.; Wei, Z.; Wang, L.; Sun, P.; Wang, Z., Characterization of the thermolysis products of Nafion membrane: A potential source of perfluorinated compounds in the environment. *Scientific reports* **2015**, *5*, 9859.

20. Springer, T. E.; Zawodzinski, T.; Gottesfeld, S., Polymer electrolyte fuel cell model. *J. Electrochem. Soc.* **1991**, *138*, 2334.

21. Kusoglu, A.; Dursch, T. J.; Weber, A. Z., Nanostructure/Swelling Relationships of Bulk and Thin-Film PFSA Ionomers. *Advanced Functional Materials* **2016**, *26*, 4961.

22. Page, K. A.; Soles, C. L.; Runt, J. *Polymers for energy storage and delivery: polyelectrolytes for batteries and fuel cells*; ACS Publications, 2012.

23. Zawodzinski, T. A.; Springer, T. E.; Davey, J.; Jestel, R.; Lopez, C.; Valerio, J.; Gottesfeld, S., A comparative study of water uptake by and transport through ionomeric fuel cell membranes. *J. Electrochem. Soc.* **1993**, *140*, 1981.

24. Laporta, M.; Pegoraro, M.; Zanderighi, L., Perfluorosulfonated membrane (Nafion): FT-IR study of the state of water with increasing humidity. *Phys. Chem. Chem. Phys.* **1999**, *1*, 4619.

25. Basnayake, R.; Peterson, G. R.; Casadonte, D. J.; Korzeniewski, C., Hydration and interfacial water in Nafion membrane probed by transmission infrared spectroscopy. *J. Phys. Chem. B* **2006**, *110*, 23938.

26. Wang, Y.; Kawano, Y.; Aubuchon, S. R.; Palmer, R. A., TGA and Time-Dependent FTIR Study of Dehydrating Nafion− Na Membrane. *Macromolecules* **2003**, *36*, 1138.

27. Su, G. M.; Cordova, I. A.; Yandrasits, M. A.; Lindell, M.; Feng, J.; Wang, C.; Kusoglu, A., Chemical and Morphological Origins of Improved Ion Conductivity in Perfluoro Ionene Chain Extended Ionomers. *J. Am. Chem. Soc.* **2019**.

28. Shimoaka, T.; Wakai, C.; Sakabe, T.; Yamazaki, S.; Hasegawa, T., Hydration structure of strongly bound water on the sulfonic acid group in a Nafion membrane studied by infrared spectroscopy and quantum chemical calculation. *Phys. Chem. Chem. Phys.* **2015**, *17*, 8843.

29. Menczel, J. D.; Judovits, L.; Prime, R. B.; Bair, H. E.; Reading, M.; Swier, S., Differential scanning calorimetry (DSC). *Thermal analysis of polymers: Fundamentals and applications* **2009**, 7.

30. Berens, A. R.; Hodge, I., Effects of annealing and prior history on enthalpy relaxation in glassy polymers. 1. Experimental study on poly (vinyl chloride). *Macromolecules* **1982**, *15*, 756.

31. Struik, L. C. E., Physical aging in plastics and other glassy materials. *Polym. Eng. Sci.* **1977**, *17*, 165.

32. Hutchinson, J. M.; Smith, S.; Horne, B.; Gourlay, G. M., Physical Aging of Polycarbonate: Enthalpy Relaxation, Creep Response, and Yielding Behavior. *Macromolecules* **1999**, *32*, 5046.

33. Echeverria, I.; Su, P. C.; Simon, S. L.; Plazek, D. J., Physical aging of a polyetherimide: Creep and DSC measurements. *J. Polym. Sci. Part B Polym. Phys.* **1995**, *33*, 2457.

34. Androsch, R.; Schick, C.; Schmelzer, J. W., Sequence of enthalpy relaxation, homogeneous crystal nucleation and crystal growth in glassy polyamide 6. *Eur. Polym. J.* **2014**, *53*, 100.

35. Nakano, Y.; MacKnight, W. J., Dynamic mechanical properties of perfluorocarboxylate ionomers. *Macromolecules* **1984**, *17*, 1585.

36. Kyu, T.; Eisenberg, A. In *J. Polym. Sci. C*; Wiley Online Library: 1984; Vol. 71, p 203.

37. Moore, R. B.; Martin, C. R., Morphology and chemical properties of the Dow perfluorosulfonate ionomers. *Macromolecules* **1989**, *22*, 3594.

38. Phillips, A. K.; Moore, R. B., Mechanical and transport property modifications of perfluorosulfonate ionomer membranes prepared with mixed organic and inorganic counterions. *J. Polym. Sci. Part B Polym. Phys.* **2006**, *44*, 2267.

39. Osborn, S. J.; Hassan, M. K.; Divoux, G. M.; Rhoades, D. W.; Mauritz, K. A.; Moore, R. B., Glass Transition Temperature of Perfluorosulfonic Acid Ionomers. *Macromolecules (Washington, DC, U. S.)* **2007**, *40*, 3886.

40. Chartoff, R. P.; Menczel, J. D.; Dillman, S. H., Dynamic mechanical analysis (DMA). *Thermal analysis of polymers: fundamentals and applications* **2009**, 387.

41. Lei, Z.; Xing, W.; Wu, J.; Huang, G.; Wang, X.; Zhao, L., The proper glass transition temperature of amorphous polymers on dynamic mechanical spectra. *J. Therm. Anal. Calorim* **2014**, *116*, 447.

42. Kim, J.-S.; Jackman, R. J.; Eisenberg, A., Filler and Percolation Behavior of Ionic Aggregates in Styrene-Sodium Methacrylate Ionomers. *Macromolecules* **1994**, *27*, 2789.

43. Kim, J. S.; Wu, G.; Eisenberg, A., Viscoelastic properties of poly (styrene-co-acrylate) and poly (vinylcyclohexane-co-acrylate) ionomers. *Macromolecules* **1994**, *27*, 814.

44. Lee, D.; Register, R. A.; Yang, C.; Cooper, S. L., MDI-based polyurethane ionomers. 2. Structure-property relationships. *Macromolecules* **1988**, *21*, 1005.

45. Kim, B. K.; Lee, J. C., Polyurethane ionomer dispersions from poly (neopentylene phthalate) glycol and isophorone diisocyanate. *Polymer* **1996**, *37*, 469.

46. Tesfaye, M.; Kushner, D. I.; McCloskey, B. D.; Weber, A. Z.; Kusoglu, A., Thermal Transitions in Perfluorosulfonated Ionomer Thin-Films. *ACS Macro Lett.* **2018**, *7*, 1237.

Chapter 6.

Contrast Variation in Small-Angle X-ray Scattering as a Means to Isolate and Characterize Morphological Features in Perfluorinated Ionomers of Different EWs and Sidechain Structures

Christina M. Orsino, Glenn Spiering, Mingqiang Zhang, and Robert B. Moore

6.1 Introduction

Over the last 50 years, tremendous work has been done to investigate the morphology of perfluorinated ionomers. Perfluorinated ionomers consist of a tetrafluoroethylene (TFE) backbone with perfluorovinylether sidechains terminated with sulfonic acid groups. Different variations in the sidechain chemical structure have been developed over the years starting with Nafion® and include Aquivion (short sidechain), and 3M-PFSA. Differences in the sidechain structures, illustrated in **Figure 6-1**, provide the capability to reach ion contents up to 22 mol percent while maintaining membrane mechanical integrity. These ionomers are classified by their equivalent weight (EW) which is related to the molecular weight of the sidechain structure and inversely related to the ion exchange capacity (IEC). Utilizing the EW values and molecular weights of the sidechains, the weight fraction of each phase can be calculated and is presented in **Figure 6-1**. This figure helps illustrate the different makeups of each phase for each of the ionomers to make a general relationship between different sidechain structures and EW values.

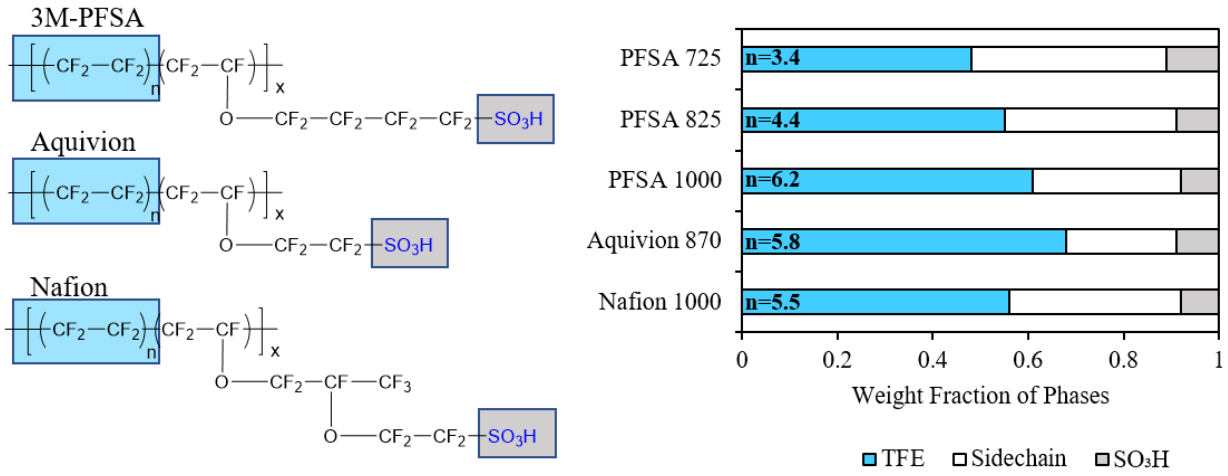

Figure 6-1. Chemical structures of Nafion®, Aquivion, and 3M-PFSA. Weight fractions of the various phases in each ionomer based on the value of *n* and ion content for each equivalent weight is shown on the right.

Small angle X-ray scattering is a useful tool in characterizing the morphological features in PFSAs. SAXS profiles for PFSA ionomers are characterized by an intercrystalline peak and a broad ionomer peak. A representative small-angle X-ray scattering pattern for PFSAs displays a maximum at ca. q = 1 – 2 nm^{-1} that is termed the "ionomer peak" consistent with inter-aggregate correlations arising from contrast in electron density between the ionic domains and the amorphous PTFE matrix. A second peak is observed at lower scattering vectors (ca. q = 0.5 nm^{-1}) that is attributed to scattering from ordered crystallites developed from crystallization of the PTFE runs between sidechains. This peak is generally referred to as the "matrix peak" but will be referred to as the "crystalline peak" in this study to emphasize that this scattering feature is associated with intercrystalline characteristic dimensions.

The primary challenge of studying multiphase systems with SAXS lies in determining how each phase contributes to the measured scattering. The scattered intensity measured by SAXS can be expressed by the equation

$$I(\boldsymbol{q}) \propto F(\boldsymbol{q})S(\boldsymbol{q})(\Delta\rho)^2 \quad (1)$$

Where the intensity of scattering is a function of F(**q**), S(**q**) and Δρ.[1] The form factor, F(**q**), is the scattering contribution related to the size and shape of the scattering particle while the structure factor, S(**q**), provides information on the interference between particles. Scattering intensity is also related to the contrast between scattering length density (SLD) of the scattering particles and the polymer matrix, Δρ. The relationship between scattering intensity and contrast is a phenomenon commonly used in small angle neutron scattering (SANS) to elucidate the origins of scattering features.[2] It is most commonly used in neutron scattering where there is a large difference in SLD between hydrogen and deuterium, which allows mixtures of water and deuterated water to be used in order to contrast match the SLD of a feature of interest.[3] When the contrast between SLD of a scattering feature and the matrix is matched, e.g., $(\Delta\rho)^2=0$, then the intensity of scattering from that feature is diminished to zero and it is no longer observed.

Contrast variation has been applied in SAXS to study latex particles in solution by varying the electron density of the solution with added sucrose.[4,5] More recently, SAXS contrast variation has been used in protein DNA solution systems by following a similar sucrose solution method to the latex particle studies, but also by monovalent counterion replacement.[6,7] In this counterion replacement method, which the authors termed "heavy atom isomorphous replacement," the cations around a standard 25-base pair DNA were replaced with Na^+, K^+, Rb^+, and Cs^+. Heaver cations increased the contrast and accordingly increased the scattering signal allowing for the authors to distinguish weaker underlying features.[6] While contrast variation in SAXS has found some use in solution studies, it is not generally used in studying PFSA solutions due to difficulty in finding solvent mixtures to match the different phases within PFSAs. Additionally, there is yet to be a systematic study specifically of SAXS contrast variation in PFSA membranes.

SAXS studies of Nafion membranes that have been conducted over the years have hinted at contrast variation within these ionomers in different counterion forms. In a study conducted by Fujimura, Hashimoto, and Kawai in 1981, it was observed that dry Nafion in the Na^+-form did not have an observable ionomer peak that was otherwise observed in the H^+- and Cs^+-forms.[8] The authors attributed this to a small difference in electron density between the ionic clusters and the matrix in the Na^+-form causing the magnitude of that scattering peak to diminish. Gierke, Munn, and Wilson observed that the ionomer peak in fully hydrated Nafion did not shift in position but decreased in intensity with increasing counterion size, which was attributed to both a change in electron density contrast and hydration of the ionic phase with counterion size variation.[9] More recent SAXS data published on water-equilibrated Nafion membranes in different counterion forms agreed with the observations of Gierke, Munn, and Wilson that ionomer peak intensity decreased with increasing counterion size and was attributed to a decrease in water content within the fully hydrated membrane with larger counterions.[10] However, the authors noted that changing counterion sizes would alter the electron density difference between phases, so it may be hard to distinguish whether that decrease in scattering intensity was due to lower hydration levels or just changes in contrast. Based on these observations, it may be possible to use these different counterions in order to systematically vary the contrast of the ionomer and intercrystalline peaks in PFSA membranes as a means to isolate each of the morphological features.

A recent study from our group identified that alkali metal counterions could be used in Nafion to vary scattering contrast and ultimately isolate the two scattering features for characterization.[11] It was observed that in the Cs^+-form, only the ionomer peak was present while the crystalline peak was eliminated. Additionally, in the Na^+- and Li^+-forms, the ionomer peak was indistinguishable while the crystalline peak was present. Variable temperature SAXS experiments

demonstrated that these scattering behaviors were the result of electron density contrast between the crystalline, amorphous, and ionic phases. In Na^+- and Li^+-form, it was proposed that the electron density of the ionic phase matched the electron density of the amorphous phase, thus eliminating the contrast between the two phase and suppressing the ionomer peak observed by scattering. In the Cs^+-form, it was proposed that the electron density of the ionic phase was increased so greatly that it also increased the electron density of the amorphous region such that it matches the electron density of the crystalline phase. By isolating the two scattering features, a model fit was able to be better applied to the crystalline peak in order to characterize the long period between crystallites in the sample.

While this previous study provided the first example of the true use of contrast variation in solid-state Nafion as a method to isolate morphological features, it is important to gain further understanding on how this method can be applied to PFSAs with different ion contents, degrees of crystallinity, and sidechain structures. If scattering contrast arises from the delicate differences between the electron density of the three phases within these samples, it is expected that the relative volume included within each phase would have an effect on scattering contrast. The present study utilizes a series of PFSAs of different sidechain structures and equivalent weight (EW) values in different alkali metal counterion-forms in order to develop a more quantitative understanding of which properties lead to scattering contrast in PFSAs. Electron densities of each phase are predicted based on the densities of model compounds and an equation for calculating the theoretical SAXS invariant (Q). The theoretical scattering contribution from the crystalline and ionic phases can be isolated and compared to the experimental Q values. From these comparisons, a relationship can be observed between EW (ion content and degree of crystallinity) and scattering contrast in SAXS, independent of sidechain structure. Finally, contrast variation proves to be a

useful technique for isolating the morphological features observed by SAXS in all of the PFSAs in this study, allowing for better model fits to be applied.

6.2 Experimental

6.2.1 Materials

Nafion® 117CS (1100 EW extruded membrane) was purchased from FuelCellStore and Nafion® NRE 211 (1000 EW solution cast membrane) was purchased from Fuel Cell Earth. Aquivion® E87-05S (870 EW extruded membrane) was purchased from Sigma Aldrich. 3M-Perfluorosulfonic acid (3M-PFSA) ionomer powders of 725, 825, and 1000 g/mol equivalent weight were provided by 3M. Nitric acid, lithium hydroxide, sodium hydroxide, potassium hydroxide, rubidium hydroxide, and cesium hydroxide were obtained from Fisher Chemical Co., and used without further purification.

6.2.2 Membrane preparation

The 3M PFSA membranes were prepared by casting a concentrated dispersion from alcohol and water onto polyimide film. The dispersions were dried in an oven with the temperature of 80°C followed by annealing for 10 minutes at 200°C. Membranes were removed from the polyimide film by soaking in water. Aquivion and Nafion membranes were used as-received. To remove impurities, all membranes were soaked in 8 M HNO_3 for 16 hours then rinsed thoroughly with deionized water. The cleaned membranes were immersed in 1 M solutions of either lithium hydroxide, sodium hydroxide, potassium hydroxide, rubidium hydroxide, or cesium hydroxide for 24 hours and then rinsed thoroughly with DI water prior to drying overnight between Kimwipes under vacuum at 70°C.

6.2.3 SAXS Experiments

SAXS experiments were performed on a Rigaku S-Max 3000 3 pinhole SAXS system, equipped with a rotating copper anode generating X-rays with a wavelength of 0.154 nm (Cu Kα). Two-dimensional SAXS patterns were obtained using a fully integrated 2D multiwire, proportional counting, gas-filled detector, with an exposure time of 2 hours. All SAXS data were analyzed using the SAXSGUI software package to obtain radially integrated SAXS intensity versus scattering vector q, where $q=(4\pi/\lambda)\sin(\theta)$, θ is half the scattering angle and λ is the wavelength of the X-rays. For all scattering experiments, the sample-to-detector distance was 1603 mm and the q-range was calibrated using a silver behenate standard. Scattering data were normalized for sample thickness and transmission using a glassy carbon standard.[12]

6.3 Results and Discussion

Figure 6-2 shows a representative SAXS curve for K^+-form PFSA 1000 EW membrane, which includes both scattering maxima from the intercrystalline dimensions and the ionic phase dimensions. A 2D schematic representation is provided on the right that demonstrates the origins of each scattering maxima observed by SAXS. The distance between crystallites (L_c) and the distance between ionic phases (L_i) are labeled in both the 2D diagram and the corresponding scattering maxima that arises from those dimensions.

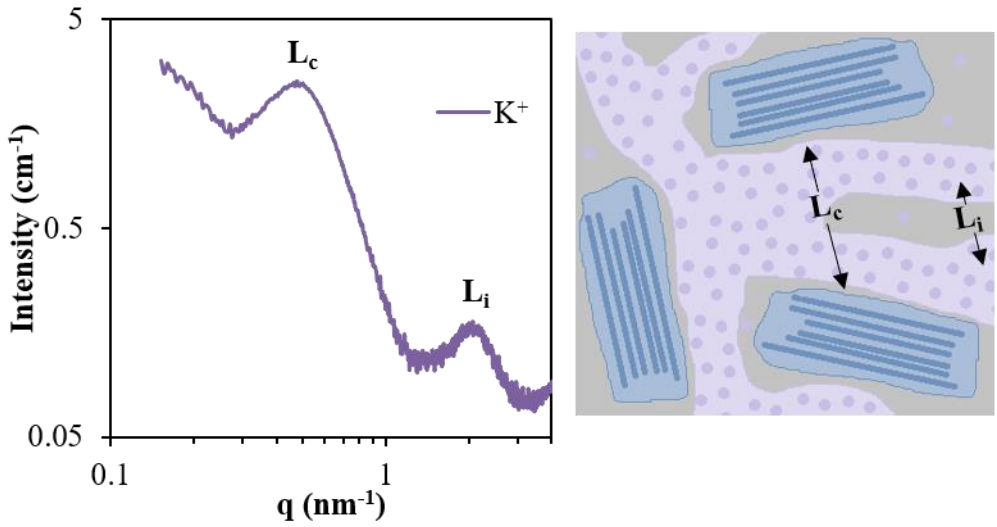

Figure 6-2. SAXS data of K+-form PFSA 1000 EW and a representative 2D drawing of the three morphological phases within PFSA membranes that lead to the two scattering maxima observed. In this schematic, the blue structure represents crystalline features, purple represents the ionic domains, and grey represents amorphous matrix.

In small angle x-ray scattering, the intensity of scattering in a sample of *n* independent particles can be expressed as:

$$I(q) = S(q)\sum_i^n[(\Delta\rho_i V_i)^2 F_i(q)] \quad (2)$$

where the intensity is related to S(q) and the sum of scattering from every particle, *i*, in the sample.[13] S(q) is defined as the structure factor which describes interparticle interactions and F(q) is the form factor, which characterizes the shape and size of the particles. In addition, I(q) is dependent on the volume-squared of each particle, V_i^2, and the difference in electron density between the scattering particle and the matrix, $\Delta\rho_i^2$.

In PFSA membranes, scattering arises from the electron density contrast between the crystalline and amorphous phases ($\Delta\rho_c$), and the contrast between the ionic and amorphous phases ($\Delta\rho_i$). This leads to the I(q) vs. q profile with two maxima, one arising from intercrystalline

scattering and the other from ionic domains. In an ionomer of a specific EW and sidechain structure, where the weight fraction of crystallites, amorphous material, and ionic content is constant, it is possible to change the intensity of the scattering peaks by manipulating electron density of the ionic domains. Since changing the counterion is done by submerging the already developed membrane into an alkali metal solution at room temperature, the morphology of the ionomer does not change (see Section 6.3.6). In this case, the F(q) and S(q) remain the same but the $\Delta\rho_i$ changes. When ρ_i "matches" ρ_a, then $\Delta\rho_i$ is equal to zero and both that term and the cross-term are eliminated from the equation and scattering only arises due to the crystalline phase. In contrast, if ρ_i is very different from ρ_a, then $\Delta\rho_i$ can become large enough that $\Delta\rho_c$ is negligible.

6.3.1 Effect of Sidechain Structure

Figure 6-3 shows the SAXS profiles of 1000 EW Nafion NRE 211, 870 EW Aquivion, and 1000 EW 3M PFSA in different alkali metal counterion forms. In all three ionomers, there is a clear decrease in the intensity of the crystalline peak at ca. 0.5 nm^{-1} and increase in the ionomer peak intensity at ca. 2.5 nm^{-1} with increasing counterion size. In Nafion, Cs^+-form shows a large and distinct ionomer peak and no crystalline peak, while Li^+-form has a large crystalline peak with no ionomer peak. Similar results are seen for 1000 EW 3M PFSA and 870 EW Aquivion. For the intermediate-sized counterions, Na^+ and K^+, both peaks are observed in all three sidechain ionomers. While there are clear changes in intensity of these peaks, there is very little change in the q-position of them, indicating that there are negligible morphological changes with counterion size and the changes in intensities can be presumed to result from electron density differences associated with the different counterion forms.[14]

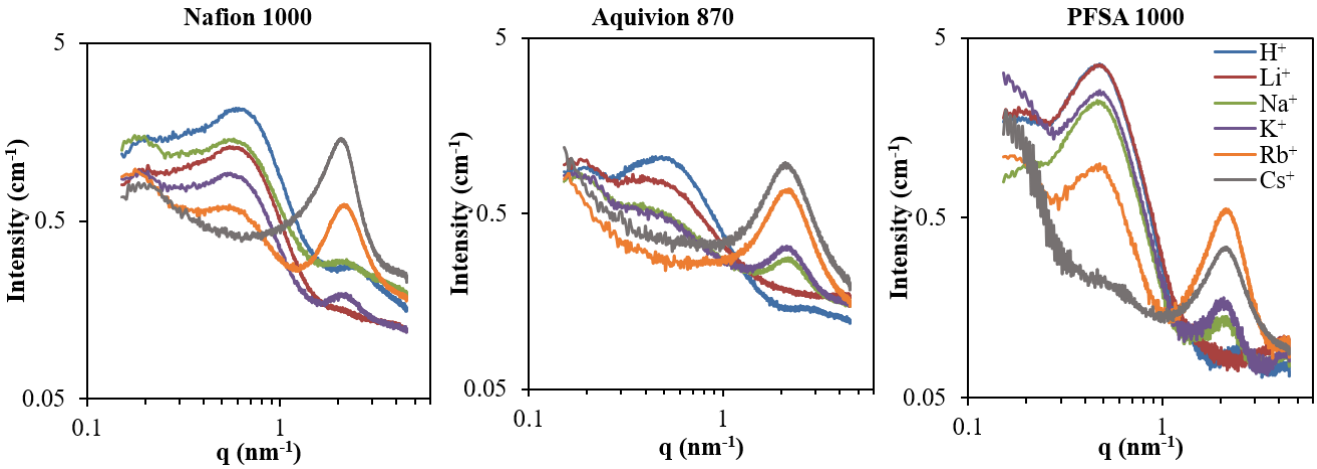

Figure 6-3. SAXS profiles of 1000 EW Nafion, 870 EW Aquivion, and 1000 EW PFSA in different alkali metal counterion forms.

Figure 6-4 shows plots of peak intensities vs. counterion size for both the crystalline peak and ionomer peak in this sidechain structure series. The crystalline peak intensity across all counterions is larger for 3M PFSA 1000 EW than Nafion and Aquivion. This increased scattering intensity relative to the other two ionomers across all counterion forms can be attributed to increased crystallinity in these ionomers. From **Figure 6-1**, it is noted that 3M PFSA 1000 EW has the highest *n* value of *n*=6.2 (average of 6.2 TFE monomers in the backbone between sidechains), followed by Aquivion with *n*=5.8 and Nafion with *n*=5.5. Resulting from the larger *n* values, the 1000 EW 3M PFSA has a high degree of crystallinity of 17%, followed by Nafion with 12% and Aquivion with 10% crystallinity determined from WAXS studies.[15,16] Increased intensity of the crystalline peak has also been observed in PFSA annealing studies, where an increase in the degree of crystallinity led to an increase in intensity of the crystalline peak.[17]

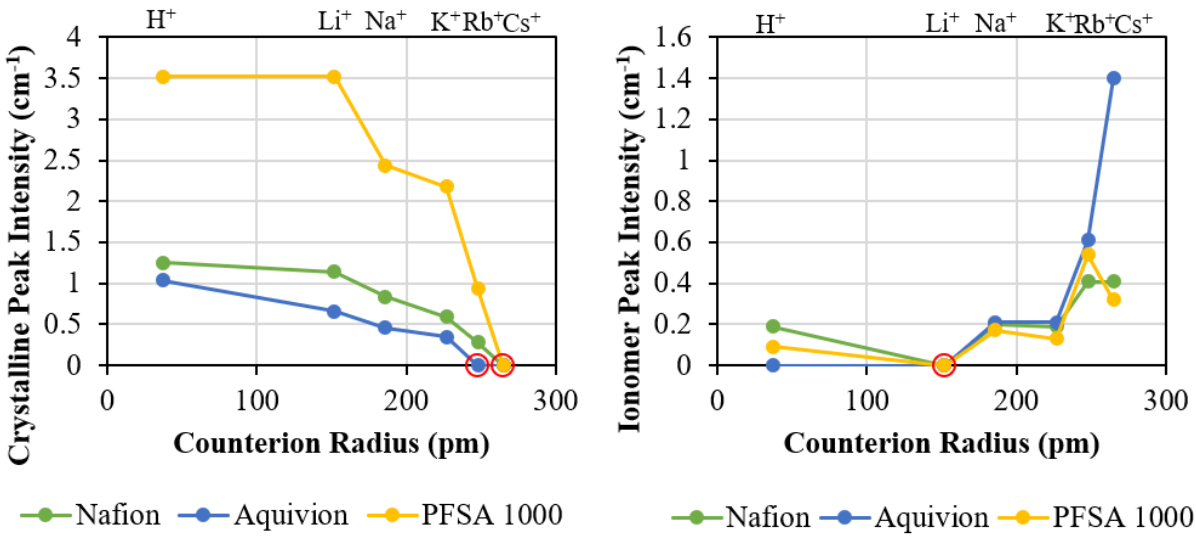

Figure 6-4. Plots of peak intensity at q_{max} vs. counterion size of the crystalline peak (left) and ionomer peak (right) for 3M PFSA 1000, Aquivion, and Nafion. The red circle indicates where there is no observable peak for each ionomer.

In the plot of ionomer peak intensity vs. counterion size, all three PFSA membranes have an observable ionomer peak in all counterions except for Li^+-form. With increasing counterion size, the ionomer peak intensity increases as expected for the increase in electron density within the ionic domains with larger counterions. Interestingly, the fact that all three PFSAs have no visible ionomer peak in the Li^+-counterion form, indicates that there is a "contrast match" between the ionic phase and amorphous phase in that counterion form. This will be explored further in the following sections.

In the plot of crystalline peak intensity vs. counterion size, the red circles indicate at which counterion a peak is no longer observed. In Aquivion membranes, a crystalline peak is observed in H^+-, Li^+-, Na^+-, and K^+-form, decreasing in intensity with increasing counterion size. In Rb^+- and Cs^+-forms, there is no observable crystalline peak in Aquivion. However, in Nafion and 3M PFSA 1000 EW, the crystalline peak is observed in all counterion forms except for Cs^+. The

disappearance of the crystalline peak in the Cs^+-form may be indicative of "contrast matching" between the electron density of the crystalline phase and the electron density of the ionic matrix phase (including both the ionic domains and amorphous matrix). However, it is interesting that in Aquivion, it is not just one counterion that causes this contrast matching phenomena to occur. In this case, the exact matching of electron densities between the two phases with two counterions of different electron densities does not make sense.

Based on this series of PFSAs with different sidechain structures, it is evident that the contrast of the ionomer and crystalline peaks are a result of EW effects as opposed to sidechain structure. Membranes with less crystallinity have a lower crystalline peak intensity, and in the case of Aquivion, that peak disappears with smaller counterion sizes than those with higher crystallinity. All of the membranes in this sidechain series have somewhat similar ion contents ranging from 14 to 15 mol % ion content. In this case, it makes sense that all three membranes lose contrast of the ionomer peak at the same counterion size, considering the ionomer peak arises from contrast between the ionic and amorphous phase, and is unaffected by crystallinity.

6.3.2 Effect of Equivalent Weight

Utilizing a series of PFSAs with the same sidechain structure, but different ion content and degree of crystallinity can help provide more detail on the electron densities of each phase and how they affect contrast in SAXS. **Figure 6-5** shows SAXS profiles for a series of 3M PFSA membranes in 1000 EW, 825 EW, and 725 EW in a series of alkali metal counterion forms. The 1000 EW PFSA shows the most dramatic effect of counterion size on both the crystalline and ionomer peaks. A crystalline peak is observable in 825 and 725 EW membranes in the H^+ and Li^+ forms, that decreases in intensity with increasing counterion size, and the ionomer peaks increase in intensity with counterion size.

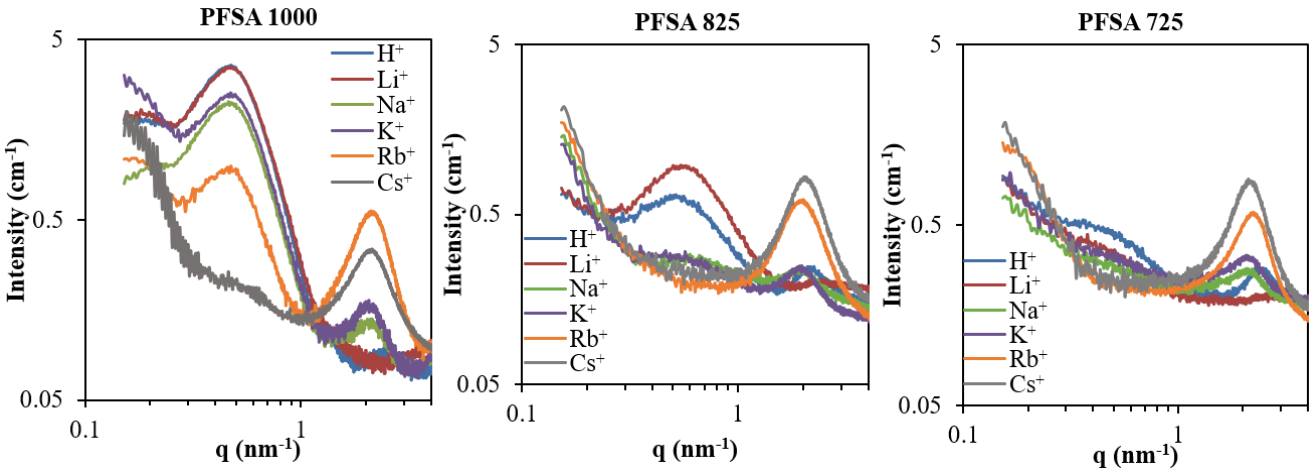

Figure 6-5. SAXS profiles of 1000 EW, 825 EW, and 725 EW 3M PFSA membranes in different alkali metal counterion forms.

Figure 6-6 shows plots of peak intensities vs. counterion size for both the crystalline peak and ionomer peak in this 3M PFSA EW series. The ionomer peak intensity again follows the same trend as the sidechain series. Here, all three EW membranes have no observable ionomer peak in the Li^+-form, regardless of ion content. The ionomer peak is attributed to electron density differences between the ionic phase and amorphous phase, independent of the crystalline component. For all of the PFSA ionomers probed in this work, the electron density of Li^+-sulfonate groups appears to match that of the electron density of the amorphous phase, thus eliminating any scattering contribution from SAXS profiles in this counterion form.

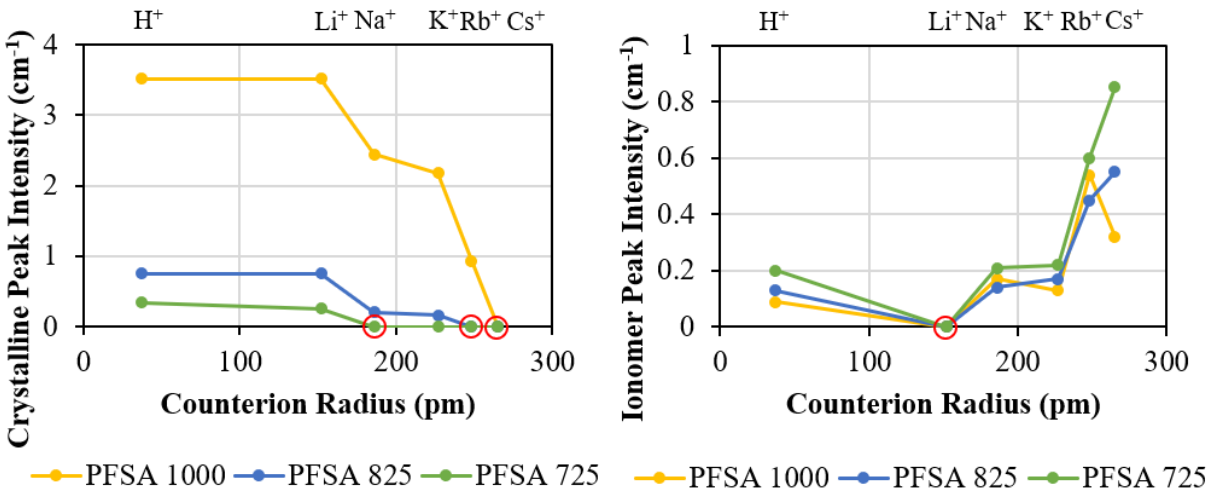

Figure 6-6. Plots of peak intensity at q_{max} vs. counterion size of the crystalline peak (left) and ionomer peak (right) for the 3M PFSA EW series. The red circle indicates where there is no observable peak for each ionomer.

The crystalline peak intensity across all counterions is larger for 100 EW 3M PFSA than 825 and 725 EW. As discussed for the sidechain series, this increased scattering intensity relative to the other two ionomers can be attributed to increased crystallinity, leading to an increase in electron density of those regions. The degree of crystallinity appears to have a more profound effect on the intensity of the crystalline peak compared to the effect of ion content on the ionomer peak intensity. Additionally, the crystalline peak does not "contrast match" at a specific counterion. In the lowest EW PFSA, the crystalline peak is observable only in Li^+ and H^+-form, but disappears in the Na^+-form and larger counterion sizes. The 3M PFSA of intermediate EW, PFSA 825, has an observable crystalline peak that decreases to extinction in the Rb^+-form and larger. Lastly, 1000 EW PFSA has an observable crystalline peak in all counterion sizes except the largest, Cs^+. This is a new consideration, that changing the electron density of the ionic phase

can affect the scattering intensity of the crystalline phase beyond just a contrast match between the ionic matrix (amorphous + ions) and crystalline phase at one counterion size.

Figure 6-7 shows a schematic diagram of the effect of counterion on the electron density contrast between phases and the resulting scattering profile observed for each representative counterion. In an intermediate counterion size, like K^+, the three phases all consist of different electron densities $\rho_i \neq \rho_c \neq \rho_a$, and thus the crystalline scattering peak arises from contrast between the crystalline phase and the ionic matrix, and the ionomer peak arises from contrast between the ionic and amorphous phases. In the Li^+-form, it is apparent that the electron density of the Li^+-sulfonates is very close in value to the electron density of the amorphous, and thus independent of ion content or crystallinity, there is no distinguishable scattering maximum for the ionomer peak. This is an example of "contrast matching."

A different phenomenon is observed for the intercrystalline peak, where it disappears above a certain counterion size as opposed to at one specific counterion size as would be assumed for a contrast match. The size of the counterion that first causes the disappearance of the crystalline peak, decreases with decreasing degree of crystallinity. From this evidence, it is suggested that the electron density contrast between the crystalline phase and the matrix in an ionomer with low crystallinity (e.g., PFSA 725 EW) is much lower than the contrast between the ionic phase and amorphous, such that at a certain electron density of the ionic phase, the intercrystalline contrast becomes negligible. This has been observed in other multiphase systems where the electron density of one phase is much higher than that of the remaining phases allowing for a two-phase approximation to be made.[18,19] Because the scattering intensity in SAXS arises from electron density contrast between phases squared, very large differences in electron density give rise to a large scattering contribution. Two-phase approximations such as this have been used to study

multiple systems such as metal alloys,[20,21] pore structures in fibers,[22,23] and many different biological samples.[24]

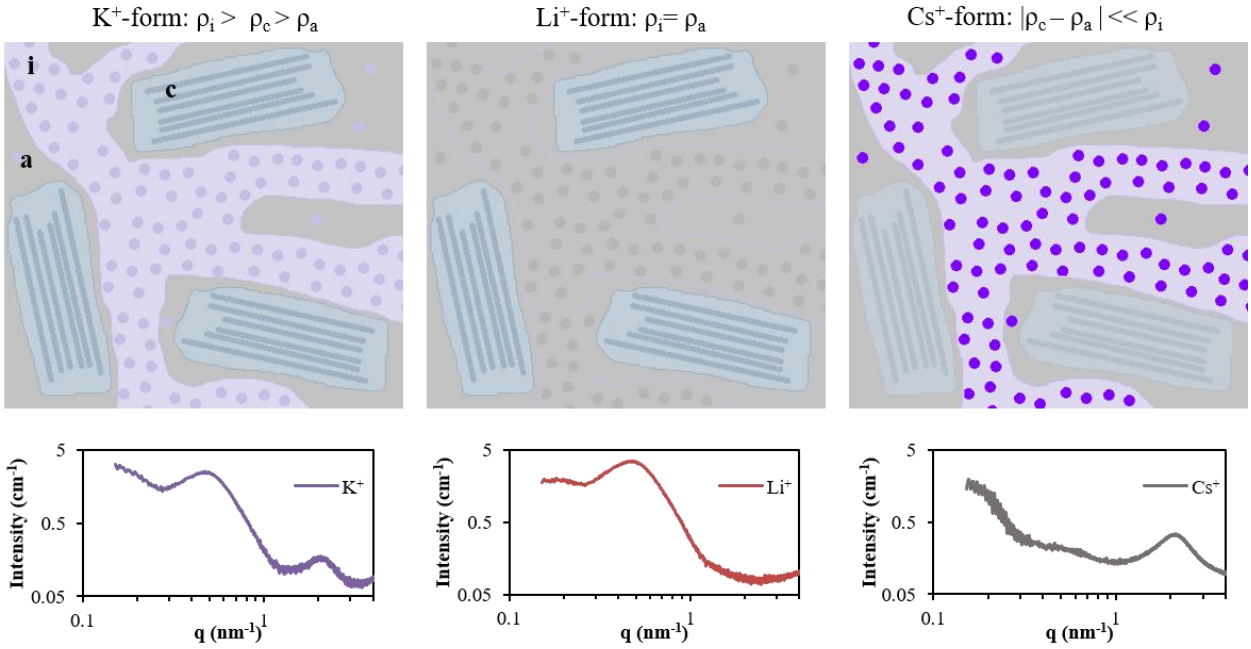

Figure 6-7. Schematic of the effect of counterion on scattering contrast and the resulting scattering profile observed for that representative counterion.

6.3.3 Correlating Experimental Findings to the Electron Density of Each Phase

In order to estimate the electron density contrast between the crystalline, ionic, and amorphous phases, we need to calculate the electron density of each component separately. For X-rays, electron density is defined as

$$\rho_x = \frac{b_e \rho_m N_A}{M} \sum_i n_i z_i \qquad (3)$$

Where b_e is the scattering length of an electron (b_e = 2.85 x 10^{-5} Å), ρ_m is the mass density, M is molecular weight, N_A is Avogadro's Number, n_i is the number of atoms of type *i*, and z_i is the

charge of each atom of type *i*. For each component, the mass density (ρ_m) must be known. In these PFSA systems, the different phases consist of amorphous PTFE, crystalline PTFE, and the ionic sulfonate groups with each corresponding counterion. In these cases, an exact mass density is not easily found. The values for the densities of amorphous and crystalline PTFE have been documented in the literature and are listed in **Table 6-1**. Using the provided mass density values and the known atomic fractions, the values for electron density (ρ_x) were calculated using the Scattering Contrast Calculator available in the Irena program in Igor Pro.[25] Because there are no readily available values for mass density of the ionic sulfonate pairs, counterion-trifluoromethyl sulfonate compounds were used as model compounds. The density of each triflate compound was obtained from published small molecule crystal structures and utilized to calculate the electron density of each group.[26-30]

Table 6-1. Mass densities and corresponding electron densities of the different components in PFSA membranes.

Group	ρ_m (g/cm^3)	ρ_x x 10^{10} (cm^{-2})
C_2F_4 Amorphous[14]	1.9	15.47
C_2F_4 Crystalline[14]	2.2	17.92
F_3CSO_3H	1.7	14.59
F_3CSO_3Li [30]	1.9	15.77
F_3CSO_3Na [29]	2.2	18.48
F_3CSO_3K [28]	2.2	18.33
F_3CSO_3Rb [26]	2.6	20.52
F_3CSO_3Cs [27]	2.9	21.95

The scattering, or Porod, invariant (Q) is a model-independent quantity that can be easily calculated from scattering data and compared to theoretical calculations utilizing the electron density of each phase. The invariant comes from the mean square fluctuation in scattering length

density and is insensitive to the distribution of phases.[31] This value for total scattered intensity of the sample is defined as

$$Q = \frac{1}{2\pi^2}\int_0^\infty I(q)q^2dq \tag{4}$$

for the experimental SAXS data and can be compared to the theoretical Q value, for an ideal two-phase system, represented by:[32]

$$Q = 2\pi^2\phi_1\phi_2(\rho_1 - \rho_2)^2 \tag{5}$$

where φ is the volume fraction and ρ is the electron density for each phase. For a multiphase system, this equation can be expanded to:[33]

$$Q = 2\pi^2 \sum_{i\neq j} \phi_i\phi_j(\rho_i - \rho_j)^2. \tag{6}$$

While PFSAs are a more complicated three-phase system consisting of ionic domains, crystalline phase, and matrix, we expand and simplify the above equation to:

$$Q = 2\pi^2[\phi_c\phi_{im}(\rho_c - \rho_{im})^2 + \phi_i\phi_a(\rho_i - \rho_a)^2] \tag{7}$$

Where the first part of the term is the scattering contribution from the intercrystalline peak with φ_c and φ_{im} representing the volume fraction of crystallites and ionic matrix $(1 - \varphi_c)$, respectively, and ρ_c and ρ_{im} are the electron densities of the crystalline and ionic matrix phases. Electron density of the ionic matrix is calculated from the electron density and volume fraction of the ionic domains and amorphous PTFE by the equation $\rho_{im} = \varphi_i \rho_i + \varphi_a\rho_a$. Using this equation for the ionic matrix density takes into consideration the changing density of the ionic matrix based on counterion, thus the intercrystalline scattering intensity is also dependent on counterion size, as observed in the experimental data. The second part of this equation is the scattering contribution from the ionic

phase where φ_i and φ_a representing the volume fraction of ions and amorphous matrix, and ρ_i and ρ_a are the electron densities of the each counterion-sulfonate calculated in **Table 6-1** and the electron density of amorphous PTFE, respectively. The values for volume fraction of ion content were derived from the EW of each ionomer, and the volume fraction of crystalline component were estimated from the degree of crystallinity determined by WAXS measurements.

The experimental SAXS data were plotted and extrapolated to q=0 and q=∞ for calculating the scattering invariant. In order to extrapolate to q=∞, the tail region of the data was defined and fitted out to q = 20 nm. At low q, the upturn was defined and a Guinier fit[34] was performed to extrapolate the data to q=0. A low pass filter (Savitsky Golay smoothing algorithm)[35] was used to filter out high frequency components in the data where the fit functions and measured data are combined. Finally, the data was plotted as a Kratky plot,[33] $I(q)q^2$ vs. q, and integrated over the entire dataset following Equation 4 to get an experimental invariant value, Q. To separate the scattering invariant into scattering contributions from both the intercrystalline peak and the ionomer peak, the data was integrated from q=0 to q=~1 nm^{-1} for Q_c and q=~1 nm^{-1} to q=∞ for Q_i.

Figure 6-8 shows a comparison of the experimental and theoretically calculated total invariant values for 1000 EW 3M PFSA and 825 EW 3M PFSA. The purpose of this calculation is to show how well the theoretical and experimental results agree. It is noticeable that the theoretical Q values follow a similar counterion dependence as the experimental Q values. However, the experimental Q values are an order of magnitude smaller than the theoretical Q values. A similar observation was made in a study conducted on a polycaprolactone/polycarbonate (PCL/PC) blend system.[32] In this study, they calculated the total scattering invariant, Q, by a theoretical calculation based on a similar equation to Equation 6 used in this study, extrapolated to fit their system of PCL/PC blends, and experimental determination by Equation 4. They

observed that the experimentally and theoretically calculated invariant values followed the same trend with PC content, but the experimental values were lower by ~50%. The authors of this study attribute the discrepancy in values to a combination of inadequacy of the model and the finite q-range accessible by SAXS experiments. However, in spite of this discrepancy in invariant values between the two methods, it was still able to produce the composition dependence and predict the absolute magnitude of the invariant.

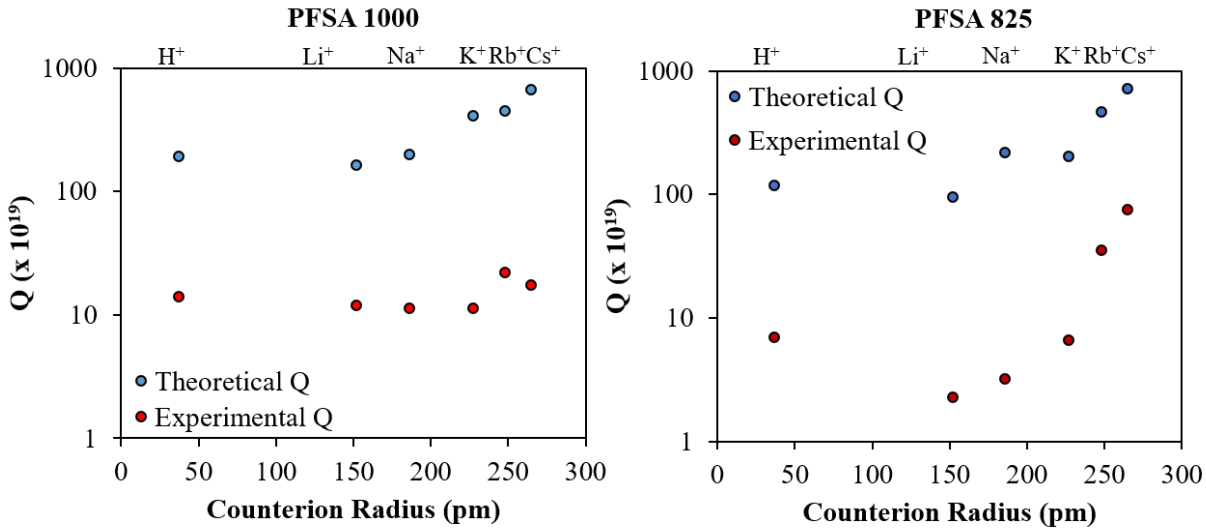

Figure 6-8. Total scattering invariant, Q, from experimental data and theoretical calculations for both PFSA 1000 EW and PFSA 825 EW.

In our PFSA system, some of the same considerations can be made based on the limitations of this invariant model. First, the experimental integration is extrapolated to q=0 and q=20 to try to account for the 0 to ∞ q-range in the theoretical calculation, but the values may still be inherently lower due to the finite range of the integration. A second consideration is that the compounds used to calculate the electron density of the ionic phase in the theoretical calculation are simply model compounds and may not be an exact representation. While the model compounds include the sulfonate-counterion pair plus a CF_3 group, the actual aggregates are proposed to only contain

ionic material.[36] Therefore, the predicted electron densities used in the theoretical calculations based on the available model compounds may be projecting higher values for density than the actual densities of the ionic phase within the phase-separated polymer. The last consideration comes from the extrapolation of Equation 6 into Equation 7 for the calculation of theoretical invariant. In theory, there may be more terms involved than this simplified equation. However, this equation provides the best representation of the experimentally observed results where changing the counterion within the ionic phase affects the scattering contribution of the crystalline phase.

Despite some discrepancy between the calculated and experimental total scattering invariant values, they both still follow the same trend with counterion size and can provide information on the scattering contributions from both the crystalline and ionic domains. By splitting the Q equations up into Q_i and Q_c, we can calculate the total scattering contributions from those two terms. The theoretical values are then calculated by

$$Q_i = 2\pi^2[\phi_i\phi_a(\rho_i - \rho_a)^2] \;\&\; Q_c = 2\pi^2[\phi_c\phi_{im}(\rho_c - \rho_{im})^2] \quad (8)$$

where the total scattering invariant is equal to the sum of the two contributions: $Q = Q_i + Q_c$. The experimental scattering invariants are determined by

$$Q_i = \frac{1}{2\pi^2}\int_0^{\sim 1} I(q)q^2dq \;\&\; Q_c = \frac{1}{2\pi^2}\int_{\sim 1}^{\infty} I(q)q^2dq \quad (9)$$

where the total scattering invariant is equal to the sum of the two components, or the integration over the entire q-range 0 to ∞.

Figure 6-9 shows the relative scattering contributions from the ionic and crystalline phases for 1000 EW 3M PFSA. To account for the discrepancies from the order-of-magnitude difference

between the total scattering invariant determined experimentally and theoretically, the values are normalized to the total scattering invariant, Q, calculated by each method. In the theoretical calculation, it is observed that at low ion contents, majority of the scattering contribution is expected to arise from the crystalline component. In the Li^+-form, there is almost negligible scattering from the ionic phase. In intermediate counterion sizes, you see scattering contributions from both phases and would expect to see both features in the experimental data. Finally, at the largest counterion size, majority of the scattering contribution results from the ionic phase.

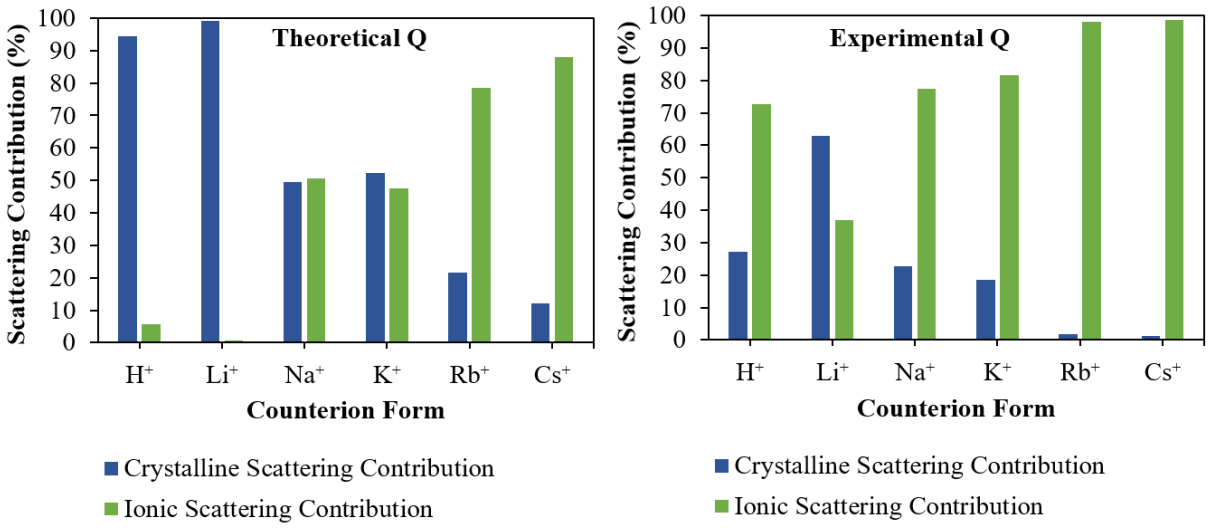

Figure 6-9. Total calculated scattering invariant, Q, divided into its two components Q_c and Q_i (scattering contributions from the crystalline phase and the ionic phase) calculated from both the theoretical calculation and experimental data for 1000 EW 3M PFSA.

While the trend from this theoretical calculation matches the observed SAXS data, it can also be compared directly to the invariant values determined from the experimental results as shown in the right-side of **Figure 6-9**. From the experimental invariant calculations, it is observed that the Li^+-form is the only sample to show more scattering contribution from the crystalline component than the ionic. The large counterions, Rb^+ and Cs^+ show a large scattering contribution

from the ionic phase and very little from the crystalline. While the overall trends are still similar between the theoretical and experimental calculations, the ionic scattering contribution appears to be much larger from the experimental calculation. This is likely due to limitations of this calculation, since in the actual SAXS profiles for 1000 EW PFSA in the Na^+- and Li^+-form, there is no ionomer peak at all, but when plotted as $I*q^2$ vs. q, the q-range across the ionic scattering region is nonzero.

Although comparisons of the theoretical to the experimental invariant values do not completely agree, the theoretically calculated scattering contributions appear to provide a good estimate of determining scattering contrast in PFSAs. The theoretically calculated contributions (normalized for overall scattering invariant, Q) for the three EW 3M PFSAs are shown in **Figure 6-10**. In all three PFSAs, the Li^+-counterion form shows strong scattering from the crystalline phase and very little from the ionic phase. This agrees with the experimental data where the Li^+-form for all of the PFSAs investigated in this study showed no ionomer peak and only a crystalline peak, regardless of ion content or degree of crystallinity. This confirms the observed "contrast matching" that occurs with the Li^+ counterion for all of the PFSAs used in this study.

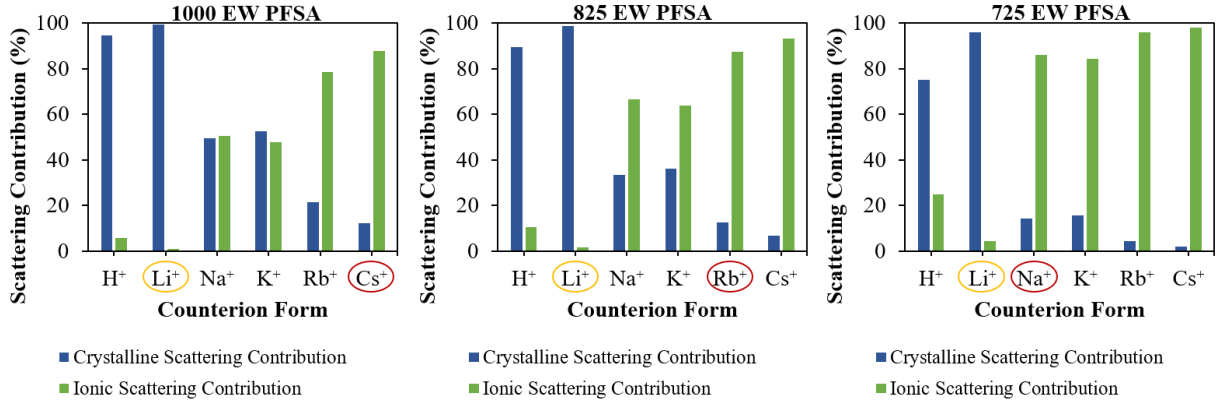

Figure 6-10. Theoretical scattering contributions from the crystalline and ionic phases for 1000 EW, 825 EW, and 725 EW 3M PFSA membranes in different counterion forms. The yellow circle

represents where the ionomer peak is contrast-matched in the experimental data and the red circle represents where the crystalline peak is contrast-matched (at that counterion-size and larger) in the experimental data for the three different PFSAs.

Interestingly, this model also fits very well to the disappearance of the crystalline peak at a certain counterion size and above for each ionomer. In **Figure 6-10**, the red circle indicates which counterion (and larger) does not have an observable crystalline peak in the SAXS data. For 1000 EW 3M PFSA, a crystalline peak is observed in the experimental data for all of the counterion-forms from H^+ to Rb^+ and disappears in the Cs^+-form. From the theoretical calculation, the ratio of ionic scattering contribution to crystalline contribution is also highest in the Cs^+-form. In 825 EW 3M PFSA, the crystalline peak is observed in counterions smaller than Rb^+. Based on the theoretical invariant calculations, the ratio of ionic to crystalline scattering is very large in Rb^+ and Cs^+-forms. Lastly, for 725 EW 3M PFSA, the crystalline peak was only observed in H^+ and Li^+-forms. The theoretical model also shows this, where there is an inversion of the dominant scattering contribution between Li^+ and Na^+ counterions. It appears based on this theoretical calculation, that when the scattering contribution of the ionomer peak reaches over 80%, the crystalline peak is no longer observed in the SAXS data. Based on these findings that used just Equation 7, the electron densities of the model compounds, and the estimated volume fraction of the crystalline, ionic, and amorphous phases based on EW, we can predict which counterions will isolate the ionomer peak in PFSAs of different physical structure properties.

6.3.4 Effect of Processing Conditions.

Processing methods have been shown to have a profound effect on the physical properties and morphology of PFSA membranes.[37] Thermal treatments used during processing can increase the degree of crystallinity,[9,38-41] but in addition, high enough temperatures (above the principle

relaxation temperature) may allow the ionic functionalities to rearrange themselves resulting in a change of the cluster morphology.[37,40,42,43] SAXS profiles of Nafion membranes of the exact same chemical structure and EW but different processing conditions are shown in **Figure 6-11**. Nafion 117 was processed by extrusion in the melt-processable $-SO_2F$ form before hydrolysis to the $-SO_3H$ form, while Nafion NRE 211 was dispersed in solvent in the $-SO_3H$ form and cast into a membrane from dispersion. As expected from the previous sections, for PFSAs of the same EW, the intensities of the scattering features vary with counterion size and contrast match at the same counterions. In both membranes, the crystalline peak is not observed in only the Cs^+-form, and the ionomer peak is not observed in the Li^+-form. This shows that the model used in the last section to determine the scattering contributions from each phase can still be applied to PFSAs that were processed by different methods.

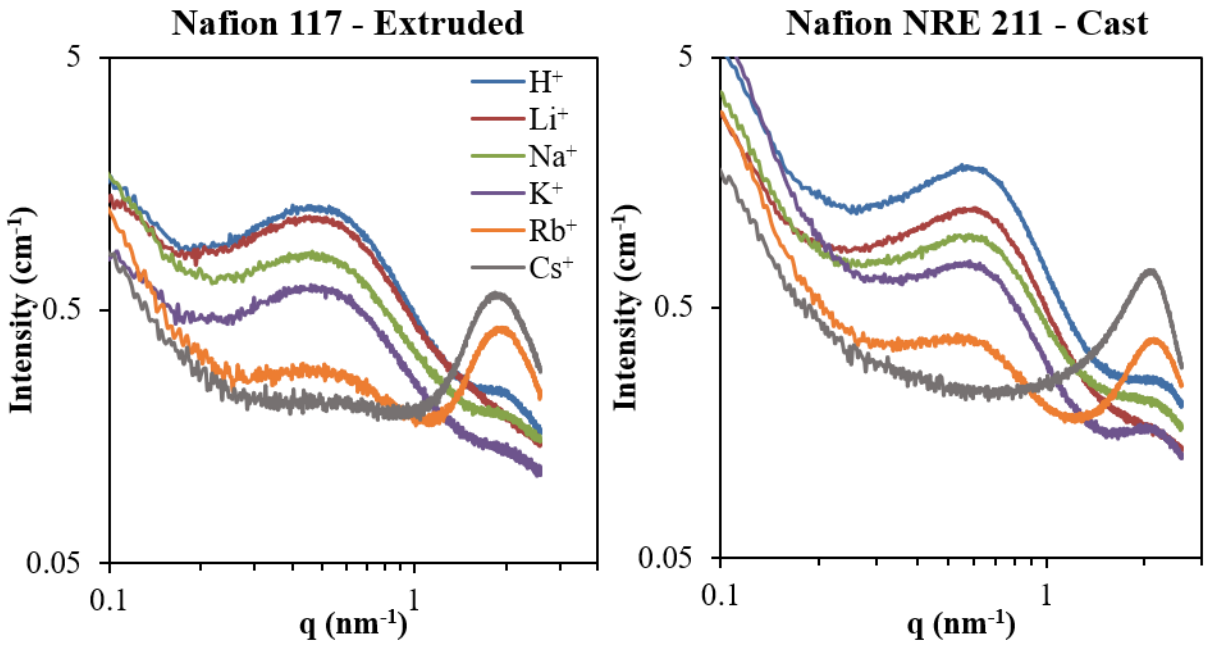

Figure 6-11. SAXS data for dry Nafion membranes processed by extrusion (left) and solution-casting (right) in varying alkali metal counterion forms.

The noticeable difference between the scattering profiles is the shape of each scattering feature in the extruded compared to the cast membranes for all counterions. In the extruded form, both the crystalline and ionic peaks are broad whereas the solution-cast membranes have narrower scattering features. This narrowing of the scattering features is an evidence of increased ordering, as generally a broader peak indicates a greater distribution of characteristic dimensions.[44,45] This has been specifically observed for the ionomer peak in polystyrene-based ionomers with different sidechain lengths.[45] The peak maximum (q) can be related to the average of a collection of characteristic distances between scattering particles (d) by $d=2\pi q^{-1}$, so a broad peak represents a large distribution of characteristic lengths compared to a narrow peak.[33,45] Longer sidechains in polystyrene ionomers were observed to have a narrower ionomer peak, which was attributed to a narrower distribution of scattering distances and thus increased order compared to ionomers with short sidechains.[45]

In Nafion membranes, both the crystalline and ionomer peak widths appear narrower in the solution-cast form than the extruded. Based on the relationship between scattering maxima and characteristic distance between scattering particles, this peak narrowing is evidence of a decrease in the distribution of characteristic distances between both the ionic and the crystalline domains, indicative of increased ordering of both morphological features. While the exact processing conditions and thermal history of these as-received membranes are unknown, there is some literature-basis for increased organization in a solution-cast membrane compared to extruded.

As mentioned previously, extrusion involves melt processing the nonionic sulfonyl fluoride precursor into sheets prior to hydrolysis into the sulfonic acid form. This means that the ionic domains are most likely locked into a defined morphology during the melt-processing phase and not able to reorganize upon hydrolysis. Evidence of this comes from the observed anisotropy

of the ionic domains in extruded Nafion membranes in the machine direction that can only be eliminated by biaxial stretching at a temperature above the principle relaxation temperature or by annealing above the melting temperature for longer 24-hour time periods.[46,47] In contrast, solution-cast membranes have improved proton conductivity and mechanical properties when cast at elevated temperatures, attributed to the formation of an entangled polymer network during the casting process.[48-50] While it is unclear how these as-received solution-cast membranes are explicitly processed, the fact that these solution-cast membranes have clearly developed some crystallinity and have increased ordering of the morphological features observed by this SAXS data, it appears that Chemours (the manufacturer of Nafion) uses some type of elevated temperature in their solution-casting process. It is plausible, based on this evidence, that the membranes cast from dispersion at elevated temperatures have the mobility (from a combination of the solvent plasticizing the polymer chains and elevated temperatures providing thermal energy)[49] to increase the degree of phase separation with the sulfonic acid interactions providing a driving force to form ordered aggregates. Melt-processing of the sulfonyl fluoride form likely provides less of a driving force for phase separation than the sulfonic acid form in dispersion, and therefore, these extruded membranes have a more disordered nanostructure. Despite the changes in nanostructure with processing condition, the effect of counterion size on contrast matching the morphological features does not seem to change. Both membranes are contrast-matched at the same counterion size, confirming that contrast-matching is affected only by the chemical structure of the ionomers.

6.3.5 Using Scattering Contrast as a Means of Isolating Morphological Features.

Contrast-matching of morphological features in SAXS simplifies the scattering data by isolating one of the morphological features that can then be modeled without interference from the

second feature. An example of this is the one-dimensional correlation function, which provides information about the long periodicity of the crystalline domains in semicrystalline polymers.[51,52] The 1-D correlation function analysis is essentially a Fourier transform of the experimental scattering data. In this analysis, the data must be extrapolated to q=0 and q=∞, and therefore the tail of the data must be fit correctly in order to estimate out to q=∞. However, in PFSAs, when applying the 1-D correlation function to the crystalline peak, scattering contributions from the ionic domains overlap with the tail of the crystalline scattering feature. Thus, isolation of the crystalline peak is necessary for this analysis.

An example of the 1-D correlation function results for Na^+ and Li^+-form extruded Nafion 117 are shown in **Figure 6-12**. For both of these counterion forms, the ionomer peak is either not present at all (Li^+-form) or very small/negligible (Na^+-form) in the experimental SAXS data. The first peak in the 1-D correlation function represents the long period, L_c. For Li^+- and Na^+-form Nafion, L_c was found to be 87 Å and 93 Å, respectively. The small difference between the calculated L_c values for the two different counterion forms demonstrates that exchanging the counterion does not affect the morphology of PFSA ionomers and thus can be used as a method of contrast-matching for isolating the morphological features. The weak maxima in the 1-D correlation function data is attributed to relatively low degrees of crystallinity in Nafion compared to other semicrystalline polymers.

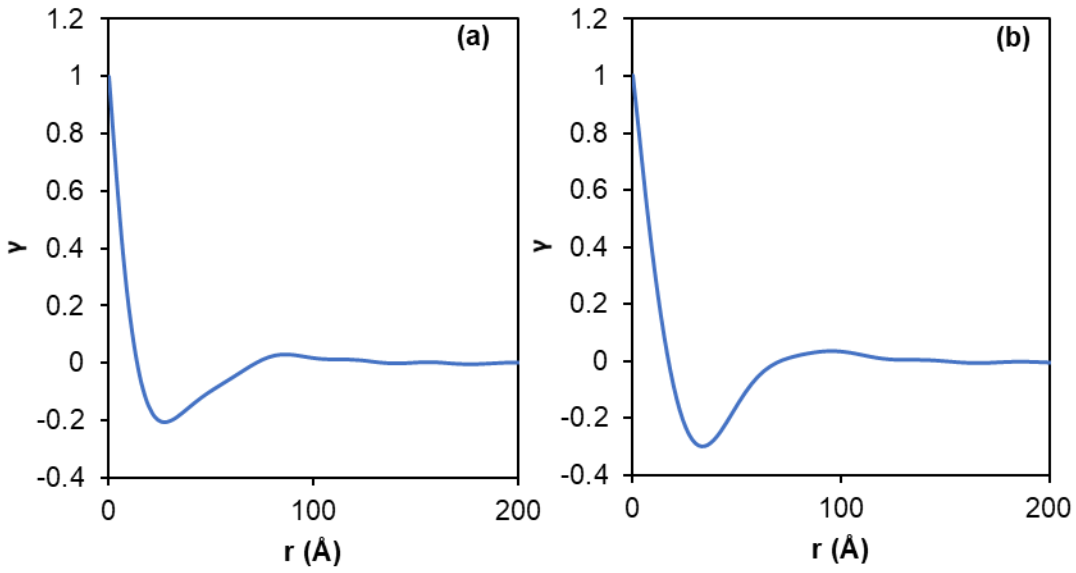

Figure 6-12. One-dimensional correlation data of (a) Li^+- and (b) Na^+-form Nafion 117.

The experimental SAXS data for H^+-form Nafion 117 and the corresponding 1-D correlation function results are shown in **Figure 6-13**. In contrast to the Li^+- and Na^+-form 1-D correlation function data, the results from H^+-form Nafion show large fluctuations in the function that indicate that this analysis cannot be applied to polymers containing additional peaks in their scattering profiles. This demonstrates the importance of contrast-matching to isolate morphological features in order to apply some quantitative analyses.

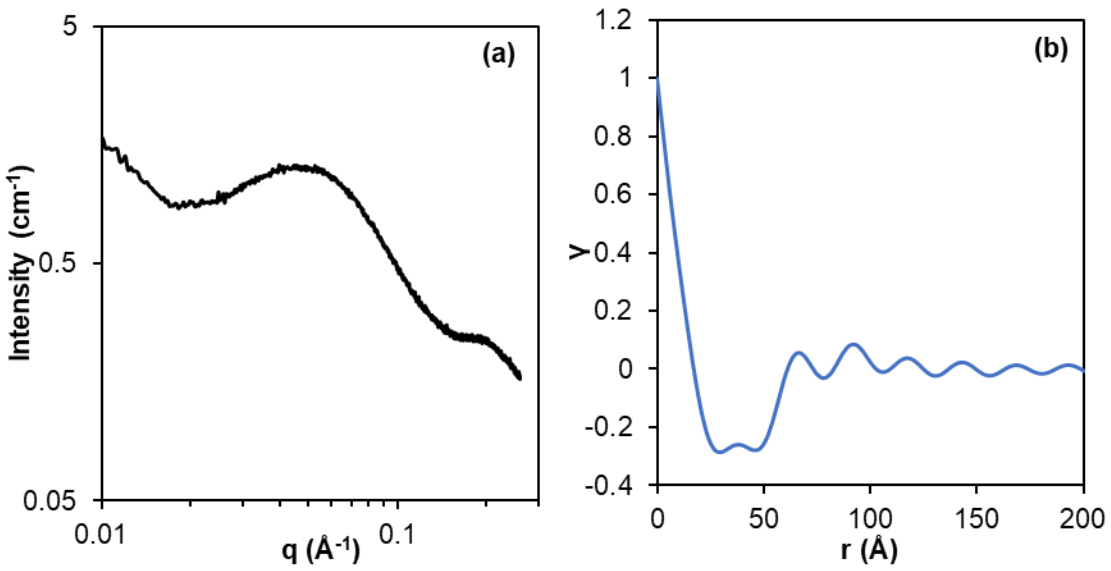

Figure 6-13. (a) SAXS profile of H^+-form Nafion 117 and (b) the resulting 1-D correlation data for H^+-form Nafion 117.

6.3.6 Effect of exchanging counterion on the same sample

In order to confirm that the observed changes in scattering intensity from each of the morphological features are due to changes in contrast and not physical changes, a membrane was counterion-exchanged from Cs^+-form to Li^+-form and SAXS experiments were performed before and after the ion exchange. The results of this experiment are shown in **Figure 6-14**. The 1000 EW 3M PFSA membrane was originally converted from the H^+- to the Cs^+-form prior to running SAXS. That curve is shown in gray, where the crystalline peak is indistinguishable and the ionomer peak is isolated. Then, the Cs^+-form membrane was submerged in 1 M LiOH for 48 hours, washed with water, and vacuum dried at 70 °C (below the principle relaxation temperature of Nafion so no morphological reorganization is expected to occur) overnight. The SAXS profile of that now-Li^+-form membrane is also shown in **Figure 6-14** in red. Upon conversion to the Li^+-form, the ionomer peak is now contrast-matched and not detected by X-rays, allowing the crystalline peak to be isolated. This is evidence that the scattering intensity of these peaks are solely being affected

by the electron density contrast from the different counterions, and not some type of structure change induced by the different counterions.

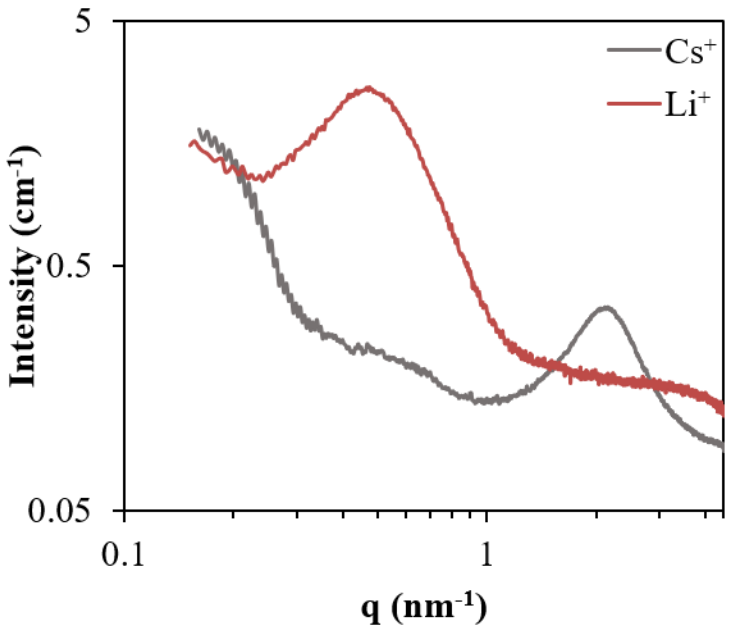

Figure 6-14. SAXS scattering profile for 1000 EW 3M PFSA in the Cs^+-form and after ion-exchanging the Cs^+ counterions to Li^+ counterions in the same membrane.

6.4 Conclusions

A systematic study of counterion effect on scattering contrast in a variety of PFSA membranes has been presented. In all membranes, regardless of EW or sidechain structure, the ionomer peak was contrast-matched (undistinguishable to X-rays) in the Li^+-form. This was evidence that the electron density of Li^+-sulfonate domains and the surrounding amorphous perfluorinated phase are the same or similar enough that there is no contrast between them. This was confirmed by calculating the electron density of a lithium trifluoromethylsulfonate model compound, which had a very similar electron density to that of amorphous PTFE. Additionally, it was observed that the crystalline peak disappeared at a certain counterion size and larger for all of

the PFSAs, but was dependent on the EW of the PFSA as opposed to sidechain structure. This observation indicated that the crystalline phase was not just contrast matching the ionic matrix at a specific counterion size, but instead, the contrast between the crystalline PTFE and the ionic matrix was much less than the contrast between the ionic domains and amorphous PTFE that it was effectively acting as a two-phase system. In order to quantify this, the scattering invariant (Q) was calculated by a theoretical method using the volume fraction of ions and crystalline phase for each ionomer based on EW, and experimentally by integrating the experimental SAXS data over an extrapolated range from q=0 to q=∞. Although the calculated invariant values had some discrepancy between the theoretical calculation and the experimental, they still showed the same trend with counterion size. In addition, a theoretical calculation of scattering contribution from the crystalline phase and the ionic phase provided a good prediction for which counterions will isolate the crystalline peak and the ionic peak based on the EW of the PFSA. Finally, this contrast-matching method was observed to be valuable for applying more quantitative modeling and data fitting methods to characterize the two morphological features observed by SAXS.

6.5 Acknowledgments

The authors acknowledge 3M for providing PFSA materials for this study and for funding this research.

6.6 References

1. Roe, R.-J.; Roe, R. *Methods of X-ray and neutron scattering in polymer science*; Oxford University Press New York, 2000; Vol. 739.

2. Hedden, R. C.; Lee, H.-J.; Bauer, B. J., Characterization of nanoporous low-k thin films by small-angle neutron scattering contrast variation. *Langmuir* **2004**, *20*, 416.

3. Glatter, O.; Kratky, O. *Small angle X-ray scattering*; Academic press, 1982.

4. Dingenouts, N.; Ballauff, M., Small-angle x-ray analysis of latex particles using contrast variation. *Acta polymerica* **1993**, *44*, 178.

5. Dingenouts, N.; Kim, Y.; Ballauff, M., The interface between immiscible polymers in composite latexes: a small-angle x-ray scattering study employing contrast variation. *Colloid and Polymer Science* **1994**, *272*, 1380.

6. Tokuda, J. M.; Pabit, S. A.; Pollack, L., Protein–DNA and ion–DNA interactions revealed through contrast variation SAXS. *Biophysical reviews* **2016**, *8*, 139.

7. Schneidman-Duhovny, D.; Hammel, M.; Tainer, J. A.; Sali, A., Accurate SAXS profile computation and its assessment by contrast variation experiments. *Biophysical journal* **2013**, *105*, 962.

8. Fujimura, M.; Hashimoto, T.; Kawai, H., Small-angle x-ray scattering study of perfluorinated ionomer membranes. 2. Models for ionic scattering maximum. *Macromolecules* **1982**, *15*, 136.

9. Gierke, T. D.; Munn, G. E.; Wilson, F. C., The morphology in nafion perfluorinated membrane products, as determined by wide- and small-angle x-ray studies. *J. Polym. Sci., Part B: Polym. Phys.* **1981**, *19*, 1687.

10. Shi, S.; Weber, A. Z.; Kusoglu, A., Structure-Transport Relationship of Perfluorosulfonic-Acid Membranes in Different Cationic Forms. *Electrochim. Acta* **2016**, *220*, 517.

11. Zhang, M. Ph.D. Dissertation, Virginia Tech, 2014.

12. Zhang, F.; Ilavsky, J.; Long, G. G.; Quintana, J. P.; Allen, A. J.; Jemian, P. R., Glassy carbon as an absolute intensity calibration standard for small-angle scattering. *Metall. Mater. Trans. A* **2010**, *41*, 1151.

13. Jeffries, C. M.; Graewert, M. A.; Blanchet, C. E.; Langley, D. B.; Whitten, A. E.; Svergun, D. I., Preparing monodisperse macromolecular samples for successful biological small-angle X-ray and neutron-scattering experiments. *Nature Protocols* **2016**, *11*, 2122.

14. Roche, E. J.; Pineri, M.; Duplessix, R.; Levelut, A. M., Small-angle scattering studies of nafion membranes. *J. Polym. Sci., Part B: Polym. Phys.* **1981**, *19*, 1.

15. Hamrock, S. J. *Membranes and MEA's for Dry, Hot Operating Conditions*, 3M Company, 2011.

16. Moukheiber, E.; De Moor, G.; Flandin, L.; Bas, C., Investigation of ionomer structure through its dependence on ion exchange capacity (IEC). *J. Membr. Sci.* **2012**, *389*, 294.

17. Herring, A. M.; Yandrasits, M. A.; Aieta, N. V.; Stanis, R. J.; Hamrock, S. J.; Cookson, D. J., Dynamics of PFSA polymer hydration measured in situ by SAXS. *ECS Trans.* **2006**, *3*, 915.

18. Pauw, B. R., Everything SAXS: small-angle scattering pattern collection and correction. *Journal of Physics: Condensed Matter* **2013**, *25*, 383201.

19. Kostorz, G., Small-angle scattering studies of phase separation and defects in inorganic materials. *J. Appl. Crystallogr.* **1991**, *24*, 444.

20. Deschamps, A.; Sigli, C.; Mourey, T.; De Geuser, F.; Lefebvre, W.; Davo, B., Experimental and modelling assessment of precipitation kinetics in an Al–Li–Mg alloy. *Acta materialia* **2012**, *60*, 1917.

21. Fratzl, P., Small-angle scattering in materials science-a short review of applications in alloys, ceramics and composite materials. *J. Appl. Crystallogr.* **2003**, *36*, 397.

22. Pauw, B. R.; Vigild, M. E.; Mortensen, K.; Andreasen, J. W.; Klop, E. A., Analysing the nanoporous structure of aramid fibres. *J. Appl. Crystallogr.* **2010**, *43*, 837.

23. Chu, B.; Hsiao, B. S., Small-angle X-ray scattering of polymers. *Chem. Rev.* **2001**, *101*, 1727.

24. Koch, M. H.; Vachette, P.; Svergun, D. I., Small-angle scattering: a view on the properties, structures and structural changes of biological macromolecules in solution. *Quarterly reviews of biophysics* **2003**, *36*, 147.

25. Ilavsky, J.; Jemian, P. R., Irena: tool suite for modeling and analysis of small-angle scattering. *J. Appl. Crystallogr.* **2009**, *42*, 347.

26. Hildebrandt, L.; Dinnebier, R.; Jansen, M., Crystal structure and ionic conductivity of three polymorphic phases of rubidium trifluoromethyl sulfonate, RbSO3CF3. *Inorganic chemistry* **2006**, *45*, 3217.

27. Hildebrandt, L.; Dinnebier, R.; Jansen, M., Crystal structure and ionic conductivity of cesium trifluoromethyl sulfonate, CSSO3CF3. *Zeitschrift für anorganische und allgemeine Chemie* **2005**, *631*, 1660.

28. Korus, G.; Jansen, M., Kristallstruktur, Phasenumwandlung und Kaliumionenleitfaehigkeit von Kaliumtrifluormethylsulfonat. *Zeitschrift für anorganische und allgemeine Chemie* **2001**, *627*, 1599.

29. Sofina, N.; Peters, E. M.; Jansen, M., Kristallstrukturanalyse und Natriumionenleitung von wasserfreiem α-Natriumtrifluoromethylsulfonat. *Zeitschrift für anorganische und allgemeine Chemie* **2003**, *629*, 1431.

30. Dinnebier, R.; Sofina, N.; Jansen, M., The Structure of the High Temperature Modification of Lithium Triflate (γ-LiSO3CF3). *Zeitschrift für anorganische und allgemeine Chemie* **2004**, *630*, 1613.

31. McDermott, A. G.; Budd, P. M.; McKeown, N. B.; Colina, C. M.; Runt, J., Physical aging of polymers of intrinsic microporosity: a SAXS/WAXS study. *J. Mater. Chem. A* **2014**, *2*, 11742.

32. Cheung, Y. W.; Stein, R. S.; Lin, J.; Wignall, G. D., Small-angle scattering investigations of poly (. epsilon.-caprolactone)/polycarbonate blends. 2. Small-angle x-ray and light scattering study of semicrystalline/semicrystalline and semicrystalline/amorphous blend morphologies. *Macromolecules* **1994**, *27*, 2520.

33. Vonk, C. G.; Glatter, O.; Kratky, O., Small Angle X-ray Scattering. *Synthetic Polymers in the Solid State, O. Glatter and O. Kratky, Eds., Academic Press, London* **1982**, *433*.

34. Guinier, A.; Fournet, G.; Yudowitch, K. L., Small-angle scattering of X-rays. **1955**.

35. Savitzky, A.; Golay, M., Analytical Chemistry. *vol* **1964**, *36*, 1.

36. Eisenberg, A.; Hird, B.; Moore, R. B., A new multiplet-cluster model for the morphology of random ionomers. *Macromolecules* **1990**, *23*, 4098.

37. Kusoglu, A.; Weber, A. Z., New Insights into Perfluorinated Sulfonic-Acid Ionomers. *Chem. Rev.* **2017**, *117*, 987.

38. Fujimura, M.; Hashimoto, T.; Kawai, H., Small-angle X-ray scattering study of perfluorinated ionomer membranes. 1. Origin of two scattering maxima. *Macromolecules* **1981**, *14*, 1309.

39. Page, K. A.; Cable, K. M.; Moore, R. B., Molecular Origins of the Thermal Transitions and Dynamic Mechanical Relaxations in Perfluorosulfonate Ionomers. *Macromolecules* **2005**, *38*, 6472.

40. Li, J.; Yang, X.; Tang, H.; Pan, M., Durable and high performance Nafion membrane prepared through high-temperature annealing methodology. *J. Membr. Sci.* **2010**, *361*, 38.

41. Yin, C.; Wang, Z.; Luo, Y.; Li, J.; Zhou, Y.; Zhang, X.; Zhang, H.; Fang, P.; He, C., Thermal annealing on free volumes, crystallinity and proton conductivity of Nafion membranes. *Journal of Physics and Chemistry of Solids* **2018**, *120*, 71.

42. Divoux, G. M.; Finlay, K. A.; Park, J. K.; Song, J.-M.; Yan, B.; Zhang, M.; Dillard, D. A.; Moore, R. B., Morphological Factors Affecting the Behavior of Water in Proton Exchange Membrane Materials. *ECS Trans.* **2011**, *41*, 87.

43. Taylor, E. P.; Landis, F. A.; Page, K. A.; Moore, R. B., Counterion dependent crystallization kinetics in blends of a perfluorosulfonate ionomer with poly (vinylidene fluoride). *Polymer* **2006**, *47*, 7425.

44. Su, G. M.; Cordova, I. A.; Yandrasits, M. A.; Lindell, M.; Feng, J.; Wang, C.; Kusoglu, A., Chemical and Morphological Origins of Improved Ion Conductivity in Perfluoro Ionene Chain Extended Ionomers. *J. Am. Chem. Soc.* **2019**.

45. Moore, R. B.; Bittencourt, D.; Gauthier, M.; Williams, C. E.; Eisenberg, A., Small-angle x-ray scattering investigations of ionomers with variable-length side chains. *Macromolecules* **1991**, *24*, 1376.

46. Elliott, J.; Hanna, S.; Newton, J.; Elliott, A.; Cooley, G., Elimination of orientation in perfluorinated ionomer membranes. *Polym. Eng. Sci.* **2006**, *46*, 228.

47. Mauritz, K. A.; Moore, R. B., State of Understanding of Nafion. *Chem. Rev.* **2004**, *104*, 4535.

48. Moore, R. B.; Martin, C. R., Procedure for preparing solution-cast perfluorosulfonate ionomer films and membranes. *Anal. Chem.* **1986**, *58*, 2569.

49. Moore, R. B.; Martin, C. R., Chemical and morphological properties of solution-cast perfluorosulfonate ionomers. *Macromolecules* **1988**, *21*, 1334.

50. Kim, Y. S.; Welch, C. F.; Hjelm, R. P.; Mack, N. H.; Labouriau, A.; Orler, E. B., Origin of Toughness in Dispersion-Cast Nafion Membranes. *Macromolecules* **2015**, *48*, 2161.

51. Vonk, C.; Kortleve, G., X-ray small-angle scattering of bulk polyethylene. *Kolloid-Zeitschrift und Zeitschrift für Polymere* **1967**, *220*, 19.

52. Koberstein, J. T.; Stein, R. S., Small-angle x-ray scattering measurements of diffuse phase-boundary thicknesses in segmented polyurethane elastomers. *J. Polym. Sci., Part B: Polym. Phys.* **1983**, *21*, 2181.

Chapter 7.
Crystalline-Like Ordering of Tetramethylammonium Counterions within the Ionic Domains of Perfluorosulfonic Acid Ionomers

7.1 Introduction

Perfluorosulfonic acid ionomers (PFSAs) are most commonly used as proton exchange membranes in fuel cells due to their excellent proton transport properties and chemical and mechanical stability.[1-3] The general structure of a PFSA consists of a polytetrafluoroethylene (PTFE) backbone containing perfluorovinyl ether sidechains with pendant sulfonic acid groups. While Nafion, originally developed by DuPont and now owned by Chemours, was the first of its class and most widely studied PFSA, several other PFSAs have been developed in recent years that have the same general structure but slight differences in sidechain structures. The structures of these different PFSAs are shown in **Figure 7-1**, including Solvay's Aquivion (short sidechain, SSC), and 3M's PFSA and perfluoroimide acid ionomer, 3M PFIA. New sidechain structures are developed with the purpose of increasing the fuel cell performance of PFSA membranes in regard to their mechanical integrity and proton conductivity.[4-7] These properties are governed by the quantity of functional sidechains and length of crystallizable PTFE units between sidechains, referred to as equivalent weight (EW). EW represents the average grams of dry membrane per moles of proton exchange groups, thus has a relationship to the molecular weight of the sidechain for each PFSA.[1,8,9]

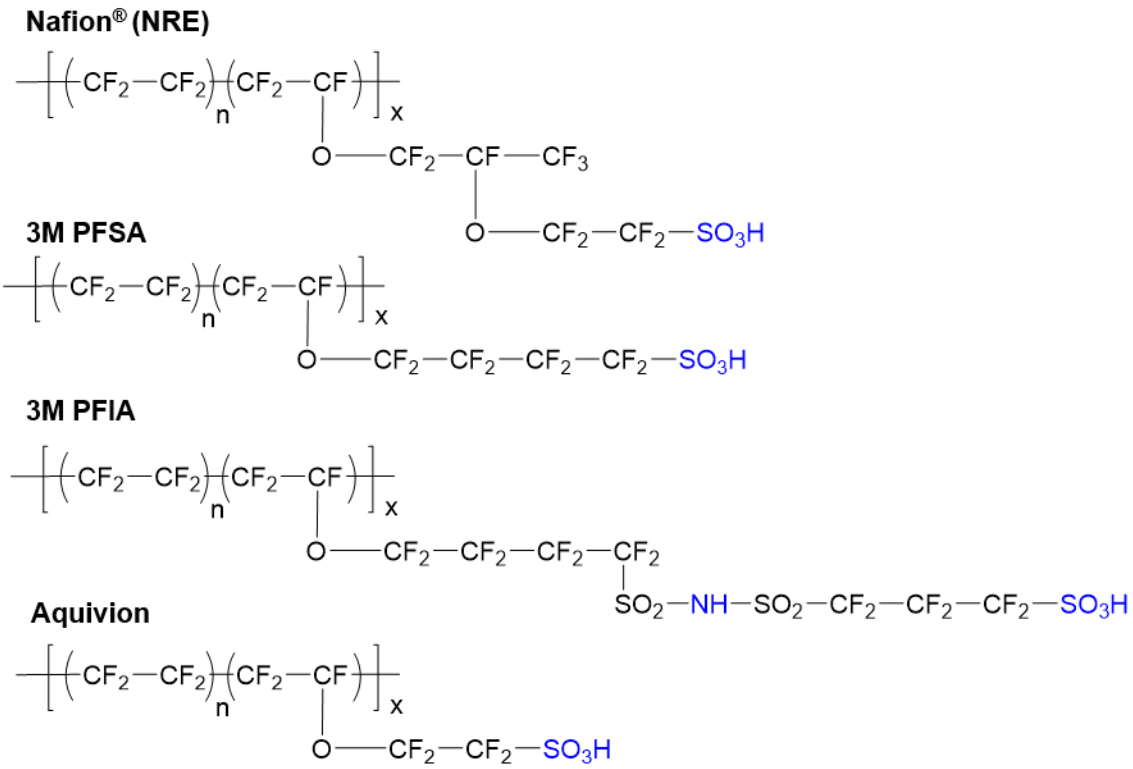

Figure 7-1. Chemical structures for Nafion, 3M PFSA, 3M PFIA, and Aquivion containing the same TFE backbone with slight differences in sidechain structure.

As a result of the dissimilarities between the polar sulfonic acid-containing sidechains and nonpolar PTFE backbones, the sulfonic acid sidechains have been shown to phase separate to form ionic domains.[10,11] These ionic domains, referred to as clusters, are randomly distributed throughout the PTFE matrix and give rise to the "ionomer peak" at ca. $q = 0.15$ Å^{-1} that appears in small angle X-ray scattering (SAXS).[1] In addition to the ionomer peak, a second peak is observed in the SAXS profiles of PFSAs at lower scattering angles that is attributed to intercrystalline dimensions at $q = 0.02$ to 0.05 Å^{-1}. Wide angle X-ray scattering (WAXS) patterns of PFSAs also show the presence of a Bragg peak reflection at ca. $2\theta = 18°$, attributed to the *hkl* (100) crystal plane of the PTFE backbone overlapping a large amorphous halo, and an additional PTFE crystalline reflection *hkl* (101) at ca. $2\theta = 39°$.[12] The 18° 2θ Bragg reflection in WAXS patterns of

PFSAs is generally very small and difficult to deconvolute from the amorphous halo, however, some studies have shown that this reflection can be manipulated by annealing the membranes at various temperatures.[13,14]

Various studies over the years have looked at the effect of annealing PFSA membranes on the resulting morphology and properties. One of the earliest of these studies was conducted on sulfonyl fluoride precursor Nafion membranes by Gierke, Munn and Wilson in 1981.[10] Wide-angle X-ray diffraction (WAXD) results for thermally annealed sulfonyl fluoride form Nafion showed the crystalline reflection at 18° 2θ that decreased in intensity as the sample annealing temperature was increased from 50 to 270 °C. However, the intercrystalline peak observed in SAXS increased with annealing temperature, ultimately disappearing above 270 °C but returned again upon cooling back to room temperature. The decrease in the wide-angle scattering reflection at 18° 2θ with annealing temperature was also observed by Fujimura and coworkers.[15] The authors of this study noted that when the Nafion membrane was cooled back down to room temperature from 275 °C, the crystalline reflection reappeared, characteristic of melting and recrystallization of the polymer. Gierke, Munn, and Wilson determined the melting temperature of the Nafion precursor to be 275 °C by differential scanning calorimetry (DSC) experiments, but noted that melting occurred over a broad temperature range compared to PTFE crystallites that melt at ca. 330 °C.[10]

Several other studies have looked at the effect of annealing in the sulfonic acid or other counterion forms on the morphology and properties of PFSA membranes. In the Cs^+-form, one study showed an increase in the SAXS ionomer peak scattering intensity and a shift to larger scattering angles with increasing temperature from 50 to 275 °C.[15] The shift in the peak maximum was attributed to a decrease in the inter-cluster distance. In the Na^+-form, Nafion membranes that were heated to 250 °C in a melt press prior to dynamic mechanical analysis (DMA) experiments

were shown to be completely amorphous after the heating step.[16] The thermal and mechanical properties were not affected by the lack of crystallinity.

In 2004, a study from our group on the molecular origins of thermal transitions in Nafion showed the effect of annealing in Na^+ and Cs^+-counterion forms on crystallinity observed by DSC experiments.[17] In both counterion-forms, the initial heat showed a broad endotherm between 200 and 250 °C that disappeared upon reheat. This endotherm could be induced to reappear by annealing in the DSC at 200 °C for increasing lengths of time ranging from 0.5 to 24 hours. Based on the slow crystallization kinetics in semicrystalline polymers, this endotherm was assigned to the melting of PTFE-like crystallites. An additional, broad endotherm was observed in the first heat scan of Cs^+-form Nafion spanning ca. 100 to 150 °C. Upon annealing in the DSC for 2 hours at temperatures ranging from 120 to 240 °C, this endotherm was observed to shift approximately 20-30 °C above the temperature at which it was annealed. Based on this finding, the low-temperature endotherm was assigned to the melting of small, imperfect crystals that develop in the sample due to annealing conditions.

Other studies observed an increase in relative degree of crystallinity in annealed Nafion membranes and related the increase in crystallinity to the conductivity of annealed membranes compared to unannealed. Li and coworkers looked at the effects of annealing Nafion NRE 211 (solution-cast membrane) in the H^+-form and the Na^+-form. Membranes were annealed at 160 °C in the H^+-form and 270 °C in the Na^+-form.[18] They observed an overall increase in relative degree of crystallinity based on WAXD measurements for both counterion-types after annealing, which led to an overall improvement in mechanical properties (determined from an increase in tensile strength). However, they noted that annealing the H^+-form reduced conductivity while annealing in the Na^+-form enhances conductivity. The authors attributed the increase in conductivity in the

annealed Na^+-form membranes to the strong electrostatic interactions that become a driving force for cluster formation when activated at high temperatures. An additional study by Yin and coworkers in 2018 also showed an increase in degree of crystallinity with annealing of H^+-form solution-cast Nafion at different temperatures.[19] This increase in crystallinity led to increased mechanical properties (increased break stress values) but a decrease in overall conductivity.

In 1996, Sone, Ekdunge, and Simonsson performed proton conductivity measurements in a range of relative humidities on Nafion annealed at 80, 105, and 120 °C.[20] Proton conductivity values at 100% relative humidity decreased from 0.09 S/cm to 0.03 S/cm with increasing annealing temperature. The authors concluded that increasing the annealing temperature to close to the α-relaxation temperature (the dominant thermomechanical relaxation in PFSAs) of Nafion led to a reduction in both water uptake and conductivity. In 2012, Maldonado and coworkers performed a systematic study on sorption and transport properties of extruded and solution-cast Nafion membranes dried at temperatures ranging from 60 to 110 °C.[21] In heat-treated membranes, they observed reduction in water uptake values that was attributed to shrinking of the polymer structure during drying. As a result of this, the water self-diffusion coefficient and proton conductivity were also reduced in the thermally treated samples.

While several of the aforementioned studies have shown a decrease in conductivity with annealing, some investigations have observed positive effects on conductivity by annealing PFSAs in different counterion-forms or at high temperatures/extended annealing times. An example of this came from Thomas and coworkers in 2003, where an increase in conductivity was observed for Nafion membranes that were annealed at 140 °C in different alkylammonium counterion forms (ranging from tetramethylammonium to tetrapentylammonium).[22] The authors attributed the increase in conductivity to a restructuring of the membrane above the α-relaxation temperature

based on fluorescence data that showed evidence that the alkylammonium salts changed the physical characteristic of the conducting channels. Contrary to findings by other annealing studies that showed a decrease in conductivity after annealing in the H^+-form, DeLuca and Elabd observed maximum proton conductivity values for Nafion membranes that were annealed in the H^+-form at 210 °C for ten minutes,[23] and Hensley and coworkers also observed an increase in conductivity after annealing H^+-form Nafion at 165 °C for three hours.[24]

In 2012, a SAXS study was conducted to look at the development of morphology in PFSA membranes during and after annealing above the α-relaxation temperature.[25] Unified fits from scattering data were used to quantify the sizes of the crystalline and ionic cluster phases in 3M PFSA membranes annealed 180, 190, and 200 °C. The authors observed an increase in the size of both the crystalline and cluster regions when annealed at 180 and 190 °C, but at 200 °C observed a decrease in size of the ionomer phase at certain relative humidities. This finding suggested that there is a maximum annealing temperature that exists for these PFSA membranes.[26] From this study, it was proposed that annealing at 200 °C increases the degree of crystallinity to such an extent that reduces the mobility of the polymer chains and prevents the ionic clusters from swelling upon hydration.[25]

Our research group has utilized different alkylammonium counterions to manipulate the strength of the electrostatic network in Nafion membranes.[14,17,27-33] A series of DMA studies on Nafion ion-exchanged to alkylammonium counterions ranging in size from tetramethylammonium (TMA^+) to tetradecylammonium showed a systematic decrease in both the α- and β-relaxations with increasing counterion size.[17] From this study, the α- and β-relaxations were determined to both be coupled to the strength of the physical crosslinked network, which led to their ultimate assignments. The β-relaxation in PFSAs was attributed to the onset of main-chain mobility

facilitated through sidechain mobility in the presence of a static physically crosslinked network. The α-relaxation was attributed to the onset of long-range mobility resulting from the destabilization of the physically crosslinked network facilitated by ion hopping processes (e.g., ion pairs "hop" to from one aggregate to another). It has been shown that using a bulky counterion like tetrabutylammonium (TBA^+) can reduce the electrostatic network strength such that the TBA^+-form Nafion membranes can be melt-processed.[30] Additionally, substituting the counterion for the small TMA^+ counterion has shown interesting morphological and property changes upon annealing.[29,32,33]

The first evidence of morphological changes upon heating Nafion membranes in the TMA^+-form resulted from a study of variable temperature ^1H and ^{13}C solid-state NMR (SS-NMR) experiments.[29] In this study, Nafion membranes were neutralized with TMA^+, tetraethylammonium (TEA^+), tetrapropylammonium (TPA^+) and TBA^+ counterions, then annealed at temperatures ranging from 25 to 200 °C for ten minutes. From SS-NMR studies, it was determined that TMA^+ and TEA^+ counterions may better ordered within the ionic domains of Nafion compared to TPA^+ and TBA^+ counterions due to their small size and stronger Coulombic interactions with sulfonate groups. This was further confirmed by the increased observed melting points for the TMA^+ and TEA^+-form membranes, which were attributed to melting of local crystalline-like ordering of TMA^+ and TEA^+ counterions within the crystalline domains. Additional SAXS data of the annealed TMA^+-form membranes showed a profoundly sharpened ionomer peak after annealing at 200 °C, which was attributed to a narrower distribution of inter-cluster dimensions likely due to the improved packing of counterions within the ionic domain. Although the underlying mechanism of this thermal reorganization is not well understood, it was proposed that the strong electrostatic interactions between ion pairs disfavor rotational tumbling

or translational hopping movements of the TMA^+ counterion. Instead, the TMA^+ counterions likely fill gaps that form upon the thermally-induced movement of polymer chains, contributing to the electrostatic interactions between the counterions and sulfonate groups that reinforce the integrity of the membrane.

Since this initial study revealed that a substantial morphological reorganization of Nafion membranes occurs after annealing in the TMA^+-form, our research group has been very interested in the underlying mechanism of this thermal reorganization and how it can be utilized to tailor the morphology of membranes in order to improve properties such as proton conductivity and fuel cell performance. In 2009, Osborn looked at the effect of annealing time and temperature on the morphology and mechanical properties of TMA^+-neutralized dispersion-cast Nafion membranes.[14] In this study, it was observed that the ionomer peak progressively sharpened, increased in intensity, and shifted to higher q-values with increasing annealing time at temperatures below 200-225 °C. Above 225 °C, the ionomer peak broadened and its intensity decreased slightly. Additionally, the intercrystalline SAXS peak was observed to shift to lower q-values with increasing annealing temperature and disappear at temperatures above 225 °C. From this data, Osborn determined that the maximum change in morphology in TMA^+-form Nafion membranes occurs during the first fifteen minutes of annealing. In wide-angle X-ray diffraction (WAXD) experiments, Park observed the appearance of an additional scattering reflection at ca. $2\theta = 12°$ in TMA^+, TEA^+, TPA^+, and TBA^+-form Nafion that shifted to lower scattering angles with increasing counterion size.[32] While this scattering reflection was unaffected by annealing temperature in larger counterion sizes, it was observed to become much more pronounced with increasing annealing temperature in the TMA^+-form. This observation was attributed to an increase in (crystalline-like) packing order of the TMA^+ counterions within the ionic aggregates.

In 2012, Divoux looked at the effect of thermal annealing of Nafion in the TMA^+-form on the mechanical properties and fuel cell performance.[33] DMA studies of the TMA^+-form membranes showed that the α- and γ-relaxations were unaffected by annealing, but the β-relaxation decreased in intensity with increasing annealing temperature. This was attributed to a change in the morphology of the backbone matrix, possibly due to increased crystallinity that reduced the mobility of the matrix with annealing. Upon reacidification of the TMA^+ annealed membranes back to the sulfonic acid form, the α-relaxation became much broader with increasing annealing temperature, spanning a range of temperatures from 60 to 160 °C, which remained unexplained. DSC studies showed the presence of two endotherms for TMA^+-form Nafion. The high temperature endotherm at ca. 250 °C remained unchanged based on annealing temperature while a lower temperature endotherm appears 20-25 °C above the annealing temperature. This low temperature endotherm was attributed to melting of PTFE-like crystallites formed in the sample as a result of annealing. The high temperature endotherm was attributed to the "melting," or disordering, of well-ordered counterions within the ionic aggregates. In this work, Divoux also reacidified membranes that were annealed in the TMA^+-form to determine whether the increased ordering of the ionic aggregates could be maintained through the reacidification process and lead to any improvements in membrane properties. It was observed that the increase in intensity and narrowing of the ionomer peak after annealing was maintained after reacidifying the membranes. In turn, an improvement in proton conductivity and fuel cell performance (increased power density and decreased hydrogen crossover) was observed in Nafion membranes that were annealed at 200-250 °C in the TMA^+-form and reacidified.

The culmination of these studies provide evidence that membrane properties can be controlled by modifying the morphology through annealing in the TMA^+-counterion form.

Although the underlying mechanism of this thermal reorganization is still not fully understood, it presents a simple and efficient method for achieving desired morphologies in PFSA membranes. To this point, these studies have mostly been conducted on Nafion extruded membranes. With the introduction of new PFSAs containing higher ion contents and different sidechain structures, it is of interest to explore the effect of annealing these new membranes in the TMA^+-form on the resulting morphology and properties. In addition, using PFSAs with different ion contents and sidechain structures may provide more evidence to ultimately lead to the understanding of the mechanism of ordering of the TMA^+ counterion. In this work, we will neutralize 3M PFSA, 3M PFIA, Solvay's Aquivion, and Nafion NRE (dispersion-cast membrane opposed to the previously studied extruded membranes) to the TMA^+-form and investigate the effect of annealing temperatures on the SAXS, WAXD, thermal properties, and membrane properties upon reacidifying. The ultimate goal is to correlate the dynamic mechanical relaxations and DSC melting endotherm to the temperatures necessary for observed ordering by X-ray experiments in these ionomers in order to gain some understanding on the molecular motions required for this ordering to occur. Additionally, reacidifying these membranes after annealing in the TMA^+-form will show whether this improvement in membrane properties can be achieved by this annealing method in a broad range of PFSAs. Although a lot of work has been conducted on this phenomenon already, some of the mechanisms are still not well understood and assigning them are beyond the scope of a single graduate student. Therefore, this chapter will serve more as a "chapter of observations" and will outline some future work that may help with the further understanding of the mechanism of TMA^+ crystalline-like ordering within ionic domains of ionomers.

7.2 Experimental

7.2.1 Materials.

3M-Perfluorosulfonic acid (3M-PFSA) ionomer of 800 equivalent weight (EW, g polymer/mol sulfonate groups) and 3M-perfluoroimide acid (3M-PFIA) ionomer of 625 EW were provided by 3M. Nafion NRE211 was purchased from FuelCellStore and Aquivion 870 EW membrane (E87-05S) was purchased from Sigma Aldrich. Tetramethylammonium hydroxide (TMAOH), 1 M in water, was obtained from Fisher Scientific and used without further purification.

7.2.2 Membrane preparation

3M-PFSA and 3M-PFIA membranes were prepared by casting a dispersion from alcohol and water onto polyimide film. The dispersions were dried in an oven with the temperature of 80°C followed by annealing for 10 minutes at 200°C. Membranes were removed from the polyimide film by soaking in water. Aquivion and Nafion membranes were used as-received. To remove impurities, all membranes were soaked in 8 M HNO_3 for 16 hours then rinsed thoroughly with deionized water. Ion exchange to 100% TMA^+-form was carried out by stirring the pretreated membranes in 1 M TMAOH in water for 24 hours. The membranes were thoroughly rinsed with water and dried under vacuum at 70 °C overnight. Once in the TMA^+-form, the membranes were annealed in a forced air oven at temperatures ranging from 125 to 300 °C for 10 minutes. They were removed from the oven and allowed to cool back to room temperature under ambient conditions.

The TMA^+/TEA^+ mixed counterion series was prepared by stirring each membrane in aqueous solutions containing specified quantities of TMAOH and TEAOH for 24 hours. TEAOH

quantities ranging from 5 to 30 mol % for each membrane were calculated on the basis of equivalent weight of dry membranes. All prepared membranes were thoroughly rinsed with water before drying under vacuum at 70°C overnight.

7.2.3 Small Angle X-ray Scattering

SAXS experiments were performed on a Rigaku S-Max 3000 3 pinhole SAXS system, equipped with a rotating copper anode generating X-rays with a wavelength of 0.154 nm (Cu Kα). Two-dimensional SAXS patterns were obtained using a fully integrated 2D multiwire, proportional counting, gas-filled detector, with an exposure time of 2 hours. All SAXS data were analyzed using the SAXSGUI software package to obtain radially integrated SAXS intensity versus scattering vector q, where $q=(4\pi/\lambda)\sin(\theta)$, θ is half the scattering angle and λ is the wavelength of the X-rays. For all scattering experiments, the sample-to-detector distance was 1603 mm and the q-range was calibrated using a silver behenate standard. Scattering data were normalized for sample thickness and transmission using a glassy carbon standard.[34]

7.2.4 Wide Angle X-Ray Scattering

Wide angle X-ray diffraction (WAXD) experiments were performed using a Rigaku MiniFlex II X-ray diffractometer emitting X-rays with a wavelength of 0.154 nm (Cu Kα). Samples were scanned from 5° to 50° 2θ at a scan rate of 0.250° 2θ /min and a sampling window of 0.050° 2θ at a potential of 30 kV and current of 15 mA. All WAXD data were analyzed using the PDXL 2 software package to obtain WAXD intensity versus 2θ profiles.

7.2.5 Variable Temperature SAXS

Variable temperature SAXS data was collected at beam line 9-ID-C at the Advanced Photon Source (APS) at Argonne National Laboratory (Lemont, Illinois).[35,36] Membrane samples

were mounted in a Linkam THMS600 with Kapton windows. The temperature was ramped from 50 to 350 °C at a rate of 5 °C/min and SAXS measurements were collected for 15 seconds once every minute. SAXS profiles were reduced using the Nika program for Igor Pro.[37] SAXS data was corrected for sample thickness and transmission and converted to absolute intensity using a glassy carbon standard.[34]

7.2.6 Differential Scanning Calorimetry

DSC data were collected for the TMA^+-form PFSAs on a TA Instruments Q2000 at a 10 °C/min ramp rate under nitrogen purge. Initial DSC thermograms were obtained after thoroughly drying the samples in the DSC at 120 °C for 2 hours. Samples were held in the DSC at 120 °C for two hours to remove water from the membranes, then cooled to the starting temperature of 0 °C. The first heat was collected from 0 to 350 °C at a heating rate of 10 °C/min, then samples were cooled from 350 to 0 °C at a rate of 10 °C/min, followed by a second heat from 0 to 350 °C at 10 °C/min. Samples that were annealed at different temperatures were annealed in the DSC at the specified temperature for 10 minutes before cooling to the starting temperature of 0 °C. The first heat data is presented from 0 to 350 °C at a heating rate of 10 °C/min.

7.2.7 Dynamic Mechanical Analysis

Dynamic mechanical analysis was performed on a TA Instruments DMA Q800 analyzer in tensile mode using clamps for thin film samples. All samples were cut from vacuum dried membranes with a width of 6.35 mm. The membranes were analyzed at a frequency of 1 Hz from −120 to 200°C with a heating ramp of 2°C/min.

7.2.8 Proton Conductivity

Prior to proton conductivity analysis, the TMA^+-annealed membranes were reacidified by stirring in an 8 M HNO_3 solution at room temperature for 24 hours, then rinsed well and stored in water until measurements were taken. Each sample was loaded into a two-point conductivity cell developed by Bekktech and placed in an Espec SH-241 temperature and humidity chamber. The cell and membrane were equilibrated at 80 °C and 95% relative humidity (RH) for two hours. Conductivity measurements were then taken starting at 95% RH and decreasing to 85, 75, 65, 55, 45, 35, and 30% RH while maintaining a constant temperature of 80 °C. Measurements were taken from 0.1 to 500,000 Hz using a Solatron Impedance Analyzer SI 1260 and Electrochemical Interface SI 1287. Data analysis was carried out using Zplot™ and Zview™ software from Scribner and Associates, Inc. The resistance was calculated from the bulk resistivity and geometry of the cell following the equation:

$$R = \frac{\rho \times L}{A} = \frac{\rho \times L}{W \times T} \quad (1)$$

where R is the resistance of the membrane, ρ is the resistivity, A is the cross-sectional area of the membrane, W is the width of the sample, L is the distance between the two reference electrodes, and T is the thickness of the membrane. The membrane resistance is taken as the real Z-axis intercept of the complex impedance plot. Conductivity (σ) is then calculated from:

$$\sigma = \frac{1}{\rho} = \frac{L}{R \times W \times T} \quad (2)$$

where conductivity, in units of S/cm, is the inverse of resistivity, ρ.

7.2.9 Dynamic Vapor Sorption

Dynamic vapor sorption (DVS) water uptake experiments were performed on a TA Instruments VTI-SA+ high performance sorption analyzer at 3M Company in St. Paul, MN. All

samples were reacidified from the TMA^+-form by stirring in 8 M HNO_3 for 24 hours, then rinsed well and stored in water. Samples were blotted dry and shipped to 3M Company in St. Paul, MN for analysis. Upon loading into the instrument, the membranes were equilibrated at 60 °C for 1 hour then the temperature was set to 25 °C for water uptake experiments. The relative humidity (RH) level was stepped from 5% to 95% RH and back with 5% increments. At each RH step, the sample was held until the weight change was less than 0.001% in 5 minutes for a maximum equilibration time of 2 hours. Water content (λ = mol H_2O/mol SO_3^-) is calculated from the mass water uptake and EW of the membrane by

$$\lambda = \left(\frac{\Delta M_{H_2O}}{M_P}\right)\frac{EW}{MW_{H_2O}} \quad (3)$$

where ΔM_{H2O} is the mass uptake of water and M_P is the initial mass of the polymer, EW is the equivalent weight of the membrane and MW_{H2O} is the molar mass of water.[9]

7.3 Results and Discussion

7.3.1 Small Angle X-ray Scattering

Small angle X-ray scattering (SAXS) has been used to characterize the distribution in domain sizes in Nafion to provide an idea of the homogeneity of the ionomer phase. Previous studies from our group have shown that annealing Nafion 117 (extruded membrane) in the TMA^+-form leads to a narrowing of the ionomer peak, which was attributed to increased phase homogeneity.[32,33] The SAXS profiles for TMA^+-form 3M PFSA, 3M PFIA, Aquivion, and Nafion NRE-211 (NRE) before and after annealing at various temperatures for ten minutes are displayed in **Figure 7-2**. The SAXS data in this figure are limited to the q-range surrounding the ionomer

peak for simplification, but the intercrystalline peak is also present at lower scattering angles and disappears above the melting temperature of each ionomer.

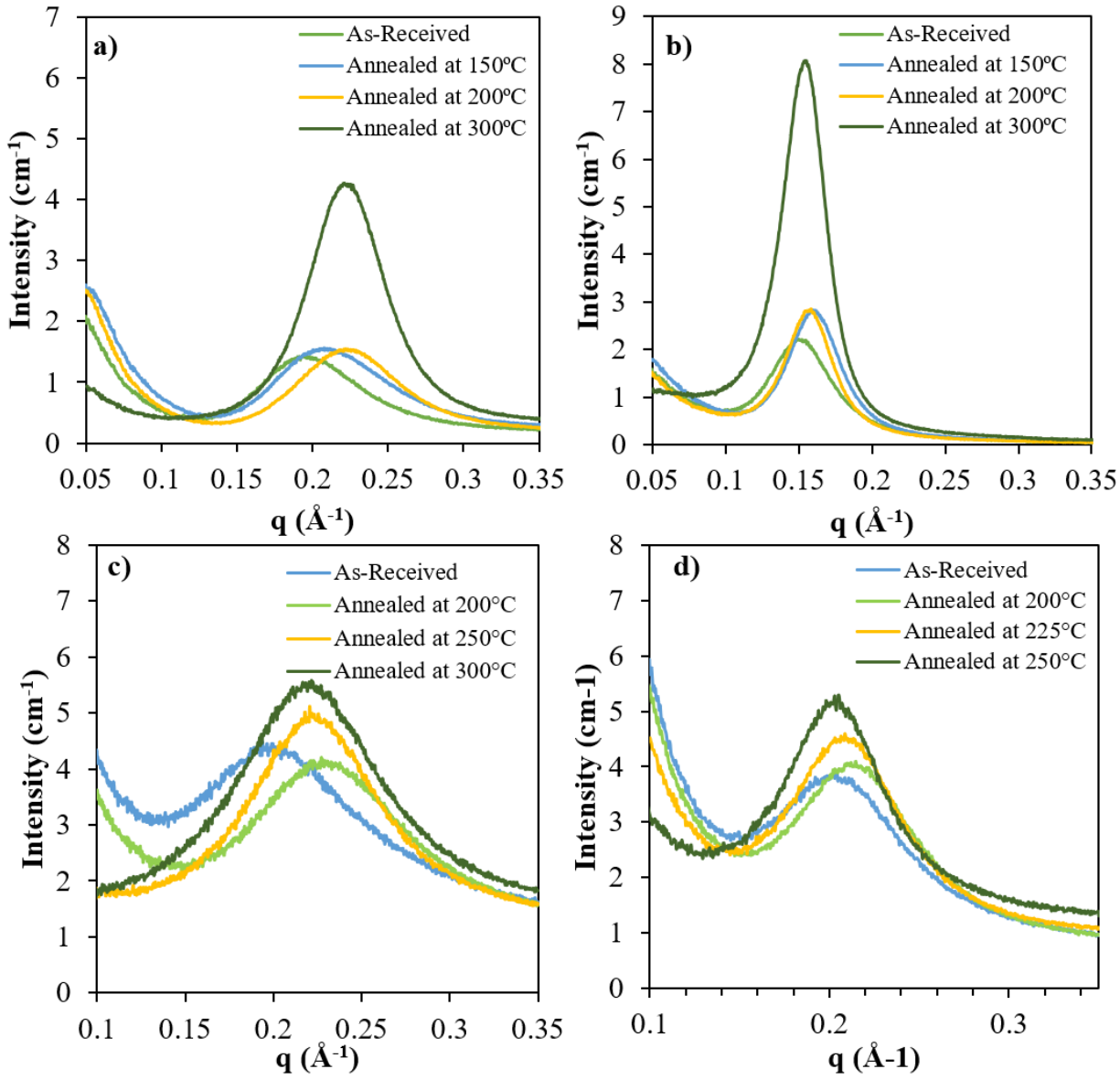

Figure 7-2. SAXS profiles of a) 825 EW 3M PFSA , b) 3M PFIA, c) Nafion NRE, and d) Aquivion as cast and annealed at increasing temperatures.

The ionomer peak is attributed to inter-aggregate correlations arising from contrast in electron density between the ionic domains and the PTFE matrix.[9] In **Figure 7-2**, there is a clear

shift in the ionomer peak to higher q-values with increasing annealing temperature. For each ionomer, the breadth of the peak decreases after annealing at an elevated temperature in the TMA^+-form. The temperature at which this peak narrowing occurs is different for each PFSA as listed in **Table 7-2**. The minimum temperature at which this peak narrowing begins to occur is lowest for Aquivion, followed by NRE. The 3M PFSA and 3M PFIA require temperatures in the vicinity of 300 °C to see any change in the ionomer peak. Evidence of this sharpening of the ionomer peak is also observed in the 2D scattering pattern for each ionomer, an example of which is shown for 3M PFSA in **Figure 7-3**. The diffuse scattering ring for the as-cast 3M PFSA in the TMA^+-form is altered into a very distinct scattering ring upon annealing at 300 °C. A reduced peak width in the ionomer peak is attributed to a narrower distribution of domain sizes, which likely is attributed to increased packing within the ionic domains.

Table 7-1. Minimum annealing temperature to see narrowing of the ionomer peak in SAXS for the different PFSA structures in the TMA^+-form.

PFSA Structure	Minimum Annealing Temp for Sharpening of Ionomer Peak (°C)
3M PFSA	300
3M PFIA	300
NRE	250
Aquivion	225-250

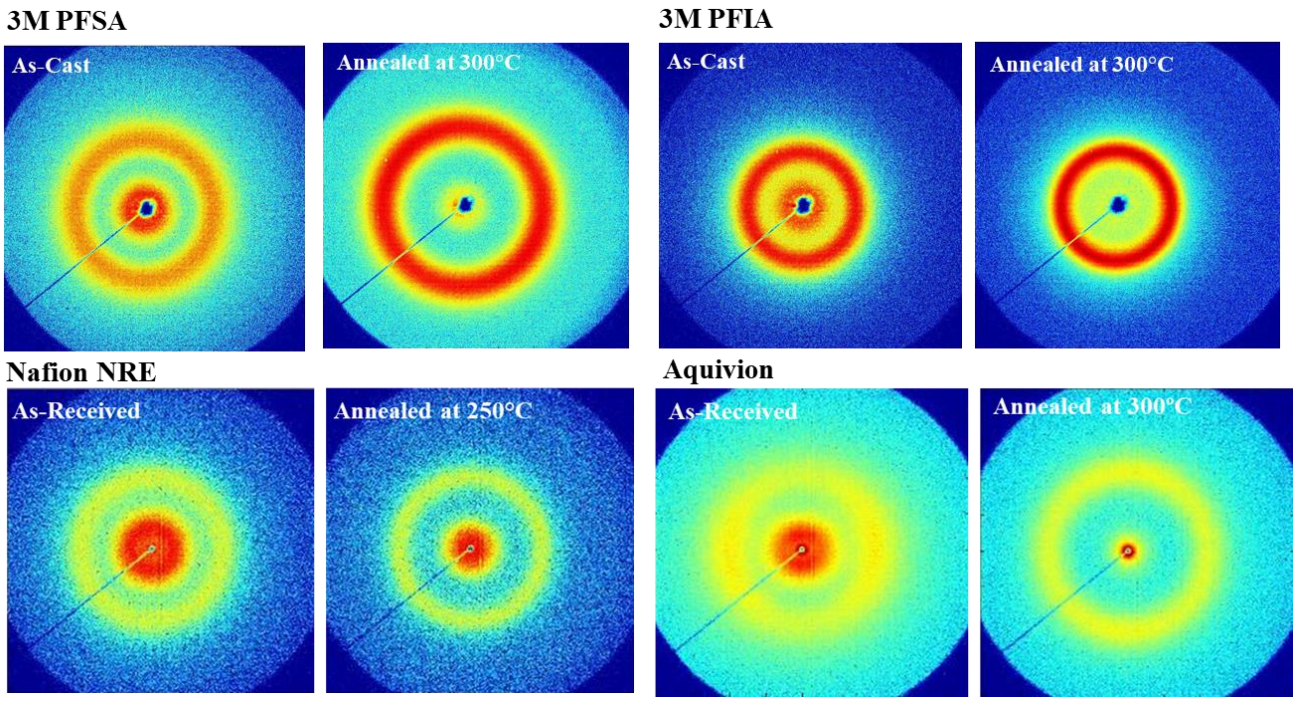

Figure 7-3. 2D SAXS scattering pattern for TMA^+-form 3M PFSA, 3M PFIA, Nafion NRE, and Aquivion as-cast/as-received and annealed at 250/300 °C.

Another profound difference between the SAXS data before and after annealing each PFSA in the TMA^+-form is the increase in intensity of the ionomer peak at the same temperature at which the narrowing occurs. This increase in intensity is most profound in 3M PFSA and 3M PFIA. While an increase in intensity was noted in the original studies of Nafion 117 annealed in the TMA^+-form,[33] it was much less than what is observed here for the 3M ionomers. An increase in intensity of a scattering feature is generally the result of increased electron density contrast between the scattering feature and the surrounding matrix.[38] While the exact morphological structure of PFSAs is still unknown despite decades of research,[1,9] the intensity of the ionomer peak is thought to be attributed to the electron density contrast between the ionic domains and the amorphous matrix. If the ionomer peak scattering feature was the result of electron density difference between the ionic domains and the entire PTFE matrix, including crystalline domains,

then an increase in intensity of the ionomer peak would be expected upon melting of the PTFE-like crystallites. However, based on our current understanding of the morphology of PFSAs, the inter-cluster dimensions are on the size-range of 3 to 6 nm while the intercrystalline dimensions are on the size-range of 10 to 25 nm, meaning that the crystallite sizes are too large to be incorporated between ionic domains.[9] Thus, we propose that the increase in scattering contrast of the ionomer peak by annealing at 300 °C is not due to melting of the PTFE crystallites, but a result of some increase in electron density of the ionic domains at these elevated temperatures in the TMA^+-form. As demonstrated in **Chapter 6**, scattering contrast of the ionomer peak in PFSAs is affected by electron density differences between the ionic aggregates and amorphous PTFE matrix and the volume fraction of each phase. In this TMA^+ annealing study, the increase in intensity may be attributed to lone TMA^+ counterion pairs being incorporated into the ionic aggregates upon annealing,[29] which then increases the volume fraction of the ionic phase. In 3M PFSA and 3M PFIA, where the content of sulfonate groups (plus additional sulfonimide groups in PFIA) and TMA^+ counterions is much higher than Aquivion and Nafion, this effect is much more pronounced and therefore leads to a larger increase in scattering intensity upon annealing.

To determine whether this morphology obtained by annealing in the TMA^+-form persists upon reacidification to the H^+-form, the TMA^+-annealed membranes were stirred in 8 M nitric acid for 24 hours at room temperature and SAXS experiments were performed on the reacidified membranes. SAXS profiles for reacidified, hydrated 3M PFSA and 3M PFIA membranes are shown in **Figure 7-4**. The ionomer peaks for all four samples in the reacidified, hydrated-form are observed at lower scattering angles than the dry TMA^+-form. This is typical of PFSA membranes where the ionomer peak shifts to lower scattering angles (larger dimensions) upon hydration, due to swelling of the ionic domains.[39] From this experiment, it is clear that the increase in intensity of

the ionomer peak upon annealing at 300 °C in the TMA^+-form persists upon reacidification for both 3M PFIA and 3M PFSA. Again, the increase is more profound in PFIA. In 3M PFSA, while the annealed sample still shows an increase in the intensity of the ionomer peak, the breadth of the peak is less narrow than it was in the TMA^+-form. This was also observed in the TMA^+-annealed Nafion 117 samples, where it was concluded that the reacidification process leads to a more heterogeneous distribution of domain sizes.[33] However, based on the increased intensity of the ionomer peak after the TMA^+-annealing step and reacidification, there is evidence that this annealing method can be used to manipulate the morphology of H^+-form PFSA membranes and ultimately improve membrane properties, which will be investigated in following sections.

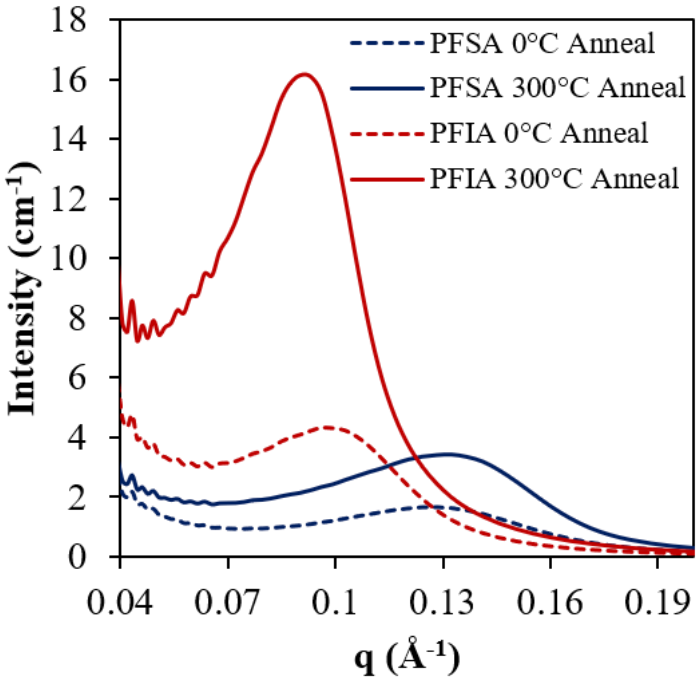

Figure 7-4. SAXS profiles for 3M PFSA and PFIA before and after annealing in the TMA^+-form at 300 °C then converted to the hydrated H^+-form.

7.3.2 Wide Angle X-ray Diffraction

While SAXS probes long-range phase homogeneity of the ionic domains, wide-angle X-ray diffraction (WAXD) can provide information about short-range ordering inside the ionic clusters. Previous studies from our group have documented the appearance of a new peak in WAXD patterns for Nafion 117 in alkylammonium counterion forms ranging in size from TMA^+ to TBA^+ at scattering angles below that of the amorphous halo.[32] With increasing counterion size, this diffraction peak shifts to lower scattering angles. Additionally, upon annealing Nafion membranes in the TMA^+-form, this extra peak increases in intensity and a second sharp peak appears at 17.5° 2θ with increasing annealing temperatures up to 250 °C. The previous studies from our group have attributed this increase in peak intensity with annealing temperatures to a crystalline-like ordering of the TMA^+ counterions within the ionic aggregates.[29,32,33]

WAXD data for 3M PFSA and 3M PFIA annealed at increasing temperatures for ten minutes in the TMA^+-form are presented in **Figure 7-5**. In the as-cast (No Anneal) samples, there is a broad amorphous halo in the 18° 2θ range and an additional peak at 39° 2θ. In PFSAs with higher degrees of crystallinity, an additional reflection is observed at ca. 18° 2θ, which is attributed to the *hkl* (100) plane of PTFE-like crystallites. In these low EW PFSAs, the weak crystalline reflection at 18° 2θ is difficult to deconvolute from the broad amorphous halo in the same vicinity. The reflection at 39° 2θ is attributed to intrachain distances associated with both the amorphous- and crystalline-phase.[9] An additional shoulder to the left of the amorphous halo is also observed in the as-cast samples. With increasing annealing temperature, that shoulder increases in intensity and prominence. This increase is most profound in the 3M PFIA membranes where the reflection becomes extremely sharp (well-ordered) at the 300 °C annealing temperature. An additional sharp reflection appears at 18° 2θ with increasing annealing temperature in both the 3M PFSA and 3M

PFIA membranes. Both of these reflections continue to increase in intensity at annealing temperatures well above the melting temperature of PTFE-like crystallites in PFSAs (ca. 250-275 °C) and thus must be attributed to crystalline-like ordering of the TMA^+ counterions within the ionic domains as opposed to an increase in PTFE-like crystallinity.

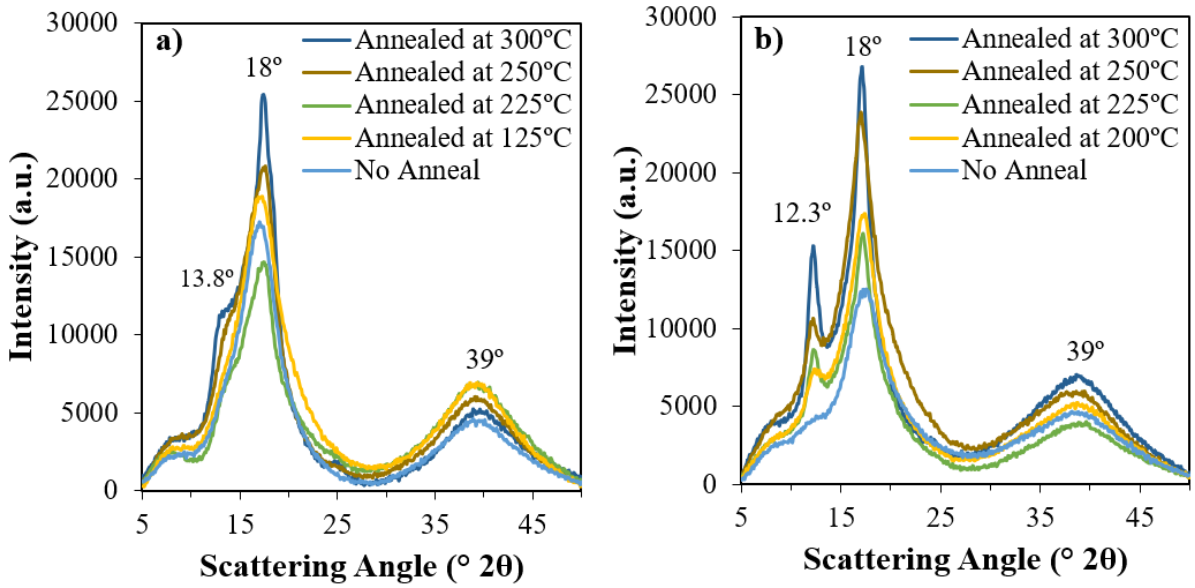

Figure 7-5. WAXD profiles of a) 3M PFSA and b) 3M PFIA annealed at various temperatures in the TMA^+-form.

7.3.3 Thermal and Thermomechanical Characterization

Differential scanning calorimetry (DSC) thermograms for the first heat of TMA^+-form 3M PFSA, 3M PFIA, Aquivion and NRE are shown in **Figure 7-6**. The first heat scans were taken after a drying step for two hours at 120 °C prior to cooling to the starting temperature of 0 °C. The small endotherm observed at ca. 150 °C in all of the samples is attributed to melting of small crystallites formed in the sample during the drying step and can be disregarded.[17] A second small melting endotherm is observed in 3M PFSA and 3M PFIA at ca. 250 °C. Both of these melting endotherms disappear upon cooling and second heat, and are attributed to melting of PTFE-like

crystallites in the samples. In all four PFSAs, a large endotherm is observed at higher temperatures than the PTFE-melting temperatures (likely overlapping with the PTFE-melting endotherm in NRE and Aquivion). This temperature persists upon cooling and reheating. In previous studies from our group on Nafion 117, this endotherm was attributed to the melting, or disordering, of well-ordered TMA^+ counterions within the ionic aggregates.[33] The temperature at which this disordering appears varies depending on the PFSA type. In 3M PFIA and 3M PFSA, this melting endotherm appears at temperatures of 300 °C and higher, while it occurs at lower temperatures for NRE and Aquivion.

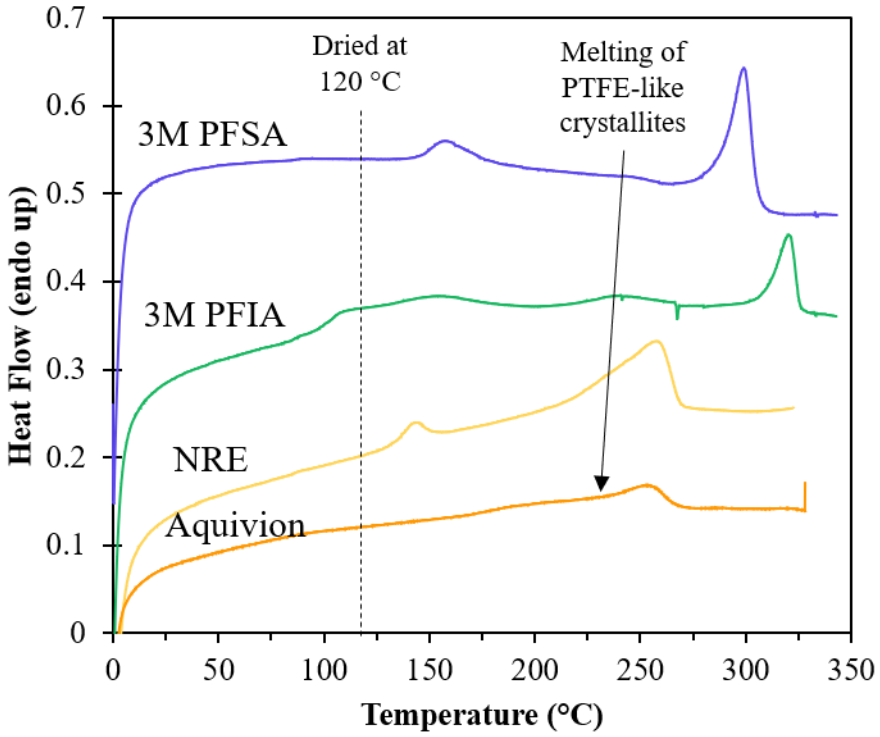

Figure 7-6. DSC first heat thermograms for TMA^+-form 3M PFSA, 3M PFIA, NRE, and Aquivion after a drying step at 120 °C for two hours.

Dynamic mechanical analysis of TMA^+-form 3M PFSA, 3M PFIA, NRE, and Aquivion are shown in **Figure 7-7**. In the three PFSAs (excluding 3M PFIA), two relaxations are observed

in the tanδ data. As mentioned previously, the lower temperature β-relaxation is attributed to the onset of segmental motions, primarily of the backbone, within a static electrostatic network.[17] The second relaxation at higher temperatures, termed the α-relaxation, is attributed to long-range motions of the main and sidechains upon destabilization of the electrostatic network due to the onset of ion-hopping. The temperature of the α-relaxation for each of the PFSAs is approximately in the same temperature range of the melting endotherm observed by DSC, as listed in **Table 7-2**. From this data, a link between the melting of ordered TMA^+ counterions and the onset of long-range polymer chain mobility is established. At elevated temperatures that melt the crystalline-like ordering of the TMA^+ counterions in the ionic domains of PFSAs, long-range mobility of the main and sidechains begin to occur. The strange behavior of 3M PFIA compared to the PFSAs will be discussed at the end of this section.

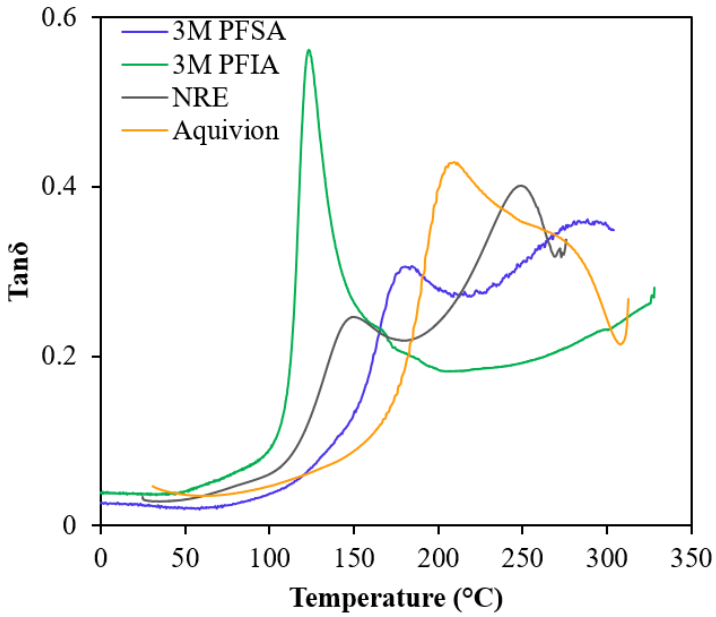

Figure 7-7. Dynamic mechanical tanδ versus temperature for 3M PFSA, 3M PFIA, NRE, and Aquivion in the TMA^+-form.

Table 7-2. Temperature of the DSC endotherm and α-relaxation from the dynamic mechanical tanδ data for 3M PFSA, 3M PFIA, NRE, and Aquivion.

	DSC Endotherm	**α-Relaxation**
3M PFSA	300 °C	290 °C
3M PFSA	320 °C	120 °C
NRE	260 °C	260 °C
Aquivion	270 °C	270 °C

DSC cooling thermograms of 3M PFSA, 3M PFIA, NRE, and Aquivion in the TMA^+-form are presented in **Figure 7-8**. Upon heating to 350 °C and cooling back to 0 °C at a cooling rate of 10 °C/min, a large exotherm is observed for all four PFSAs. This exotherm persists regardless of cooling rate, even appearing at cooling rates in excess of 60 °C/min (data not shown), emphasizing how rapidly this ordering occurs upon cooling. More information is necessary to explain the mechanism behind the increased magnitude and narrowing of the ordering exotherm in 3M PFSA, although it may be related to the ionic sidechain length and sidechain content compared to NRE and Aquivion. The 800 EW 3M PFSA has functional sidechain content of 19 mol %, NRE has 13 mol %, and Aquivion has 14.5 mol % ion content. Similar to a polymer in the nucleation-controlled regime at temperatures above the crystallization temperature, short-range diffusion occurs rapidly and a kinetically stable surface must be established in order to begin nucleation. In these TMA^+-form PFSAs at elevated temperatures, chain mobility is high and the likelihood of two TMA^+-sulfonate groups colliding to begin the crystalline-like ordering process is low. In 3M PFSA, the higher fraction of TMA^+-sulfonated in the polymer increase the probability of collisions between contact-ion pairs, and thus ordering begins at higher temperatures. In Nafion and Aquivion, the fraction of TMA^+-sulfonates in the system are lower and the probability of two coming into contact

at high thermal energies is decreased, so their exotherm appears at lower temperatures. Additionally, Aquivion has a shorter sidechain than Nafion, also reducing mobility and the temperature at which this ordering occurs. I must emphasize here that this is an initial attempt to explain the different exotherm temperatures for this ordering process that has not been observed in ionomers previously. More investigation of this this thermal behavior will be necessary to uncover the underlying mechanism of this thermal ordering, but these sharp exotherms that appear regardless of cooling rate in these TMA^+-form PFSAs is very intriguing.

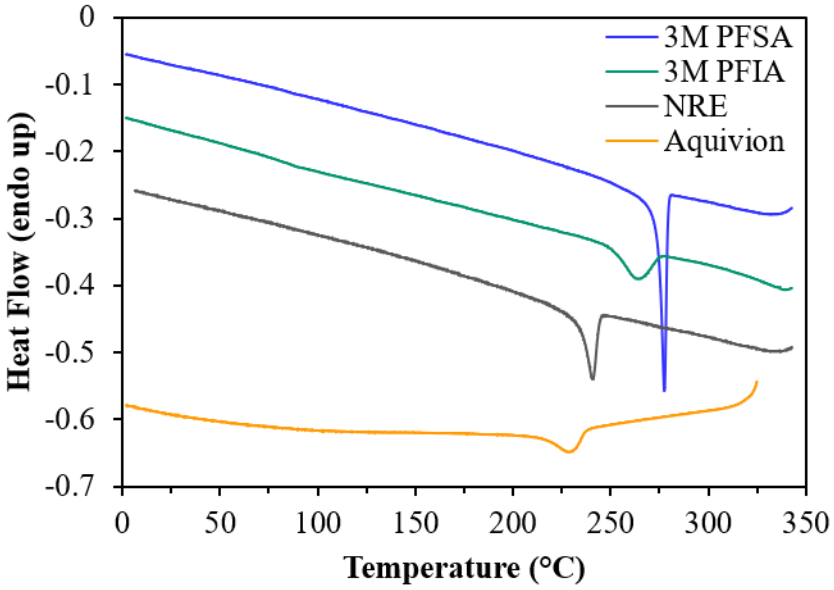

Figure 7-8. DSC cooling thermograms for TMA^+-form 3M PFSA, 3M PFIA, NRE, and Aquivion.

Figure 7-9 shows the DSC thermograms of TMA^+-form 3M PFSA annealed at various temperatures for ten minutes. Two endotherms are visible in the thermograms of the membranes annealed below 280 °C. Upon annealing at 280 °C, the high temperature endotherm increases in magnitude and sharpens. Park showed that annealing Nafion 117 in the TMA^+-form at 200 °C for

different lengths of time led to a second melting endotherm approximately 20-30 °C above the annealing temperature, that increased in magnitude with increasing annealing time. In agreement with a study by Page and coworkers, this low temperature endotherm was assigned as melting of PTFE-like crystallites that are formed from annealing.[17] Divoux then annealed TMA^+-form Nafion 117 at different temperatures and showed that the low temperature endotherm increased with increasing annealing temperature.[33] Upon annealing TMA^+-form Nafion at 250 °C for ten minutes, only one endotherm was observed that was attributed to the disappearance of well-ordered counterions. The DSC thermograms for 3M PFSA annealed at different temperatures in the TMA^+-form are in good agreement with these previous studies. Melting of the PFSA crystallites occurs below 280 °C, and thus the high temperature endotherm that is observed in the 280 °C-annealed sample must be attributed to disordering of the TMA^+ counterions. The increased sharpness of that peak indicates increased ordering as a result of the ten-minute annealing step.

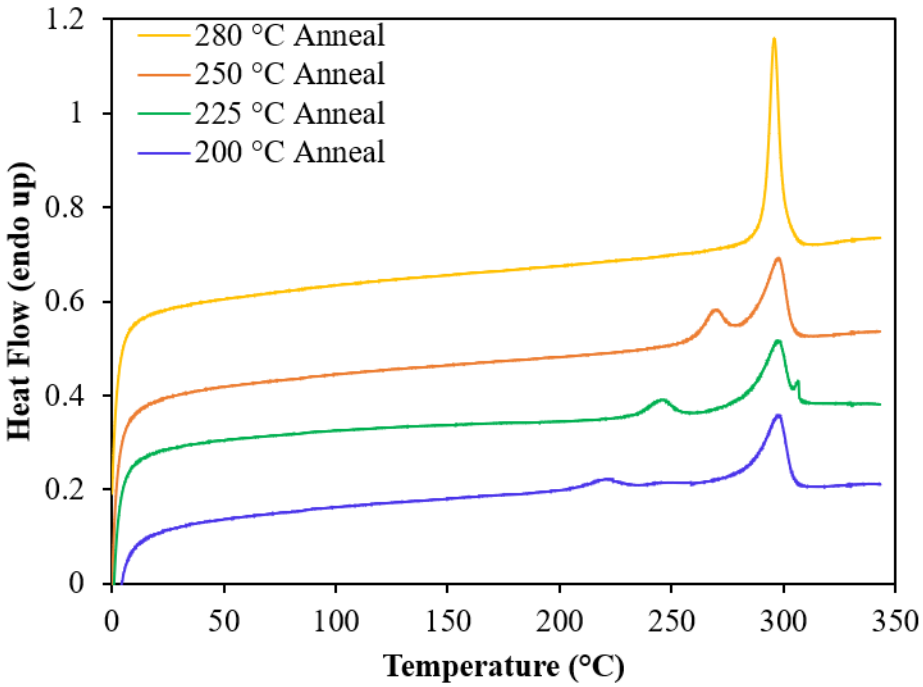

Figure 7-9. DSC thermograms for 3M PFSA annealed at various temperatures in the TMA^+-form.

In the TEA^+-form, this ordering peak is no longer observed the DSC thermograms for 3M PFSA. In TEA^+-form Nafion 117, an endotherm attributed to disordering of well-ordered counterions was observed, as well as evidence of ordering at elevated temperatures by X-ray scattering experiments.[32] However, in 3M PFSA, it appears that the bulkier size of TEA^+ counterions are not able to efficiently pack within the ionic aggregates. In order to emphasize the disruption of counterion packing by introduction of a bulky counterion, we look at DSC thermograms of mixed counterion membranes of 3M PFSA with varying ratios of TMA^+ to TEA^+ shown in **Figure 7-10**. In these thermograms, the samples were heated up to 350 °C to erase thermal history, then cooled back to the starting temperature of 0 °C at a rate of 10 °C/min before collecting the second heat data. Upon second heat, the "melting" endotherm for the disordering of TMA^+ counterions is observed at ca. 300 °C in the 100% TMA^+-form membrane. With increasing TEA^+ counterion content, that endotherm decreases in magnitude and temperature. It appears that adding in a bulkier counterion to the system serves to disrupt the packing of the TMA^+ counterions that is observed in the 100% TMA^+-form. It is important to note that the ordering affect is observed in TEA^+-form Nafion but not in 3M PFSA. Further investigation is required to understand the different counterion sizes and their ability to order within the ionic domains of different PFSA structures.

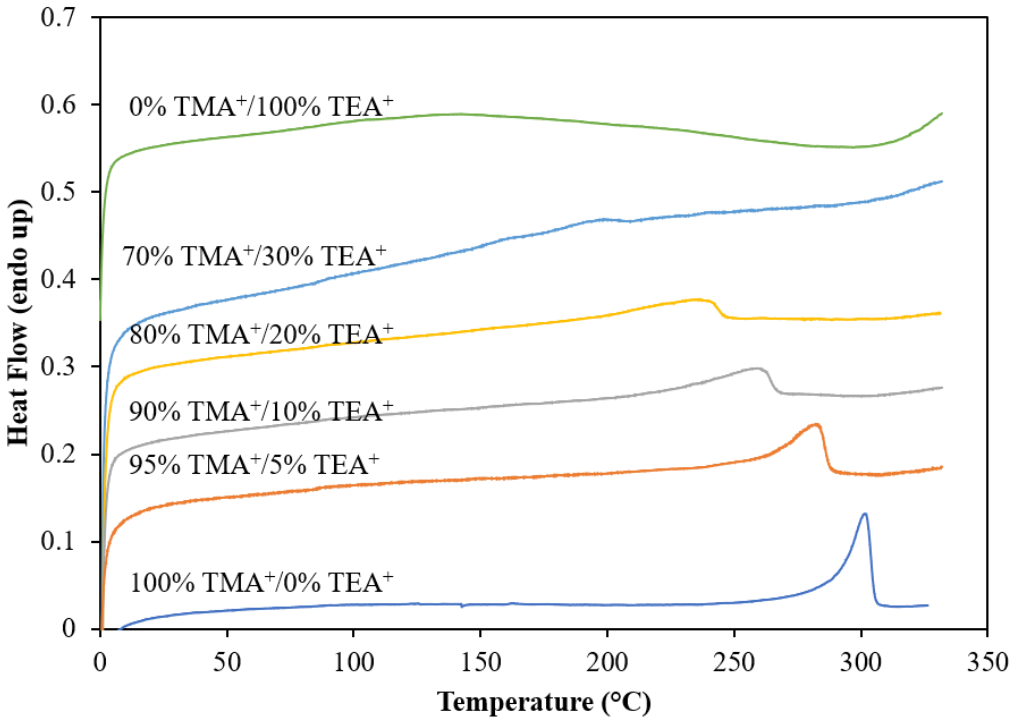

Figure 7-10. DSC second heat thermograms for mixed counterion TMA^+/TEA^+ 3M PFSA membranes.

For the three single sulfonic acid PFSAs, the melting endotherm observed by DSC occurs at the same temperature as the α-relaxation in DMA. This is not the case for 3M PFIA, which requires some further explanation. The 3M PFIA has been shown to have some anomalous thermomechanical behavior in comparison to 3M PFSA, as discussed in **Chapter 4**. DMA data of Na^+-form and TMA^+-form 3M PFIA are shown in **Figure 7-11**. In the Na^+-form, PFIA passes through, what we previously assigned as the α-relaxation, at ca. 180 °C. While we attribute this large peak in tanδ and drop in the storage modulus to long-range mobility of the ionomer main chains and sidechains as a result of destabilization of the electrostatic network, there is still some mechanical integrity maintained above this relaxation as observed by the rubbery plateau in the storage modulus. It is to be noted that 3M PFIA has two ionic groups per sidechain, both of which act as anchors restricting the sidechains within physically crosslinked aggregates.[40] Although the

chains become much more mobile at temperatures above the α-relaxation, the probability that both anchors on the sidechain participate in ion hopping (i.e., thermally activated process of ion pairs "hopping" from one aggregate to another)[17] at the same time is low, meaning that there are still some physical crosslinks at these elevated temperatures. In the TMA^+-form, there is an increase in storage modulus above the α-relaxation. This can only be attributed to some additional ordering within the membrane that increases the stiffness of the material. The storage modulus then drops off below the instrument sensitivity after reaching the temperature of the melting endotherm observed in DSC (320 °C). In 3M PFIA, clearly this additional ionic site increases the effect of this thermal ordering in the TMA^+-form. This is evidenced by the large increase in intensity of the SAXS peak, very well-ordered sharp crystalline peak in WAXD, high temperature melting endotherm observed by DSC, and now this increase in storage modulus above the α-relaxation.

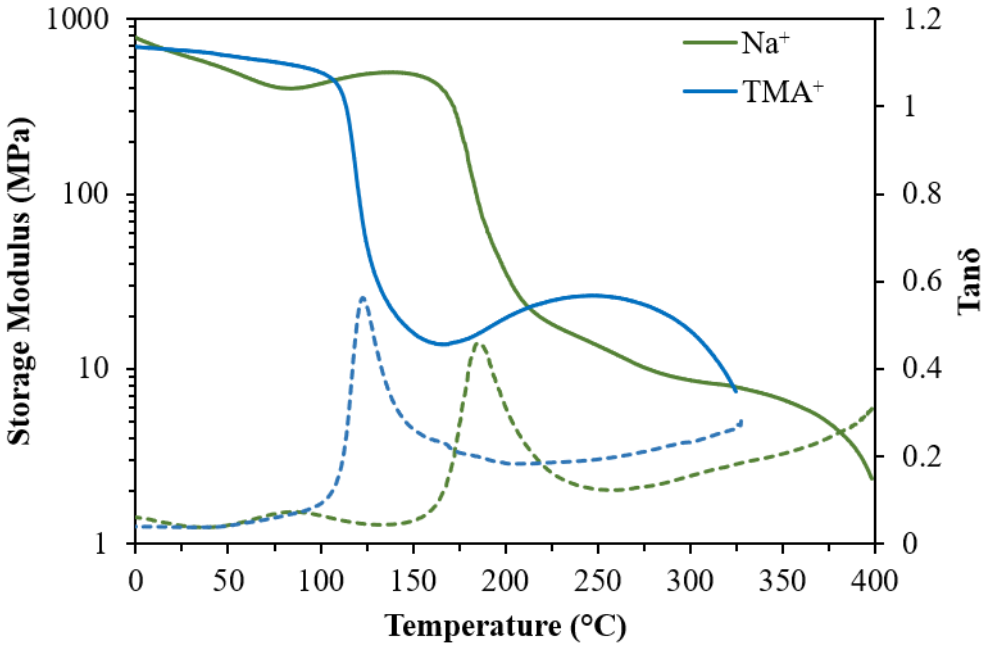

Figure 7-11. Dynamic mechanical storage modulus and tanδ data for TMA^+ and Na^+-form 3M PFIA.

7.3.4 Variable Temperature SAXS

Variable temperature SAXS (VT-SAXS) has been used to assign the morphological origins of thermomechanical relaxations in Nafion counterion-exchanged with TMA^+, TEA^+, TPA^+, and TBA^+.[17] In all four counterions, the ionomer peak was observed in at room temperature, but decreased in intensity upon heating through the α-relaxation temperature up to 300 °C. This was attributed to the destabilization of the electrostatic network as the process of ion hopping begins in order to reduce local stress from elastic stresses exerted on the chains in the vicinity of the aggregates. It was noted that the decrease in ionomer peak intensity through this relaxation was likely due to an increase in the time-averaged distribution of ion pairs on the time-scale of the measurement (1 minute).

A similar experiment was performed on TMA^+-form 3M PFSA and 3M PFIA as shown in **Figure 7-12** and **Figure 7-13**. Dry, TMA^+-form membranes were heated from 50 to 350 °C at a heating rate of 5 °C/min and data was collected for 15 seconds every one minute. In 3M PFSA, the initial SAXS profile at 50 °C shows the appearance of the intercrystalline peak at ca. q = 0.05 $Å^{-1}$ and the ionomer peak at q = 0.2 $Å^{-1}$. With increasing temperature, the intensity of the intercrystalline peak increases due to thermal expansion of the amorphous phase, which alters the scattering contrast for that feature.[17] Around 250 °C, the intensity of the intercrystalline peak decreases to extinction, marking the melting of the PTFE-like crystallites. The ionomer peak also appears to decrease in intensity as temperature increases. At temperatures between 115 °C and 250

°C, the ionomer peak becomes convoluted with the intercrystalline peak. However, as temperatures approach the α-relaxation temperature (290 °C), the ionomer peak appears to have completely disappeared, similar to the observations of the previous study on Nafion, and attributed to the destabilization of the electrostatic network.[17]

Intriguingly, the ionomer peak reappears as the membrane approaches temperatures of 300 °C and above. This phenomenon is profound and unexpected from the evidence gathered in the previous sections. Based on DSC evidence, TMA^+-form 3M PFSA passes through a *disordering* phase at 300 °C, resulting in an endothermic peak at that temperature. The *ordering* exotherm appears upon cooling. Yet, there appears to be long-range ordering at temperatures above this melting endotherm observed by VT-SAXS. While this finding is preliminary and will require further studies to confirm this new phenomenon, we may attribute the discrepancy between the melting endotherm in DSC and the increase in ionomer peak in variable temperature SAXS by the different length scales that are probed by each method. DSC and WAXS are capable of measuring material properties related to short-range ordering. In WAXS, the sharp crystalline-like reflection observed in TMA^+-annealed PFSAs is associated to a Bragg dimension of 6-7 Å and attributed to a crystalline-like spacing between ordered TMA^+ counterions within in the ionic domains. When disordering of these TMA^+ counterions occurs, a melting endotherm is visible by DSC. In SAXS, however, the ionomer peak is associated with long-range inter-aggregate dimensions of ca. 30 Å in length. The decrease in the ionomer peak intensity with increasing temperature means that the

distribution in domain sizes very broad, due to the onset of ion hopping, such that the ionomer peak disappears. Above 300 °C, the distribution in domain sizes begins to narrow, meaning that some unknown driving force for the TMA^+-sulfonates to aggregate arises at these high temperatures, but the ion pairs within these domains are likely still mobile and the TMA^+ counterions do not form the crystalline-like packing until cooling (as observed by the exotherm in DSC on cooling). Obviously, future studies are necessary to verify this hypothesis and will be outlined in the Future Work section of this chapter.

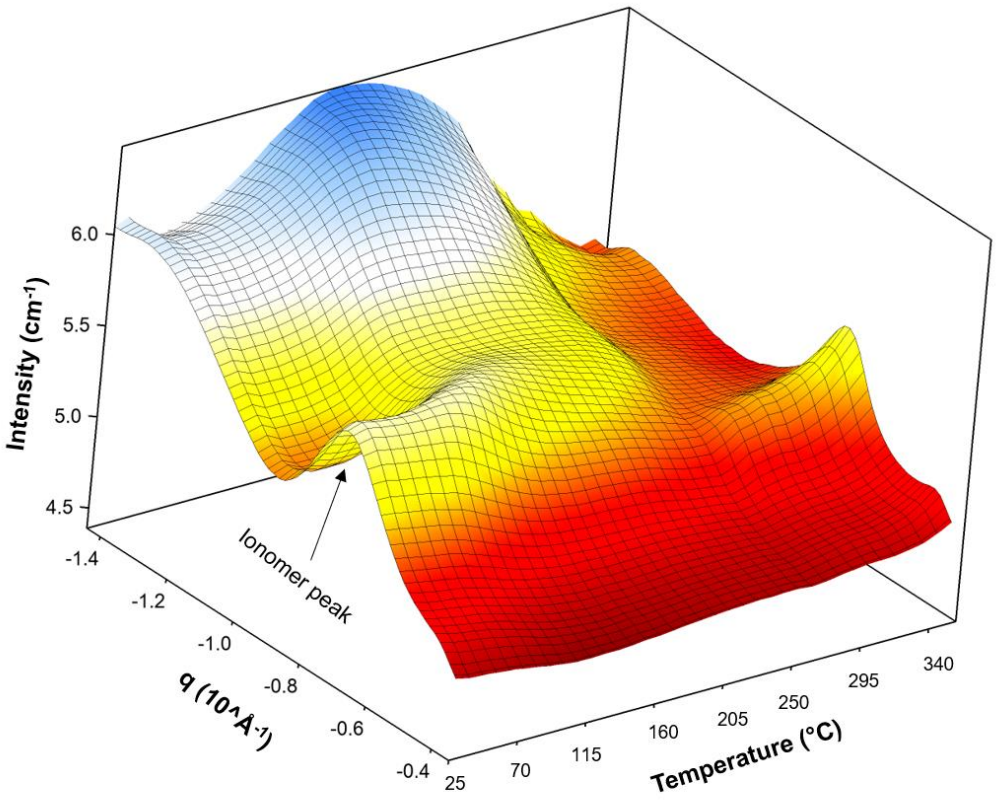

Figure 7-12. Variable temperature SAXS profiles for 3M PFSA in the TMA^+-form.

Variable temperature SAXS data for TMA^+-form 3M PFIA are shown in **Figure 7-13**. Similar to 3M PFSA, an intercrystalline peak is present at q = 0.05 $Å^{-1}$ and ionomer peak at q = 0.15 $Å^{-1}$ in the 50 °C SAXS profile. As the temperature is ramped, the intercrystalline peak follows the same trend as observed for 3M PFSA and disappears above the melting temperature of 250 °C. Contrary to TMA^+-form 3M PFSA, the ionomer peak never disappears with increasing temperature. As hypothesized previously to explain the anomalous DMA data for PFIA, although the PFIA structure passes through an α-relaxation at lower temperatures than 3M PFSA, full disruption of the electrostatic network is unlikely due to the two ionic sites per sidechain anchoring each sidechain within the aggregates. Even with the onset of ion hopping, the probability of both ionic groups on a sidechain being able to "hop" to another aggregate at the same time is low. Although the ionomer peak for TMA^+-form 3M PFIA does not disappear with increasing temperature, it does decrease in intensity slightly. Above the 320 °C (the temperature at which the melting endotherm is observed by DSC) the ionomer peak increases in intensity, similar to what was observed for 3M PFSA.

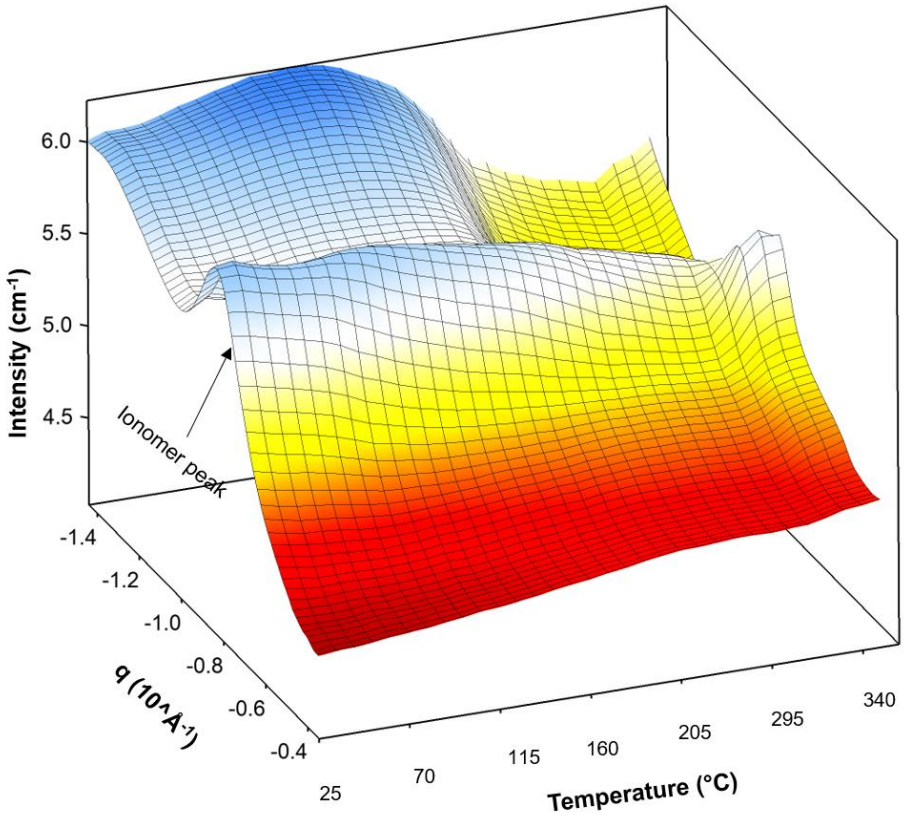

Figure 7-13. Variable temperature SAXS profiles for 3M PFIA in the TMA^+-form.

7.3.5 Proton Conductivity

It has been established that annealing PFSA membranes in the TMA^+-form allows for a reorganization of the morphology that increases the ordering of the ionic domains that appears to be maintained upon reacidification to the sulfonic acid-form. It is of interest to our research group and the fuel cell community to determine whether this improved ordering leads to improvements in fuel cell performance. One of the critical properties of a proton exchange membrane for fuel cell performance is its proton conductivity. **Figure 7-14** shows the proton conductivity versus relative humidity (RH) of reacidified 3M PFSA, 3M PFIA, Aquivion, and NRE before and after

annealing in the TMA^+-form. For each ionomer, the annealing temperature was chosen based on the maximum observed reordering from SAXS data and DSC data in the previous sections. For each PFSA, the proton conductivity increases across all RH levels after annealing in the TMA^+-form. On a linear scale, the difference is noticeable, but on the log scale NRE has the largest increase in proton conductivity upon annealing, especially at low relative humidities where water uptake plays less of a role.[9] Divoux has shown that a small improvement in proton conductivity can lead to a large improvement in fuel cell performance of Nafion membranes that were annealed in the TMA^+-form.[33] Therefore, it appears that this annealing method prior to reacidification is a simple method for improving fuel cell performance of 3M PFSA, 3M PFIA, Aquivion, and Nafion (both NRE and 117) membranes.

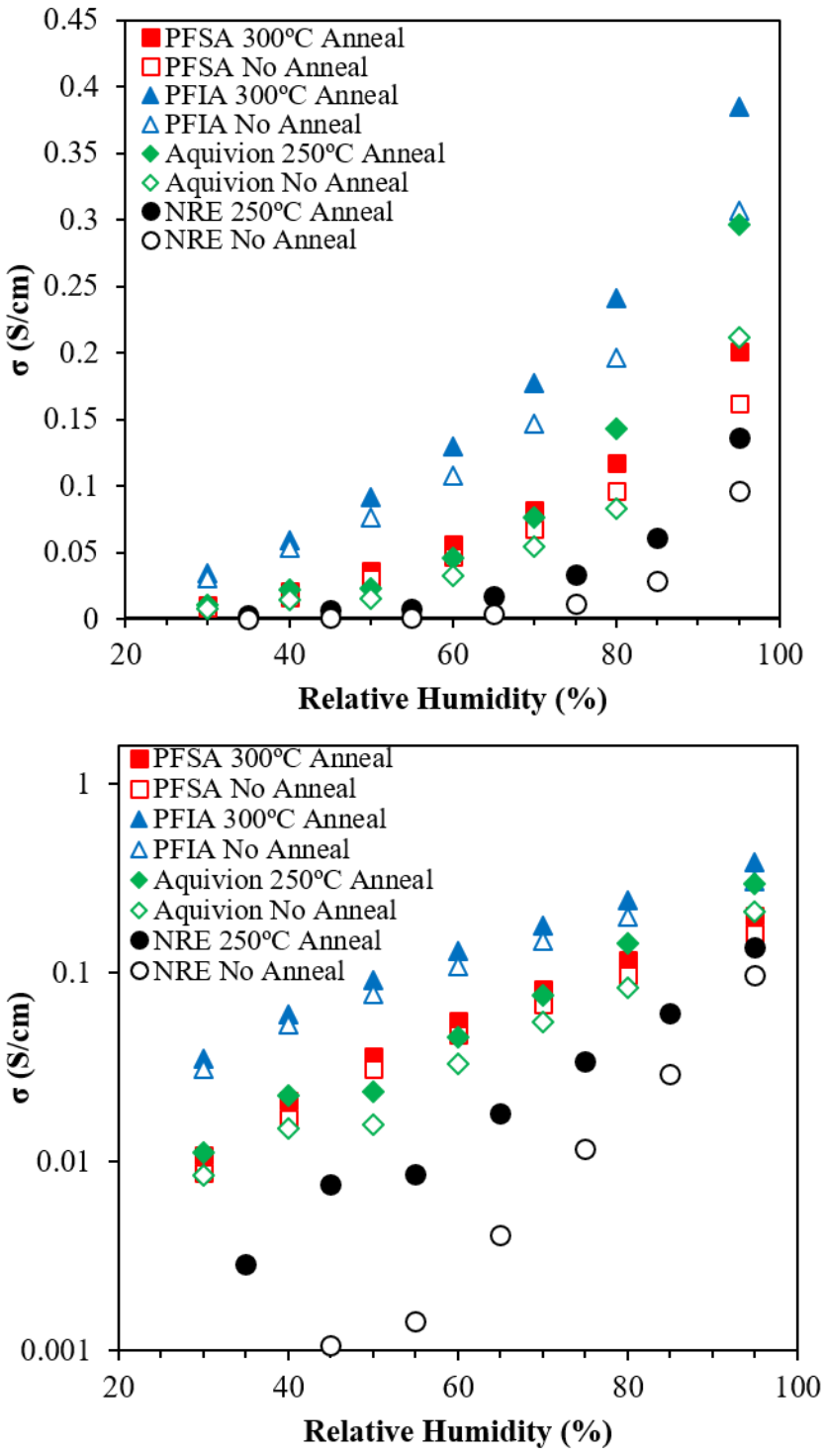

Figure 7-14. Proton conductivity of 3M PFSA, 3M PFIA, Aquivion, and NRE before and after annealing in the TMA-form.

7.3.6 Water Uptake

While Nafion and Aquivion show signs of ordering after annealing at temperatures near or below the melting temperature of the PTFE-like crystallites, 3M PFSA and 3M PFIA require temperatures of 300 °C to see the effects of annealing. In this case, it is important to establish whether the improvement in proton conductivity is the result of decreased crystallinity in these membranes that allows for greater levels of hydration, or if it is a result of the increased ordering of the ionic domains. Water uptake isotherms for the reacidified PFSA membranes at room temperature (25 °C) before and after annealing in the TMA^+-form are shown in **Figure 7-15**. All membranes were annealed at the maximum temperature of 300 °C in the TMA^+-form then reacidified by submersing in 8 M HNO_3 at room temperature. In relative humidity (RH) ranges below 75%, there is no discernable difference between the water uptake isotherms for any of the ionomers with annealing. Only at high RH values do you see a slight increase in water uptake after the annealing step. This is not surprising, as crystallinity has been shown to affect the uptake of water by PFSAs within the "free-water regime" at high RH levels.[9] Although the annealing step appears to increase the water content at high RH levels, which likely contributes to an increase in proton conductivity,[20,41] the proton conductivity also appears improved across all water contents and therefore, is likely a result of the ordering of the ionic domains.

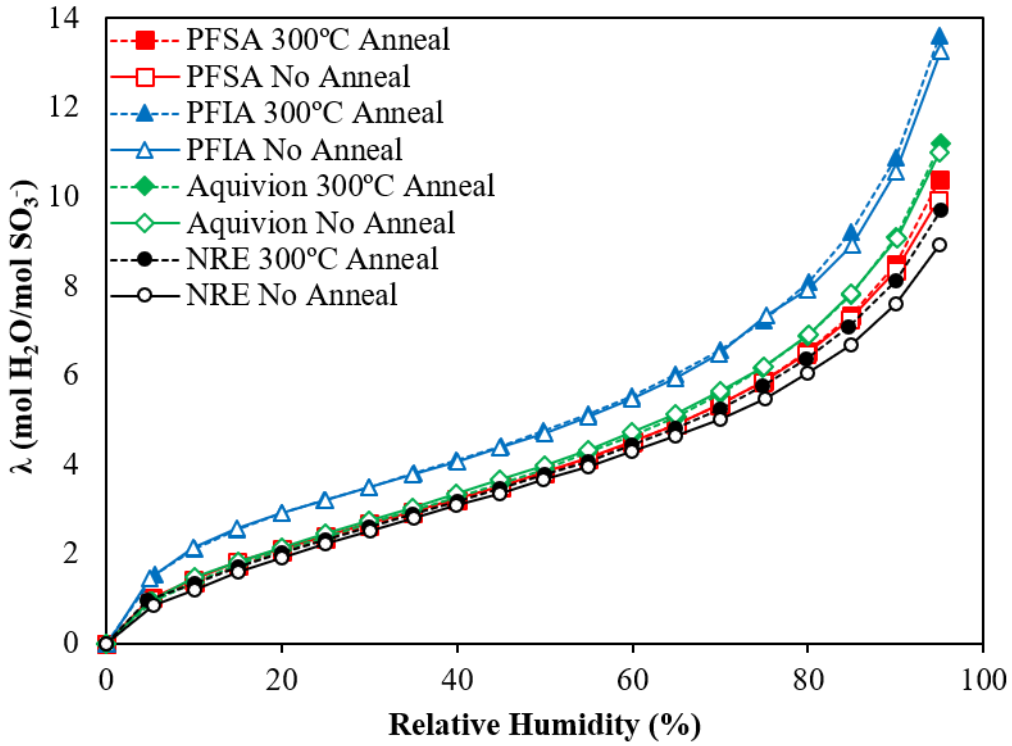

Figure 7-15. Water uptake isotherms for 3M PFSA, 3M PFIA, Aquivion, and NRE before and after annealing in the TMA^+-form and reacidified.

7.4 Conclusions

Here we have presented a method of altering the morphology of the ionic domains in PFSAs by annealing in the TMA^+-counterion form. TMA^+-form PFSAs of different sidechain structures and contents show an increase in long-range and short-range ordering by SAXS and WAXD measurements upon annealing at elevated temperatures. The short-range ordering is attributed to a crystalline-like packing of TMA^+ counterions within the ionic domains. This packing is observed to disorder at temperatures in the vicinity of the α-relaxation for each ionomer as observed through an endotherm in DSC. Ordering then occurs upon cooling of the membranes, and the temperature at which ordering happens is dependent on the sidechain structure and/or ion content. Variable temperature SAXS showed that the ionomer peak decreased in intensity through

the α-relaxation but then increased in intensity again at the same temperature at which the melting endotherm is observed by DSC. This phenomenon of an order-disorder-order transition in PFSAs has never been documented before and requires further studies to explain the underlying mechanism. Static SAXS of TMA^+-annealed membranes after reacidifying to the sulfonic acid form showed that the increased long-range ordering is maintained even after the reacidifying, indicating that this method can be used as a simple processing method for obtaining improved morphologies in fuel cell membranes. This is further emphasized by the increase in proton conductivity of membranes that were annealed in the TMA^+-form and reacidified.

7.5 Future Work

The observed phenomenon of ordering of TMA^+ counterions in PFSAs has now been studied by multiple students in our research group and is an ongoing effort. Although the goal of the work in this chapter was to use different sidechain structures and ion contents to provide more evidence on the underlying mechanism of this ordering, it has only left us with more questions than answers. However, based on some of the findings in this chapter, some new experiments may provide the answers that we are looking for. To start, we will address some of the remaining questions:

1. Why is this ordering phenomenon only observed with TMA^+ counterions and not in any alkali counterions like Na^+, K^+, or Cs^+?
2. What is the driving force for ordering between TMA^+ counterions?
3. What is the origin of the increase in ionomer peak intensity at these elevated temperatures, and how does it relate to the scattering reflection observed by WAXS and the melting endotherm in DSC?

4. Is this phenomenon limited to PFSAs or does it occur in other hydrocarbon-based ionomer systems?

To address the first question, molecular modeling studies may be required. Does the size of the TMA^+ counterion allow it to pack within the ionic domains better than other counterions? The crystallographic radius of the TMA^+ counterion is 3.20 – 3.47 Å.[28,42,43] This radius is already two times the radius of the largest alkali metal counterion, Cs^+, with an ionic radius of 1.67 Å.[44] While solid state NMR studies have provided some information on the molecular motions of TBA^+ and TPA^+ counterions in Nafion at temperatures spanning the α-relaxation,[29] the strong electrostatic interactions between TMA^+ counterions and the sulfonate groups lead to an α-relaxation temperature above the range of standard variable temperature NMR probes, making it impossible to collect direct evidence of ordering at these high temperatures. Solid state ^1H T_1 experiments show some indirect evidence of ordering of the TMA^+ counterions as temperatures increase, however this method looks at the protons on the methyl groups of the TMA^+ counterion so it is impossible to compare with other counterions of the similar dimensions, such as Cs^+. Because some of these investigations go beyond the capability of experimental studies, molecular modeling studies may be useful to provide some insight on the mechanism behind the ordering of the TMA^+ counterion.

Model compounds may also provide insight into this ordering phenomenon. We specifically began looking for a small molecule compound, such as a perfluorinated sulfonate-TMA^+. However, in light of the environmental impacts of those perfluorinated small molecules (e.g., PFOA), a polymer-based model compound may be best. For example, our group has demonstrated the ability to brominate poly(ether ether ketone) and react a perfluorinated sidechain onto the bromine groups.[45] The same reaction may be performed on polystyrene to provide a simplified

model compound. Upon creating this compound, DSC, WAXD, and SAXS studies would show whether this ordering phenomenon is also observed.

Further studies on the work presented in this chapter are also needed to confirm some of the conclusions hypothesized. First, using a 3M PFSA of the same ion content as the Nafion and Aquivion would help eliminate the experimental variable of sidechain content on the temperatures of the observed order/disorder endotherms and exotherms by DSC. Additionally, with a 1000 EW 3M PFSA, which contains the most crystallinity, we could anneal at 300 °C in the TMA^+-form, then anneal again at temperatures below the melting point to re-induce crystallinity in the membrane. Then the intercrystalline peak should still be visible by SAXS and the increase in intensity of the ionomer peak would be attributed to ordering of the ionic domains and not just an increase in contrast from melting of the PFSA-like crystallites.

More variable temperature X-ray experiments are also necessary. First, the ordering at high temperatures observed in variable temperature SAXS is very interesting, and necessitates the SAXS data upon cooling. Since a DSC exotherm is observed upon cooling that we associate with ordering of the ionic domains, do we see any change in the SAXS patterns when cooling from 350 to 50 °C, that may support this? Additionally, the endotherm and exotherm in DSC are attributed to short range order/disorder while the SAXS data is associated with long-range ordering. Variable temperature WAXS should confirm the observed DSC data where the short-range ordering (sharp scattering reflection observed) disappears above temperatures of the melting endotherm in DSC.

7.6 Acknowledgments

The authors acknowledge 3M for providing PFSA materials for this study and for funding this research. This research used resources of the Advanced Photon Source (APS) and a U.S.

Department of Energy (DOE) Office of Science User Facility operated for the DOE Office of Science by Argonne National Laboratory under General User Proposal Number 49574. Variable temperature SAXS data were collected on the 9-ID-C beam line at the APS, Argonne National Laboratory.

7.7 References

1. Mauritz, K. A.; Moore, R. B., State of Understanding of Nafion. *Chem. Rev.* **2004**, *104*, 4535.
2. Doyle, M.; Rajendran, G., Perfluorinated membranes. *Handbook of fuel cells* **2010**.
3. Hamrock, S. J.; Yandrasits, M. A., Proton Exchange Membranes for Fuel Cell Applications. *J. Macromol. Sci., Rev. Macromol. Chem. Phys.* **2006**, *46*, 219.
4. Stassi, A.; Gatto, I.; Passalacqua, E.; Antonucci, V.; Arico, A.; Merlo, L.; Oldani, C.; Pagano, E., Performance comparison of long and short-side chain perfluorosulfonic membranes for high temperature polymer electrolyte membrane fuel cell operation. *J. Power Sources* **2011**, *196*, 8925.
5. Arcella, V.; Ghielmi, A.; Merlo, L.; Gebert, M., Membrane electrode assemblies based on perfluorosulfonic ionomers for an evolving fuel cell technology. *Desalination* **2006**, *199*, 6.
6. Hamrock, S., New membranes for PEM fuel cells. *Advances in Materials for Proton Exchange Membrane Fuel Cell Systems, Pacific Grove, CA* **2005**.
7. Emery, M.; Frey, M.; Guerra, M.; Haugen, G.; Hintzer, K.; Kai; Lochhaas, H.; Pham, P.; Pierpont, D.; Schaberg, M.; Thaler, A.; Yandrasits, M.; Hamrock, S., The Development of New Membranes for Proton Exchange Membrane Fuel Cells *J. Electrochem. Soc.* **2007**, *11*, 3.

8. Grot, W. G., Perfluorinated ion exchange polymers and their use in research and industry. *Macromol. Symp.* **1994**, *82*, 161.

9. Kusoglu, A.; Weber, A. Z., New Insights into Perfluorinated Sulfonic-Acid Ionomers. *Chem. Rev.* **2017**, *117*, 987.

10. Gierke, T. D.; Munn, G. E.; Wilson, F. C., The morphology in nafion perfluorinated membrane products, as determined by wide- and small-angle x-ray studies. *J. Polym. Sci., Part B: Polym. Phys.* **1981**, *19*, 1687.

11. Hsu, W. Y.; Gierke, T. D., Ion transport and clustering in nafion perfluorinated membranes. *J. Membr. Sci.* **1983**, *13*, 307.

12. Gebel, G.; Aldebert, P.; Pineri, M., Structure and related properties of solution-cast perfluorosulfonated ionomer films. *Macromolecules* **1987**, *20*, 1425.

13. Luan, Y.; Zhang, Y.; Zhang, H.; Li, L.; Li, H.; Liu, Y., Annealing effect of perfluorosulfonated ionomer membranes on proton conductivity and methanol permeability. *J. Appl. Polym. Sci.* **2008**, *107*, 396.

14. Osborn, S. J. Morphological and Mechanical Properties of Dispersion-Cast and Extruded Nafion Membranes Subjected to Thermal and Chemical Treatments. Ph.D. Dissertation, Virginia Tech, Blacksburg, VA, 2009.

15. Fujimura, M.; Hashimoto, T.; Kawai, H., Small-angle X-ray scattering study of perfluorinated ionomer membranes. 1. Origin of two scattering maxima. *Macromolecules* **1981**, *14*, 1309.

16. Kyu, T.; Hashiyama, M.; Eisenberg, A., Dynamic mechanical studies of partially ionized and neutralized Nafion polymers. *Can. J. Chem.* **1983**, *61*, 680.

17. Page, K. A.; Cable, K. M.; Moore, R. B., Molecular Origins of the Thermal Transitions and Dynamic Mechanical Relaxations in Perfluorosulfonate Ionomers. *Macromolecules* **2005**, *38*, 6472.

18. Li, J.; Yang, X.; Tang, H.; Pan, M., Durable and high performance Nafion membrane prepared through high-temperature annealing methodology. *J. Membr. Sci.* **2010**, *361*, 38.

19. Yin, C.; Wang, Z.; Luo, Y.; Li, J.; Zhou, Y.; Zhang, X.; Zhang, H.; Fang, P.; He, C., Thermal annealing on free volumes, crystallinity and proton conductivity of Nafion membranes. *J. Phys. Chem. Solids* **2018**, *120*, 71.

20. Sone, Y.; Ekdunge, P.; Simonsson, D., Proton conductivity of Nafion 117 as measured by a four-electrode AC impedance method. *J. Electrochem. Soc.* **1996**, *143*, 1254.

21. Maldonado, L.; Perrin, J.-C.; Dillet, J.; Lottin, O., Characterization of polymer electrolyte Nafion membranes: Influence of temperature, heat treatment and drying protocol on sorption and transport properties. *J. Membr. Sci.* **2012**, *389*, 43.

22. Thomas, T. J.; Ponnusamy, K. E.; Chang, N. M.; Galmore, K.; Minteer, S. D., Effects of annealing on mixture-cast membranes of Nafion® and quaternary ammonium bromide salts. *J. Membr. Sci.* **2003**, *213*, 55.

23. DeLuca, N. W.; Elabd, Y. A., Nafion®/poly (vinyl alcohol) blends: effect of composition and annealing temperature on transport properties. *J. Membr. Sci.* **2006**, *282*, 217.

24. Hensley, J. E.; Way, J. D., The relationship between proton conductivity and water permeability in composite carboxylate/sulfonate perfluorinated ionomer membranes. *J. Power Sources* **2007**, *172*, 57.

25. Liu, Y.; Horan, J. L.; Schlichting, G. J.; Caire, B. R.; Liberatore, M. W.; Hamrock, S. J.; Haugen, G. M.; Yandrasits, M. A.; Seifert, S.; Herring, A. M., Small-Angle X-ray

Scattering Study of the Development of Morphology in Films Formed from the 3M Perfluorinated Sulfonic Acid Ionomer. *Macromolecules (Washington, DC, U. S.)* **2012**, *45*, 7495.

26. Hamrock, S. J. *Membranes and MEA's for Dry, Hot Operating Conditions*, 3M Company, 2011.
27. Landis, F. A.; Moore, R. B.; Page, K. A.; Han, C. C., SAXS Analysis of the Thermal Relaxation Behavior of Oriented Perfluorosulfonate Ionomer Membranes. *Polymeric Materials: Science & Engineering* **2002**, *87*, 121.
28. Page, K. A.; Park, J. K.; Moore, R. B.; Garcia Sakai, V., Direct analysis of the ion-hopping process associated with the α-relaxation in perfluorosulfonate ionomers using quasielastic neutron scattering. *Macromolecules* **2009**, *42*, 2729.
29. Park, J. K.; Spano, J.; Moore, R. B.; Wi, S., Counterion motions and thermal ordering effects in perfluorosulfonate ionomers probed by solid-state NMR. *Polymer* **2009**, *50*, 5720.
30. Moore, R. B.; Cable, K. M.; Croley, T. L., Barriers to flow in semicrystalline ionomers. A procedure for preparing melt-processed perfluorosulfonate ionomer films and membranes. *J. Membr. Sci.* **1992**, *75*, 7.
31. Cable, K. M.; Mauritz, K. A.; Moore, R. B., Effects of hydrophilic and hydrophobic counterions on the Coulombic interactions in perfluorosulfonate ionomers. *J. Polym. Sci. Part B Polym. Phys.* **1995**, *33*, 1065.
32. Park, J. K. Anisotropic Morphologies and Properties in Perfluorosulfonate Ionomer-Based Materials. Ph.D. Dissertation, Virginia Tech, Blacksburg, VA, 2009.
33. Divoux, G. M. M. Properties and Performance of Polymeric Materials Used in Fuel Cell Applications. Ph.D. Dissertation, Virginia Tech, Blacksburg, VA, 2012.

34. Zhang, F.; Ilavsky, J.; Long, G. G.; Quintana, J. P.; Allen, A. J.; Jemian, P. R., Glassy carbon as an absolute intensity calibration standard for small-angle scattering. *Metall. Mater. Trans. A* **2010**, *41*, 1151.

35. Ilavsky, J.; Zhang, F.; Allen, A. J.; Levine, L. E.; Jemian, P. R.; Long, G. G., Ultra-Small-Angle X-ray Scattering Instrument at the Advanced Photon Source: History, Recent Development, and Current Status. *Metall. Mater. Trans. A* **2013**, *44*, 68.

36. Ilavsky, J.; Jemian, P. R.; Allen, A. J.; Zhang, F.; Levine, L. E.; Long, G. G., Ultra-small-angle X-ray scattering at the Advanced Photon Source. *J. Appl. Crystallogr.* **2009**, *42*, 469.

37. Ilavsky, J., Nika: software for two-dimensional data reduction. *J. Appl. Crystallogr.* **2012**, *45*, 324.

38. Roe, R.-J.; Roe, R. *Methods of X-ray and neutron scattering in polymer science*; Oxford University Press New York, 2000; Vol. 739.

39. Schmidt-Rohr, K.; Chen, Q., Parallel cylindrical water nanochannels in Nafion fuel-cell membranes. *Nat Mater* **2008**, *7*, 75.

40. Eisenberg, A.; Hird, B.; Moore, R. B., A new multiplet-cluster model for the morphology of random ionomers. *Macromolecules* **1990**, *23*, 4098.

41. Kreuer, K.-D.; Dippel, T.; Meyer, W.; Maier, J., Nafion® membranes: Molecular diffusion, proton conductivity and proton conduction mechanism. *MRS Proceedings* **1992**, *293*.

42. Coetzee, J.; Cunningham, G., Evaluation of single ion conductivities in acetonitrile, nitromethane, and nitrobenzene using tetraisoamylammonium tetraisoamylboride as reference electrolyte. *J. Am. Chem. Soc.* **1965**, *87*, 2529.

43. Gill, D. S., Evaluation of solvated radii of ions in non-aqueous solvents. *Electrochim. Acta* **1979**, *24*, 701.

44. Shannon, R. D., Revised effective ionic radii and systematic studies of interatomic distances in halides and chalcogenides. *Acta Crystallogr. Sec. A* **1976**, *32*, 751.

45. Anderson, L. J. Controlled Heterogeneity in Semicrystalline Gels by Chemical and Physical Modification. Ph.D. Dissertation, Virginia Tech, Blacksburg, VA, 2018.

Chapter 8.
Conclusions and Suggested Future Work

8.1 Conclusions

The work presented in this dissertation has helped to provide a better understanding of the influence of sidechain structures and interactions on the morphology and physical properties of perfluorinated ionomers. PFSAs with C2 and C4 sidechains (Solvay's Aquivion and 3M PFSA, respectively) were observed to have slightly different thermomechanical properties than what has been observed and assigned for Nafion in the past.[1] Particularly, DMA data for 3M PFSA and Aquivion membranes in the H^+-form showed only two dynamic mechanical relaxations compared to the three observed in Nafion. Partial neutralization with the bulky tetrabutylammonium (TBA^+) counterion demonstrated that the β-relaxation (attributed to the onset of segmental motions of mainchains induced by sidechain mobility) appears to grow in with increasing TBA^+ content, which was attributed to the large size of the counterion that increases chain mobility by reducing the strength of the physical crosslinks. Additionally, partial hydrolysis of these membranes confirmed that the β-relaxation is suppressed in these new PFSAs due to their shorter sidechain lengths and higher ion contents that reduce the mobility of the mainchains at temperatures below the α-relaxation (the onset of long-range mobility of mainchains and sidechains as a result of destabilization of the physically-crosslinked network).

In addition to the discrepancy in DMA data observed for short and intermediate sidechain PFSAs, anomalous glass transition behavior was observed for 3M's multiacid sidechain ionomer, perfluoroimide acid (3M PFIA). Although the addition of more ion exchange groups in 3M PFIA was expected to decrease chain mobility by introducing additional sites for physical crosslinking,

it was observed to have a lower α-relaxation temperature in the Na^+-form than its parent ionomer (same average number of TFE units between sidechains), 3M PFSA. Both spherical and cylindrical model fits for the ionomer peak in small angle X-ray scattering (SAXS) profiles for 3M PFIA and 3M PFSA provided information on the estimated size of the aggregates formed in each membrane, and space-filling calculations shed light on the average number of sidechains participating in each aggregate. Based on these calculations, it was determined that the aggregate structure in 3M PFIA must incorporate the fluorocarbon segment between the ionic groups on each sidechain, likely reducing the strength of the ionic aggregates by spacing out the ion pairs constituting the electrostatic crosslinks within each aggregate. Additionally, by calculating the surface area and ion density of the aggregates, the space between each sidechain was estimated to be larger in 3M PFIA compared to 3M PFSA, and thus the amount of mobility of the sidechains increased, leading to a lower α-relaxation temperature. Despite this finding, the dynamic mechanical storage modulus provides evidence that some physical crosslinks remain in 3M PFIA that provide mechanical integrity to the membrane above the α-relaxation temperature. This is attributed to the second acidic site, which reduces the ability of a sidechain to "hop" between ionic aggregates.

In general, temperatures in the vicinity of the α-relaxation are required to see any significant morphological reorganization in PFSAs. This is especially observed when PFSAs are neutralized with tetramethylammonium (TMA^+) counterion and annealed at temperatures in the vicinity of the α-relaxation. Crystalline-like ordering of the TMA^+ counterions as a result of this annealing step was observed in Nafion, Aquivion, 3M PFSA, and 3M PFIA. This ordering is maintained upon reacidification of the membranes, leading to improved proton conductivity. This processing method may be used to achieve desirable membrane morphologies for improved fuel cell performance.

Throughout these studies on the molecular origins of thermomechanical relaxations observed in 3M PFSA, 3M PFIA, and Aquivion, it was necessary to find an additional technique for probing glass transition behavior that complements the DMA data. A new pretreatment method for differential scanning calorimetry (DSC) was presented that completely removed water and any additional artifacts from the thermograms for H^+-form PFSAs, and demonstrated a step-change in heat flow in the second heat. This step change was ultimately attributed to the same molecular motions as the β-relaxation in counterion-exchanged PFSAs (i.e., SO_3TBA) and the α-relaxation in H^+-form PFSAs. This observed endotherm in DSC was associated with a single peak in the loss modulus DMA data, which occurs for either the α- or the β-relaxation. The peak in loss modulus and corresponding thermal transition in DSC was attributed to the onset of segmental motions, a relaxation that is enthalpic in nature. Thus, the molecular motions underlying the α-relaxation in H^+-form PFSAs (where there is no observable β-relaxation) is coupled with the enthalpic onset of segmental motions.

Another method for characterizing PFSAs was presented for small angle X-ray scattering data in the form of contrast variation for isolation of the two morphological features. In Nafion, Aquivion, and 3M PFSA membranes of varying equivalent weights (EW), the ionomer peak was "contrast-matched" and undistinguishable to X-rays in the Li^+-form. This was attributed to similar electron density between the Li^+-sulfonate domains and the surrounding amorphous perfluorinated phase such that there was no contrast between the two. Additionally, it was observed that the crystalline peak disappeared at a certain counterion size and larger for all of the PFSAs, but was dependent on the EW of the PFSA as opposed to sidechain structure. This observation indicated that the crystalline phase was not just contrast matching the ionic matrix at a specific counterion size, but instead, the contrast between the crystalline PTFE and the ionic matrix was much lower

than the contrast between the ionic domains and amorphous PTFE such that it was effectively acting as a two-phase system. This finding was shown to be useful for isolating the intercrystalline peak for modeling to the 1-D correlation function without interfering scattering from the ionomer peak.

These insights contribute to the understanding of PFSA structure-property relationships and characterization techniques for these materials. Recently, the PFSA community has begun to shift gears toward the development of novel PFSA structures for use in the catalyst layer of the fuel cell, which require increased gas permeability properties compared to the that of the current PFSA structures.[1,2] The importance of developing simple methods for characterizing these ionomers, and fine tuning the morphology and properties of PFSAs will be crucial in the success of commercialization of fuel cell technology.

8.2 Suggested Future Work

8.2.1 PFSA Blends to Fine Tune Morphology and Properties

In **Chapter 4** we discovered anomalous glass transition behavior in 3M's perfluoroimide acid ionomers as a result of the second ion exchange site on each sidechain. In an effort to determine the origin of the large relaxation for Na^+-form PFIA, we have blended 3M PFIA with its parent ionomer, 800 EW 3M PFSA (containing the same number of average TFE units between sidechains) by co-dispersing the two ionomers in solvent and casting into membranes. DMA data for the Na^+-form blends are shown in **Figure 8-1**. While we originally expected the two ionomers to be miscible and show a shift in the large relaxation temperature with increasing 3M PFSA content, the data actually appears to be that of an immiscible blend with two different glass

transitions. With increasing 3M PFSA incorporation, the α-relaxation observed for 3M PFIA reduces in intensity while the α-relaxation in 3M PFSA increases in intensity. There is also a small β-relaxation for all of the membranes that remains at the same temperature and intensity regardless of PFSA/PFIA content. DSC data of the Na^+-form blends is shown in **Figure 8-2**, where you can see the appearance of the enthalpic glass transition for 3M PFIA begin to increase in intensity with increasing PFIA content.

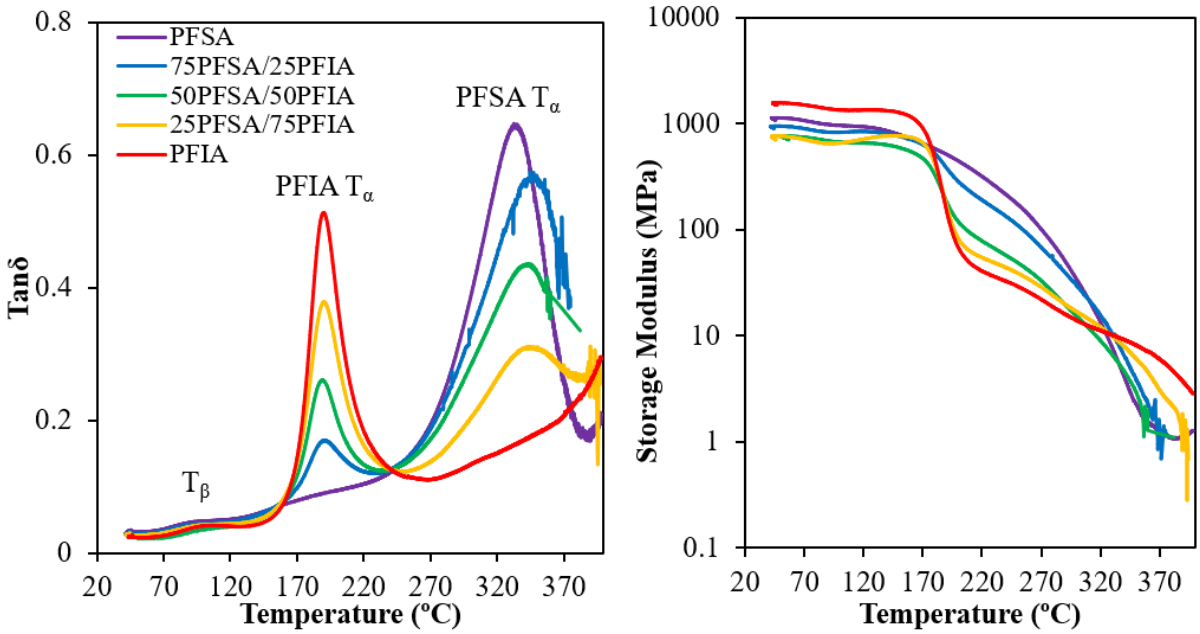

Figure 8-1. Dynamic mechanical tanδ and storage modulus versus temperature for 3M PFIA/PFSA blends in the Na^+-form.

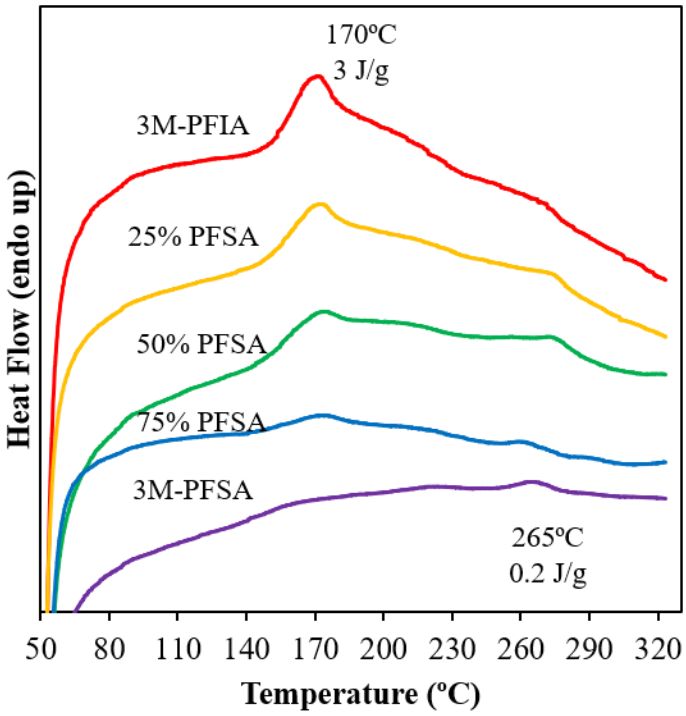

Figure 8-2. DSC thermograms for Na^+-form 3M PFIA/PFSA blended membranes.

This finding presents a new method of blending PFSAs to manipulate the morphology and thermomechanical properties. While it is difficult to believe that two structures that are so similar would be immiscible in solution, it is our prediction that because PFSAs do not fully dissolve in solution and rather form aggregates in dispersion, they are not able to blend on a molecular level. An illustration of this is shown in **Figure 8-3**. It is predicted that the aggregate sizes in solution will ultimately form the domain sizes of the different PFSAs in the membrane. This may be fine-tuned by disrupting the aggregate morphology in dispersion possibly by dispersing at high temperatures and pressures in a reactor or by sonicating the dispersion. If the domain sizes could be manipulated in dispersion, it may provide a facile method of fine tuning the morphology and thermomechanical properties of PFSAs. With increasing focus on PFSAs as binders in the catalyst layer of fuel cells, ionomers with better oxygen permeability properties are of interest.[1] While new

structures are being synthesized to fill this role as the ionomer binder, it is possible that blending two PFSAs may provide a simpler method for fine-tuning the properties to increase gas permeability. 3M PFIA and 3M PFSA blends in the Na^+-form provided an extreme case where the α-relaxations are very different, which led to our observation of the phase-separated behavior. However, blends of PFSAs with different EWs may be of interest as well. A lower EW PFSA may provide increased proton conductivity properties while a higher EW PFSA allows for gas transport. An exploration of the morphology of PFSA dispersion blends and their resulting properties may be useful for this application.

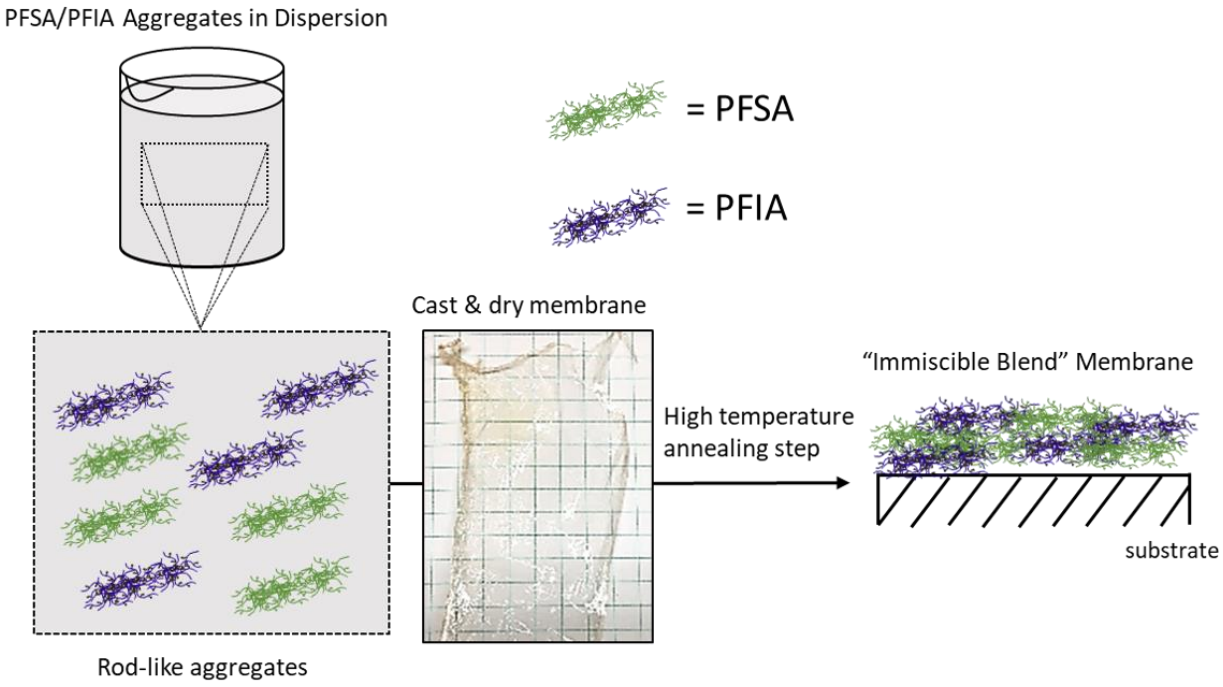

Figure 8-3. Casting method for the formation of "immiscible blend" membranes of 3M PFSA and 3M PFIA.

8.2.2 Thermomechanical Analysis as a Complementary Tool for Probing the Thermal Relaxations in PFSAs

With the development of new PFSAs with shorter sidechain lengths and higher ion contents, the thermomechanical relaxations are being driven to higher temperatures. In the H^+-form, higher relaxation temperatures allow for increased operating temperature range in fuel cell applications. When the sulfonic acid groups are neutralized with a small counterion, such as Na^+, the α-relaxation temperature increases to over 300 °C in an 800 EW 3M PFSA. These very high temperatures make it hard to find a complementary method to DMA for probing the glass transition behavior in PFSAs. As discussed in this dissertation, DSC is not sensitive enough to detect any glass transition behavior in Na^+-form PFSAs except for 3M PFIA. Other complementary techniques, such as variable temperature NMR, likely cannot reach temperatures in excess of 300 °C. Variable temperature SAXS provides information on the glass transition of these semicrystalline polymers below the melting temperature of the PTFE-like crystallites, which is well below 300 °C. Therefore, an additional technique for probing glass transition behavior in PFSAs may be useful for future studies.

Thermomechanical analysis (TMA) measures changes in length or volume of a sample under load as a function of temperature.[3] As opposed to DMA, the load used in TMA measurements should be negligible and just enough to keep the probe in contact with the sample. The relative change in length with temperature is measured to determine the coefficient of linear thermal expansion (CLTE), denoted by the symbol α, which is the slope of dimension change versus temperature. A change in the CLTE occurs through the glass transition temperature of a polymer and is attributed to the expansion in free volume. TMA is estimated to be about 15 times more sensitive to glass transitions than DSC, but still 67 times less sensitive than DMA.[4]

For the detection of the glass transition behavior in PFSAs, initial TMA experiments with an expansion probe were unsuccessful due to the small thickness of each PFSA membrane (ca. 25 μm) which led to low sensitivities and did not show any expansion upon heating. However, by using a film (tensile) probe and sample dimensions of 16 mm x 2 mm, changes in sample length as a function of temperature were successfully measured. Upon heating from −50 °C to 200 °C, H^+-form 3M PFSA showed multiple increases and decreases in dimension with increasing temperature. In order to resolve the thermal expansion across the full temperature range, we used modulated temperature TMA (MTTMA) experiments. In this technique, the temperature was ramped at 1 °C/min while modulated ±5°C every 300 seconds. MTTMA allows for separation of the reversible signal, which is associated with properties that depend on the temperature change, and nonreversible signal, which results from kinetic events associated with time and temperature.[5] From this technique, we can use the reversible signal to measure the coefficient of thermal expansion, while the nonreversible signal is used for detecting things like stress relaxations, softening, and heat shrinking. The MTTMA data including total, reversible, and nonreversible dimension change for an H^+-form 800 EW 3M PFSA is shown in **Figure 8-4**. From this MTTMA experiment, it's clear that some nonreversible dimension changes affect the overall profile of the total dimension change data. Using MTTMA to separate out the nonreversible and reversible data will be useful for determining where there are changes in the CLTE that are attributed to relaxations of the material.

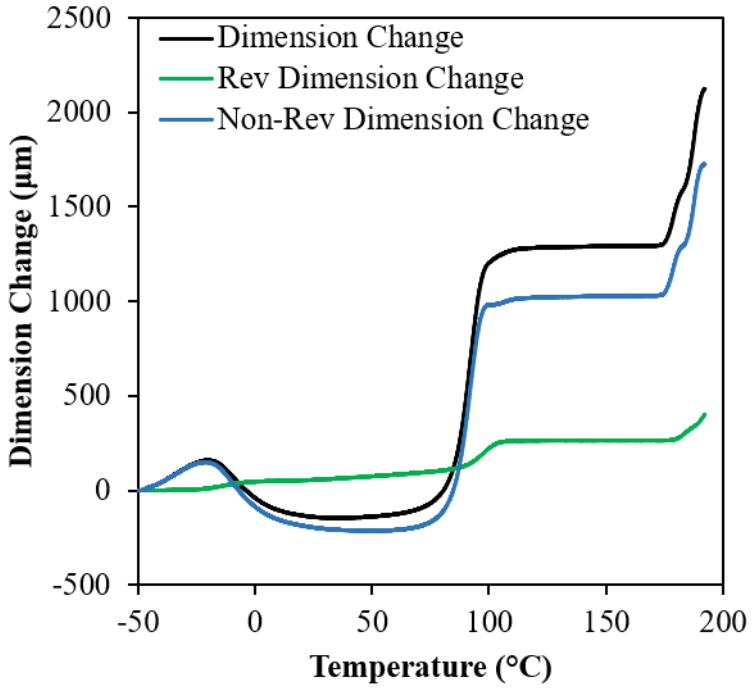

Figure 8-4. Reversible, non-reversible, and total dimension change of an 800 EW H^+-form 3M PFSA membrane from modulated thermomechanical analysis in tensile mode.

Figure 8-5 shows preliminary data comparing the reversible dimension change from MTTMA to the tanδ from DMA for a series of H^+- to TBA^+-form partially neutralized 800 EW 3M PFSA membranes. In the H^+-form, we observe two relaxations in the DMA tanδ that are also observed as changes in the slope of reversible dimension change versus temperature MTTMA data. In the 45% and 75% TBA^+-form samples, we observe three peaks in the tanδ data that also correspond to three slope changes in the MTTMA. In the 100% TBA^+-form sample, the two peaks in tanδ are slightly overlapping so it's difficult to correlate them to the slope changes observed in MTTMA. However, I believe that this technique is demonstrating slope changes for each relaxation temperature as expected and may be a useful complementary technique to DMA for the characterization of glass transition behavior in PFSA membranes.

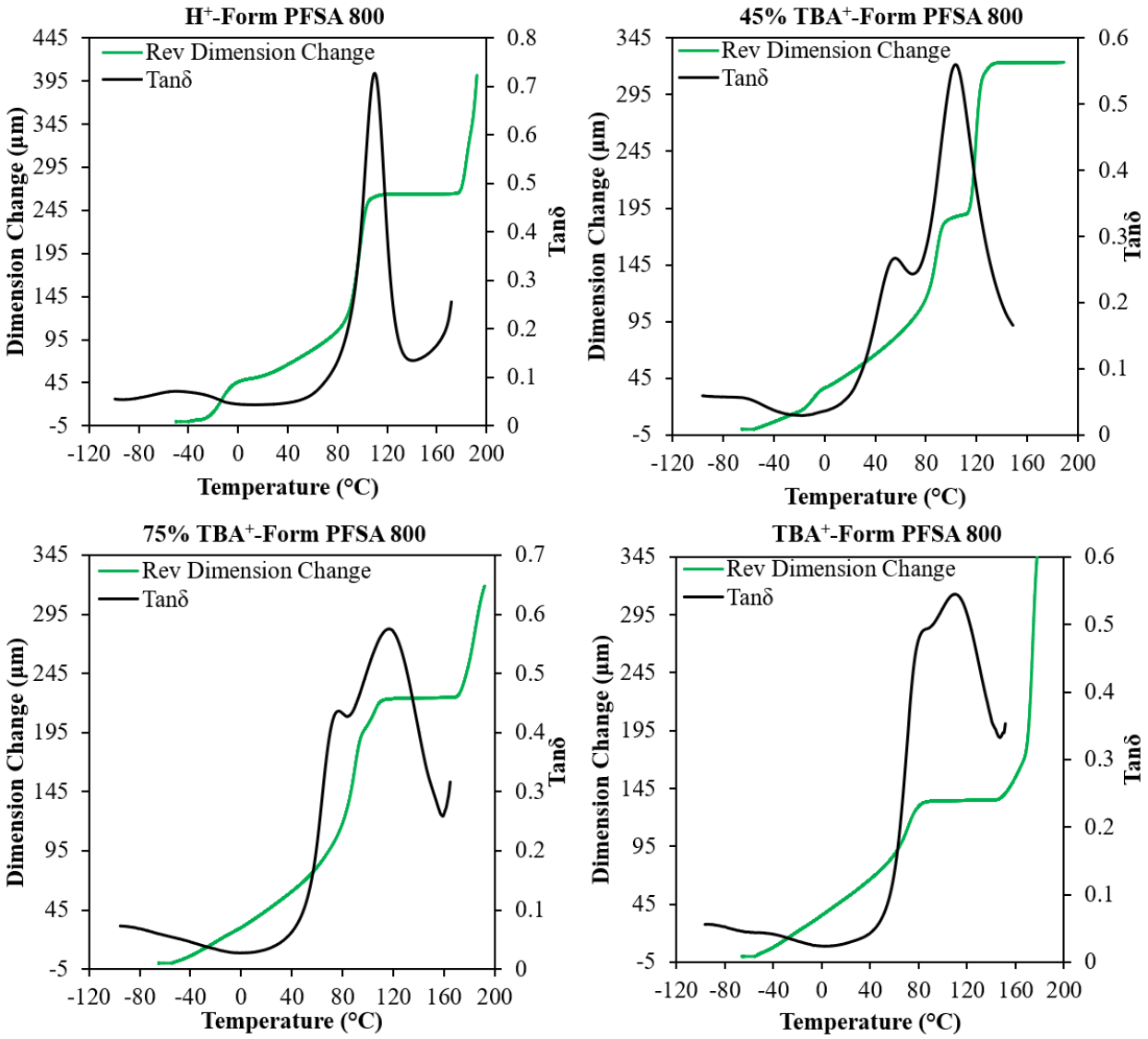

Figure 8-5. Reversible dimension change compared to dynamic mechanical tanδ for a series of partially neutralized 800 EW 3M PFSA membranes with tetrabutylammonium counterions.

8.3 References

1. Page, K. A.; Cable, K. M.; Moore, R. B., Molecular Origins of the Thermal Transitions and Dynamic Mechanical Relaxations in Perfluorosulfonate Ionomers. *Macromolecules* **2005**, *38*, 6472.

2. Katzenberg, A.; Mukherjee, D.; Dudenas, P. J.; Okamoto, Y.; Kusoglu, A.; Modestino, M. A. Dynamic Emergence of Nanostructure and Transport Properties in Perfluorinated Sulfonic Acid Ionomers. Published Online: 2020. https://doi.org/10.26434/chemrxiv.12302693.v1.
3. Bair, H. E.; Akinay, A. E.; Menczel, J. D.; Prime, R. B.; Jaffe, M., Thermomechanical analysis (TMA) and thermodilatometry (TD). *Thermal Analysis of Polymers* **2009**, 319.
4. Foreman, J.; Sauerbrunn, S.; Marcozzi, C., Exploring the sensitivity of thermal analysis techniques to the glass transition. *TA Instruments: Applications Library Search [online]* **2006**.
5. Blaine, R. L.; Instruments, T., Modulated Thermomechanical Analysis–Measuring Expansion and Contraction Simultaneously. *TA Instruments* **2003**.

Appendix A.

Modified Perfluorosulfonic Acid Ionomers for Use in the Catalyst Layer of Hydrogen Fuel Cells

Christina M. Orsino,[a] Gregg Dahlke,[b] Lisa Chen,[b] Denis Duchesne,[b] Robert B. Moore[a]

[a]*Department of Chemistry, Macromolecules Innovation Institute, Virginia Tech, Blacksburg, VA, 24060, USA*

[b]*3M Company, St. Paul, MN, 55144, USA*

A.1 Introduction

Proton exchange membrane fuel cells (PEMFCs) are considered a promising technology for clean and efficient power sources for transportation applications. The heart of a PEMFC is the membrane electrode assembly (MEA) which consists of a proton exchange membrane (PEM), catalyst layers, and gas diffusion layers. The anode and cathode catalyst layers, of micrometers in thickness, is coated onto either side of a PEM (i.e. 3M PFSA, Nafion, or Aquivion membrane).[1] The catalyst layer itself is comprised of a carbon support, platinum catalyst, and an ionomer binder. The carbon support serves to increase the available surface area while the platinum particles act as the catalyst for the reactions. The ionomer binder consolidates the carbon and platinum particles together and allows for proton conduction from the membrane to the catalyst. The combination of these three components of the catalyst layer form the "triple-phase boundary," or a confined spatial site where the electrolyte, gas, and catalyst regions are in contact to allow for the oxygen reduction reaction (ORR) or hydrogen oxidation reaction (HOR) to occur.[2]

The limiting factor to widespread commercialization of PEMFCs is their high cost.[3] In particular, the cost of the electrode is high due to the high platinum catalyst loading, predominantly in the cathode for accelerating the otherwise slow ORR (the rate limiting factor for performance

in a fuel cell). One of the highest priorities in reducing the cost of the electrode is to decrease the load of precious metal in the cathode. Optimization of the tripe phase boundary is crucial to the reduction of catalyst loading. The electrodes must have appropriate ionomer coating for transport of protons and porosity for transport of gas and water to the catalyst. Since the platinum particles are predicted to be coated with a thin film of ionomer, oxygen transport through the ionomer layer is critical to the performance of the cathode.[4,5]

Currently, perfluorosulfonic acid (PFSA) ionomers are typically used as the binder in MEA catalyst layers. Although the perfluorinated structure of PFSAs makes them relatively permeable to gases, they are not optimized for this application. PFSAs are typically developed to act as the proton exchange membrane in the middle of the MEA, which requires barrier properties against the crossover of hydrogen and oxygen gases. Primarily, the crystallinity that is formed from runs of polytetrafluoroethylene (PTFE) backbone between sidechains in PFSA membranes serves to reduce oxygen permeability.[6,7]

Recently, a new strategy has been implemented to improve oxygen permeability of PFSA membranes for use as the catalyst binder by introducing an additional sidechain or backbone group that reduces the crystallinity of the matrix and/or increases the free volume in the polymer.[8] These recent investigations involve the introduction of dioxole structures, which are commonly used to reduce chain packing in common commercial materials such as Cytop, Teflon AF, and Hyflon AD.[8,9] These studies successfully showed a reduction in gas transport resistance after incorporation of the dioxole monomer into an Aquivion (short sidechain, SSC) based ionomer,[9] and a Nafion (long sidechain, LSC) based ionomer.[8]

While these bulky dioxole monomers were shown to reduce the crystallinity in these new PFSA membranes and thus improve the oxygen permeability, there was an observed trade-off

between oxygen transport and proton conductivity attributed to the reduced ability of the ionic domains to swell as a result of their stiffer matrix.[8,10] The glass transition temperature of the dioxole homopolymer was higher than that of pure PTFE, indicating that the mobility of the dioxole chains is more restricted than the mobility of PTFE. Upon copolymerizing the dioxole with the Nafion sidechain, the glass transition temperature of the sulfonyl fluoride precursor was increased in the dioxole copolymer compared to the standard Nafion sulfonyl fluoride polymer. This decreased mobility of the backbone matrix was attributed to the decrease in ion conductivity of these dioxole-modified LSC ionomers.

Recently, 3M has developed their own version of a modified PFSA for use in the catalyst layers of MEAs based on their 3M PFSA structure, shown in **Figure A-1**. While the exact chemical structure has not been published, a general structure for this modified PFSA is shown in **Figure A-2**. These modified PFSAs are essentially a terpolymer of PTFE, 3M PFSA sidechain, and an unspecified modifier. The samples explored in this study are listed in **Table A-1**, and characterized by low, medium, and high modifier content. The goal of this preliminary study is to probe the effect of modifier content on the thermomechanical relaxations in these new modified PFSAs. By investigating the thermomechanical properties, we hope to gain information on the chain mobility that may allow for improved proton conductivity in addition to gas permeability properties. Additionally, we use small angle X-ray scattering and ultra-small angle X-ray scattering to provide some initial information on the effect of modifier on the morphology of these new PFSAs.

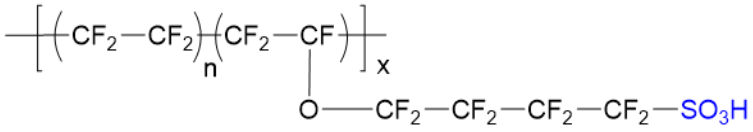

Figure A-1. Chemical structure of 3M PFSA.

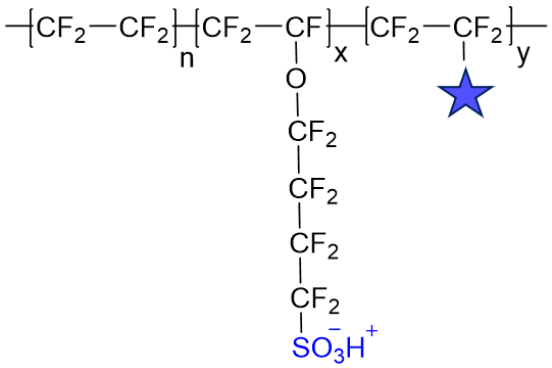

Figure A-2. General chemical structure of new modified PFSA membranes.

Table A-1. Modified PFSA membrane sample names and relative content of modifier.

Sample Name	Modifier Content
04-2006	Low
04-2007	Intermediate
04-2008	High

A.2 Experimental

A.2.1 Materials.

Modified PFSAs of low, intermediate, and high modifier content and 800 EW 3M PFSA were provided by 3M. All other reagents were purchased from the Virginia Tech Chemistry Stockroom and used without further purification.

A.2.2 Membrane Preparation

Modified PFSA and 800 EW 3M PFSA membranes were prepared by casting a dispersion from alcohol and water onto polyimide film. The dispersions were dried in an oven with the temperature of 80°C followed by annealing for 10 minutes at 200°C. Membranes were removed

from the polyimide film by soaking in water. To remove impurities, all membranes were soaked in 8 M HNO_3 for 16 hours then rinsed thoroughly with deionized water and dried under vacuum at 70 °C overnight.

A.2.3 Thermomechanical Characterization

Dynamic mechanical analysis (DMA) was performed on a TA Instruments DMA Q800 analyzer in tensile mode using clamps for thin film samples. All samples were cut from vacuum dried membranes with a width of 6.35 mm. The membranes were analyzed at a frequency of 1 Hz from −120 to 200°C with a heating ramp of 2°C/min.

Differential scanning calorimetry (DSC) data were collected for the H^+-form Modified PFSAs on a TA Instruments Q2000 at a 20 °C/min ramp rate under nitrogen purge. Initial DSC thermograms were obtained after thoroughly drying the samples in the DSC at 120 °C for 2 hours then cooling to the starting temperature of −50 °C. The first heat was collected from −50 °C to 240 °C at a heating rate of 10 °C/min to remove all thermal history, then samples were cooled from 240 to −50 °C at a rate of 10 °C/min, followed by a second heat from −50 °C to 240 °C at 10 °C/min. The second heat data are presented.

A.2.4 X-Ray Characterization

Small and ultra-small angle X-ray scattering (SAXS/USAXS) data were collected at beamline 9-ID-C at the Advanced Photon Source (APS) at Argonne National Laboratory (Lemont, Illinois).[11,12] Dry membrane samples were run under ambient conditions. Hydrated membrane samples were run while sealed in capsules of water between Kapton, which were then background subtracted during data processing. Dispersions were also sealed in capsules between Kapton that were background subtracted. SAXS profiles were reduced using the Nika program for Igor Pro.[13]

USAXS profiles were reduced and merged with the SAXS profiles using the Irena program for Igor Pro.[14] All X-ray scattering data were corrected for sample thickness and transmission and converted to absolute intensity using a glassy carbon standard.[15]

A.3 Preliminary Results

A.3.1 Thermomechanical Properties

A study on the modified Nafion ionomers containing a dioxole backbone provided glass transition data for the sulfonyl fluoride form to describe chain mobility without the impact of physical crosslinks from the sulfonic acid functionalities.[8] In that investigation, it was observed that the glass transition of the precursor for the dioxole-containing polymers increased with increasing dioxole content. The dioxole-containing polymer had an increased glass transition (in the range of 60 to 100 °C in the sulfonyl fluoride form) compared to the Nafion sulfonyl fluoride precursor (T_g = 20 °C). Based on this evidence, it was concluded that the dioxole monomers increased the stiffness of the backbone and led to decreased proton conductivity.

Table A-2 shows the glass transition temperatures of the nonionic sulfonyl fluoride-form 3M Modified PFSAs compared to an 800 EW 3M PFSA copolymer from DSC measurements. With increasing modifier content, the glass transition temperature of the precursor decreases. Even the lowest modifier content has a significantly reduced T_g compared to the PFSA copolymer. This demonstrates that the introduction of this new modifier into these PFSA membranes does not increase the stiffness of the polymer matrix, and in fact may increase the polymer chain mobility with increasing modifier content.

Table A-2. Glass transition temperature of the sulfonyl fluoride precursor for 3M Modified PFSA ionomers.

Ionomer	SO_2F T_g (°C)
800 EW 3M PFSA	25
04-2006*	5.9
04-2007*	0.4
04-2008*	−3.8

*Data provided by 3M.

The DMA data for the modified PFSAs in the hydrolyzed H^+-form are presented in **Figure A-3**. In 800 EW 3M PFSA, the dominant α-relaxation is observed at ca. 110 °C in the H^+-form. This relaxation is attributed to long-range mobility of the polymer chains upon destabilization of the hydrogen-bonded physically-crosslinked network.[16] In the modified PFSAs, the presence of this α-relaxation at temperatures much higher than the glass transition of the sulfonyl fluoride precursor indicates that the sulfonic acid groups are still capable of aggregating to form a crosslinked network in the presence of the additional modifier. However, the clear decrease in α-relaxation temperature with increasing modifier content can be attributed either to less functional sidechain content in the ionomers with higher mole percent modifier content or some disruption of the sulfonic acid aggregates by the modifier.

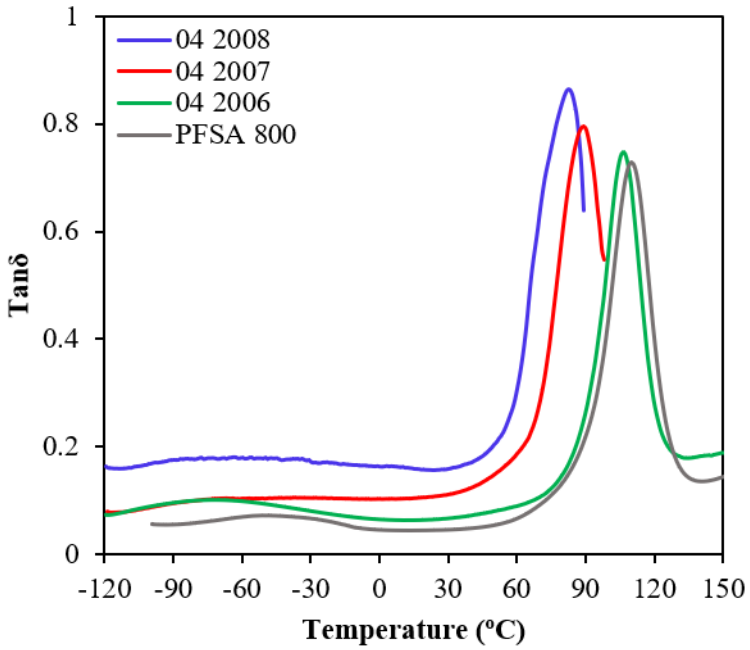

Figure A-3. Dynamic mechanical tanδ versus temperature data for 3M Modified PFSAs compared to an 800 EW 3M PFSA copolymer in the H^+-form.

DSC thermograms for the modified PFSAs and an 800 EW 3M PFSA in the sulfonic acid-form are shown in **Figure A-4**. For all four PFSAs, a clear step-change transition is observed in the second heating scan. This step-change was attributed to the molecular motions underlying the α-relaxation of H^+-form PFSAs in **Chapter 5** of this dissertation. As such, the decrease in thermal transition temperature with increasing modifier content is expected based on the same trends observed for the α-relaxation in the DMA data presented above. Again, the decrease in thermal transition behavior may provide evidence of increasing polymer chain mobility with increasing modifier content.

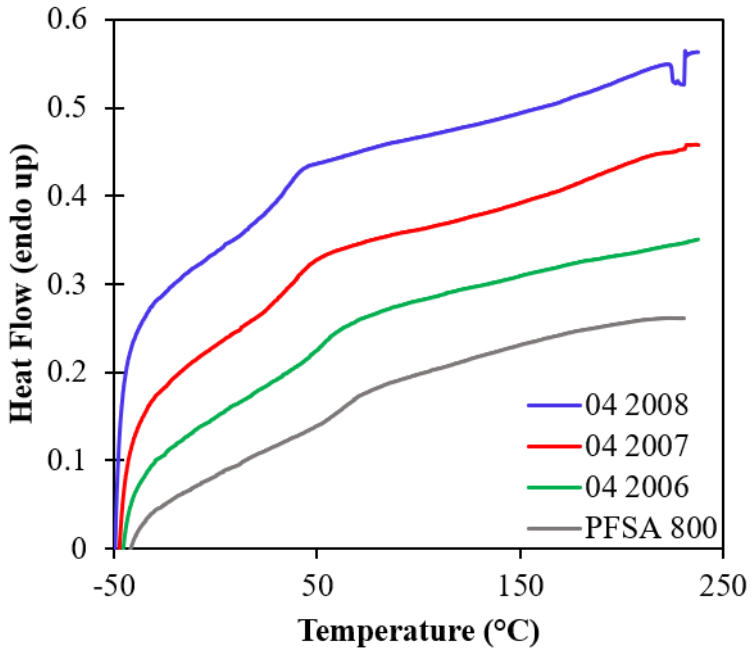

Figure A-4. Second heat DSC thermograms for 3M Modified PFSA ionomers in the H^+-form.

A.3.2 Small and Ultra-Small Angle X-Ray Scattering

In the making of the catalyst layer in PEMFCs, the catalyst ink typically consists of ionomer and supported catalyst (Pt/carbon) dispersed in solvent. The morphology of the ionomer (aggregate structure and size) in dispersion dictates the viscosity and ultimately the chemical and physical properties of the resulting membrane.[17] Small angle X-ray scattering profiles of concentrated dispersions of the 3M modified PFSAs are shown in **Figure A-5**. A single peak is observed in the vicinity of q = 0.1 $Å^{-1}$ for all three dispersions. This peak has been observed in SAXS profiles of concentrated Nafion solutions and attributed to the interference between rod-like aggregates in dispersion.[18] The peak position, q_{max}, can be expressed as a Bragg distance by $d_{Bragg}=2\pi/q_{max}$ and used as an estimate of the interaggregate dimension. The introduction of modifier does not appear to show any meaningful trend in regard to the dispersion peak position and thus interaggregate distance in dispersion. The intermediate modifier-content sample, 04-

2007, has the lowest q_{max}, followed by 04-2006 and 04-2008, respectively. The peak shape, however, appears narrower in the modified PFSAs, indicating a lower distribution of dimensions in the modified PFSAs compared to the 800 EW 3M PFSA. Bragg dimensions for these peaks range from 60 to 80 Å, but specific model fits may provide more information on the size and shape of these aggregates in dispersion.[19] The larger slope in the low-q range for the modified PFSAs compared to the 800 EW 3M PFSA may suggest larger aggregates of aggregates,[20] but further investigation is necessary to confirm that assumption. Overall, there does not appear to be a trend in dispersion morphology with increasing modifier content.

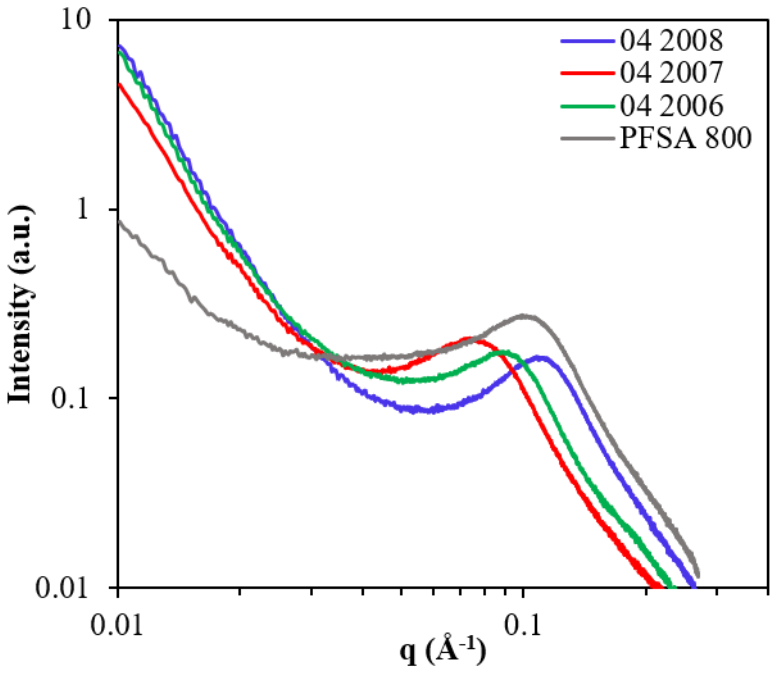

Figure A-5. Small angle X-ray scattering profiles of 3M Modified PFSA dispersions of relatively high weight percent in an alcohol/water solvent mixture.

SAXS profiles of the dry H^+-form membranes are shown in **Figure A-6**. In the 800 EW 3M PFSA, there are two scattering features in the SAXS profile. The first feature, at q = 0.05 $Å^{-1}$,

is attributed to intercrystalline scattering from ordered crystallites developed from crystallization of the runs of PTFE between sidechains. The second scattering feature at q = 0.2 $Å^{-1}$ is termed the "ionomer peak" and is associated with inter-aggregate correlations arising from contrast in electron density between the ionic domains and the amorphous PTFE matrix. In the modified PFSA with the lowest amount of modification, 04-2006, the intercrystalline feature is weakly present and is decreased in intensity from the 800 EW 3M PFSA. In the 04-2007 and 04-2008 intermediate and highly modified PFSAs, that intercrystalline feature is no longer observed. The ionomer peak is present in all four membranes, indicating the aggregation of the sulfonic acid groups into ionic domains. The ionomer peak also shifts slightly to lower scattering angles with increasing modifier content, which signifies an increase in the characteristic distance between ionic domains. Most unusual, is the appearance of an additional scattering feature at q = 0.35 $Å^{-1}$ (d_{Bragg} length scale of ~ 18 Å) that is not observed in unmodified PFSAs but appears to grow in with increasing modifier content. The origin of this scattering feature is unknown at this time, but may signify an interesting new morphology attributed to some form of association between the modifier units for these modified PFSA ionomers.

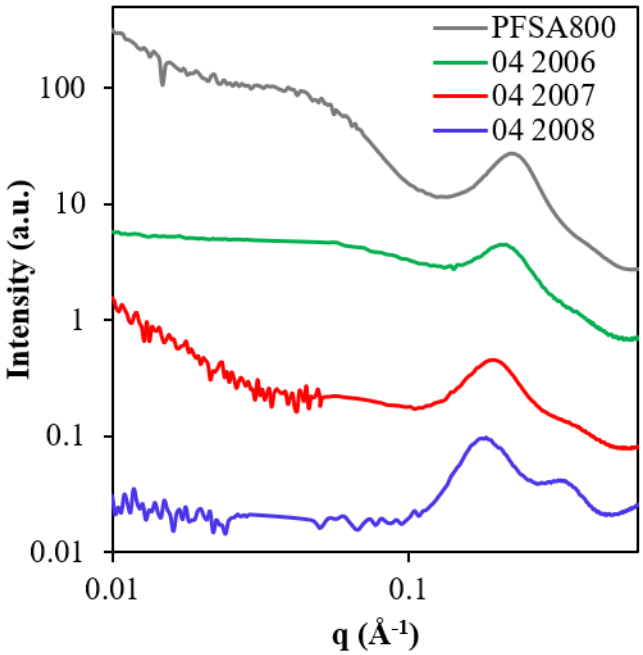

Figure A-6. SAXS profiles for dry, H^+-form modified PFSAs.

Combined ultra-small-angle and small-angle X-ray scattering profiles of hydrated H^+-form modified PFSAs are shown in **Figure A-7**. The ionomer peak for each PFSA shifts to lower scattering angles upon hydration, characteristic of swelling of the ionic domains and is well-documented in the literature.[21] The ionomer peak q_{max} decreases with increasing modifier content, as observed for the dry H^+-form. Interestingly, the extra scattering feature in the high-q region has decreased in intensity and a new scattering feature at ultra-small angles appears for the modified PFSAs upon hydration. This feature, of large characteristic dimensions, is new to the PFSA literature. In USAXS studies of Nafion, the ultra-low scattering region typically shows a strong upturn that is attributed to large scale electron density inhomogeneities of thousands of angstroms in size.[22] The existence of a new scattering peak at such small scattering angles may indicate a significantly large structure (in the range of 300 nm) for these new modified PFSAs.

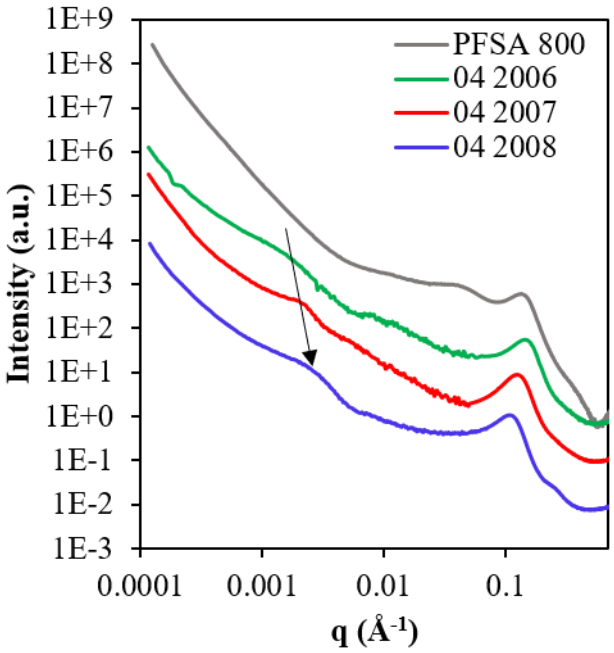

Figure A-7. Ultra-small angle X-ray scattering profiles of hydrated H^+-form 3M modified PFSAs.

A.4 Conclusions

Here we have presented preliminary characterization studies of new modified PFSAs from 3M. DSC data of the sulfonyl fluoride precursors showed a decrease in glass transition temperature with increasing modifier content. Upon hydrolysis to the sulfonic acid-form, DMA data showed a prominent α-relaxation for each of the modified PFSAs, indicating the existence of a physically crosslinked network from hydrogen-bonding between sulfonic acid groups on the functional sidechains. The temperature of the α-relaxation was observed to decrease with increasing modifier content. Similarly, a thermal transition observed by DSC decreased with increasing modifier content. This is the first evidence that the addition of this new modifier serves to increase the mobility of the polymer chains and sidechains, which may ultimately lead to improved proton conductivity.

X-ray scattering studies showed the presence of a weak intercrystalline peak in the PFSA with the least modifier content, and no intercrystalline peak in the intermediate and high modifier samples. An ionomer peak was observed in all of the membranes and shifted to lower scattering angles with increasing modifier content, indicating larger inter-ionic domain dimensions. Interestingly, SAXS of the dry H^+-form membranes showed the existence of a new scattering feature at scattering angles in between the ionomer peak and the wide-angle region in the highly modified PFSA, that decreased in intensity upon hydration. The hydrated membranes showed a new scattering feature at ultra-small scattering angles. The SAXS data indicate a new structure for these modified PFSAs. Ultimately, gas permeability and fuel cell studies are necessary to determine the functionality of these modified PFSAs as ionomer binders in the catalyst layer of a PEM fuel cell.

A.5 Acknowledgments

The author acknowledges 3M for providing PFSA materials for this study and for funding this research. This research used resources of the Advanced Photon Source (APS) and a U.S. Department of Energy (DOE) Office of Science User Facility operated for the DOE Office of Science by Argonne National Laboratory under General User Proposal Number 49574. USAXS and SAXS data were collected on the 9-ID-C beam line at the APS, Argonne National Laboratory.

A.6 References

1. Garsany, Y.; Atkinson III, R. W.; Sassin, M. B.; Hjelm, R. M.; Gould, B. D.; Swider-Lyons, K. E., Improving PEMFC performance using short-side-chain low-equivalent-weight PFSA ionomer in the cathode catalyst layer. *J. Electrochem. Soc.* **2018**, *165*, F381.
2. Karuppanan, K. K.; Raghu, A. V.; Panthalingal, M. K.; Ramanathan, S.; Kumaresan, T.; Pullithadathil, B., Triple phase boundary augmentation in hierarchical, Pt grafted N-doped mesoporous carbon nanofibers for high performance and durable PEM fuel cells. *J. Mater. Chem. A* **2018**, *6*, 12768.
3. Moreno, N. G.; Molina, M. C.; Gervasio, D.; Robles, J. F. P., Approaches to polymer electrolyte membrane fuel cells (PEMFCs) and their cost. *Renewable and Sustainable Energy Reviews* **2015**, *52*, 897.
4. Sambandam, S.; Parrondo, J.; Ramani, V., Estimation of electrode ionomer oxygen permeability and ionomer-phase oxygen transport resistance in polymer electrolyte fuel cells. *Phys. Chem. Chem. Phys.* **2013**, *15*, 14994.
5. Morawietz, T.; Handl, M.; Oldani, C.; Friedrich, K. A.; Hiesgen, R., Quantitative in situ analysis of ionomer structure in fuel cell catalytic layers. *ACS Appl. Mater. Interfaces* **2016**, *8*, 27044.
6. Van Cleve, T.; Khandavalli, S.; Chowdhury, A.; Medina, S.; Pylypenko, S.; Wang, M.; More, K. L.; Kariuki, N.; Myers, D. J.; Weber, A. Z., Dictating Pt-based electrocatalyst performance in polymer electrolyte fuel cells, from formulation to application. *ACS Appl. Mater. Interfaces* **2019**, *11*, 46953.

7. Schuler, T.; Chowdhury, A.; Freiberg, A. T.; Sneed, B.; Spingler, F. B.; Tucker, M. C.; More, K. L.; Radke, C. J.; Weber, A. Z., Fuel-cell catalyst-layer resistance via hydrogen limiting-current measurements. *J. Electrochem. Soc.* **2019**, *166*, F3020.

8. Katzenberg, A.; Mukherjee, D.; Dudenas, P. J.; Okamoto, Y.; Kusoglu, A.; Modestino, M. A., Dynamic Emergence of Nanostructure and Transport Properties in Perfluorinated Sulfonic Acid Ionomers 2. **2020**.

9. Rolfi, A.; Oldani, C.; Merlo, L.; Facchi, D.; Ruffo, R., New perfluorinated ionomer with improved oxygen permeability for application in cathode polymeric electrolyte membrane fuel cell. *J. Power Sources* **2018**, *396*, 95.

10. Katzenberg, A.; Chowdhury, A.; Fang, M.; Weber, A. Z.; Okamoto, Y.; Kusoglu, A.; Modestino, M. A., Highly Permeable Perfluorinated Sulfonic Acid Ionomers for Improved Electrochemical Devices: Insights into Structure–Property Relationships. *J. Am. Chem. Soc.* **2020**, *142*, 3742.

11. Ilavsky, J.; Zhang, F.; Allen, A. J.; Levine, L. E.; Jemian, P. R.; Long, G. G., Ultra-Small-Angle X-ray Scattering Instrument at the Advanced Photon Source: History, Recent Development, and Current Status. *Metall. Mater. Trans. A* **2013**, *44*, 68.

12. Ilavsky, J.; Jemian, P. R.; Allen, A. J.; Zhang, F.; Levine, L. E.; Long, G. G., Ultra-small-angle X-ray scattering at the Advanced Photon Source. *J. Appl. Crystallogr.* **2009**, *42*, 469.

13. Ilavsky, J., Nika: software for two-dimensional data reduction. *J. Appl. Crystallogr.* **2012**, *45*, 324.

14. Ilavsky, J.; Jemian, P. R., Irena: tool suite for modeling and analysis of small-angle scattering. *J. Appl. Crystallogr.* **2009**, *42*, 347.

15. Zhang, F.; Ilavsky, J.; Long, G. G.; Quintana, J. P.; Allen, A. J.; Jemian, P. R., Glassy carbon as an absolute intensity calibration standard for small-angle scattering. *Metall. Mater. Trans. A* **2010**, *41*, 1151.

16. Page, K. A.; Cable, K. M.; Moore, R. B., Molecular Origins of the Thermal Transitions and Dynamic Mechanical Relaxations in Perfluorosulfonate Ionomers. *Macromolecules* **2005**, *38*, 6472.

17. Holdcroft, S., Fuel cell catalyst layers: a polymer science perspective. *Chemistry of materials* **2014**, *26*, 381.

18. Loppinet, B.; Gebel, G.; Williams, C. E., Small-Angle Scattering Study of Perfluorosulfonated Ionomer Solutions. *J. Phys. Chem. B* **1997**, *101*, 1884.

19. Buitrago, C. F.; Bolintineanu, D. S.; Seitz, M. E.; Opper, K. L.; Wagener, K. B.; Stevens, M. J.; Frischknecht, A. L.; Winey, K. I., Direct comparisons of X-ray scattering and atomistic molecular dynamics simulations for precise acid copolymers and ionomers. *Macromolecules* **2015**, *48*, 1210.

20. Welch, C.; Labouriau, A.; Hjelm, R.; Orler, B.; Johnston, C.; Kim, Y. S., Nafion in dilute solvent systems: Dispersion or solution? *ACS Macro Lett.* **2012**, *1*, 1403.

21. Mauritz, K. A.; Moore, R. B., State of Understanding of Nafion. *Chem. Rev.* **2004**, *104*, 4535.

22. Rubatat, L.; Rollet, A. L.; Gebel, G.; Diat, O., Evidence of Elongated Polymeric Aggregates in Nafion. *Macromolecules* **2002**, *35*, 4050.

Appendix B.

PFSA Electrode Coating for Detecting Heavy Metal Analytes in Ground Water

B.1 Introduction

Heavy metal pollutants such as arsenic, chromium, lead, mercury, and cadmium are known to be toxic even at trace levels.[1] Additionally, iron is thought to be environmentally hazardous as a contaminant in rivers and oceans.[2] Highly sensitive techniques are required for detection of these heavy metals in environmental water sources. There are several spectroscopic methods for detecting trace quantities of heavy metal contaminants including inductively coupled plasma mass spectrometry, atomic absorption spectrometry, atomic emission/fluorescence spectrometry, and X-ray fluorescence.[3] However, these methods require large and expensive instrumentation and are not suitable for in situ applications.[4] Electrochemical techniques offer low cost, user friendly, and in situ, real-time monitoring of heavy metals.[5] Nanosonic, Inc. (Pembroke, VA) has recently developed a portable sensor that incorporates chemical field effect transistors (ChemFET) technology in combination with stripping voltammetry that can be modified for the detection of mercury, lead and chromium ions.[6]

While these new sensors have been proven to detect some heavy metal analytes, they are not yet sensitive for detection of iron in ppb concentrations. Detection of these low concentrations of iron usually require a preconcentration method,[7] and ligands are typically added to the analyte solutions to complex with either iron (III) or iron (II) in order to separate the two uniquely-reactive species.[8] In order for these new chemical sensors to be modified for detection of iron, it is

necessary to employ a method for preconcentrating iron species on the electroactive surface and possibly a ligand to distinguish between oxidation states.

Perfluorosulfonic acid ionomer (PFSA) film-modified electrodes have been demonstrated to be useful in preconcentrating cationic species to the electrode surface for detecting low concentrations of analyte.[9] PFSA polymers are nonelectroactive, insoluble in water, and chemically inert, which make them ideal for coatings on modified electrodes.[10] They are also easily coated onto the surface of an electrode from dispersion and can be removed and re-casted. PFSA membranes have a high selectivity for cations,[11,12] resulting in preconcentration within the membrane at the surface of the electrode for electrochemical reaction. Nafion, has been the most studied membrane for use in modified electrodes, but new 3M PFSA and perfluoroimide acid (PFIA; containing two ion exchange sites per sidechain) ionomers provide higher ion contents that increase the available ion exchange groups for improved sensitivity.

In this study, we are looking to ultimately combine PFSA coatings with a ligand for complexation and preconcentration of iron (III) ions on the electrode surface of new portable electrochemical sensors produced by Nanosonic, Inc. In order to achieve this ultimate goal, we start with a simplified system of detecting copper (II) on a glassy carbon electrode (GCE) coated with Nafion to develop a refreshing method. Then, we will test different PFSAs with higher ion contents, referred to by equivalent weight (EW), in grams of polymer per moles of ion exchange groups, to determine whether these lead to improvements in sensitivity. Last, we will switch to a gold electrode (comparable to the gold sensors developed by Nanosonic, Inc.) for the detection of iron (III) using a 1-nitroso-2-naphthol ligand and Nafion coating.

B.2 Experimental

B.2.1 Materials

The 3M-Perfluorosulfonic acid (3M-PFSA) ionomer of 800 and 725 equivalent weight (EW, g polymer/mol sulfonate groups) and PFIA of 625 EW were provided by 3M. Nafion D521 dispersion (1100 EW, 5 wt % in alcohol-based solvent) was purchased from FuelCellEarth. Iron standards (1000 μg/mL in 2% HNO_3) were purchased from Inorganic Ventures and copper standards (1000 ppm) were provided by Nanosonic, Inc. Sodium acetate buffer solution (3 M, pH=5.2) was purchased from Sigma-Aldrich and 1-nitroso-2-naphthol (99% purity) was purchased from Fisher Scientific. Glassy carbon and gold working electrodes and their polishing kits were purchased from BASi. All other reagents were purchased from the Virginia Tech Chemistry stockroom and used without further purification.

B.2.2 Solution Preparation

All electrochemical measurements were carried out in a 0.01 M sodium chloride, 0.01 M sodium acetate buffer. A 3 M solution of sodium acetate buffer was diluted to 0.01 M and sodium chloride was added to make a concentration 0.01 M to make the buffer. All solutions were made in polypropylene volumetric flasks and were stored in polyethylene bottles that were washed with 5% nitric acid to remove any trace metals. The 1000 ppm stock solutions of Cu (II) and Fe (III) were diluted with Millipore water to make stock solutions of 100 ppm. A 0.1 mM (17.3 ppm) 1-nitroso-2-naphthol (NN) solution was prepared by first dissolving NN in methanol at a 0.01 M concentration. The NN/methanol solution was then diluted to 0.1 mM with Millipore water.

B.2.3 Electrode Coating Method

Glassy carbon electrodes and gold electrodes were first cleaned and polished using an alumina slurry and diamond slurry (for the gold electrode only) on electrode polishing pads following a procedure provided by BASi. The electrode was clamped so the active surface was facing up and 10 μL of a 0.5 wt % PFSA dispersion was dropped onto the electrode surface and allowed to dry at ambient conditions. The electrode and coating were then placed into a forced-air oven at 200 °C for 1 minute to anneal the thin-film coating. The volume and weight percent of PFSA dispersion were chosen to achieve a theoretical film thickness of 0.7 μm, assuming a density of 2 g/cm for PFSA.[13] After coating, the electrode was submerged in a 5 M NaCl solution for several hours to ion-exchange all sulfonic acid groups to Na^+-sulfonates, then stored in the 0.01 NaCl/0.01 acetate buffer until use.

B.2.4 Electrochemical Measurements

Electrochemical measurements were taken using either a glassy carbon or gold working electrode, silver wire reference, and platinum mesh auxiliary electrode. The electrodes are wrapped together by Parafilm as shown in **Figure B-1** to simplify the process of switching between samples in small containers. Differential pulse stripping voltammetry (DPSV) was used for the detection of copper (II) and iron (III) in a 0.01 M sodium chloride/0.01 M sodium acetate buffer solution. For each analyte, a 25 mL solution of blank electrolyte was first measured, then the specified concentration of analyte was pipetted in and allowed to stir for 30 minutes prior to measuring. For collecting measurements of analyte solutions containing NN, the NN was added to the blank buffer to make a concentration of 1 ppm, and each additional concentration of Fe(III) was pipetted into the NN/buffer solution and allowed to complex for 1 hour prior to measurements.

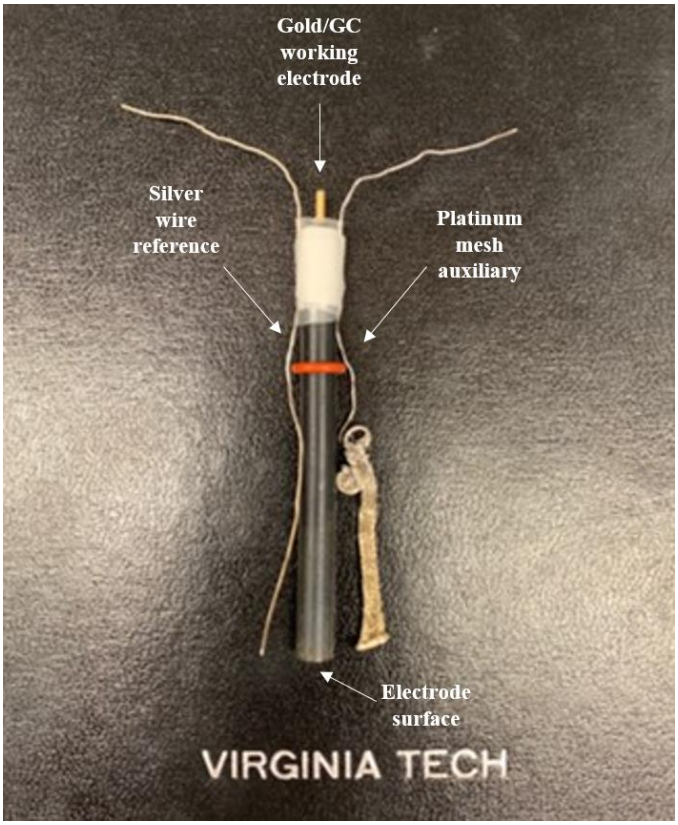

Figure B-1. Electrode setup for electrochemical measurements.

DPSV Method for Detection of Copper (II):

- Deposition at -700 mV for 180 s.
- Sweep from -700 to 700 mV at 4 mV step, 50 ms pulse width, 200 ms pulse period, 40 mV amplitude.

DPSV Method for Detection of Iron (III):

- Deposition at 500 mV for 120 s.
- Sweep from 500 to −400 mV at 4 mV step, 100 ms pulse width, at a 20 mV/s scan rate.

B.3 Results and Discussion

B.3.1 PFSA Coating on Glassy Carbon Electrode for the Detection of Copper (II)

In order to optimize the PFSA film coating on electrochemical sensors, we start with a simplified system for detecting copper (II) on a glassy carbon electrode (GCE). We utilize differential pulse stripping voltammetry (DPSV), which employs a deposition step at negative potentials to reduce copper (II) to solid copper that then plates onto the surface of the electrode. Upon sweeping from negative to positive potentials, solid copper is then oxidized back to copper (II) and released from the electrode, leading to a peak in measured current. **Figure B-2** shows the DPSV voltammogram for the detection of 0.01 ppm copper (II) on a bare GCE and a GCE coated with a thin (ca. 0.7 μm) Nafion film. There is a clear increase in signal for the Nafion-coated GCE compared to the bare GCE. However, after running the measurement and re-running a blank on the Nafion-coated GCE, the signal for oxidation of copper is still present, indicating that copper is still present within the Nafion membrane. This is typical for Nafion-coated electrodes because the cationic species is preferentially retained in the membrane due to a thermodynamic driving force for the partitioning of the analyte into the membrane from the solution.[9] Thus, a method for "refreshing" the membrane is required if the membrane-modified electrode is to be reused for more than one analysis.

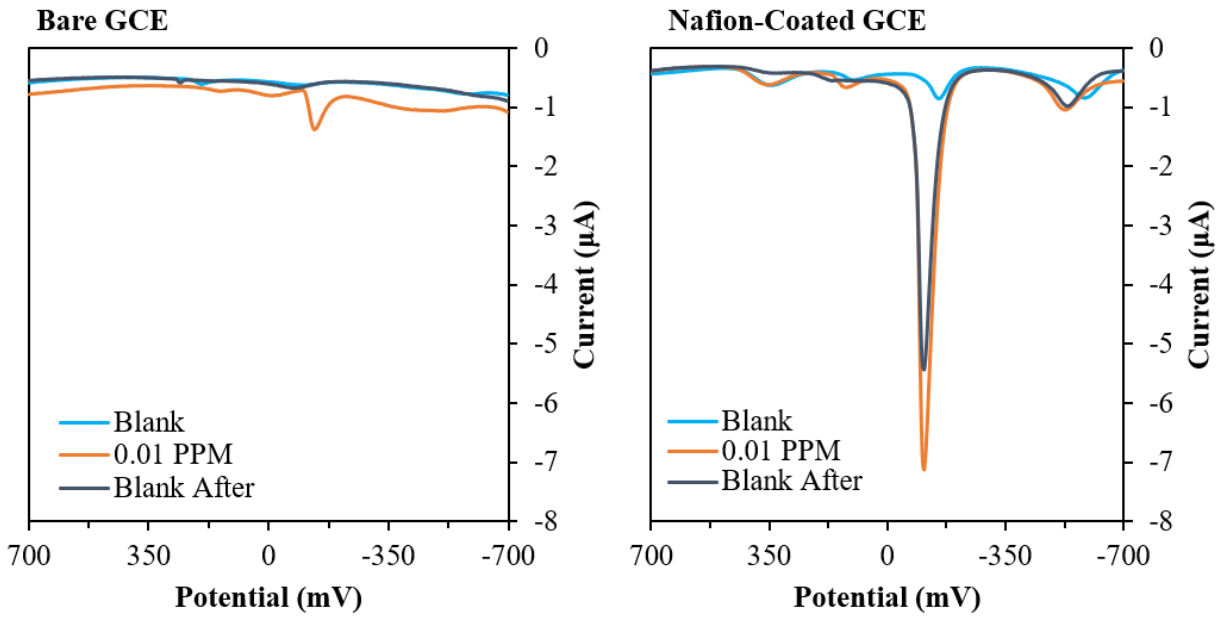

Figure B-2. DPSV voltammograms for detection of 0.01 ppm copper (II) with a bare GCE and a Nafion-coated GCE.

Figure B-3 shows the voltammograms of the Nafion-coated GCE before, during, and after the detection of a 0.01 ppm copper (II) solution and different refreshing methods. Apart from the one voltammogram labeled "0.01 ppm copper," the rest of the voltammograms included in this figure are of blank solutions either before or after a refreshing method. The first method consisted of rinsing the electrode with Millipore water, which showed only a slight decrease in the copper signal. Then, the membrane was refreshed by submersing in NaCl solutions of increasing concentration for 15 minutes prior to analysis of a blank solution. The copper signal decreases dramatically from these NaCl refreshing steps. With increasing NaCl concentration, the copper (II) signal decreases further, likely due to the increased ionic strength of the refreshing solution that increases the driving force for Na^+ ions to replace the Cu^{2+} ions.[9,12] Lastly, the Nafion-coated GCE was refreshed in a high concentration (8 M) nitric acid solution, which is typically used to reacidify Nafion membranes in the literature.[14-16] While this nitric acid refreshing method appears

to reduce the copper peak observed in DPSV, it also alters the baseline. Since the buffer solution contains a small concentration of NaCl, it is best to have the sulfonic acid groups all ion-exchanged to sodium-sulfonate groups prior to analysis to avoid any baseline changes as a result of SO_3H → SO_3Na exchanges.

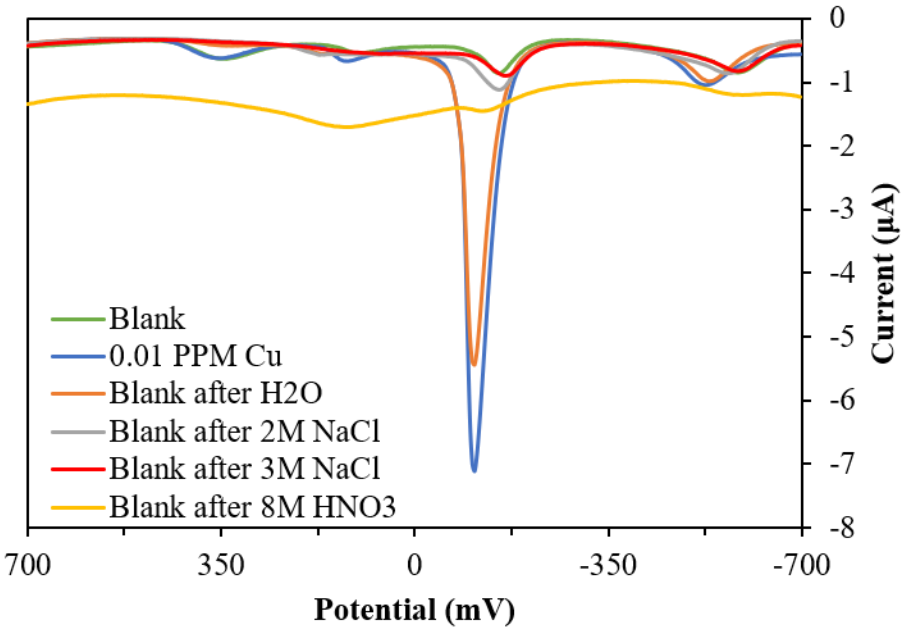

Figure B-3. DPSV voltammograms of blank solutions after analysis of a 0.01 ppm Cu^{2+} solution with a Nafion-coated GCE and subsequent refreshing of the Nafion coating by different methods.

While working with this well-behaved (reproducible) system of Cu^{2+} detection on GCEs, we tested different PFSA coatings to determine if EW (inversely related to ion content) has an effect on the copper signal in DPSV. The PFSAs used are from 3M, and contain a shorter sidechain than the previously analyzed Nafion coatings. In comparison to the 1000 EW (13 mol % ion content) Nafion coating used in the previous analysis, PFSA 800 contains 19 mol %, PFSA 725 contains 22.5 mol %, and PFIA contains ca. 38 mol % ion content. DPSV voltammograms for the detection of 0.1 ppm Cu^{2+} with the different PFSA-coated GCEs are shown in **Figure B-4**. There

is an increase in the signal (current) with decreasing EW (increasing ion content) for the three single sulfonic acid PFSAs. The 3M PFIA shows a slightly lower signal than the 725 EW 3M PFSA despite having a higher ion content. This analysis confirms that high ion content PFSAs membrane may be useful for optimizing the signal from low concentrations of analyte in DPSV.

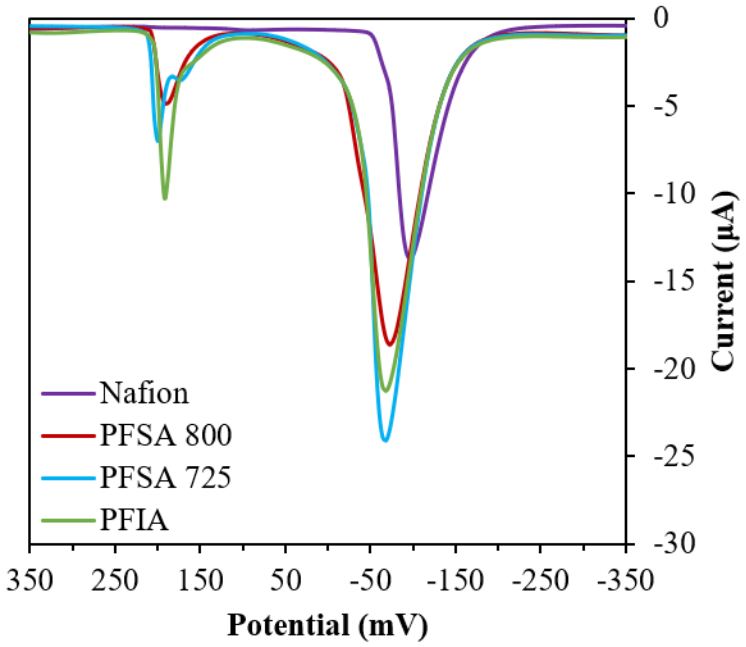

Figure B-4. DPSV voltammograms of the detection of 0.1 ppm Cu^{2+} by GCEs coated with Nafion, 3M PFSA 800, 3M PFSA 725, and 3M PFIA.

B.3.2 Detection of Iron (III) by Gold Electrode

The next phase of this project aimed to investigate the detection of iron (III) by a gold working electrode in order to better compare to the sensors developed by Nanosonic, Inc., which utilize a gold electroactive surface. In this system, we add a 1-nitroso-2-naphthol (NN) ligand, which has been shown to be selective for complexing with iron (III).[17,18] Addition of iron (III) analyte to the buffer + NN solution is followed by stirring for an hour to allow for complete complexation. Cathodic stripping voltammetry (CSV) is then conducted by depositing the iron-

NN complexes at positive potentials and then stripping by sweeping to negative potentials. CSV voltammograms for solutions containing 1 ppm NN and varying concentrations of iron (III) are shown in **Figure B-5**. A visible oxidation peak is observed at −0.15 V that is sensitive to iron concentration. This peak appears at concentrations as low as 0.05 ppm, and appears to reach a maximum at concentrations of 5 ppm.

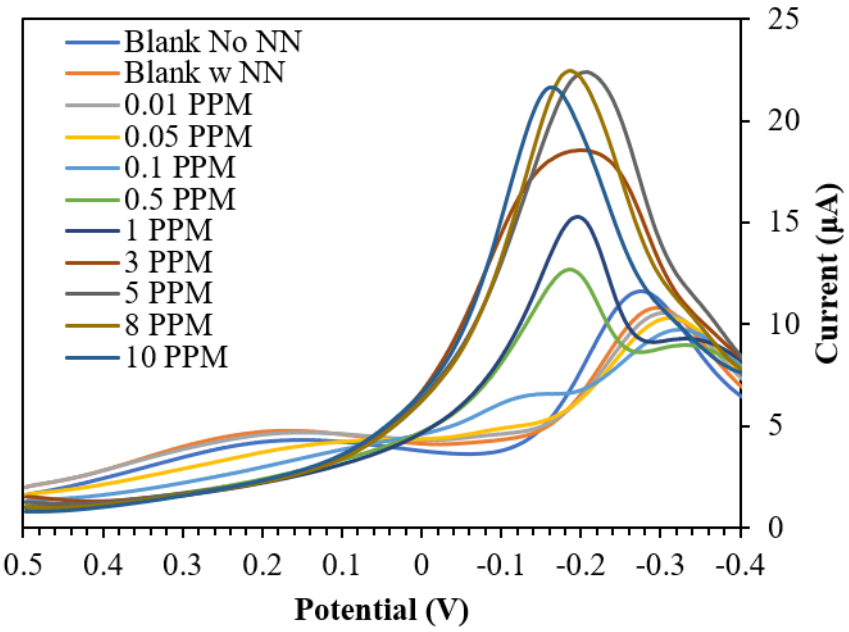

Figure B-5. CSV voltammograms of solutions containing various concentrations of Fe^{3+} in addition to 1-nitroso-2-naphthol complexing agent by a bare gold electrode.

While this method is sensitive to the detection of these iron-NN complexes, we are looking to achieve even lower limits of detection in the ppb range. Coating the electrode surface may assist in preconcentrating iron ions to the surface of the electrode and increasing the signal of the stripping voltammogram as observed in the previous section with PFSA-coated GCEs. **Figure B-6** shows CSV voltammograms for solutions containing varying concentrations of iron (III) using a

Nafion-coated gold working electrode with no addition of NN. Without the complexing ligand, we still see a strong signal appear with increasing iron (III) content. This signal has now shifted to a more positive potential (ca. 0.25 V) than what was previously observed for the iron-NN complexes on a bare gold electrode. A signal is observed for concentrations as low as 0.05 ppm in this Nafion-coated electrode system.

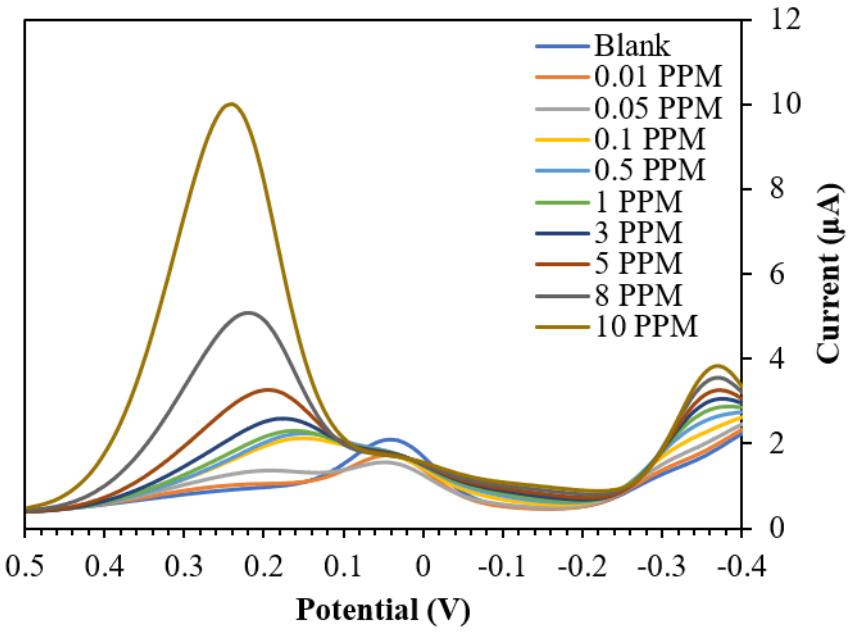

Figure B-6. CSV voltammograms of solutions containing varying concentrations of Fe^{3+} by a Nafion-coated gold electrode.

B.4 Conclusions

In this investigation, we demonstrated the utility of applying a PFSA coating to glassy carbon and gold working electrode surfaces for increasing the detection limit of copper (II) and iron (III). In the GCE/copper (II) system, a method of refreshing the PFSA membrane was found by submersing the Nafion-coated electrode in a high ionic strength sodium chloride solution for

15 minutes between each measurement to remove any leftover copper ions from the membrane. Additionally, PFSAs of increasing ion contents showed an increase in the signal for detecting copper ions. In the gold/iron(III) system, both the addition of a 1-nitroso-2-naphthol complexing agent and the addition of a Nafion-coating on a gold electrode were shown to be sensitive for the detection of iron ions in solution. Future work for this project includes incorporating the NN ligand within a PFSA membrane on a gold electrode surface to possibly achieve synergistic improvement in signal from combining the two techniques. Ultimately, a PFSA-coating will be applied to Nanosonic, Inc.'s new sensors for a facile and portable method of detecting heavy metals in water samples.

B.5 Acknowledgments

The authors acknowledge Nanosonic, Inc for providing materials and funding for this research. Materials used for the PFSA coatings were provided by 3M.

B.6 References

1. Mohiuddin, K.; Ogawa, Y.; Zakir, H.; Otomo, K.; Shikazono, N., Heavy metals contamination in water and sediments of an urban river in a developing country. *Int. J. Environ. Sci. Technol* **2011**, *8*, 723.
2. Hirata, S.; Yoshihara, H.; Aihara, M., Determination of iron (II) and total iron in environmental water samples by flow injection analysis with column preconcentration of chelating resin functionalized with N-hydroxyethylethylenediamine ligands and chemiluminescence detection. *Talanta* **1999**, *49*, 1059.

3. Helaluddin, A.; Khalid, R. S.; Alaama, M.; Abbas, S. A., Main analytical techniques used for elemental analysis in various matrices. *Trop. J. Pharm. Res.* **2016**, *15*, 427.

4. Grieshaber, D.; MacKenzie, R.; Vörös, J.; Reimhult, E., Electrochemical biosensors-sensor principles and architectures. *Sensors* **2008**, *8*, 1400.

5. Bansod, B.; Kumar, T.; Thakur, R.; Rana, S.; Singh, I., A review on various electrochemical techniques for heavy metal ions detection with different sensing platforms. *Biosens. Bioelectron.* **2017**, *94*, 443.

6. Ruan, H.; Kang, Y.; Gladwin, E.; Claus, R. O., Selective detection of heavy metal ions by self assembled chemical field effect transistors. *Appl. Phys. Lett* **2015**, *106*, 163102.

7. Chen, J.; Lin, J., Determination of dissolved iron (II) and iron (III) in water with 5-Br-PAN-S by solid phase spectrophotometry. *Anal. Lett.* **2001**, *34*, 2169.

8. Hirayama, T.; Nagasawa, H., Chemical tools for detecting Fe ions. *J. Clin. Biochem. Nutr.* **2017**, *60*, 39.

9. Espenscheid, M. W.; Ghatak-Roy, A. R.; Moore, R. B.; Penner, R. M.; Szentirmay, M. N.; Martin, C. R., Sensors from polymer modified electrodes. *J. Chem. Soc., Faraday Trans. 1* **1986**, *82*, 1051.

10. Hoyer, B.; Florence, T. M.; Batley, G. E., Application of polymer-coated glassy carbon electrodes in anodic stripping voltammetry. *Anal. Chem.* **1987**, *59*, 1608.

11. Steck, A.; Yeager, H., Water sorption and cation-exchange selectivity of a perfluorosulfonate ion-exchange polymer. *Anal. Chem.* **1980**, *52*, 1215.

12. Yeager, H.; Steck, A., Ion-exchange selectivity and metal ion separations with a perfluorinated cation-exchange polymer. *Anal. Chem.* **1979**, *51*, 862.

13. Zook, L. A.; Leddy, J., Density and Solubility of Nafion: Recast, Annealed, and Commercial Films. *Anal. Chem.* **1996**, *68*, 3793.

14. Osborn, S. J.; Hassan, M. K.; Divoux, G. M.; Rhoades, D. W.; Mauritz, K. A.; Moore, R. B., Glass Transition Temperature of Perfluorosulfonic Acid Ionomers. *Macromolecules (Washington, DC, U. S.)* **2007**, *40*, 3886.

15. Page, K. A.; Cable, K. M.; Moore, R. B., Molecular Origins of the Thermal Transitions and Dynamic Mechanical Relaxations in Perfluorosulfonate Ionomers. *Macromolecules* **2005**, *38*, 6472.

16. Zook, L. A.; Leddy, J., Density and solubility of Nafion: recast, annealed, and commercial films. *Anal. Chem.* **1996**, *68*, 3793.

17. Van Berg, C. D.; Nimmo, M.; Abollino, O.; Mentasti, E., The determination of trace levels of iron in seawater, using adsorptive cathodic stripping voltammetry. *Electroanalysis* **1991**, *3*, 477.

18. Gledhill, M.; van den Berg, C. M., Measurement of the redox speciation of iron in seawater by catalytic cathodic stripping voltammetry. *Mar. Chem.* **1995**, *50*, 51.